**AALBORG UNIVERSITY**

DENMARK

**Multiple Antenna Systems for Mobile Terminals**

Nguyen, Hung Tuan

# Multiple Antenna Systems

## for

## Mobile Terminals

This thesis is submitted to
The Faculty of Engineering and Science
Aalborg University, Denmark
in defense of the PhD degree
by

Hung Tuan Nguyen

This thesis is typeset by the author using LaTeX $2_\varepsilon$.

Printing: Aalborg University, Denmark

Supervisors:

Prof. dr.techn Jørgen Bach Andersen
Prof. dr. Gert Frølund Pedersen

Opponents:

Prof. A. Molisch, Lund University,Sweden

Prof. L. Correia, Technical University of Lisbon, Portugal

Assoc. Prof. Søren Holdt Jensen, Aalborg University, Denmark

Committee Chairman:

Assoc. Prof. Søren Holdt Jensen, Aalborg University, Denmark

Moderator:

Assis. Prof. Persefoni Kyritsi, Aalborg University, Denmark

# Abstract

Recently Multiple Input Multiple Output (MIMO) systems, where an antenna array is applied at both ends of the transmission link, have been a major focus of research. The main reason for such interest is that a MIMO system has the potential of providing more spectral efficiency and better transmission quality. Hence, beyond the original purpose of transmitting and receiving speech, it is possible to provide more services which require a higher data rate. The first part of the project is devoted to the characterization of the measured MIMO radio channel in various propagation environments. Several parameters of the measured MIMO radio channel are extracted and the system performance is analyzed. The influence of the propagation conditions and some real-life usage effects on the channel capacity is evaluated. Based on the measurement data, a simple stochastic model for a spatio-temporally correlated MIMO radio channel is proposed. The capability of the model in replicating the spatial and temporal characteristic of the measured channel is assessed.

The second part of the project aims at analysing and evaluating the performances of several link adaptation (LA) techniques for multiple elements antenna (MEA) systems. With a premise that the channel knowledge is available at both ends of the transmission link, the performances of the proposed LA techniques for single user scenario narrowband MIMO systems are evaluated. It is shown that an efficient use of the channel information can improve the system performance significantly. However, the performance of the LA techniques strongly depends on the quality of the estimated channel coefficients. Imperfection in the estimation of the channel coefficient could lead to degradation in the performance of any MIMO system. We study the impact of the time-varying channel, as the only source of such imperfection, on the MIMO system performance. An expression of the signal to interference plus noise ratio (SINR) quantifying the effect of time-varying channel on the spatial multiplexing MIMO system is derived. It is shown that for a channel varying with time, increasing the transmitted power does not really help in improving the performance of a MIMO system. As a remedy for this problem, a precoder/decoder prediction scheme for the time-varying frequency flat MIMO channel is proposed and evaluated. Using the prediction scheme in a slowly time-varying narrowband channel, improvement of the MIMO system performance by a factor of two is shown to be possible.

In a wideband transmission, the frequency selective fading causing the inter symbol interference (ISI) remains a big challenge for point to point wireless communication in general. Moreover, interferences caused by other users in the multi-user environment also degrade the system performance significantly. It is especially true for MEA systems where the received signals are not only mixed in space but also in time. The last part of the project is devoted to the investigation of the performance of the time reversal technique (TR) in wireless communications. The feasibility of applying TR in MEA wireless systems to combat the effect of time dispersion and interference is illustrated. The results show that TR is a very promising solution for interference reduction and time dispersion in multi-user MISO system.

# Dansk resume

Der har i den senere tid været meget fokus på "Multiple Input, Multiple Output (MIMO)" systemer, hvor der er opstillet en række antenner i begge ender af transmissionsforbindelsen. Grunden til at denne interesse er først og fremmest at MIMO systemer har mulighed for at yde en højere spektral virkningsgrad og en bedre transmissionskvalitet. Der er således mulighed for at tilbyde flere tjenester, som kræver et højere datahastighed end det oprindelige formål med at sende og modtage tale

Første del af projektet beskriver målinger af MIMO radiokanalen i forskellige udbredelsesmiljøer. Der er uddraget flere forskellige parametre af MIMO radiokanalen, og systemkapaciteten er blevet undersøgt. Der er foretaget en evaluering af hvilken indflydelse udbredelsesforholdene og visse former for dagligdags brug har på kanalkapaciteten. Med udgangspunkt i disse målinger er der foreslået brug af en simpel stokastisk model af en rum-tid MIMO kanal. Der er foretaget en vurdering af modellens evne til at gendanne den rumlige og tidsmæssige karakteristik af den målte kanal.

Anden del af projektet har til hensigt at analysere og evaluere resultatet af flere link adapteringer (LA) til multiantenne systemer (MEA). Forudsat at kanaloplysningerne er tilgængelige i begge ender af transmissionslinket, foretages der en evaluering af LA teknikkernes ydeevne i forbindelse med enkeltbruger smalbånds-MIMO systemer. Det har vist sig, at hvis man bruger kanal informationerne rationelt og effektivt, så vil systemets ydeevne forbedres væsentligt. Dog afhænger LA teknikkernes ydeevne i høj grad af kvaliteten af de estimerede kanal koefficienter. Ukorrekt estimering af kanal koefficienter kan føre til en forringet ydeevne i ethvert MIMO system. Der er undersøgt betydningen af den tidsvarierende kanal som den eneste kilde til uregelmæssigheder i forhold til MIMO systemets ydeevne. Der er udledt et udtryk for forholdet mellem signal og summen af interferens og støj (SINR), der udtrykker indflydelsen af den tids-varierende kanal på den rumligt multipleksede MIMO kanal. Med hensyn til den tidsvarierende kanal har det vist sig, at selvom man øger sendestyrken har dette ikke nogen forbedrende effekt på MIMO systemets ydeevne. Som en afhjælpende foranstaltning på dette problem er der foreslået og undersøgt brug af et prekodet system for den tidsvarierende smalbånds MIMO kanal. Det har vist sig muligt at benytte det prekodede skema i en langsomt tidsvarierende smalbåndskanal MIMO system med en forbedringsfaktor på to.

I bredbåndstransmission er frekvensselektiv fading, der leder til inter-symbol-interferens stadig en stor udfordring for punkt-til-punkt trådløs kommunikation. Desuden er forstyrrelser forårsaget af andre brugere i multi-bruger omgivelserne også med til i væsentlig grad at forringe systemets ydeevne. Dette gælder især for MEA systemer, hvor de signaler der bliver modtaget ikke kun er forskellige med hensyn til rum men også med hensyn til tid.

Den sidste del af projektet er en undersøgelse af tidsinversionsteknikkens (TR) ydeevne i trådløs kommunikation. Muligheden for at benytte TR til at bekæmpe eller eliminere effekten af tidsdispersion og interferens i et MEA trådløst system er behandlet. Resultaterne viser, at TR er en lovende løsning på at reducere interferens og tidsdispersion i et multi-bruger MIMO system.

# Acknowledgements

# Contents

i

# List of Figures

# Chapter 1

# Introduction

## 1.1 Objective

The goals of this PhD project are to do research in the multiple antennas systems for wireless communications with focus on mobile terminals. In this thesis, we intend to address the two key issues as follows.

- Performance evaluation and characterization of MIMO radio channels in various real-life usage scenarios. Based on the measurement data of a MIMO system, with eight antenna output at the base station and four antennas at the small terminal in different propagation environments the measured channels are characterized. Crucial factors those significantly affect the MIMO performance in some real-life usage scenarios are indicated.

- Study and propose suitable transmitting/receiving techniques which are capable of reducing the complexity of antenna system and signal processing algorithm at the mobile terminal. The main drawback of deploying multiple antennas in small terminals is the need for extra hardware cost and higher power consumption. Therefore, focus is put on to decrease complexity handset without performance degradation.

## 1.2 Outline

In chapter 2 we present some background on the working principle of the wireless systems which use multiple antennas either at the transmitter, the receiver or at both sides. It starts with a brief overview of the smart antennas system and numerous diversity techniques to reduce the multipath fading effect. The second part of the chapter focuses on the MIMO techniques. Numerous metrics, parameters and basic concepts which are often used in the MIMO techniques are presented. This chapter provides a good background on MEA systems and is useful for the understanding of the chapters that follow.

Chapter 3 to chapter 5 are the summary and discussion based on a number of published/submitted papers. Each chapter is constituted by a number of small but related topics. In each topic, the problem definition, motivation and obtained results are organized in terms of a paper. These chapters are organized in such a way that the flow of the thesis is retained.

Chapter 3 describes major findings in the channel characterization of the measured MIMO radio channel for both outdoor and indoor scenarios. The measurement setup was done to mimic some real-life usage scenarios where the antennas and the channel propagation are integral parts of the MIMO systems. These findings area taken from the three following papers

[**P1** ] H.T.Nguyen, J.B.Andersen and G.F.Pedersen, *Characterization of the indoor/outdoor to indoor MIMO radio channel at 2.140GHz* accepted to Wireless Personal Communication, An International Journal, 2005.

[**P2** ] H.T.Nguyen, J.B.Andersen and G.F.Pedersen, *The influence of outdoor environment on MIMO system performance*, WPMC 2005, Aalborg, Denmark.

[**P3** ] H.T.Nguyen, J.B.Andersen and G.F.Pedersen, *A stochastic model of spatio-temporally correlated narrowband MIMO channel based on indoor measurement*, $15^{th}$ IEEE International symposium on Personal, Indoor and Mobile Communications Barcelona Spain, September, 2004, Vol 3, 1827-1831.

Chapter 4 focuses on the link adaptation techniques for narrowband MIMO systems when the channel state information is assumed to be known at both ends of the transmission link. It also discusses one of the major issues in MIMO systems applying spatial multiplexing, that is the performance degradation due to the time-varying channel. A prediction scheme for the precoder/decoder of the spatial multiplexing MIMO system operating in a time-varying channel is presented in the same chapter. The chapter is the summarization of the three papers

[**P4** ] H.T.Nguyen, J.B.Andersen and G.F.Pedersen, *On the performance of link adaptation technique in MIMO systems*, submitted to Wireless Personal Communication, An International Journal, 2005.

[**P5** ] H.T.Nguyen, J.B.Andersen and G.F.Pedersen, *Capacity and performance of MIMO system under the impact of feedback delay*, $15^{th}$ IEEE International symposium on Personal, Indoor and Mobile Communications Barcelona Spain, September, 2004, Vol 1, 53-57.

[**P6** ] H.T.Nguyen, G.Leus and N.Khaled, *Prediction of the eigenvectors for spatial multiplexing MIMO systems in time-varying channels*, The 5th IEEE International Symposium on Signal Processing and Information Technology December 18-21, 2005, Athens, Greece.

Chapter 5 is devoted to a recently hot topic: the time reversal technique (TR) for wireless communications. Experimental and analytical studies on the performance of TR in RF wireless communications from wideband to ultra-wideband are performed. The results from the following three papers are summarized in this chapter.

[**P7** ] H.T.Nguyen, J.B.Andersen and G.F.Pedersen, *The potential use of time reversal technique in multiple elements antenna system*, IEEE Communications Letters, January, 2005, vol 9, no 1, 40-42.

[**P8** ] H.T.Nguyen, J.B.Andersen, G.F.Pedersen, P. Kyritsi, P. Eggers, *Time Reversal in Wireless Communications: a Measurement Based Investigation*, accepted to IEEE Transactions on Wireless Communications, 2005.

[**P9** ] H.T.Nguyen, I.Z.Kovács and P.C.F.Eggers, *A Time Reversal Transmission Approach for Multi-user UWB Communications*, submitted to IEEE Transaction on Antennas and Propagation, 2005.

Chapter 6 is for conclusions and remarks. Major results and findings of the thesis are summarized in this chapter. Some discussions and directions for future work are also introduced.

# Chapter 2

# Smart antenna systems in wireless communications

## 2.1  Adaptive antennas in mobile communications

Major impairments such as multipath fading, delay spread, Doppler spread and co-channel interference make the wireless channel a hostile medium for mobile communications. Degradation in the system performance is inevitable if only a single omnidirectional antenna is used for communication. To reduce the above mentioned impairment, one can use a directional antenna with the main beam pointed toward the direction where most of the signal energy is expected to come from. However, this approach is only suitable for a point to point fixed wireless communication and the system performance is very sensitive to the variations of the channel.

With extra antenna elements and complex signal processing algorithm, the impairment factors mentioned above can be reduced or even mitigated. As long as the signal at different antenna elements undergoes independent fading, all of these signals probably will not go in deep fade simultaneously. In the transmit mode, by changing the weight at each antenna array port, the radiation pattern of the antenna array is dynamically adapted to the channel variations. The whole antenna array can be considered as a single antenna with an adjustable radiation pattern both in phase (direction) and magnitude (pattern shape). The transmitted signal is focused on the intended user, and the interference from other users in the same cell as well as in other cells is thus limited. Because the beam is formed in certain directions and nulls in others, some delayed arrivals can also be cancelled. Thereby, the inter symbol interference is alleviated. In the receive mode, by using proper weight factors, it is possible to steer the main beam of the antenna array to the intended user and at the same time steering nulls to interference sources. In this way, the co-channel interference is suppressed. In all, the transmission range, the capacity and the data rate of the wireless communications can be improved by the use of adaptive antennas systems [1, 2, 3, 4].

There is a number of definitions in literature about the "*adaptive antennas system*". The simplest definition could be a system with multiple antennas and a signal processing unit to adapt to the variations of the channel. This definition highlights the important of both the antennas elements as well as the signal processing unit in an adaptive antenna

system. The degree of intelligent in an adaptive (smart) antenna system is defined in [5] as in the order of Switched lobe, Dynamically phased array and Adaptive array. In a Switched lobe system, the antenna array comprises of several directive antenna elements. A basic switching function is used to select an active antenna element. The radiation pattern of this element will determine the radiation pattern of the whole array. The Direction of Arrival (DoA) information of the received signal from the user is included in the Dynamically phased array system, whereby continuous tracking can be achieved. In the Adaptive array system, the DoA information of the desired signal as well as interference signal is used in order to form nulls towards the interference and a main lobe to the intended signal sources.

In the receiving mode, to steer the antenna array main lobe to the direction that maximum gain would appear, one can change the phase or both the phase and the gain of the signal at each antenna output. In the first approach, the phase of the received signal is adjusted such that the signals are coherently added in phase. The second approach gives an optimal performance because the signal at each antenna elements is adjusted both in gain and phase. With this approach, not only is the signal strength increased but also the interference is suppressed. Optimum signal to noise ratio (SNR) and maximum signal to interference plus noise ratio (SINR) can be obtained by properly adjusting the gain and phase of each antenna element. This is also called the optimum combining techniques in literature and some of them will be discussed in more detail in the section 2.3.

## 2.2   Diversity dimensions

From the antenna and propagation point of view, the basic principle to achieve diversity gain is to configure the antenna elements in such a way that each element can capture independent or at least partly uncorrelated versions of the signal. Moreover, in order to obtain a good diversity performance the mean branch power differences should be limited. If the branch power difference is significant, the strongest branch will dominate and the diversity performance will degrade even though the correlation between the branches signals is still low. Space, polarization and angle domain are the three diversity dimensions which are often employed in wireless communications systems nowadays. It should be noted that the performance of each diversity scheme is heavily dependent on the conditions of the propagation channel.

**Spatial diversity:** By separating the antenna elements in space it is possible to get independent versions of the signal because the electromagnetic waves often travel through unique paths before reaching a certain antenna element. As a rule of thumb, for a rich multipath environment and omnidirectional antennas only a quarter wavelength separation is required for low multipath fading correlation [6]. Due to the space limitation, employing spatial diversity on a small handset can be difficult. However, when operating at a higher frequency regime (i.e. 2.1GHz for UMTS, 5.1GHz for Wireless LAN), since the electric size of the handset becomes larger, it is still possible to enhance the performance by the use of multiple antennas at the handset. Employing spatial diversity at the BS seems to be feasible because the constraint on the size of the antenna array is not too strict. However, normally the angular spread of the signals arriving at the BS is narrower than that at the handset. Therefore, separation between BS's antennas elements must be higher in order

to get the same performance improvement as achieved at the handset.

**Polarization diversity:** The electromagnetic wave contains two vertical and horizontal polarization components. They are orthogonal to each other and perpendicular to the propagation path. Even if the transmitting antenna emits a well defined polarization wave, after some reflections, and diffractions the polarization of the wave is totally random. Moreover, these two vertical and horizontal components fade independently. Therefore, it is possible to use both vertical and horizontal polarizations to obtain dual diversity without spatial separation. Since polarization only provides two branches of diversity, combination with other forms of diversity is often used when more diversity branches is required. It was shown that the correlation coefficient of the combined space and polarization diversity is equivalent to the product of the spatial correlation coefficient and the polarized correlation coefficient [7].

In general, the two polarizations are mutually uncorrelated and the average power ratio is set to unity for convenient. However, experiment results show that it is not always the case. The ratio of the average powers of the two polarizations is denoted as the cross polarization discrimination (XPD). For urban environment it ranges from 0dB to 18dB, [8]. It was found that in an indoor environments along the corridor horizontal polarization attenuates faster than the vertical polarization [9], meanwhile the opposite is true for outdoor environment due to the large opening volume in the horizontal plane. Therefore care must be taken in deploying polarization diversity so that the influence of branches power difference to the diversity performance is not severe. For example, dual polarization slanted at $45^o$ is used in outdoor environment to avoid the above mentioned problem [10].

**Angle (pattern) diversity:** Using the same principle, if the radiation pattern of each antenna element can point toward different directions there is a potential that the captured signals becomes mutually uncorrelated. This is the main argument for using angle diversity. Maximum diversity performance is obtained only when the radiation pattern of the antenna elements is separated well enough. Moreover, the scatterers or in other words the signal sources must be uniformly distributed over a wide angular spread. By fulfilling this condition, we can avoid the case that the pattern of the antenna element is pointed toward a direction with weak or even no signal.

From a signal space point of view, there are other ways to obtain diversity gain. They are the temporal diversity, the frequency diversity and the path diversity.

**Temporal diversity:** By transmitting copies of signal at different instants, the variation of the propagation channel will give rise to the temporal diversity. In order to assure that different copies of the transmitted symbol will undergo independent fading, the intervals between transmissions of the same symbol should be at least equivalent to the coherence time of the channel. The temporal diversity finds its application in error control coding with repetition code and interleaving techniques.

**Frequency diversity:** The frequency diversity technique works also in the same manner. When the same signal is simultaneously transmitted over two or more independent frequencies separated from the each other by at least a coherence bandwidth, they will fade independently. Thereby, a diversity gain can be obtained. It should be noted that in both temporal and frequency diversities there is a trade off between the diversity gain and the redundancy. For temporal diversity the redundancy will reduce the actual transmission rate. Meanwhile, for using frequency diversity extra spectrum is required.

**Path diversity:** The delayed version of the transmitted signal in an environment with a larger delay spread can also be used to improve the performance of the system. By coherently combining the signal received in the delay domain more signal energy is collected. Moreover, because the signal at each delayed tap is normally uncorrelated (i.e. uncorrelated scattering) achieving diversity in the delay domain is possible. The Rake receiver is one example of a system that exploits this type of diversity. However, in a system applying path diversity, the interval between two consecutive transmitted signal symbols must be larger than the delay spread of the system to avoid the interference caused by the neighboring symbols. The advantage of the path diversity scheme is that no explicit expansion of the bandwidth is required.

## 2.3   Diversity combining

Diversity combining is used to combat the mutipath fading problem in wireless communications. It exploits the diversity (i.e. one of the dimensions mentioned above or the combination of these) of the signals received at multiple antenna ports. The signals induced on different antennas are combined in one of many ways to avoid the deep fade and in some case to null out the interference. The average received signal power is improved and it can be used to increase the capacity or transmission quality of the system. Because of its simplicity, yet effective, a diversity combining technique is often deployed in the user terminal.

The simplest form of the diversity combining technique is the switched combining technique. The principle of this technique is simple; when the signal quality of the currently used branch is good (i.e. the signal strength, SNR value or the average BER meet certain requirements) there is no need to use other branch. This will reduce the complexity of the receiver as only one RF chain is required. A more advance form of the switched combining technique is the selection combining technique. The quality of the currently used branch is examined and compared with those of the other branches continuously (i.e. at the end of each received frame or even during the communication reception/detection process [11]). The performance of this scheme is better than the switched combining technique, yet requiring only a single RF chain. However, a system using the selection combining technique is more prone to the error caused by the discontinuities in the combined signal amplitude and phase than the simple switched combining technique. Nevertheless, utilizing these two techniques one could get a good compromise between the system complexity and performance.

Other form of the diversity combining techniques is the equal gain combining (EGC). The phase of the signal at each antenna output is adjusted. After being equally weighted the signals are combined in-phase. The combined signals can be described by

$$r = \sum_{i=1}^{N_r} e^{-j\theta_i} r_i = x \sum_{i=1}^{N_r} A_i + \sum_{i=1}^{N_r} e^{-j\theta_i} n_i \qquad (2.1)$$

where $A_i$, $\theta_i$ and $n_i$ are the gain, the phase shift and the additive noise of the $i^{th}$ branch; $r_i$ is the received signal before combining $r_i = xA_i e^{j\theta_i} + n_i$, $x$ is the transmitted symbol;

and $N_r$ is the number of receiving branches. The SNR of the EGC technique is given by

$$SNR_{EGC} = \left(\sum_{i=1}^{N_r} A_i\right)^2 \frac{SNR_o}{N_r} \tag{2.2}$$

where $SNR_o$ is the average signal to noise value of one receiving branch.

The EGC is a simple version of the maximal ratio combining technique (MRC). For the MRC, the signal at each antenna port is first weighted proportional to the SNR at this port. The weighted signals are then combined in-phase. The SNR of the system using MRC is

$$SNR_{MRC} = \left(\sum_{i=1}^{N_r} A_i^2\right) SNR_o \tag{2.3}$$

Figure 2.1 illustrates the Cumulative Distribution Function (CDF) of the gains obtained by different combining techniques. It is observed that when the number of diversity branches $N_r$ is small the performance differences among the SC, EGC and MRC techniques is negligible. When $N_r$ is large there is a significant difference between the performance of the SC and MRC technique. However, the performance of the EGC is still very close to that of the MRC technique.

It should be noted that when the signals at the receiving antenna outputs are correlated or there is considerable difference in the received branch power, the performance of these diversity combining techniques mentioned above will degrade.
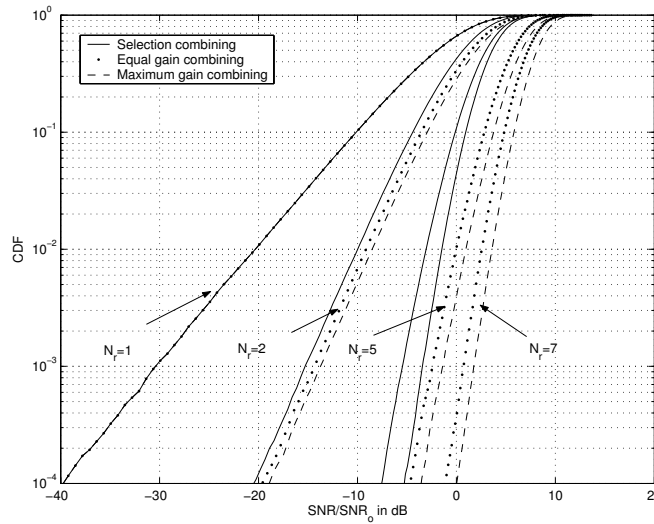


Figure 2.1: Dependence of the diversity gain on the combining methods and number of receiving antennas

## 2.4 MIMO

The beamforming and diversity combining techniques discussed above exploit the availability of multiple antennas or antenna array at one side of the transmission link. The

beamforming technique often involves the use of an array antenna at the transmit side and a single antenna at the receive side. On the other hand, diversity combining techniques require multiple antennas at the receiver and a single antenna at the transmitter. Multiple input single output (MISO) and single input multiple output (SIMO) are the two terms describing the antenna setting for beamforming and diversity combining techniques, respectively. It has been shown in numerous research works that the performance of a system using multiple antennas with proper signal processing algorithm can be significantly improved. However, the potential use of antenna arrays at both ends of the transmission link, the so called multiple input multiple output (MIMO) system, was not mentioned until recently by the work of Telatar and Foschini [12, 13, 14].

A MIMO system involves multiplexing of the input data stream between the transmitting antennas. It exploits the independence of channels to achieve very high spectral efficiency [14, 15, 16]. It has been shown in [12] that under certain assumptions the channel capacity increases linearly with the number of used antennas without increasing premium bandwidth or transmitted power. The physical MIMO channel can be considered as the combination of the multiple MISO or SIMO channels. In this sense, MIMO systems can be considered as an extension of the adaptive antenna system described in section 2.1.

In fact, the traditional use of array antennas in MISO or SIMO systems where the signals at all antenna outputs are combined into one port is often called a one-port array, [8]. At one instance, the same signal information is transmitted or received. The weight vector is adjusted to optimize under some criteria, such as maximizing the received signal power or maximizing the SINR. For a multi-port array, which is often observed in MIMO systems, several independent symbols are treated at the same time. Therefore, the signal is not only mixed in space, like that of the one-port array, but also mixed in time. For this type of transmission, signal processing is used to demultiplex the received signals. Examples are the spatial multiplexing or the Space Time Block Code (STBC) transmissions applied in MIMO systems. Self interference is a problem in a multi-port array system and it can be thought of as the co-channel interference in one-port multi-user systems.

### 2.4.1   MIMO system and the parallel sub-channels transmission

Let us consider a wireless system where there are $N_t$ transmitting antennas and $N_r$ receiving antennas. The channel matrix $\mathbf{H}$ can be realized as an $N_t \times N_r$ matrix. Each entry of $\mathbf{H}$ denoted as $h_{n_t n_r}$ is the channel state coefficient between the $n_t^{th}$ transmitting antenna and the $n_r^{th}$ receiving antenna.

$$
\begin{bmatrix}
h_{11} & h_{12} & \cdots & h_{1N_r} \\
h_{21} & h_{22} & \cdots & h_{2N_r} \\
\vdots & \vdots & \ddots & \vdots \\
h_{n_t 1} & h_{n_t 2} & \cdots & h_{N_t N_r}
\end{bmatrix}
\tag{2.4}
$$

This is the channel description of the MIMO system when the channel is frequency flat (i.e. the bandwidth-delay spread product of the channel is smaller than 0.1, $W\sigma_\tau < 0.1$). The frequency selective MIMO channel can be described by a number of frequency flat MIMO channels.

The channel transfer matrix H can be diagonalized using the Singular Value Decomposition (SVD) technique

$$\mathbf{H} = \mathbf{U}\mathbf{D}\mathbf{V}^H \tag{2.5}$$

where $\mathbf{U}$ and $\mathbf{V}$ are unitary matrices; $\mathbf{D}$ is the $N_t \times N_r$ diagonal matrix containing the real and non-negative singular values; $(.)^H$ means complex conjugate transpose. By applying the matrix $\mathbf{U}^H$ at the transmit side and the $\mathbf{V}$ matrix at the receive side, $K = \min(N_t, N_r)$ orthogonal channels can be realized. Each channel has a channel gain denoted as $\lambda_k$, which is the square of the singular value in the diagonal matrix $\mathbf{D}$.

$$\lambda_k = \mathbf{u}_k \mathbf{H} \mathbf{v}_k \tag{2.6}$$

The square of the singular values are the eigenvalues. They could also be obtained by SVD of the matrix $\mathbf{G}$

$$\mathbf{G} = \mathbf{H}\mathbf{H}^H = \mathbf{U}\mathbf{D}\mathbf{D}^T\mathbf{U}^H \tag{2.7}$$

where $(.)^T$ denotes transpose operator. The realization of the $K$ parallel channels is achieved by processing significant uncorrelated multi-path components. To study in more detail the realization of these parallel channels, the discrete time baseband interpretation of a single transmitted vector of symbols is preferred. In the baseband, it is assumed that the frequency synchronization and sampling are perfectly achieved. The received symbol vector has the form

$$\mathbf{y} = \mathbf{x}\mathbf{U}\mathbf{D}\mathbf{V}^H + \mathbf{n} \tag{2.8}$$

where $\mathbf{x}$ is the vector of transmitted symbols, and $\mathbf{n}$ is the vector of noise at the receiving RF chains. By using the weight matrix $\mathbf{U}^H$ at the transmit side and the weight matrix $\mathbf{V}^H$ at the receive side the received symbol vector becomes

$$\mathbf{y} = \mathbf{x}\mathbf{U}^H\mathbf{U}\mathbf{D}\mathbf{V}^H\mathbf{V} + \mathbf{V}^H\mathbf{n} = \mathbf{x}\mathbf{D} + \tilde{\mathbf{n}} \tag{2.9}$$

After being weighted by $\mathbf{V}$, the variance of the noise vector $\mathbf{n}$ is the same since $\mathbf{V}$ is an unitary matrix. This equation implies that the power put into $K$ parallel channels is amplified by the eigenvalues; power put into channel(s) which have indices larger than $K$ will be lost.

By applying the singular vectors $\mathbf{u}_k$ and $\mathbf{v}_k$, at the transmit side and receive side, the transmitted and received signals are matched with the channel. In essence, these singular vectors are the solutions of a joint optimization problem. As the weight vectors at the antenna ports, they form the transmitting and receiving eigenpatterns. In this context, parallel transmission of the sub-channels is also called the eigen beamforming technique.

The relation between the eigenpatterns and the propagation scenario has been discussed in, for example, [17, 18]. In general, the singular vector will shape the eigenpatterns in an effort to maximize the channel gain. When the number of the main clusters is small compared with the number of antenna elements, the antenna arrays at the transmitter and receiver can resolve the multipath signals in space. In that case, the shape of the eigenpattern is directly related to the physical distribution of the clusters in space. When the number of clusters increases, the multipath signals cannot be resolved by the antenna array. Since there is no preferred direction, the eigenpattern is shaped so that maximal signal power can be obtained.

As an example, the formulation of the eigenpatterns and how it can be adjusted according to the propagation scenario will be shown as follows. For simplicity, single reflection of the signal waves is assumed. The transmitting and receiving antenna elements radiate isotropically in the horizontal plane, Figure 2.2. The distance between antenna elements is half wave length. Given $N_s$ scatterers in the horizontal plane, the channel matrix $\mathbf{H}$
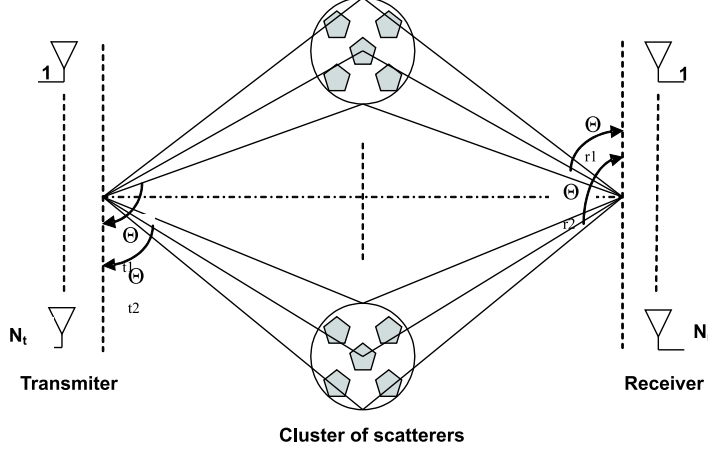


Figure 2.2: MIMO channel model with single reflection

can be described by

$$
\begin{bmatrix} \mathbf{w}_{t,1} & \cdots & \mathbf{w}_{t,N_s} \end{bmatrix}
\begin{bmatrix} a_1 & \cdots & 0 \\ \vdots & \ddots & \vdots \\ 0 & \ldots & a_{N_s} \end{bmatrix}
\begin{bmatrix} \mathbf{w}_{r,1} & \cdots & \mathbf{w}_{r,N_s} \end{bmatrix}^T
\tag{2.10}
$$

where $a_{n_s}$ is the fading gain of the $n_s^{th}$ path. The array direction vector at the transmitter and receiver can be defined as

$$
\mathbf{w}_{t,n_s} = \begin{bmatrix} 1 \\ e^{-j\frac{2\pi d}{\lambda}\cos\theta_{t,n_s}} \\ \vdots \\ e^{-j\frac{2\pi d(N_t-1)}{\lambda}\cos\theta_{t,n_s}} \end{bmatrix}
\mathbf{w}_{r,n_s} = \begin{bmatrix} 1 \\ e^{-j\frac{2\pi d}{\lambda}\cos\theta_{r,n_s}} \\ \vdots \\ e^{-j\frac{2\pi d(N_r-1)}{\lambda}\cos\theta_{r,n_s}} \end{bmatrix}
\tag{2.11}
$$

where $d$ is the distance between two closest antenna elements, $\lambda$ denotes a wave length, $\theta_{t,n_s}$ and $\theta_{r,n_s}$ are the angle of departure and angle of arrival respectively of the $n_s^{th}$ path.

Let us consider a specific MIMO system with 8 transmitting antennas and 4 receiving antennas. The multipath scattering environment contains three main clusters in the horizontal plane at the angle of $30^o$, $60^o$ and $120^o$. The field strength of each cluster is 30dB, 20dB and 5dB respectively. In each cluster, there were 10 scatterers uniformly distributed with an angular spread of $5^o$. The distribution of the scatterers and the corresponding field strength level are plotted in Figure 2.3.

Using this information together with the model described in (2.10), the channel matrix $\mathbf{H}$ is obtained. The unitary matrices and therefore the weight vectors corresponding to each eigenmode can be found by the SVD of the channel matrix $\mathbf{H}$. Based on these weight

(a) AoD                    (b) AoA
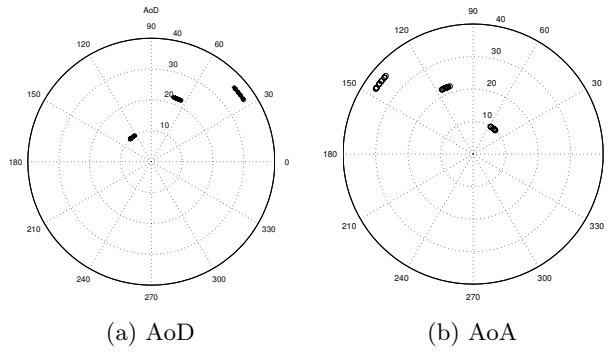
Figure 2.3: Angle of Departure and Angle of Arrival at the transmitter and the receiver

vectors the eigenpatterns at the transmit side and receive side are calculated and plotted in Figure 2.4 and 2.5.
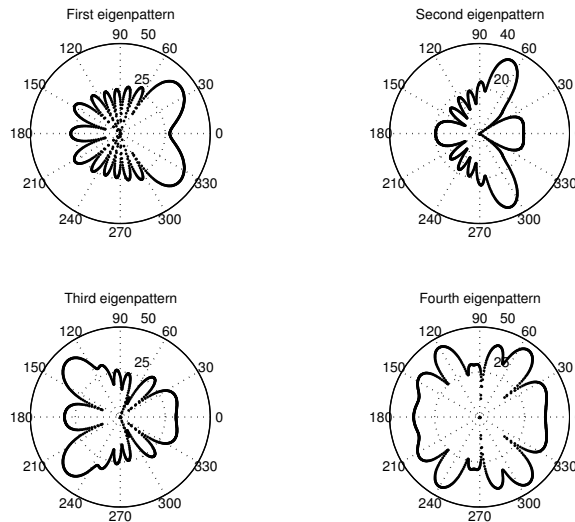


Figure 2.4: Eigenpatterns at the transmitter

One common thing which can be observed from Figure 2.4 and Figure 2.5 is that the eigenpattern does have a maximum lobe pointed toward the direction where the cluster locates. The maximum lobe of the eigenpattern corresponding to the highest eigenvalue points toward the cluster that brings about the highest signal power and so on. The directivity of the eigenpattern and its 3dB beamwidth depend strongly on the number of antenna elements, the number of the clusters and the relative strength of the signals emerging from the clusters. Having more antenna elements, the eigenpatterns observed at the transmitting antenna array are more related to the distribution of the clusters than those at the receiving antenna array.
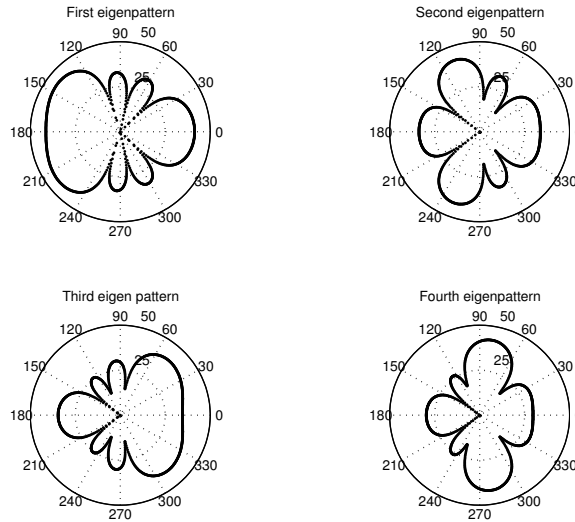
Figure 2.5: Eigenpatterns at the receiver

## 2.4.2   MIMO channel capacity

It is well known that by increasing the received SNR by 3dB, the Shannon capacity normalized to the signal bandwidth for an Additive White Gaussian Noise (AWGN) channel increases by 1bit/s/Hz, [19]

$$C = \log_2(1 + SNR) \tag{2.12}$$

Because it is very difficult to get rid of the thermal noise, increasing the transmitted power is the only solution to enhance the channel capacity. Although in principle it might be possible for wired communications, in wireless communications, due to the electromagnetic exposition regulation, there is a restriction on the total transmitted power level. Moreover, because of the signal fading, either in space, time or frequency, the capacity of a wireless channel will also fade accordingly. If we denote the gain of a wireless channel at one instant as $h$, the channel capacity at this instant can be written as

$$C = \log_2(1 + |h|SNR) \tag{2.13}$$

The absolute value of $h$ fades according to some distribution i.e. Rayleigh, Ricean, or Nakagami. Therefore, the channel capacity of a single wireless channel is also a random variable. Increasing the channel capacity in wireless communication thus becomes a very challenging problem.

Recently, it has been shown by Telatar and Foschini [12, 13] that by using multiple antennas at both the transmitter and receiver one can significantly increase the channel capacity. Because of the mathematic nature of the MIMO environment, the performance of MIMO systems can go well beyond that of the conventional adaptive/smart antenna systems [20]. For a narrowband MIMO system, when the channel is known at the receiver only the channel capacity can be calculated as

$$C = \log_2\left(det(\mathbf{I} + \frac{SNR}{N_t}\mathbf{H}\mathbf{H}^H)\right) = \sum_{k=1}^{\min(N_t,N_r)} \log_2(1 + \frac{SNR}{N_t}\lambda_k) \tag{2.14}$$

Increasing the number of antennas elements reduces the randomness of the channel capacity because the probability that all channels are in deep fade is vanishing. At the same time, the array gain is increased which gives rise to an enhancement in the channel capacity. In an extreme case, when the number of transmit or receiving antenna is infinitely large, the capacity of an uncorrelated MIMO channel can be approximated by

$$C = \sum_{k=1}^{\min(N_t,N_r)} \log_2(1 + \frac{SNR}{N_t}\lambda_k) = N_t\log_2(1 + \frac{SNR}{N_t}\lambda_{max}) = N_t\log_2(1 + SNR) \quad (2.15)$$

This illustrates an interesting fact that by the use of multiple antennas at both link ends, the channel capacity in the limit will increase linearly with the number of used antenna elements at each end. The advantage of using MIMO becomes two fold: i) increase the channel capacity, ii) reduce the impact of fading in wireless communications. In Figure 2.6, we show the channel capacity gain of MIMO systems over that of SISO (single channel), MISO or SIMO (used of multiple antenna elements at one end, beamforming or diversity combining) systems. Rayleigh fading, fully uncorrelated channels and a reference SNR of 20dB are assumed in the simulation. Because of the fading, the median capacity of
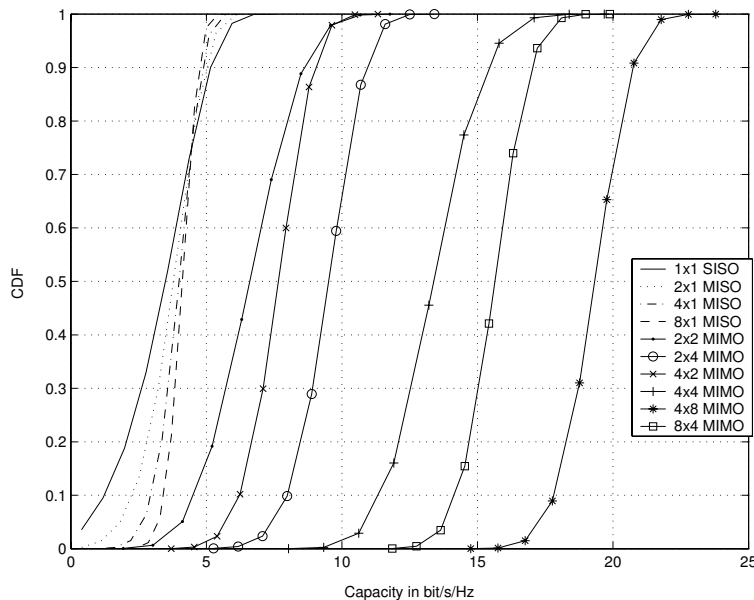


Figure 2.6: Capacity of the MIMO systems with different setups

the wireless SISO channel is about 3.5bit/s/Hz. For the AWGN channel, the channel capacity using equation (2.12) is 4.4 bit/s/Hz. Increasing the number of antenna elements does increase the channel capacity, however at a slow rate. Keeping the total number of used antenna elements at both sides constant, the channel capacity of MIMO systems (i.e. 2×2, 2×4) are always greater than that of a MISO system (i.e. 4×1, 8×1). For an asymmetric setting system, swapping the roles of the transmitter and receiver results in a difference in the channel capacity at each mode. More specifically, the channel capacity of the $N_t \times N_r$ MIMO system with $N_t$ greater than $N_r$ (i.e. 4×2, 8×4) is less than that of the $N_r \times N_t$ MIMO system (i.e. 2×4, 4×8). The fact that any $N_t \times N_r$ MIMO can support

up to $\min(N_t, N_r)$ sub-channels is the explanation for this phenomena. For an $N_t \times N_r$ MIMO system with $N_t$ greater than $N_r$, the transmitted power is equally distributed over $N_t$ ports. Since there are only $N_r$ nonzero eigenvalues, the power distributed to the rest $N_t - N_r$ ports is lost. Meanwhile all transmitted power is received in a MIMO system with $N_r \times N_t$ setting (note that the roles of the transmitter and receiver have been changed). This gives rise to an increment in the channel capacity of the $N_r \times N_t$ MIMO system over that of the $N_t \times N_r$ MIMO system.

So far we have considered the channel capacity of the MIMO systems with the assumption that the channel information is known at the receiver only. Since the transmitter does not know the channel, equal power distribution over all transmitting antenna port seems to be an optimal solution. By having the channel information at both ends of the transmission link, it is possible to distribute the transmitted power in the most efficient way, such that the channel capacity is enhanced. At the same time, the above mentioned phenomena can be avoided. When the transmitted power level is kept constant, optimal power allocation is found iteratively using the water filling method [21]

$$\gamma_k = max(\mu - \frac{1}{\lambda_k}, 0) \tag{2.16}$$

where the parameter $\mu$ is chosen such that $\sum_{k=1}^{K} \gamma_k = SNR$. The channel capacity then becomes

$$C = \sum_{k=1}^{\min(N_t,N_r)} \log_2(1 + \gamma_k \lambda_k) \tag{2.17}$$

The essence of the water filling algorithm is to allocate more transmitted power to the sub-channel with high eigenvalue and less power to the sub-channel with low eigenvalue. The capacity gain at the sub-channels with high eigenvalues is well traded for the capacity loss at the sub-channels with low eigenvalues. As a result, the overall MIMO channel capacity which is the sum of the capacities of the sub-channels is enhanced.

Equation (2.14) expresses the channel capacity of a narrowband MIMO channel. For a frequency selective channel, the capacity is calculated by integrating the channel capacity over the bandwidth $W$ of interest

$$
\begin{aligned}
C &= \frac{1}{W} \int_{f_c-W/2}^{f_c+W/2} \log_2\left( det(\mathbf{I} + \frac{SNR}{N_t} \mathbf{H}_f \mathbf{H}_f^H) \right) df \\
&= \frac{1}{W} \sum_{k=1}^{\min(N_t,N_r)} \int_{f_c-W/2}^{f_c+W/2} \log_2(1 + \frac{SNR}{N_t} \lambda_{k_f}) df
\end{aligned}
\tag{2.18}
$$

where $f_c$ is the carrier frequency. When the frequency step $df = \Delta f$ between the adjacent frequency samples is small enough so that the channel is frequency flat in that step, the channel capacity can be expressed in the discrete form as

$$C = \frac{1}{L} \sum_{l=1}^{L} log_2\left( det(\mathbf{I} + \frac{SNR}{N_t} \mathbf{H}_{f_l} \mathbf{H}_{f_l}^H) \right) \tag{2.19}$$

where $L$ is the number of frequency spots.

Using an additional diversity dimension, it is expected that there should be an enhancement in the channel capacity of a frequency selective MIMO channel. Measurement results showed that the frequency selective of the channel significantly increases the outage probability of the capacity (increasing the slope of the distribution curve), while hardly changes the mean capacity [22]. The joint space-frequency water filling algorithm could be used to improve the channel capacity when knowledge of the channel is available both at the transmitter and the receiver [23]. However, it was experimentally shown that the largest gain comes from the spatial domain and that the gain from the frequency domain is negligible [24].

### 2.4.3 MIMO under certain operation scenario

The performance of a MIMO system depends on both the setup/configuration of the antenna elements and the characteristics of the environment in which the MIMO system is operated. Depending on the operating environment and antenna setting, the channel coefficients in the matrix $\mathbf{H}$ can be fully uncorrelated with high rank (i.e. identical independently distributed (IID) components), fully uncorrelated with low rank or keyhole effect, partly uncorrelated (observed in most of the cases) or even fully correlated (strong LOS environment).

**Channel with wide angular spread at both ends, Rayleigh fading**

Also named as uncorrelated high rank, this type of channel can be found in an environment with rich scattering such as indoor to indoor or even outdoor micro cell scenarios. Each element of the channel matrix $\mathbf{H}$ is a complex number with the real and imaginary part having a Gaussian distribution. For a MIMO system with widely separated antenna elements, the channel coefficients can be taken to be a complex IID with zero mean and unit variance variable. Because full diversity order is available i.e. $N_t N_r$, this type of channel yields the highest capacity.

There is a situation that although there is a rich scattering environment around the transmitter and the receiver, the channel matrix $\mathbf{H}$ yet still has a rank one. The so called "key hole" effect happens when the signal waves stemming from the scatterers around the transmitter go through a pine or a wave guide before reaching the scatterers surrounding the receiver. There is in fact only one propagation path between the transmitter and the receiver. Everything becomes a point source and one thus can obtain only array gain. This phenomenon was theoretically studied in [25, 26]. However, it is difficult to have a key hole effect in practice and one has to control the propagation of the waves in order to observe this effect [27].

**Channel with LOS characteristic, Ricean fading**

The antenna element still radiates isotropically, however due to the LOS characteristic of the environment, the received signals become correlated. Assuming that the signal strength is unchanged compared with the uncorrelated case mentioned above, this leads to the reduction of the channel capacity and system performance of the MIMO system. The channel can be modelled as two parts, one corresponds to the LOS component and

the other corresponds to the diffuse (Rayleigh fading) component.

$$\mathbf{H}_{Ricean} = \sqrt{\frac{\mathbb{K}}{\mathbb{K}+1}}\mathbf{H}_{LOS} + \sqrt{\frac{1}{\mathbb{K}+1}}\mathbf{H}_{IID} \qquad (2.20)$$

where $\mathbb{K}$ is the Ricean factor, $\mathbf{H}_{LOS}$ is a matrix with all entries equal to 1 and $\mathbf{H}_{IID}$ is a matrix with IID entries.

Recently, it was demonstrated that even the channel capacity is affected by the correlated LOS component, the signal strength is so large that it can easy compensate for this reduction. With the same amount of transmitted power a higher channel capacity in the LOS case than in the uncorrelated case is observed [28, 29]. This highlights the fact that together with the multipath richness characteristics, the amount of received power is also an important factor that determines the performance of MIMO systems.

Figure 2.7 shows the influence of the LOS component in terms of the $\mathbb{K}$ factor on the capacity of a 2×2 MIMO channel. In all cases the SNR is kept constant. In fact, the LOS component changes the distribution of the eigenvalue of the channel matrix $\mathbf{H}$. As the $\mathbb{K}$ factor increases, the channel gain will be concentrated on the largest eigenvalue. The other eigenvalues become less and less significant. In an extreme when $\mathbb{K}$ is infinitively large, the channel matrix becomes a rank one matrix and there is only a single non-zero eigenvalue. It is observed that the capacity gain obtained by using the water filling method in the Ricean fading channel is higher than in the Rayleigh fading channel.
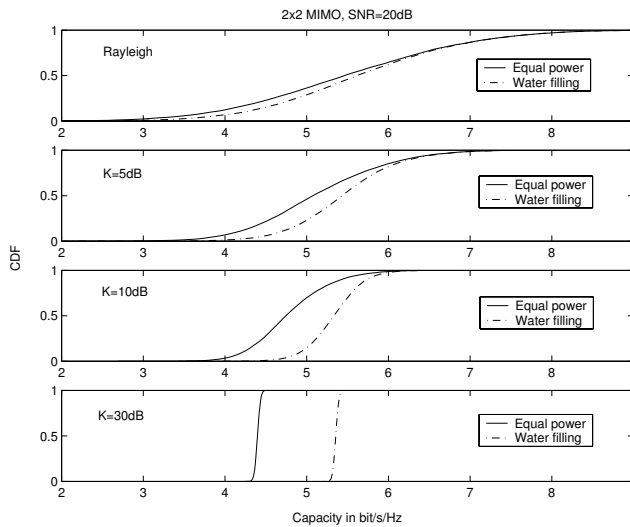


Figure 2.7: Effect of LOS component on the MIMO capacity

### Correlated channel

The correlated channel is caused by the lack of scatterers around the transmitting antennas and/or the receiving antennas. Insufficient separation between antenna elements or high cross polarization coupling among antenna elements could also make the channels correlated. As for the LOS scenario, correlated fading increases the gain of the maximum eigenmode and lowers the gain of the minimum eigenmode. The antenna array again is

still the same but the diversity gain is reduced. However, the channels need not to be fully decorrelated in order to benefit from the capacity gain. In fact, it was shown that the return by having the fading correlation goes below 0.5 is diminishing [30]. In practice, we aim at having the fading correlation coefficient lower than 0.7.

The correlated channel matrix may be described by the multiplicative product of the fading correlation matrices seen at the transmitter and the receiver and an IID entries matrix.

$$\mathbf{H}_{corr} = \mathbf{R}_{Tx}^{1/2}\mathbf{H}_{IID}\mathbf{R}_{Rx}^{T/2} \tag{2.21}$$

where $\mathbf{R}_{Tx}$ and $\mathbf{R}_{Rx}$ are the two fading correlation Hermitian matrices seen at the transmitter and receiver respectively, $()^{1/2}$ is the matrix square root operator. These two matrices can be obtained from measurements of real MIMO systems or available measurement/analytical results of the MISO and SIMO systems.

The effect of the correlated fading on the channel capacity can be evaluated numerically by using a certain correlation model, simulation or measurement. Using the above mentioned model and further assume that $N_t$ is equal to $N_r$ , at high SNR values the capacity of the MIMO channel can be expressed as [31, 32]

$$
\begin{aligned}
C_{corr} &= \log_2\left(det(\mathbf{I} + \frac{SNR}{N_t}\mathbf{H}_{corr}\mathbf{H}_{corr}^H)\right) \\
&= \log_2\left(det(\mathbf{I} + \frac{SNR}{N_t}\mathbf{R}_{Tx}^{1/2}\mathbf{H}_{IID}\mathbf{R}_{Rx}\mathbf{H}_{IID}^H\mathbf{R}_{Tx}^{H/2})\right) \\
&\approx \log_2\left(det(\mathbf{I} + \frac{SNR}{N_t}\mathbf{H}_{IID}\mathbf{H}_{IID}^H)\right) + \log_2(det(\mathbf{R}_{Tx})) + \log_2(det(\mathbf{R}_{Rx}))
\end{aligned}
\tag{2.22}
$$

Since the sum of the eigenvalues of $\mathbf{R}_{Tx}$ or $\mathbf{R}_{Rx}$ is equal to $N_t$, $\log_2(det(\mathbf{R}_{Tx}))$ is smaller or equal to zero. At a high SNR value the capacity loss due to the correlated channel can be estimated as

$$C_{loss} \approx \log_2(det(\mathbf{R}_{Tx})) + \log_2(det(\mathbf{R}_{Rx})) \tag{2.23}$$

Figure 2.8 shows the capacity loss due to the correlated fading for a 2×2 MIMO setting with different values of the fading correlation. It indeed shows that when the fading correlation is bellows 0.3, the capacity loss due to the increase in the fading correlation is negligible.

### 2.4.4 Transmission techniques

Transmission techniques for a MIMO system vary depending on the usage purposes and requirements. Beamforming can be used for increasing the transmission range or the transmission quality. In the beamforming approach, a single data stream is transmitted through multiple antennas and the receiver combines the received signals from multiple receiving antennas. Because both the transmitted and received signals are matched to the channel, full diversity gain and significant array gain can be obtained. Normally, the maximum eigen beamforming solution is used. The channel gain in the beamforming method is equivalent to the maximum eigenvalues of the channel matrix $\mathbf{H}$. As long as the channel is reciprocal, the weigh vectors at the transmitter and receiver can be found
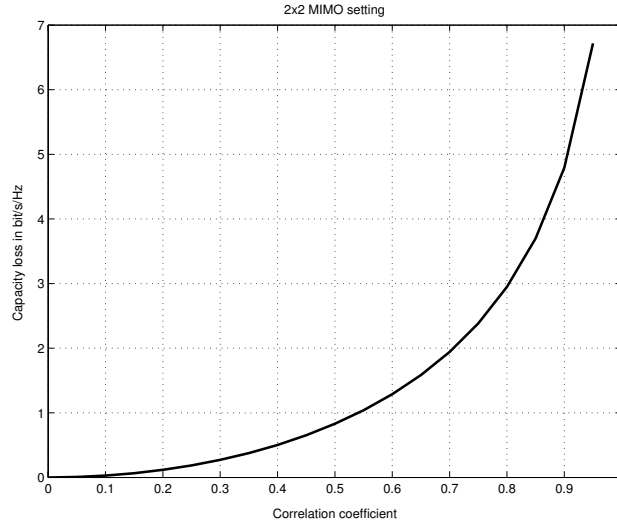
Figure 2.8: Capacity loss due to the correlated channel for a 2x2 MIMO system

by iterate transmitting and receiving a random vector [33, 34]. After some iterations or "*ping pong transmissions*", one could obtain transmitting and receiving weigh vectors at the transmitter and receiver respectively.

Spatial multiplexing is used to increase the spectral efficiency of the MIMO system. Up to $min(N_t, N_r)$ independent data streams can be transmitted simultaneously from $N_t$ transmitting antennas. Each data stream is transmitted over an eigenmode that may relate to a specific propagation scenario as illustrated in section 2.4.3. When the channel matrix has a full rank, spatial multiplexing is an optimum strategy in terms of the channel capacity. However, in this scheme in order to find the proper eigenvectors the channel matrix need to be diagonalized. Information on the channel should be available both at the transmitter and the receiver. This requirement, in principle can be met in a reciprocal channel and the channel information obtained from the uplink can be used for the downlink. For non-reciprocal channel, the downlink channel must be estimated at the receiver and feedback to the transmitter through a dedicated feedback channel. To reduce the overhead, the eigenvectors (also called the precoders) are quantized and a codebook is built at the transmitter. At the receiver, the downlink channel matrix is diagonalized, and only the index of the precoder is transmitted back to the transmitter. It was shown that using this approach significant overhead reduction can be achieved without losing system performance [35].

Spatial multiplexing can also be obtained if the channel information is available at the receiver only. There are a number of schemes to decouple the MIMO system into a set of parallel sub-channels. Depending on the complexity of each scheme, its performance varies accordingly. These schemes ordered according to the increment in their complexity are: Zero Forcing (ZF), Minimum Mean Square Error (MMSE), Vertical-Bell Labs Space Time (VBLAST) [15], Diagonal-Bell Labs Space Time (DBLAST) [14] and Maximum Likelihood Receiver (ML).

Parallel sub-streams are detected at the ZF receiver by

$$\hat{\mathbf{x}} = \mathbf{y}\mathbf{H}^H \left(\mathbf{H}\mathbf{H}^H\right)^{-1} \tag{2.24}$$

where $\mathbf{y} = \mathbf{x}\mathbf{H}$ is the received vector at the $N_r$ ports, $\mathbf{x}$ and $\hat{\mathbf{x}}$ is the transmitted and detected symbol vector respectively. Because the noise is enhanced by a factor of $\left(\mathbf{H}^H\mathbf{H}\right)^{-1}\mathbf{H}$, the performance of the ZF is degraded at low SNR. However, ZR is a linear receiver with low computation complexity.

The signal at MMSE receiver is detected by applying

$$\hat{\mathbf{x}} = \mathbf{y}\mathbf{H}^H \left(\mathbf{H}\mathbf{H}^H + \sigma_o\mathbf{I}_{N_t}\right)^{-1} \tag{2.25}$$

where $\sigma_o$ is the noise variance at one receiver branch. At high SNR, the performance of the MMSE scheme is the same as that of the ZF and it is equivalent to a matched filter at low SNR. In general the performance of the MMSE outperforms that of ZF.

VBLAST is an ordered successive cancellation receiver where the sub-stream with the highest SNR is detected first. The contribution of the detected symbol in the received signal vector is removed and the symbol of the next stream is detected in the same manner. The procedure is repeated until the received symbol of the last stream with the lowest SNR value is detected. Since the symbol in each stream is detected according to its SNR value, VBLAST outperforms the successive interference cancellation receiver. However, it is still influenced from error propagation when a symbol at one of the decoding step is incorrectly detected.

In DBLAST, the data stream is spread over all transmitting antennas through a diagonal layer structure. Although no layer ordering is needed, DBLAST is considered impractical due to its decoding complexity and space time wastage where no transmission takes place [31].

ML receiver detects the received symbol streams according to

$$\hat{\mathbf{x}} = \text{argmin}_{\mathbf{x}}|\mathbf{y} - \mathbf{x}\mathbf{H}| \tag{2.26}$$

Because it searches for every possible solution, the ML obtains an optimum performance. The computation complexity increases exponentially according to the modulation constellation order and the number of sub-streams.

Space time block code (STBC) is another transmission scheme which aims at improving the communication reliability when the channel information is only available at the receiver. In 1998, Alamouti [36] proposed a simple transmit diversity scheme by a simple processing across two transmitting antennas. The scheme is further extended for the case of 2 transmitting antennas and more than 2 receiving antennas. It has been shown that the scheme can provide a diversity order of $2N_r$ and a loss of 3dB as compared to the case of MRC.

Tarokh et.al. later generalized the Alamouti transmit diversity scheme to an arbitrary number of transmit antennas [37, 38, 39]. In essence, the STBC is a linear combination of the symbols and theirs complex conjugate. One dimension of the block code is the transmitting antenna indexes and time is the other dimension. The code is designed such that the vectors expanding the time dimension are pairwise orthogonal. In fact, it makes the effective channel matrix become orthogonal regardless of its realization. Thereby,

STBC requires only a simple linear processing at the receiver to decouple the transmitted symbols and the complex ML vector detection problem can be avoided. Redundancy is introduced in the STBC in order to achieve transmit diversity, and therefore the rate of STBC is always smaller or equal to one.

The design of the STBC is divided into real orthogonal criteria and complex orthogonal criteria. For the real orthogonal coding the codewords can be designed for a system with arbitrarily number of transmitting antennas $N_t$. For complex orthogonal coding, it has been shown that there is a codeword for any number of transmitting antenna as long as the rate is less than $\frac{1}{2}$ . For a rate greater than $\frac{1}{2}$, there are codewords for three or four transmitting antennas only. For more information and detail description of the STBC and ST trellis code the reader is referred to [37, 38, 39, 40, 41].

# Chapter 3

# Characteristics and modelling of MIMO channels

As described in the previous chapter, MIMO has a great potential in enhancing the transmission rates, the transmission quality and the outage capacity of the system. In parallel to the theoretical works, MIMO channel measurement and characterization are required. The results from the channel measurements and characterization are very useful for justifying the consistency between theoretical and empirical findings. Unknown phenomena and observations are identified which act as a general background for the development and invention of new, more efficient transmission algorithms. Since the first introduction of the MIMO technique by Telatar and Forshini, there have been a number of published works on the measurement and channel characterization of the MIMO channel. However in most of the works, the measurement settings were made such that the characteristics of the multipath environments are highlighted. The antennas configurations and measurements scenarios therefore, sometime are impractical for a normal usage purpose. There is a lack of measurements especially for MIMO channels where proper attention is put into the practical usage aspect.

In an effort to fill in this gap, the work presented in this chapter is devoted to evaluate the performance of a MIMO system designed for small terminals with different antenna configurations in different propagation environments. The study is unique in the sense that it is based on measurements of MIMO systems in some real-life settings, where space and antenna design constraints are taken into account. Due to the practical constraints, in the analyses we aimed at investing the characteristics of the MIMO radio channel where both the antennas and the propagation channel are integral parts. Based on the results, the performance of the MIMO system as a whole in some real-life scenarios can be evaluated and compared. A spatio-temporal correlated MIMO model for a narrowband indoor environment is proposed and assessed. As we shall see in the following, despite its simplicity the model is fairly good at retaining the spatial and temporal characteristics of the measured channel.

## 3.1   Indoor to Indoor, Outdoor to Indoor microcell

In paper [P1], we have evaluated the performance of the 8x4 measured narrowband MIMO channel for indoor-indoor and outdoor-indoor scenarios. To mimic a real MIMO system, a prototype of a base station (BS) with eight outputs and prototypes of small terminals such as the mobile handset and the laptop with four patch antennas were deployed in the measurement. The measurements were conducted in different offices located at the same floor of a two story building. For each type of receiver, there were one Indoor-Indoor and two Outdoor -Indoor measurement scenarios.

General properties of the measured MIMO radio channel as well as its distinct characteristics those adhere to the measurement environment and scenarios have been analyzed and discussed. The mean received power decreases steadily as the distance between the transmitting antennas and the receiving antennas increases. At the same measured location, the power level is dependent on the orientation of the receiving antenna. It was verified that a major part of the signal energy comes from large openings, such as windows or entrance doors. The multipath richness characteristics of the measured radio channel are almost independent of the measured locations, measurement scenario (indoor-indoor or outdoor-indoor) as well as the type of the receiver (either handset or laptop). The distributions of the eigenvalues or the gains of the sub-channels observed from the measurement data were spread over a larger range than that of the theoretical channels with identical independently distributed (IID) complex Rayleigh fading components, Figure 3.1.

It is shown that when there are perfect amplifiers and/or attenuators so that the mean SNR remains constant, i.e. 20dB, the median capacity of the measured MIMO channel is accountable for at least 80% of the system with IID components. This indicates that for the purpose of obtaining full diversity gain and diversity order, it is still makes sense to deploy multiple antennas in a small terminal. The gain in channel capacity which results from knowing the channel at the transmitter is significant for low SNR value. At the SNR value of 20dB, using the measured data we show that by knowing the channel at both ends of the transmission link it is possible to obtain up to 20% increase in the channel capacity as compared with the case where the channel is known at the receive side only. However, the gain gradually reduces at a higher received power or a higher SNR value, Figure 3.2.

We estimate the channel capacity where both the change in the mean received power and the change in the MIMO radio channel multipath characteristics are included. The analysis shows that the variation in the mean received power can have greater influence on the overall system performance than the change in the multipath scattering property. This highlights the fact that in the design of MIMO systems, above a certain multipath richness threshold one might want to optimize the received power level other than the uncorrelated channel in order to get a better performance enhancement. The performance gain due to the increase in the received power level may well compensate for the performance reduction due to high correlated fading.

## 3.2   Outdoor macrocell

In paper [P2], we presented initial analyses of a MIMO system performance in terms of the channel capacity and environment scattering richness. The assessments are based on
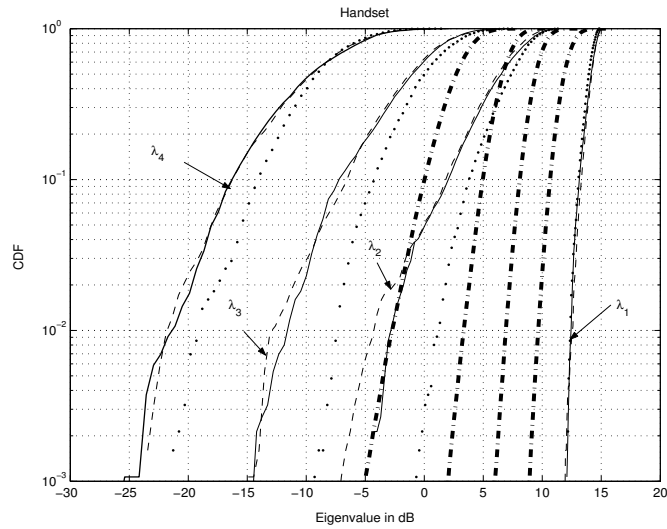
(a) Handset
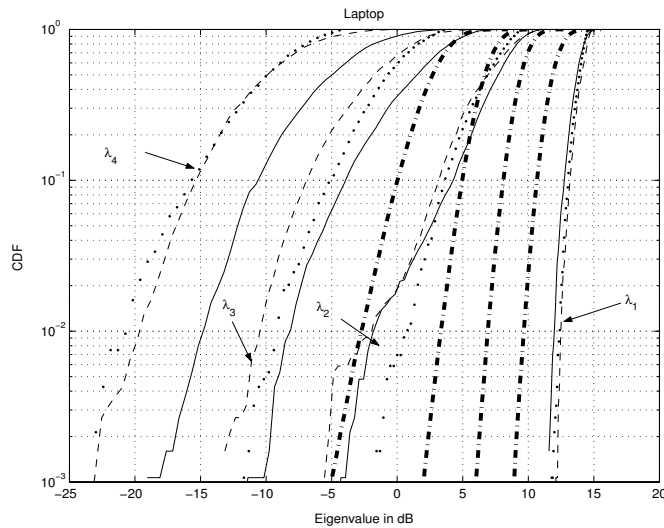


(b) Laptop

Figure 3.1: The distribution of the eigenvalues at three BS positions, straight line: BS1, dot line: BS2, broken line: BS3. For each BS position the data collected at all receiver's location are used. Thick dash lines are the distribution of eigenvalues in the IID case

acquisition data from extensive outdoor measurement campaign of an 8x4 MIMO system at 2140MHz, in downtown Aalborg. The measurement bandwidth was about 10MHz and the data collected from two measured routes was used for the analyses. Several positions of a prototype mobile handset were considered in order to evaluate the effect of local shadowing and absorption on system performance (i.e on a wooden pole in a trolley, on a phantom head in a trolley pulled by a car, on a pole inside a car and on the phantom head inside a car). It was found that the outdoor MIMO system with 4 patch antennas handset and 8 antennas array at the BS can provide up to 80% median capacity according to that of
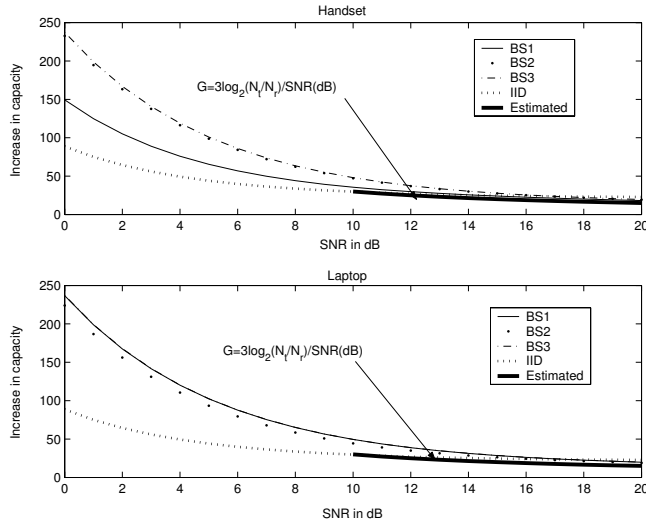
Figure 3.2: The advantage of having knowledge of the channel at the transmitter as a function of the SNR, in percentage

the IID case for a SNR=20dB. Strong correlation between the normalized capacity (using a reference SNR) and the mean received power level has been observed. The correlations of the normalized channel capacity and the mean received power are presented in Table 3.1.

| Route | Trolley - Pole | Trolley - Phantom | In car - Pole | In car - Phantom |
|-------|----------------|-------------------|---------------|------------------|
| 1     | -0.72          | -0.62             | -0.76         | -0.82            |
| 2     | -0.81          | -0.83             | -0.81         | -0.88            |

Table 3.1: Correlation coefficient between the channel capacity and the mean received power at the system SNR of 20dB

The results presented in Table 3.1 indicate that the location with low signal strength will give higher channel capacity than the location with high signal strength. High mean path loss or equivalently low received signal level could suggest that there is a richer scattering environment. This in turn, gives rise to an enhancement in the diversity gain as of richer multipath environment.

Analysis on the normalized capacity shows that local scattering (car, phantom) does not enrich the multipath scattering of the radio channel. In fact, local scattering may increase the angle spread seen from the mobile and therefore reduce the spatial correlation. However, for outdoor environment, the major paths arriving at the mobile often contain the same information. Scattering this correlated arrival paths certainly increase the multipath richness of the local environment in the vicinity of the mobile but not the multipath channel from the transmitter to the receiver. This means local scattering is related to the concept of the "keyhole" channel.

Although the local scattering does not change the multipath richness of the channel, it does influence the received power level. It was found that the shadowing and power

absorption of the phantom and car can lead to a reduction of the received power level by 2dB and 4dB respectively. By including the information of the mean path loss in the formulation of the channel capacity, it is possible to evaluate the impact of the scattering very near to the mobile (car, phantom) on the MIMO true channel capacity. Table 3.2 shows the degradation in the channel capacity due to the local absorption and shadowing.

| Route | Trolley-Phantom | In car-Pole | In car-Phantom |
|-------|-----------------|-------------|----------------|
| 1     | 10%             | 26%         | 45%            |
| 2     | 16%             | 33%         | 48%            |

Table 3.2: Median capacity lost with the best case scenario "Trolley-Pole" as reference

## 3.3   Spatial and temporal correlated channel modelling

In order to evaluate and study the data transmission algorithms at higher layers of the MIMO system, we normally need a model for modelling the behavior of the radio channel. Here we will concentrate on the measurement-based model. The advantage of the measurement-based model is that only from a few extracted parameters from the measurement it is possible to reconstruct the MIMO radio channel with the essential characteristics as the measured ones. Moreover, verification of the model thus becomes very simple since we have the measured channel information as a reference. The measurement-based model is classified into two approaches. In the first approach, the use of double directional information in the modelling process (i.e. AoA, AoD) is emphasized [42, 43]. In the second approach, which is normally called the correlation based model, the complex correlation coefficients of the transmitted and received signals observed at the transmitter and receiver are the crucial parameters for modelling the MIMO channel [44, 45, 46].

However, there is a lack of MIMO models that can retain both the spatial and temporal characteristics of the radio channel. In paper [P3] we propose a spatio-temporal model for narrowband indoor non line of sight (NLOS) MIMO channels. The model is based on parameterizations from the measured $8 \times 4$ MIMO radio channels in an indoor environment. The model can be briefly described as follows

$$\mathbf{H}(t_o + t) = \rho(t)\mathbf{H}(t_o) + \sqrt{1 - \rho(t)^2}\mathbf{E} \qquad (3.1)$$

where $\rho(t)$ is the temporal correlation coefficient obtained from the measured channel; $H(t_o + t)$ and $H(t_o)$ are the channel current and past channel matrices respectively; $\mathbf{H}(t_o)$ and $\mathbf{E}$ are the spatially correlated matrices which are independently generated from the Kronecker model as mentioned in (2.20).

The validation of the model performance is made by comparing the capacity and the temporal characteristics of the synthetic channels with those obtained from measurements. Figure 3.3 shows the capacity of the measured channel and the synthetic channel at two locations. The temporal correlation of the measured channel and the synthetic channel are shown in Figure 3.4. With the 5% median relative error in the channel capacity and a very close match in the temporal correlations, it has been proved that our model is capable of

capturing the essential characteristics of a temporally correlated multipath MIMO radio channel.
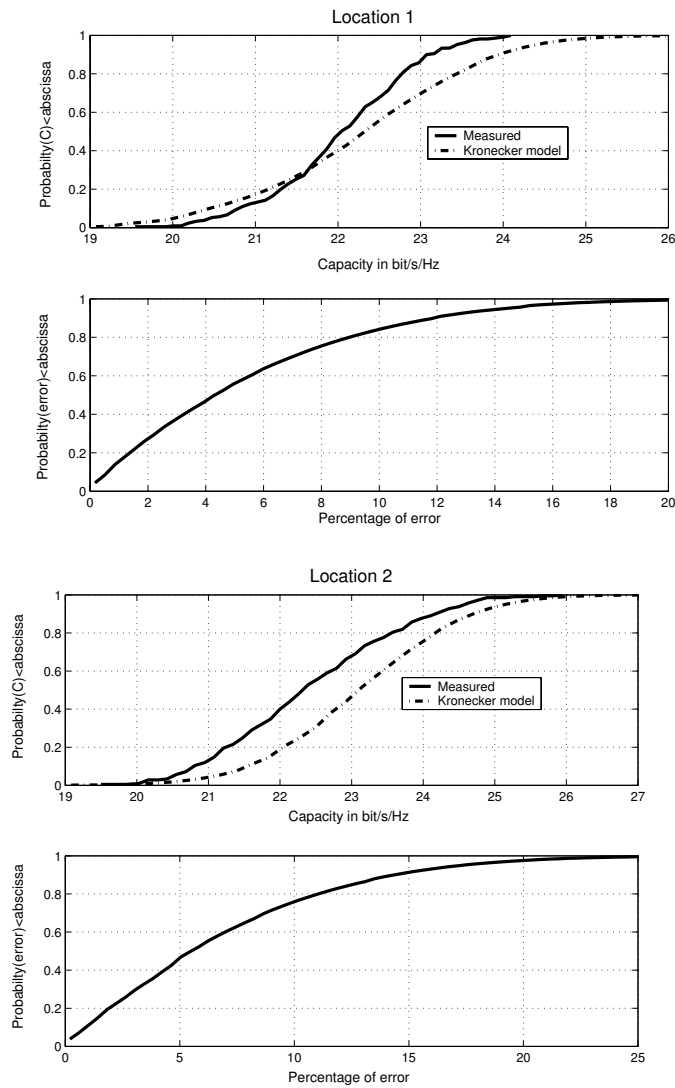


Figure 3.3: Measured and estimated capacity at SNR=20dB and the average relative error at two measured locations
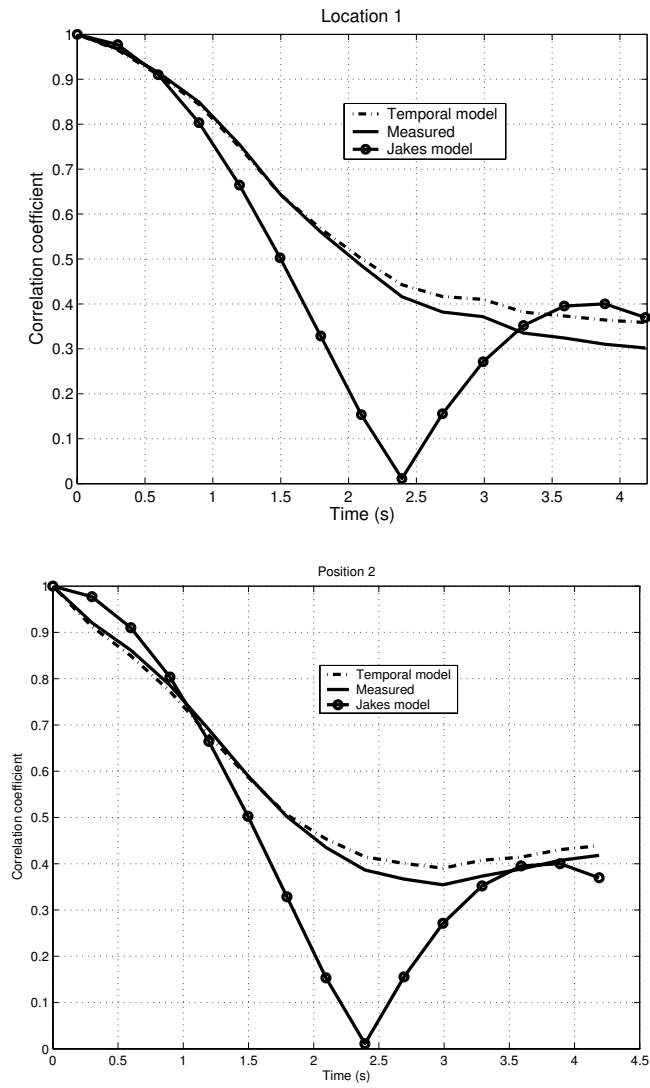
Figure 3.4: Measured and estimated temporal correlation at two measured locations, the velocity of the handset is 23.4 mm/s

# Chapter 4

# Link adaptation techniques in MIMO systems

In this chapter, with the assumption that the channel is narrowband and the channel coefficients are known at both link ends, we propose and evaluate some link adaptation (LA) algorithms applied to spatial multiplexing MIMO systems. The performance of these LA techniques in time-varying channels is also investigated. In an attempt to reduce the impact of the time-varying channel on the spatial multiplexing MIMO systems, an eigenvectors prediction scheme is introduced at the end of the chapter.

## 4.1 Adaptation techniques for spatial multiplexing MIMO systems

In paper [P4] we have investigated several link adaptation algorithms for spatial multiplexing MIMO system with the assumption on the availability of the instantaneous channel coefficients at both link ends. Depending on the requirement either at the target average bit rate or the BER, the transmitted power is optimally distributed to each parallel sub-channel according to its associated eigenvalue. Based on the approximated calculations of the BER for M-QAM and M-PSK modulations presented in [47] and the Gallager multiplier procedure, optimum power distribution solutions can be derived.

For a spatial multiplexing MIMO system in which keeping a constant total bit rate is desirable, it can be shown that the overall BER of the system using either M-QAM or M-PSK is minimized if the distributed power satisfies

$$
\gamma_k = max(\frac{1}{\beta\lambda_k}(ln(\lambda_k) - \mu), 0)
$$

$$
\beta = \begin{cases} \frac{1.6}{\sigma^2(2^{r_k}-1)} \text{ for M-QAM} \\ \frac{6}{\sigma^2(2^{1.9r_k}-1)} \text{ for M-PSK} \end{cases} \tag{4.1}
$$

where $\mu$ is chosen such that $\sum_{k=1}^{K} \gamma_k = P_t$; $P_t$ is the transmitted power level; $\sigma$ is the noise variance; and $r_k$ is the modulation order assigned to the $k^{th}$ sub-channel. For a system that aims at increasing the bit rate while keeping the BER constant the overall

throughput can be shown to be maximized if the following power distribution is met

$$\gamma_k = max(\mu - \frac{1}{\Gamma\lambda_k}, 0)$$

$$\Gamma = \begin{cases} \frac{-1.6}{\sigma^2 ln(5BER_{target})} \text{ for M-QAM} \\ \frac{-6}{\sigma^2 ln(20BER_{target})} \text{ for M-PSK} \end{cases} \tag{4.2}$$
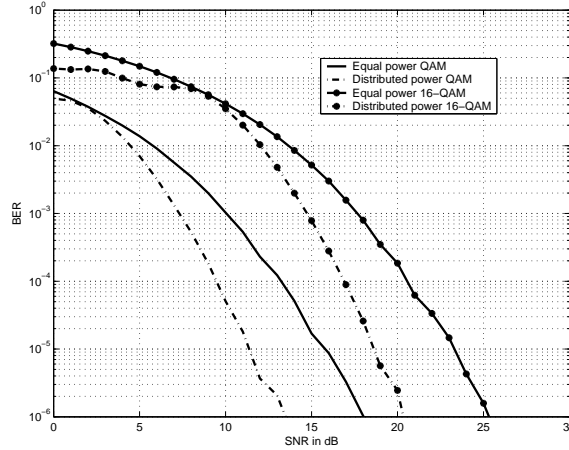


a.    M-QAM modulation
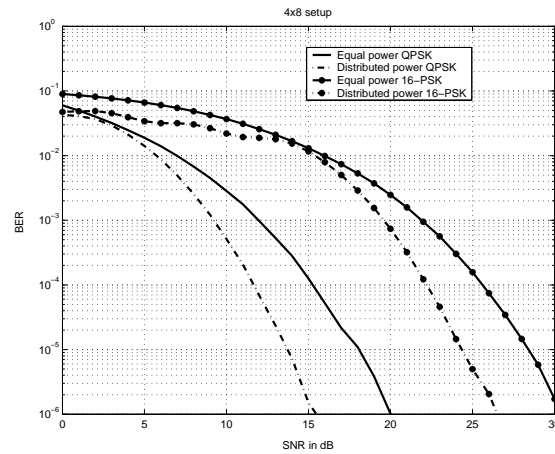


b.    M-PSK modulation

Figure 4.1: BER of MIMO system with and without optimum power distribution

Figure 4.1 shows the improvement in the BER of the 8x4 MIMO system using optimum power distribution. At a BER of $10^{-4}$, a gain of 4dB in the SNR can be observed for both M-QAM and M-PSK modulation. However, at low SNR values the improvement in the BER comes at the cost of a lower number of activated sub-channels. In Figure 4.1, this fact is manifested itself as the stair case shape of the BER curves, where each step corresponds to an increase in the number of activated sub-channels. This violates the condition that we would like to keep the system throughput constant while minimizing the overall BER. Lower transmission rate is traded for better transmission quality. In

other words, it is not possible to improve the overall BER in such low SNR values and/or eigenvalues without reducing the number of used sub-channels. In this scenario, using an equal power distribution seems to be the only solution in order to keep the total bit rate constant.

Based on the distributed power level, the modulation order or the number of bits per transmitted symbol of the $k^{th}$ sub-channel can be estimated as

$$r_k = \begin{cases} log_2(1 + \Gamma\gamma_k\lambda_k) \text{ for M-QAM} \\ \frac{1}{1.9}log_2(1 + \Gamma\gamma_k\lambda_k) \text{ for M-PSK} \end{cases} \tag{4.3}$$

where *Gamma* is defined in 4.2. Figure 4.2 illustrates the achievable transmission rate as a function of the SNR values for two types of modulation. The results are obtained from 100000 synthetic channel matrices with IID entries for 4x4 and 8x4 MIMO setups. The results indicate that at low SNR values, the algorithm does not work, illustrated by low spectral efficiency (e.g. 0 or 1 bit/s/Hz). It is expected, since the gain of each sub-channel is not high enough to support either types of modulation with the target BER. At high SNR values, M-QAM has better performance than M-PSK for the same system setup and the target BER. The reason could be that M-PSK modulation, by its constellation setup, has higher average BER than M-QAM modulation for the same modulation order. This forces the algorithm to select a lower modulation order to fulfill the target BER. However, the M-PSK modulation does not require the gain of each sub-channel to be exactly known at the receiver as does the M-QAM modulation. Therefore M-PSK modulation has an advantage of low demodulation complexity.

## 4.2 The maximum eigen beamforming approach

To reduce the system complexity, one can use a maximum eigen beamforming technique. In paper [P5] we showed that this technique can provide a higher array gain and not very sensitive to the time-varying environment as compared to the case where all sub-channels are used. Although only a single data stream is transmitted in this scheme, due to the array gain advantage one can increase the system throughput by using a higher modulation order. In some cases, at the same throughput the BER of the system using the maximum eigen beamforming can be lower than the spatial multiplexing system, Figure 4.3. As studied in section 2.4.1 the eigenvectors act as the steering vectors which steer the beam pattern toward the direction radiating maximum energy. Therefore, the maximum eigen beamforming creates some sort of spatial focusing with the resolution and the signal to interference ratio (SIR) depending on the number of supported users and the degree of correlation between them. For a multi-user MIMO system with $N_u$ users, $N_t$ transmitting antennas, $N_r$ receiving antennas, the SIR can be estimated as

$$SIR = \frac{\lambda_{max}}{N_u - 1} \tag{4.4}$$

With a target SIR value, the number of simultaneous users which the MIMO system can support is lower and upper bounded by

$$1 + \frac{max(N_t, N_r)}{SIR} < N_u < 1 + \frac{(\sqrt{N_t} + \sqrt{N_r})^2}{SIR} \tag{4.5}$$
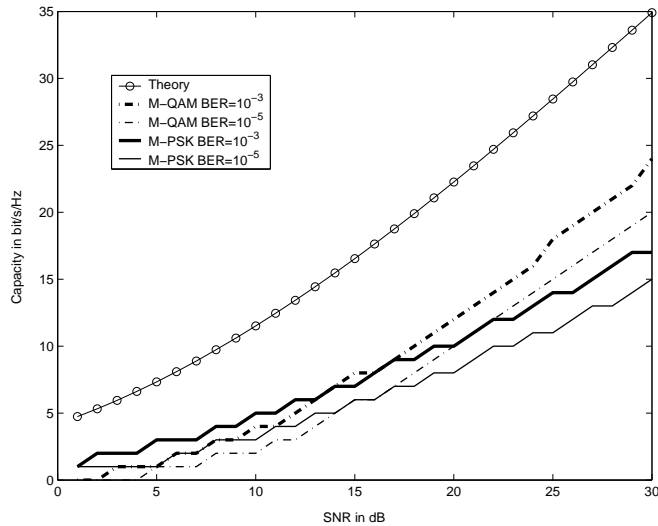
a.    4x4 setup
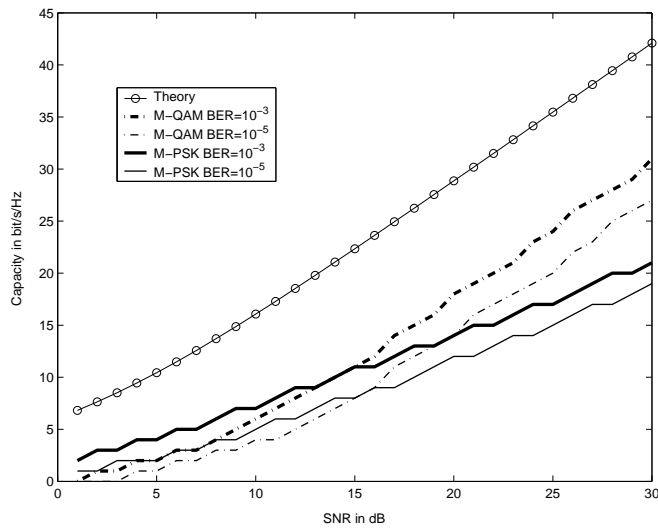


b.    8x4 setup

Figure 4.2: The obtainable throughput at different targeted BER values for M-QAM and M-PSK modulations in spatial multiplexing MIMO systems

Figure 4.4 illustrates the bound of the number supported users for MIMO systems with up to 20 antennas at each ends. The target SIR was 10dB as it is a reasonable number for achieving a BER of $10^{-3}$ in Gaussian channels with BPSK modulation.

## 4.3    The influence of the time-varying channel to the spatial multiplexing MIMO systems

A time-varying channel causes the channel information available at the transmitter or receiver to be outdated. The performance of the system is degraded since it is adapted
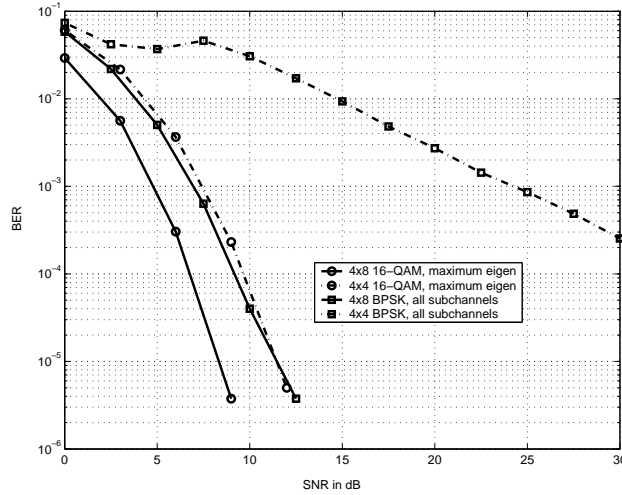
Figure 4.3: Average BER of MIMO systems using maximum eigen beamforming and spatial multiplexing approaches with the same throughput

to the past channel condition. For a MIMO system applying the spatial multiplexing the performance degradation manifests itself as the increment in the co-channel interference level. The orthogonality of the used unitary matrices $\mathbf{U}$ and $\mathbf{V}$ with the true ones is perturbed. The signal from one channel leaks to the other causing an irreducible BER. In paper [P5], using the Markov chain model the degradation is quantified by the Signal to Interference plus Noise Ratio (SINR). The average SINR of the $k^{th}$ sub-channel can be estimated as

$$
\begin{aligned}
\overline{SINR}_k &= \frac{|\rho\sqrt{\lambda_k} + \sqrt{1-\rho^2}q_{kk}|^2 P_k}{(1-\rho^2)\sum_{i\neq k, i=1}^{i=K} P_i|q_{ik}|^2 + \sigma^2} \\
&= \frac{|\rho\sqrt{\lambda_k} + \sqrt{1-\rho^2}q_{kk}|^2 SNR_k}{(1-\rho^2)\sum_{i\neq k, i=1}^{i=K} SNR_i|q_{ik}|^2 + 1}
\end{aligned}
\tag{4.6}
$$

where $\rho$ is the channel time-varying correlation coefficient, $q_{ik}$, $q_{kk}$ can be chosen as a complex Gaussian variable with zero mean and unit variance, $\sigma^2$ denotes the noise variance, $P_k$ and $SNR_k$ is the received power and the SNR of the $k^{th}$ sub-channel. In a multipath channel where the scatterers are uniformly distributed in the horizontal plane the channel time-varying correlation coefficient is related to the relative maximum Doppler frequency $f_d$ and the updated time $t$ as

$$
\rho(t) = J_o(2\pi f_d t)
\tag{4.7}
$$

The scattering model is another approach, which gives more physical insight into the evolution of the channel state of the moving terminal. This simple model assumes that the received signal is a superposition of a number of waves emitted from random scattering objects. For a narrowband MIMO system the discrete time CSI at time $to + t$ can be
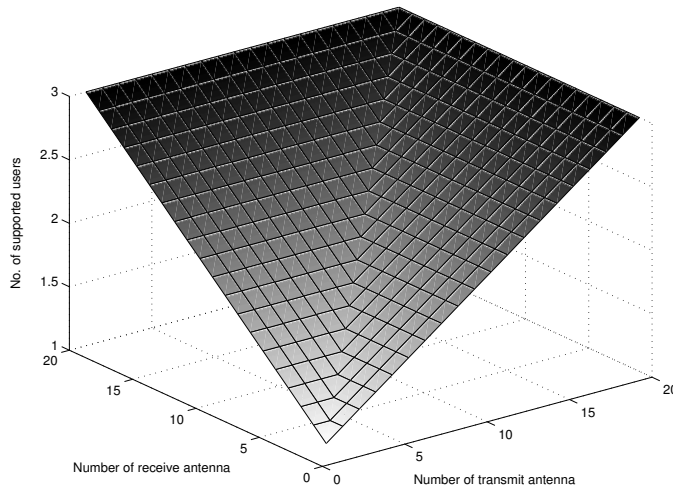
a.    Lower bound
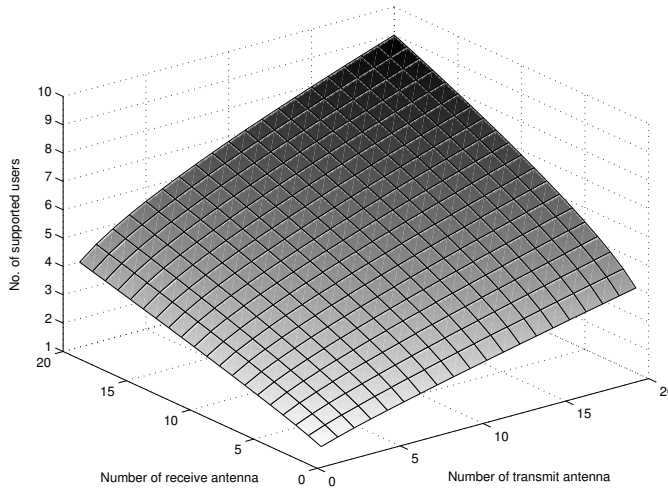


b.    Upper bound

Figure 4.4: Lower and upper bound of the number of simultaneous users with a target SIR of 10dB

described in the baseband by

$$[\mathbf{H}]_{(n_t,n_r)}(t+t_o) = \frac{1}{\sqrt{N_s}} \sum_{n_s=1}^{N_s} a_{n_s} e^{-j2\pi f_d(t+t_o)cos\theta_{n_s}} \tag{4.8}$$

where $\theta_{n_s}$ is uniformly distributed over $(0, 2\pi]$, $a_{n_s}$ is a random complex Gaussian number with zero mean and variance 1, $f_d$ is the maximum Doppler frequency and $N_s$ is the number of scatterers.

However, from this model we may not be able to derive a closed form of the average SINR. Hence, the model lacks of explanation why the time-varying channel effect degrades

the system capacity and BER performance. Nevertheless the scattering model can act as a reference to verify the results obtained from the Markov chain model. The influence of the time-varying channel to the channel capacity and BER is illustrated in Figure 4.5 and Figure 4.6. The system capacities and BER obtained from the two models are visually inline with each other. The result shows that delay in the feedback of the channel state information can degrade the capacity and performance of a MIMO system significantly. Increasing the transmitted power does not help in such case, above a certain value the capacity curve reaches a ceiling and the BER curve reaches a BER floor.
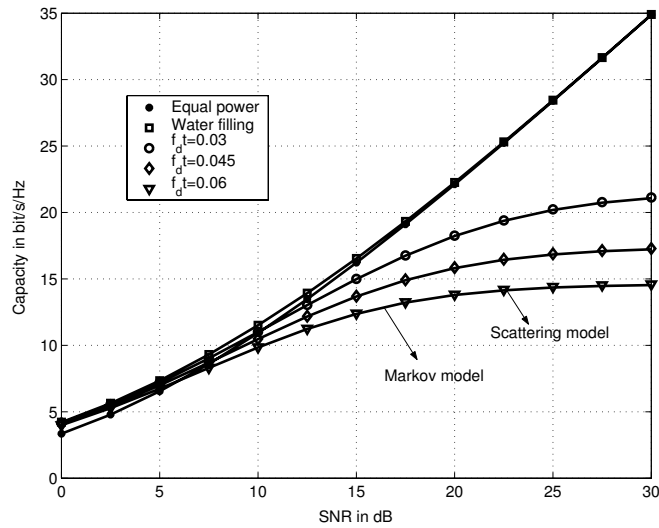


(a) 4x4 setup
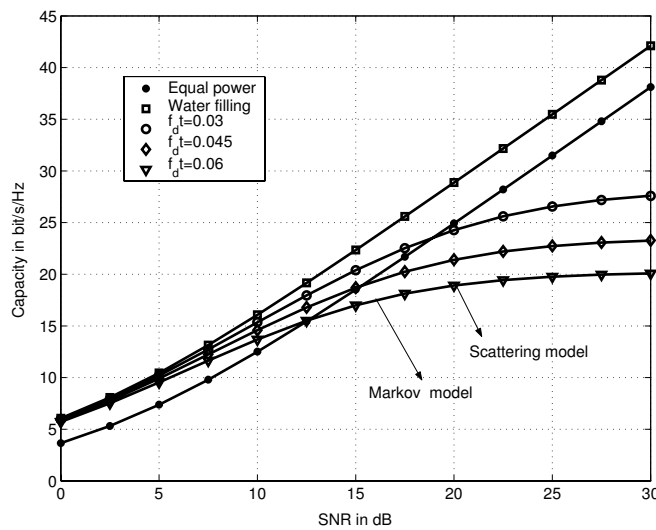


(b) 8x4 setup

Figure 4.5: Capacity of 4x4 and 8x4 MIMO systems in a time-varying channel
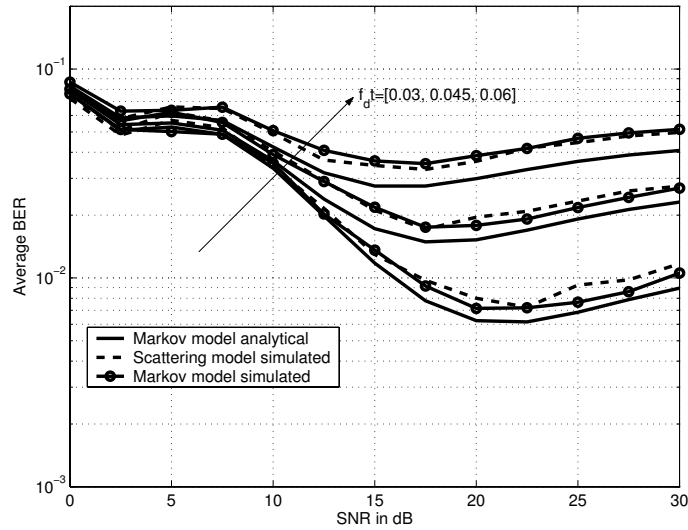
(a) 4x4 setup
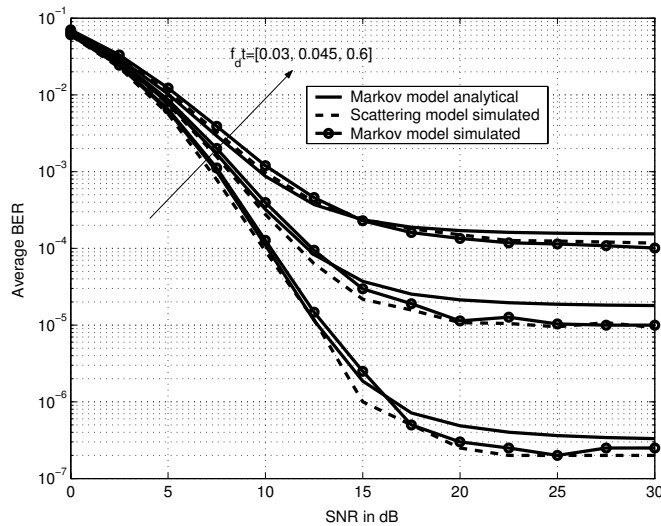


(b) 8x4 setup

Figure 4.6: The BER performance of 4x4 and 8x4 MIMO systems in a time-varying channel

## 4.4   Precoder/decoder prediction

In an effort to alleviate the impact of time-varying channel to the MIMO system performance, paper [P6] presents a prediction scheme for the precoder and decoder (e.g. the unitary matrix $\mathbf{U}^H$ and $\mathbf{V}$) in spatial multiplexing MIMO systems. The precoder and decoder are obtained from the SVD of the channel matrix. Because of the time-varying channel, the precoder/decoder gradually becomes out of date and it causes system performance degradation as investigated in section 4.3. One way to reduce the time-varying channel impact is to predict the channel matrix based on the past ones. Then, the future precoder and decoder are estimated by the SVD of the predicted channel matrix.

However, predicting all the components of the channel matrix at both ends appears to be cumbersome. Moreover, the precoder and decoder obtained from the SVD of the predicted channel matrix are more prone to estimation errors. We aim at predicting the precoder and decoder directly without going through the prediction of the channel matrix. The prediction is done in the Stiefel manifold where the precoder/decoder ($\mathbf{V}/\mathbf{U}^H$) is a unitary matrix and can be expressed as the matrix exponential of a skew Hermitian matrix.

$$\left. \begin{array}{c} \mathbf{V}{=}\mathbf{A}\Xi\mathbf{A}^{-1} \\ \mathbf{S}{=}\mathbf{A}\ln(\Xi)\mathbf{A}^{-1} \end{array} \right\} V = expm(\mathbf{S}) \tag{4.9}$$

where $expm()$ is the matrix exponential operator. The prediction is done based on the $Q$ past decoders. However, since the precoders/decoders as a solution of the SVD of the channel matrix are not unique, they have to be transformed in a way to reduce the ambiguity

$$\begin{aligned} \mathbf{V}_{nN} &\rightarrow \mathbf{I} = \mathbf{V}_{n,o}^{Tr} = expm(\mathbf{S}_{n,0}) \\ \mathbf{V}_{(n-1)N} &\rightarrow \mathbf{V}_{nN}^{-1}\mathbf{V}_{(n-1)N}\mathbf{\Theta}_{n,-1} = \\ &\qquad \mathbf{V}_{n,-1}^{Tr} = expm(\mathbf{S}_{n,-1}) \\ &\vdots \\ \mathbf{V}_{(n-Q+1)N} &\rightarrow \mathbf{V}_{nN}^{-1}\mathbf{V}_{(n-Q+1)N}\mathbf{\Theta}_{n,-Q+1} = \\ &\qquad \mathbf{V}_{n,-Q+1}^{Tr} = expm(\mathbf{S}_{n,-Q+1}) \end{aligned} \tag{4.10}$$

where $n$ is the frame index, $N$ is the number of symbols within a frame. The orientation matrix $\mathbf{\Theta}_{n,q}$, $q \subset \{-Q+1,..,-1,0\}$ is the orientation matrix that makes the two matrices $\mathbf{V}_{nN}$ and $\mathbf{V}_{(n+q)N}\mathbf{\Theta}_{n,q}$ as close as possible in Euclidean distance

$$\mathbf{\Theta}_{n,q} = diag(\mathbf{V}_{(n-q+1)N}^{-1}\mathbf{V}_{nN})/|diag(\mathbf{V}_{(n-q+1)N}^{-1}\mathbf{V}_{nN})| \tag{4.11}$$

Through these $Q$ skew-Hermitian matrices $(\mathbf{S}_{n,-Q+1}, \mathbf{S}_{n,-Q+2}, ..., \mathbf{S}_{n,0})$ we try to fit a $P^{th}$ order polynomial. When $P+1$ is equal to $Q$, for matrix $\mathbf{S}_{n,q}$ we have $P+1$ unknown matrix coefficients that can be solved by a set of $Q$ linear matrix equations:

$$\mathbf{S}_{n,q} = \sum_{p=0}^{P} \mathbf{C}_{n,p} ((n+q)N)^p \tag{4.12}$$

Based on the $Q$ coefficients, the future skew-Hermitian matrix $\hat{\mathbf{S}}_{nN+m}$ is estimated by

$$\hat{\mathbf{S}}_{nN+m} = \sum_{p=0}^{P} \mathbf{C}_{n,p}(nN+m)^p \tag{4.13}$$

where $m \in \{1..N-1\}$ The corresponding future precoders/decoders for the $(Q+1)^{th}$ frame can thus be constructed as

$$\hat{\mathbf{V}}_{nN+m} = \mathbf{V}_{nN}expm(\hat{\mathbf{S}}_{nN+m}) \tag{4.14}$$

To evaluate the prediction performance two metrics were defined, namely the square root error (SRE) and the leakage level. The square root error is the Euclidean distance between the predicted precoder/decoder and the true ones. On the other hand the leakage level is defined as

$$||\hat{\mathbf{U}}^H \mathbf{H} \hat{\mathbf{V}} - \mathbf{D}||_F \tag{4.15}$$

where $\mathbf{D}$ is a diagonal matrix which contains the singular values of the true channel matrix in the diagonal.

In the prediction of the precoder/decoder we aim at a slowly time-varying channel with a maximum Doppler spread ranging from a couple of Hz to tens of Hz. This type of channel can occur in an indoor environment. The time required to transmit a data frame is $10^{-3}s$. The channel matrices were generated using the Jakes model. We consider 1000 channel realizations and 1000 simulated frames.

In general, based on the two metrics presented above the proposed precoder/decoder prediction scheme always outperforms the scheme with no prediction (i.e. only using a delayed version of the precoder/decoder). A reduction in the leakage level by a factor of two is observed for most MIMO settings and time-varying channel conditions. Despite of using only two past samples for the prediction, linear prediction of the precoder/decoder shows a reasonable performance improvement.

# Chapter 5

# Time reversal in wireless communications

Time reversal techniques (TR) have been used in acoustic and medical application for quite some time. TR is known for being able to focus the signal both in space and in time. In the acoustic frequency range, TR has been shown to work very well in a rich scattering environment. In papers [P7,P8,P9] the applicability of the time reversal technique in wireless communication which often operates at a high frequency regime (GHz) is investigated. From a wireless communication viewpoint these two distinct characteristics of the TR can help to reduce the inter symbol interference (ISI) effect in a wideband transmission and the co-channel interference in a multi-user environment.

The essence of the TR is to convolve the transmitted signal with the complex conjugate of the time reversed version of the measured impulse response (IR). If the channel is slowly varying, the received signal will be equal to a convolution of the transmitted symbol with the autocorrelation of the IR as

$$y_j(t) = x_j(t) \star h_{ij}(-t)^* \star h_{ij}(t) + n_j(t) = x_j(t) \star R_{ij}^{auto}(t) + n_j(t) \qquad (5.1)$$

where $x(t)$ denotes the transmitted signal and $y(t)$ indicates the received signal; $\star$ denotes the convolution operator; $()^*$ is the complex conjugate operator; $i$ and $j$ are the indices of the transmitting antenna and receiving antenna respectively; $n_j(t)$ is the noise component; $R^{auto}(t)$ is the autocorrelation of the channel IR $h_{ij}(t)$. The received signal at an off-target point has the form

$$x_j(t) \star h_{ij}(-t)^* \star h_{ik}(t) + n_k = x_j(t) \star R_{ijk}^{cross}(t) + n_k(t) \qquad (5.2)$$

where $h_{ik}(t)$ denotes the IR of the channel from the transmitting point to the off-target point and $R_{ijk}^{cross}(t)$ is the cross correlation of the channel IR $h_{ik}(t)$ to the target point and the IR $h_{ij}(t)$.

Although a TR-SISO system can offer a limit spatial focusing, it can be shown that it is not possible to obtain temporal focusing. In a TR-MISO system, the autocorrelations are added coherently at their peaks as a sum of real numbers, whereas sidelobes add up randomly. The composite sidelobes are suppressed and the temporal focusing therefore is possible. For a multi-user MISO system applying TR the received signal of the $j^{th}$ user

Table 5.1: Mean RMS delay spread of the IRs and of the *equivalent time reversal channel IRs*

| Route | $\overline{\sigma_\tau}$ | |
|---|---|---|
| no | IRs, $h_{ij}$ | Equivalent channel IR, $h_j^{eq}$ |
| 1 | 0.2 $\mu$s | 0.1 $\mu$s |
| 2 | 0.6 $\mu$s | 0.3 $\mu$s |

becomes

$$y_j(t) = \underbrace{x_j(t) \star \sum_{i=1}^{N_t} R_{ij}^{auto}(t)}_{S(t)} \;+\; \underbrace{\sum_{i=1}^{N_t} \sum_{k=1; k \neq j}^{N_u} x_k(t) \star R_{ikj}^{cross}(t)}_{IF(t)} + \underbrace{n_j(t)}_{Noise} \qquad (5.3)$$

where $S(t)$ is the signal of interest and $IF(t)$ is the interfering signal, $N_t$ is the number of transmitting antennas, $N_u$ is the number of users.

The spatial focusing property of TR is qualified by the SIR which can be calculated as

$$SIR = \frac{|S(t)_{peak}|^2}{|IF(t)_{peak}|^2} = \frac{P_S}{P_{IF}} \qquad (5.4)$$

where $P_S$ and $P_{IF}$ are the signal and the interference power respectively. To avoid branch power difference the time-reversed IR is normalized so that it has a unit wideband power. In paper [P7], the average SIR of an uncorrelated Rayleigh fading channel with the power delay profile having an exponential decay can be analytically calculated as

$$\overline{SIR} \;\approx\; \frac{1}{(N_u - 1)} \left( 1 + N_t \left( 1 + \frac{2exp(-\frac{\Delta\tau}{\sigma_{\Delta\tau}})}{1 - exp(-\frac{\tau}{\sigma_\tau})} \right) \right) \qquad (5.5)$$

where $\sigma_\tau$ is the RMS delay spread, and $\Delta\tau$ is the tap resolution. For example, in a 8×1 TR-MISO system supporting two users with $\frac{\Delta t}{\sigma_\tau} = 0.82$ the estimated SIR value is 18.8dB.

In [P7], based on the measured IR of an 8x1 MISO system centered at 2.14GHz the SIR of 2 users TR-MISO system are calculated as a function of the separation distance between them. The results are presented in Figure 5.1. The spatial focusing capability of the TR in wireless communication is illustrated by a SIR values of 18dB when the separation distance between the two users is 300m. These empirical results are also inline with the analytical estimations presented in (5.5). The temporal focusing of TR is illustrated as a reduction of the RMS delay spread. The RMS delay spread of an 8×1 TR-MISO system is reduced by a factor of 2 as compared with that of the SISO system. Table 5.1 shows the mean RMS delay spread obtained from the IR of the SISO system and the equivalent IR of the TR-MISO system. Other way of evaluating the temporal focusing of TR is to compare the BER of the system with and without the use of TR. Improvement in the BER will indicate the temporal focusing performance. In Figure 5.2 we show the simulated BER of a pure single user SISO system and a single user TR-MISO system at different guard intervals or symbol rates. To highlight the temporal focusing property of TR, no equalizer was used
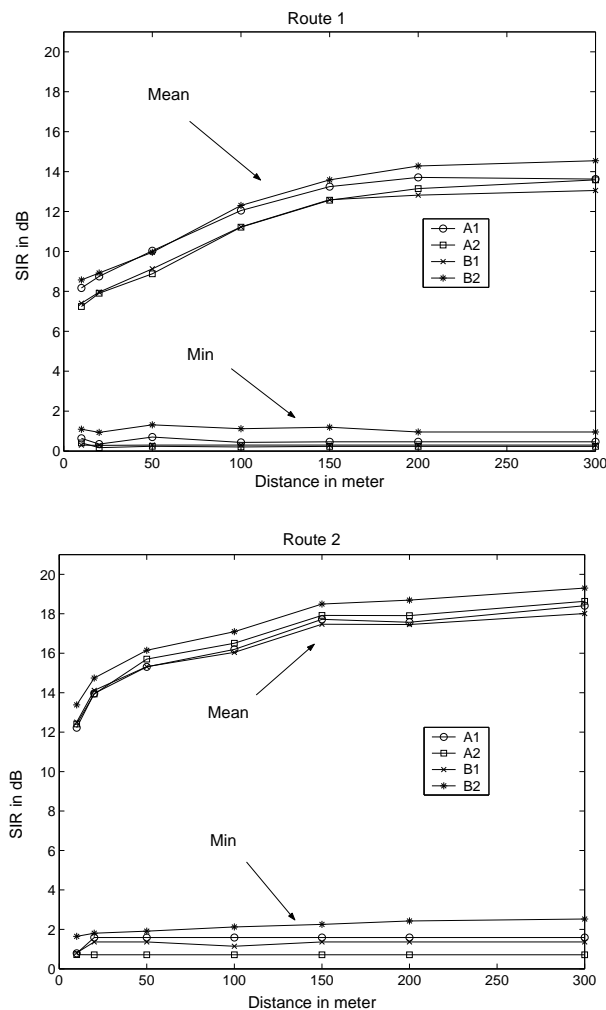
Figure 5.1: Maximum, Mean and Minimum value of the SIR vs the separation distance for 2 routes

at the receiver. Both the channel IR of the SISO system and the equivalent channel IR of the TR-MISO system were normalized so that they have unit wideband power. In general, the BER floor of the TR-MISO system is always lower than that of the SISO system by at least an order of magnitude. For a lower transmission rate (e.g. smaller than 2Mbps), while the BER of the SISO system reaches a floor at some SNR values, no BER floor is observed for the MISO-TR system in the SNR range of 0dB to 20dB. As observed in RMS delay spread results, the highly frequency selective characteristic of the environment in route 2 leads to a significant difference in the BER of these two SISO and TR-MISO systems.

The expectation of the simultaneous transmission of independent data streams to multi-user requires that the time-reversed IRs should be aligned at their maximal peak/or the first arrival path, so that one can transmit $N_u$ independent symbols simultaneously. Because of the time alignment, even though the channel IRs are uncorrelated, the mag-
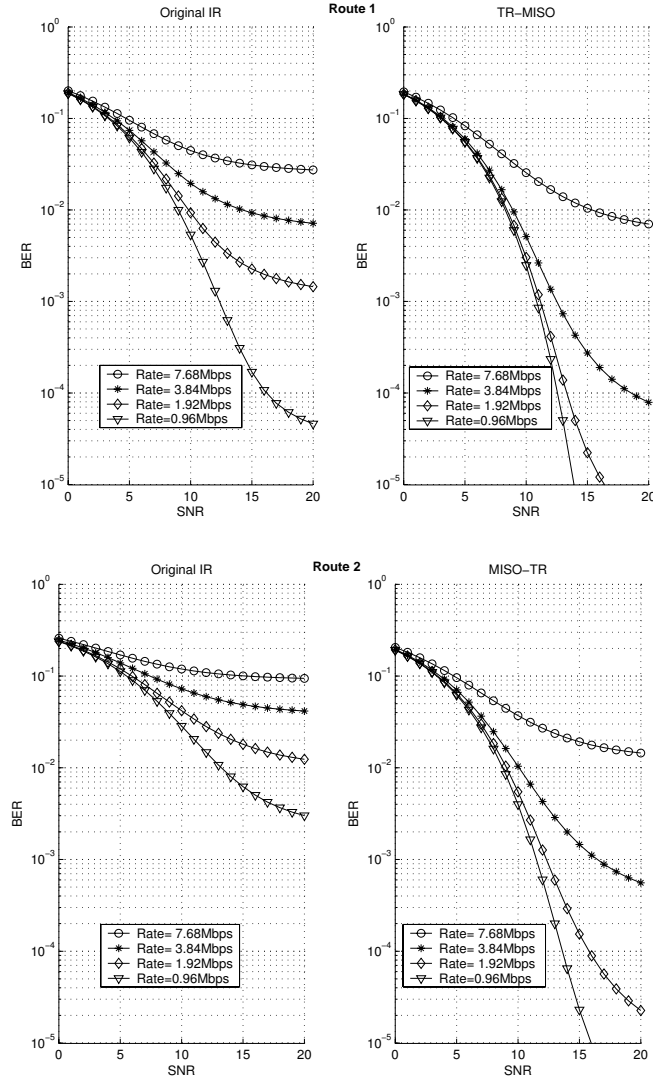
Figure 5.2: BER comparison between the SISO and the TR-MISO systems at different transmission rates

nitude of the IRs cross-correlation $R^{cross}(t)$ is still an order of magnitude smaller than that of the IR autocorrelation, $R^{auto}(t)$ . In general, the interference at the peak of the signal also increases linearly according to the number of simultaneous transmissions. Low transmission quality, i.e. low SIR is traded for more users. In [P7], we proposed an interference suppression scheme which involves an offsetting in time the time-reversed IRs intended for each user, called TR&S. The transmitted signal intended for the $j^{th}$ user at the $i^{th}$ transmitting antenna can be described as

$$circshift(s_j h_{ij}(-t)^*, \triangle TR(j-1))$$
$$\triangle TR = \triangle l \delta_t \tag{5.6}$$

where $circshift(.)$ denotes the circular shift operation, $\triangle l$ is the shifted unit calculated

as the number of taps and $\delta_t$ is the tap resolution. Figure 5.3 illustrates the signals transmitted at one transmitting antenna before and after shifting the time-reversed IRs' main peaks by $\triangle TR = 5$ taps relative to each other. In this way the taps in the propagation
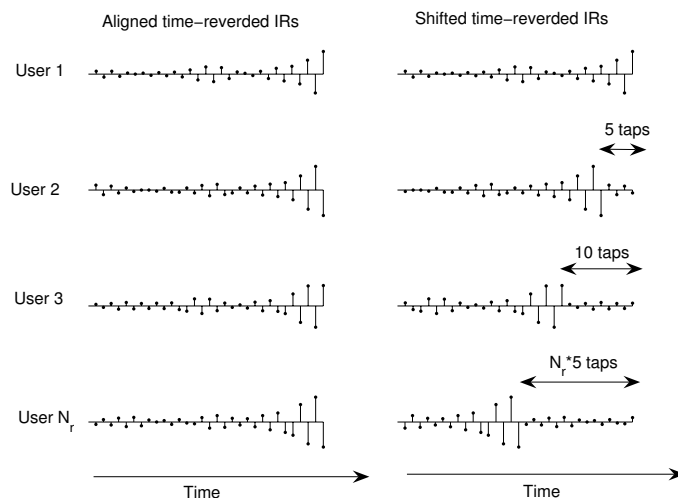


Figure 5.3: Signal applied at one antenna for MISO TR-UWB multiple-user scenario: normal TR case (left), proposed shifted TR (*TR&S*) scheme (right)

channel containing significant energy are multiplied by taps of the transmitted signal with low energy and vice versa. The peak to peak multiplication can be avoided and the interference power is significantly suppressed. Depending on the amount of the time offset $\triangle TR$, the system capacity is reduced as it requires a longer interval for all symbols to be transmitted. On the other hand, the communication quality is improved as the interference is decreased.

In paper [P9], the SIR was calculated from the measured IRs in an ultra wideband regime with the effective IR length of 100 taps (40ns). The results for both aligned time-reversed IRs and TR&S schemes are shown in Figure 5.4. It is observed that by shifting the transmitted time-reversed IRs intended for each user by 2ns ($\triangle l = 5$ taps), significant improvement in the SIR can be obtained i.e. the median SIR increases to 23dB from 12dB for 5 simultaneous users.
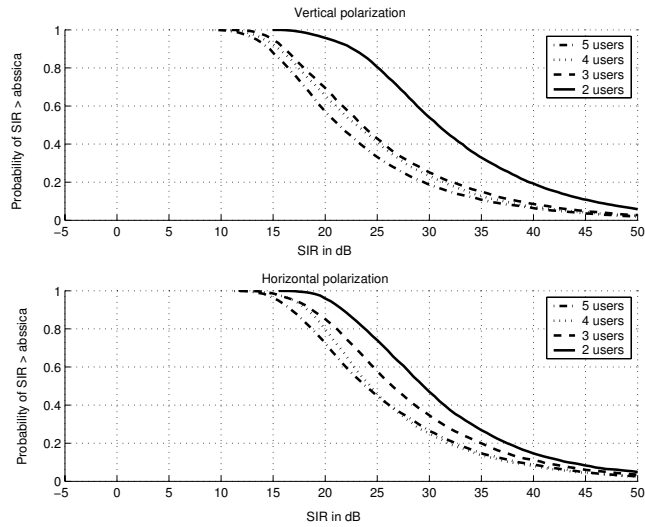
(a) SIR of aligned time-reversed IRs, simple TR
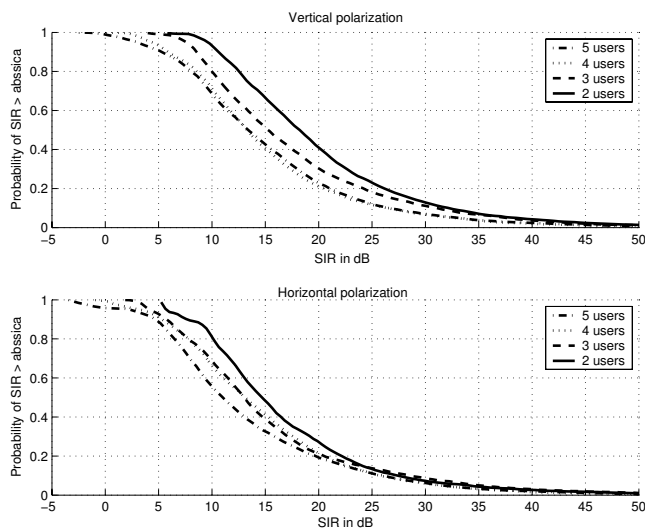


(b) SIR of shifted and time-reversed IRs, the peaks are shifted by 2ns relative to each other($\Delta l = 5$, $\Delta TR =$2ns),TR&S

Figure 5.4: SIR with different setups and transmission schemes

# Chapter 6

# Conclusions and remarks

Several topics within the antenna propagation and signal processing domain have been studied in this thesis. The emphasis was put on studying, investigating and evaluating the performance of multiple antenna systems for mobile terminals. The thesis was divided into two major parts. The first part is for experiment data processing and characterization of the measured MIMO radio channel. In Chapter 3 the characteristics of the radio channel in different operating environment and usage scenario were investigated. Applying spatial diversity at a small terminal was shown to be feasible despite the space constraint. In general, the measured channels have a good multipah richness property which leads to a channel capacity accountable for 80% of the ideal IID case. The scattering very near to the mobile was shown to be of little influence on the overall multipath richness of the measured radio channel. In the contrary, it has a significant impact on the received power level which is essentially a single antenna problem. Therefore, when taking both the multipath richness and received power level information into account the capacity of a MIMO system is very sensitive to body shadowing and absorption loss. Based on indoor narrowband measurement data, a non-physical model for MIMO radio channels was proposed. A multiplication structure of the channel covariance matrix and the temporal correlations information has been exploited to model the spatio-temporally correlated MIMO channel. Simulations have shown a good agreement between the capacity and temporal correlation of the measurement data and those from the statistical MIMO channel model.

Knowledge of the radio channel in multipath environment is crucial for the development, evaluation of the transmission technique in future wireless communication systems. In Chapter 4, several link adaptation schemes for narrowband MIMO systems applying the spatial multiplexing transmission are presented. The performance of the link adaptation schemes in time-varying channel is also investigated. It was shown that due to the delay in the update of the channel information the transmitted signals cannot be properly decoupled. Leakage among the sub-channels causes an irreducible BER at high SNR values. In an attempt to reduce the impact of time-varying channels a precoder/decoder prediction scheme was proposed. Without increasing the overhead signalling it was illustrated that using the prediction scheme, improvement in the system performance by a factor of two is possible.

Application of the time reversal technique to wireless communication and the simultaneous investigation of temporal and spatial effects were presented in Chapter 5. Because in TR, the design complexity burden is moved from the receiver to the transmitter, TR

is very suitable for wireless systems which require a very low complexity receiver. Actual channel measurements were used to quantify the benefit of time reversal in the context of wideband and ultra wideband applications. A promising spatial focusing characteristic of the TR has been illustrated with 17dB signal isolation for two simultaneous users in an outdoor environment. As for the temporal focusing, a reduction in the root mean square delay spread of the "*equivalent*" as compared to that of the true channel impulse response by a factor of three was shown to be possible. It is illustrated that the performance of the TR in wireless communication is determined by the frequency selective characteristic of the radio channel as well as the differences in the scattering medium in which the signals experience.

In conclusion, the ultimate goal of this PhD project is to study and verify several aspects relating to the design and implementation of the multiple antennas wireless communication systems in which small terminals are the receiver. It is hoped that the thesis not only gives some insight to the defined problems but also raises some new problems that may be of interest for future researchers.

# Bibliography

[1] J.H Winters. Smart antennas for wireless systems. *IEEE Personal Communications*, 5(1):23–27, 1998.

[2] J.H.Winters, J.Salz, and R.D.Gitlin. The impact of antenna diversity on the capacity of wireless communication systems. *IEEE Transactions on Communications*, 42(234):1740–1751, 1994.

[3] L.C.Godara. Applications of antenna arrays to mobile communications. i. performance improvement, feasibility, and system considerations. *Proceedings of the IEEE*, 85(7):1031–1060, 1997.

[4] L.C.Godara. Application of antenna arrays to mobile communications. ii. beam-forming and direction-of-arrival considerations. *Proceedings of the IEEE*, 85(8):1195–1245, 1997.

[5] P.H.Lehne and M.Pertersen. Smart antenna technology for mobile communications systems. *IEEE Communications Surveys*, 2(4), 1999.

[6] W.C.Jakes. Microwave mobile communications. *New York Wiley*, 1974.

[7] P.C.F.Eggers, J.Toftgard, and A.M.Oprea. Antenna systems for base station diversity in urban small and micro cells. *IEEE Journal on Selected Areas in Communications*, 11(7):1046–1057, 1993.

[8] R.G.Vaughan. Polarization diversity in mobile communications. *IEEE Transactions on Vehicular Technology*, 39(3):177–186, 1990.

[9] P.Kyritsi. Multiple element antenna systems in an indoor environment. *PhD thesis, Wireless Communications Research Group at Stanford University*, 2001.

[10] S. Kozono, T. Tsuruhara, and M. Sakamoto. Base station polarization diversity reception for mobile radio. *IEEE Transactions on Vehicular Technology*, 33(4):301–306, 1984.

[11] R.Vaughan and J.B.Andersen. Channels propagation and antennas for mobile communications. *IEE Electromagnetic Waves Series 50*, (ISBN 085296 084 0), 2003.

[12] I.E.Telatar. Capacity of multi-antenna gaussian channels. *Tech. Rep. BL0112170-950615-07TM AT&T Bell Laboratories*, 1995.

[13] G.J.Foschini and M.J.Gans. On limits of wireless communications in a fading environment when using multiple antennas. *Wireless Personal Communications*, 6:311–335, 1998s.

[14] G.J.Foschini. Layered space-time architecture wireless communication in a fading environment when using multi-element antenna. *Bell Labs Tech. J.*, pages 41–59, 1996.

[15] P.W.Wolniansky and et.al. V-blast: An architecture for realizing very high data rates over the rich-scattering wireless channel. *Proc. IEEE ISSSE*, 1998.

[16] G. D.Golden, C.J.Foschini, R.A.Valenzuela, and P.W.Wolniansky. Detection algorithm and initial laboratory results using v-blast space-time communication architecture. *IEE Letter*, 35(1):14–16, 1999.

[17] M.A.Jensen and J.W.Wallace. A review of antennas and propagation for mimo wireless communications. *IEEE Transactions on Antennas and Propagation*, 52(11):2810–2824, 2004.

[18] G.D.Durgin. Space-time wireless channels. *ISBN: 0-13-065647-X, Prentice Hall PTR*, 2003.

[19] J. G. Proakis. Digital communications. *New York: McGraw- Hill*, 1999.

[20] D.Gesbert and J.Akhtar. Breaking the barriers of shannon's capacity: An overview of mimo wireless system. *Telektronikk Telenor Journal*, 2002.

[21] T.M.Cover and J.A.Thomas. Elements of information theory. *Wiley-Interscience, ISBN: 0471062596*, 1991.

[22] A.F. Molisch, M.Steinbauer, E.Bonek M.Toeltsch, and R.S.Thoma. Measurement of the capacity of mimo systems in frequency-selective channels. *IEEE Vehicular Technology Conference*, 1:204–208, 2001.

[23] G.G.Raleigh and J.M.Cioffi. Spatio-temporal coding for wireless communication. *IEEE Transactions on Communications*, 46(3):357–366, 1998.

[24] P.Almers, F.Tufvesson, O.Edfors, and A.F.Molisch. Measured capacity gain using water filling in frequency selective mimo channels. *IEEE Personal, Indoor and Mobile Radio Communications*, 3:1347–1351, 2002.

[25] D. Gesbert, H. Bolcskei, D. Gore, and A. Paulraj. Mimo wireless channels: Capacity and performance prediction. *Proceedings of IEEE Globecom Conference*.

[26] D. Chizhik, G. Foschini, M. Gans, and R. Valenzuela. Keyholes, correlations, and capacities of multielement transmit and receive antennas. *IEEE Transactions on Wireless Communications*, 1:361–368, 2002.

[27] P.Almers, F.Tufvesson, and A.F.Molisch. Measurement of keyhole effect in a wireless multiple-input multiple-output (mimo) channel. *IEEE Communication Letters*, 7(8):373–375, 2003.

[28] J.W.Wallace, M.A.Jensen, A.L.Swindlehurst, and B.D.Jeffs. Experimental characterization of the mimo wireless channel: data acquisition and analysis. *IEEE Transaction on wireless communication*, 2(2):335–343, 2003.

[29] T.Svantesson and J.Wallace. On signal strength and multipath richness in multi-input multi-output systems. *IEEE International Conference on Communications*, 4:2683–2687, 2003.

[30] M.Chiani, M.Z.Win, and A.Zanella. On the capacity of spatially correlated mimo rayleigh-fading channels. *IEEE Transactions on Information Theory*, 49(10):2363–2371, 2003.

[31] A.Paulraj, R.Nabar, and D.Gore. Introduction to space-time wireless communications. *Campridge University Press, ISBN 0 521 82615 2*, 2003.

[32] Chen-Nee Chuah, D.N.C.Tse, J.M.Kahn, and R.A.Valenzuela. Capacity scaling in mimo wireless systems under correlated fading. *IEEE Transactions on Information Theory*, 48(3):637–650, 2002.

[33] J.B.Andersen. Array gain and capacity forknown random channels with multiple element arrays at both ends. *IEEE Journal on Selected areas in Communication*, 18(11):2172–2178.

[34] T.Dahl, N.Christophersen, and D.Gesbert. Blind mimo eigenmode transmission based on the algebraic power method. *IEEE Transactions on Signal Processing*, 52(9):2424–2431, 2004.

[35] D.J.Love and R.W.Weath. Limited feedback unitary precoding for orthogonal space-time block codes. *IEEE Transactions on Signal Processing*, 53(1):64–73, 2005.

[36] S.M.Alamouti. A simple transmit diversity technique for wireless communications. *IEEE Journal Selected Areas in Communications*, 16(8):1451–1458, 1988.

[37] V.Tarokh, N.Seshadri, and A.R.Calderbank. Space-time codes for high data rates wireless communications: Performance criterion and code construction. *IEEE Trans. Inform. Theory*, 44:774–765, 1998.

[38] V.Tarokh, A.Naguib, N.Seshadri, and A.R.Calderbank. Space-time codes for high data rate wireless communication: performance criteria in the presence of channel estimation errors, mobility, and multiple paths. *IEEE Transactions Communications*, 47(2):199–207, 1999.

[39] V.Tarokh, A.Naguib, and A.R.Calderbank. Space-time block codes from orthogonal designs. *IEEE Trans, Inform. Theory*, 45(5):1456–1467, 1999.

[40] V.Tarokh, A.Naguib, and A.R.Calderbank. Combined array processing and space-time coding. *IEEE Trans, Inform. Theory*, 45(4):1121–1128, 1999.

[41] V.Tarokh, A.Naguib, H.Jafarkhani, and A.R.Calderbank. Space-time block coding for wireless communications: performance results. *IEEE Journal of selected areas in Communications*, 17(3):451–460.

[42] M.Steinbauer, A.F.Molisch, and E.Bonek. The double-directional radio channel. *IEEE Antennas and Propagation Magazine*, 43(4):51–63, 2001.

[43] A.F.Molisch, M.Steinbauer, M.Toeltsch, E.Bonek, and R.S.Thoma. Capacity of mimo systems based on measured wireless channels. *IEEE Journal on Selected Areas in Communications*, 20(3):561–569, 2002.

[44] K.I.Pedersen, J.B.Andersen, J.P.Kermoal, and P.E.Mogensen. A stochastic multiple-input multiple-output radio channel model for evaluation of space-time coding algorithms. *Proceedings of VTC*, pages 893–897.

[45] J.P.Kermoal, L.Schumacher, K.I.Pedersen, and P.E.Mogensen. A stochastic mimo radio channel with experimental validation. *IEEE Journal on Selected Areas in Communications*, 20(6):1211–1226, 2002.

[46] L.Schumacher, L.T.Berger, and J.R.Moreno. Recent advances in propagation characterisation and multiple antenna processing in the 3gpp framework. *Proceedings of XXVI URSI General Assembly*, 2002.

[47] A.J.Goldsmith Seong Taek Chung. Degrees of freedom in adaptive modulation: a unified view. *IEEE Transactions on Communications*, 49(9):1561–1571, 2001.

**Publications included in the thesis**

**Paper 1:**
**Characterization of the indoor/outdoor to indoor MIMO radio channel at 2.140 GHz.**

H.T.Nguyen, J.B.Andersen and G.F.Pedersen.

# Characterization of the indoor/outdoor to indoor MIMO radio channel at 2.140 GHz [*]

Hung Tuan Nguyen, Jørgen Bach Andersen and Gert Frølund Pedersen
*Department of Communication Technology, Niels Jernes Vej 12, DK-9220 Aalborg , Denmark*

**Abstract.** In this paper the radio channel characteristics of the 8x4 MIMO system consisting of a base station and a small terminal equipped with multiple antennas for indoor-indoor and outdoor-indoor scenarios are presented. We study the large-scale variation and small-scale characteristics of the measured channel coefficients. Although the mean received power is very much dependent on the measured location, the channel capacity seems to be unchanged when the receiver's location is altered. The data collected from different scenarios (e.g. measurement locations, antenna setting) were used to investigate the advantage of having the knowledge of the channel at both ends of the transmission link. It is shown that using the water filling algorithm there is indeed an increase in the channel capacity. At low SNR, the benefit of knowing the channel at both link ends observed in the measurement data is much higher than which can be obtained in the channel matrix with usual assumption on identical independently distributed components. Using the small-scale and large-scale information in the formulation of the channel capacity we show that in our measurement, the variation of the mean received power has a greater influence on the change of the overall system performance than the change in the environmental multipath scattering property.

**Keywords:** MIMO, measurements, antenna configuration, mobile terminal antennas

## 1. Introduction

Applying multiple antennas at both the transmit and receive side have emerged as a new approach that promises a huge capacity gain and performance improvement. In these Multiple Input Multiple Output (MIMO) systems, the inherent multipath fading components in wireless communication are processed in a smart way such that the small-scale fading is mitigated and parallel channels created. Because of its potential, enormous amount of work has been carried out in order to understand the behavior of MIMO channel propagation. Channel measurements become very crucial for such understanding as well as for the derivation of models that can be used for system design and simulation.

Based on the measurement results, the MIMO channel can be characterized by analyzing the scattering richness or more specifically the direction of the multipath components at both link ends of the propagation channel. In this research approach, emphasis is put onto the investigation of the double directional description of the propagation channel. The antennas therefore, become independent of the analyzed results. The Time Delay of Arrival (TDoA), the Angle of Arrival (DoA), the Angle of Departure (DoD) and the Angle Power Spectrum (APS) are very important metrics in extracting the double directional information of the channel, see for example (Steinbauer, 2002), (Thoma, 2002), (Medbo, 2001) and (Fugen, 2002).

On the other hand, studies on the characteristics of the MIMO systems with the transmitting and receiving antennas taken as integral parts of the radio channel also gains a lot of interest. The results obtained from this research direction are very useful for evaluating the performance of the MIMO system as a whole. Most of the existing research is focused on the small-scale variation (multipath richness) of the MIMO radio channel in terms of the channel correlation coefficients and/or the channel capacity. There are a number of indoor to indoor or outdoor to outdoor channel characteristics results reported in the literature such as (Kermoal, 2000), (Yu, 2001), (Kivinen, 2002), (Kyritsi1, 2002) and (Chizhik, 2003). Only recently, McNamara et.al. (McNamara, 2002), Wallace et.al. (Wallace, 2002) and Svantesson et.al (Svantesson, 2003) have investigated the influence of

---

[*] This work is partly supported by Aalborg University under the Phd Fellowship grant.

the large-scale variation (mean received power) on the performance of the MIMO system. However, there is a lack of measurement results for outdoor to indoor, the scenario in which it is expected to have most applications in 3G systems. Moreover, not many measurement results of real MIMO systems have been published. Knowledge on the influences of the practical constraint to the performance of the real MIMO systems is therefore limited.

One of the main objectives of this paper is to assess the performance of a real MIMO system consisting of a base station (BS) and small receiving terminal operating in some real life measurement scenarios. Based on the measurements of indoor to indoor and outdoor to indoor of an 8x4 MIMO system we investigate the multipath richness of the radio channel and the variation of the mean received power. The two parameters are first separately evaluated and later their joint contributions to the overall MIMO performance in terms of the channel capacity are assessed. Throughout the paper, we highlight the importance of including both small-scale variation and large-scale variation in evaluating the performances of MIMO systems. Using the *measured data* the advantage of having the knowledge of the channel at both ends of the transmission link is discussed. We estimate the improvement or the gain in the channel capacity when the channel is known at the transmitter as compared with the case where it is unknown. A simple formula approximating this gain is also derived.

The rest of the paper is organized in the following way. Firstly, the measurement environment and equipments setup are described in section 2. Having the measured data collected from different scenarios such as receiver's location, receiving antenna setting, we investigate the variation of the mean received power in section 3. Next, the multipath richness of the measured radio channel is assessed by means of the theoretical channel capacity in section 4. The advantage of knowing the channel at both ends of the transmission link is also investigated in this section. In section 5, including both small-scale and large-scale information of the measured radio channel in the formulation of the channel capacity we then evaluate the performance of the measured MIMO system. In the last section we wrap up the paper by some conclusions and remarks.

## 2. Measurement environment and system set-up

Center for Personal Kommunication's (CPK) sounder system is built on post-processing and real antenna array technology. A code phase offsetting technique with the use of pseudo noise sequence (PN) is applied. In our measurement campaign a PN sequence of length 511 bits with the chip rate 7.665MHz was transmitted at a frequency of 2140MHz. It was then sampled at the rate of 15.36 MHz and the sampled data was stored in a hard disk. There, the data can be further processed in order to get the complex channel impulse responses (IR). The obtained channel data was compensated for all system components. We note that the center frequency and the measurement bandwidth are comparable to the standard center frequency and bandwidth of 3G WCDMA systems.

At the transmit side, we used 8 outputs antenna array, a BS antenna prototype made by ALLGON in Sweden. In this BS antenna both polarization and space diversity are applied. At the receive side, prototypes of the handset and the laptop were deployed. The setup of the handset, laptop and BS's position are illustrated in figure 1. The handset is equipped with 4 patch antennas at the four corners. The distance between the vertical antennas (A1-B1, A2-B2) in the handset is 0.5 wavelength and it is 0.25 wavelength for the horizontal antennas (A1-A2, B1-B2). Meanwhile four patch antennas were arranged as a linear array with an equal distance of 0.5 wavelength. They were mounted at the top edge of the open lid of a prototype laptop. The conducting cable was replaced by optical fibre to avoid radiation disturbance. The handset and laptop were mounted on a sledge capable of moving them linearly in a track over a distance of 1.64m ($\approx$ 11 wavelengths) with a speed of 23.4 mm/s. The influence of the user was not considered in the measurement

campaign as both the handset and laptop are mounted on a wooden stick in free space. The sampling distance was 7mm which made up 20 samples per wavelength. This gives a total number of 32x234 channel impulse responses at one measured location.

The layout of the measured site was an office building with number of rooms on the same floor. Each room is surrounded by walls made of plasterboard with glass windows. Inside the room, there were several tables chairs and metal furniture (cabinets, measurement equipment, and trolleys) which made a fairly rich scattering environment around the receiver. Three placements of the BS that form an indoor-indoor and two outdoor-indoor measurement scenarios were considered. The total transmitted power for the indoor-indoor and outdoor-outdoor scenario were -16dBm and +14dBm respectively. During the measurements, except the $4^{th}$ location, the laptop was mounted so that the main beams of the antennas were perpendicular to the corridor's axis. They were faced toward the main entrance door of the room, which was left open during the measurement campaign. The handset antennas' main radiation patterns were always parallel to the corridor's axis (see figure 2).



a.    Setup of the Handset & Laptop



b.    Floor plan of the measurement site
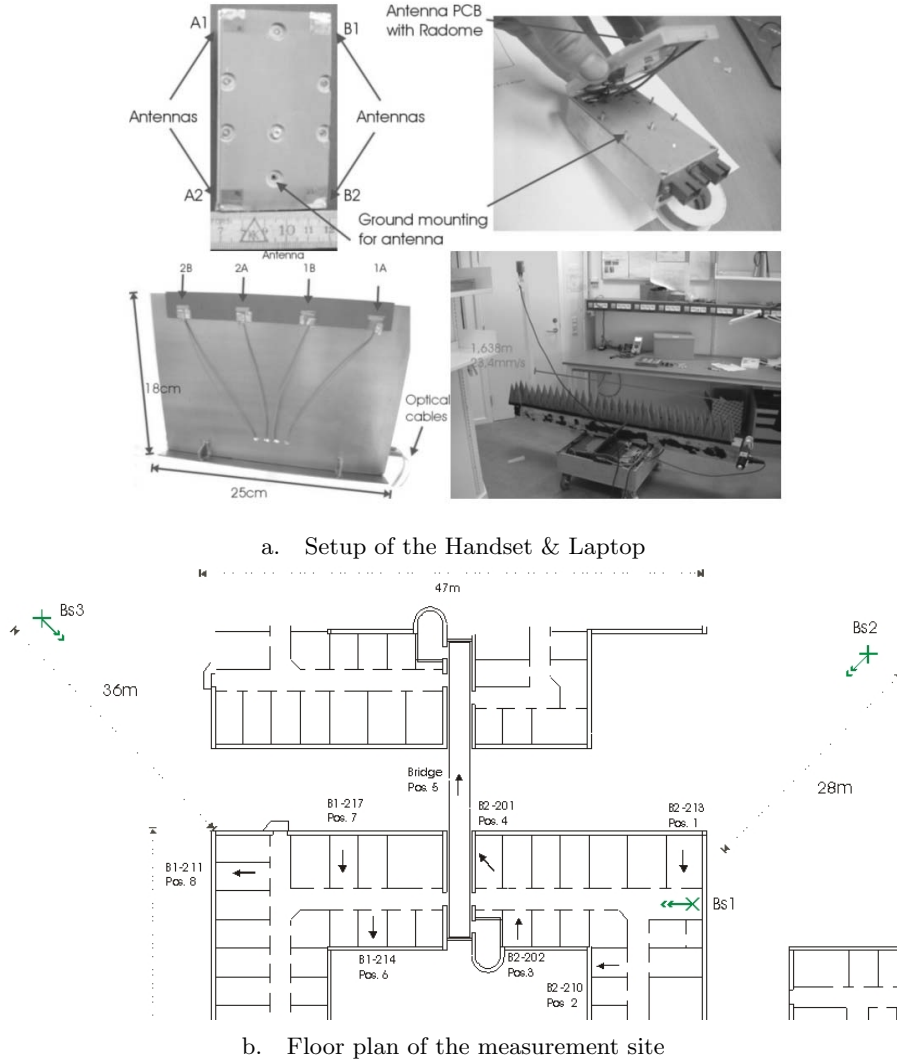
*Figure 1.* Setup and the location of the handset and base station in the measurement

In all measurement locations the distance from the center of the handset and laptop to the floor was 1.69m. For indoor-indoor measurement the height of the BS was 1.75m and it was 5.7m for outdoor to indoor measurement.

*Figure 2.* Orientation of the handset and laptop in the measurement campaign

## 3. Large-scale variation or mean received power characteristics

The mean received power at one measured location is calculated as

$$\overline{P_{received}} = \frac{1}{NN_tN_r} \sum_{n=1}^{N} \sum_{i=1}^{N_t} \sum_{j=1}^{N_r} \sum_{l=1}^{L} |IR_{ij}(l)|^2 \qquad (1)$$

where $L = 60$ is the number of taps of the IR, $N_t = 8$ is the number of transmitting antennas, $N_r = 4$ is the number of receiving antennas, and $N = 234$ is the number of measurement snapshots at one location, $IR_{ij}$ is the measured channel impulse response between $i^{th}$ transmitting antenna and $j^{th}$ receiving antenna. The mean received power at each measured location for both the handset and laptop are illustrated in figure 3. Note that this is also the mean received power of one SISO link.

The mean received power is obviously site dependent. For indoor-indoor measurements (BS1) the amount of received power tends to decrease along the corridor. At the same measured location, higher mean received power was observed at the laptop rather than at the handset. The difference in the antenna orientations as mentioned in section 2 might be the main source of the 4dB increase in the mean received power at the laptop as compared to that at the handset.

For outdoor-indoor environment it has been previously confirmed that the major part of the signal energy comes through the openings in the building such as windows and main door entrance (Knudsen, 2002). Those measured positions where the main beams of the receiving antennas are oriented toward to the openings will receive the most energy. In our outdoor-indoor measurement scenarios (BS2 and BS3), the fact that antennas at the handset have wider radiation patterns (almost omnidirectional) than those in the laptop (more directional) together with their perpendicular orientations could be the reasons for a higher mean received power observed at the handset than that at the laptop (in the order of 5dB).
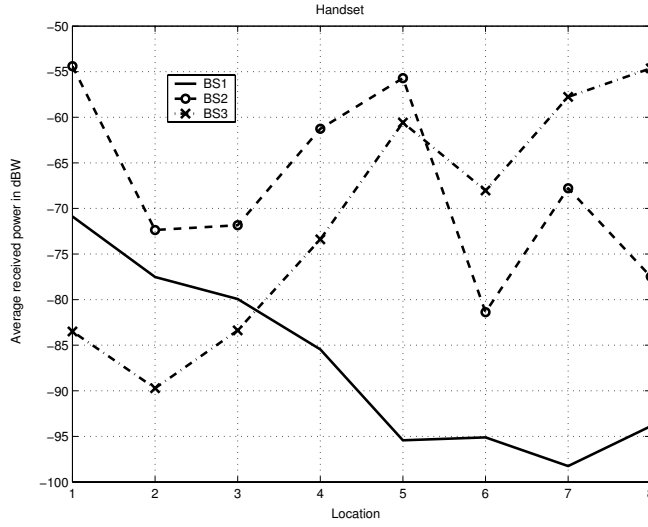
a. Handset
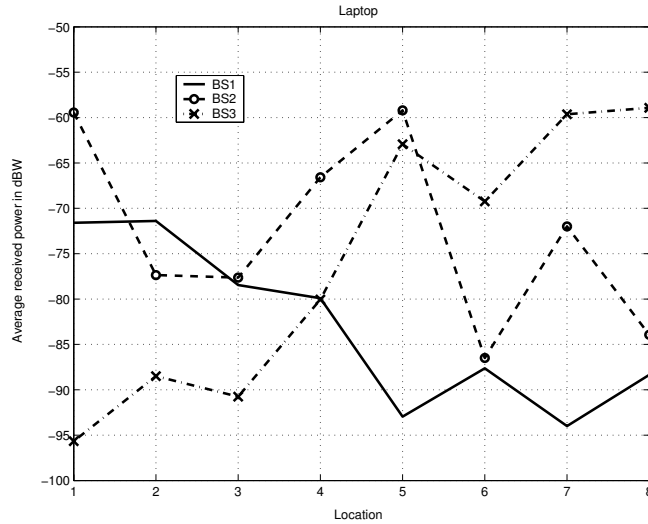


b. Laptop

*Figure 3.* The mean received power of the handset and laptop at different measured locations

## 4. Radio multipath richness or the small-scale variation characteristics

### 4.1. Channel coefficients characteristics

To quantify the time dispersion of the channel, we have assessed the root mean square (RMS) delay spread in all measured locations. To avoid the quantization and the correlation noise a threshold of 30dB is used for the power delay profile (PDP). We found that for indoor-indoor scenario in all measured locations, around 80% to 90% of the RMS delay spread is lower than the excess delay resolution of $0.135\mu$s which is an inversion of the PN chip rate. For the outdoor-indoor case, only 30% of all the paths have the time dispersion larger than the excess delay resolution. Therefore we decided to use the narrowband information of the channel for the following analysis. The channel coefficient is derived by summing up all $L = 60$ taps out of 90 available taps of the measured IR as the remaining taps often contain the quantization and correlation noise other than useful

multipath information.

$$h_{ij} = \frac{1}{L} \sum_{l=1}^{l=L} IR_{ij}(l) \qquad (2)$$

To assess the multipath richness of the measured MIMO radio channel we need to normalize the measured channel matrix. In the normalization process we simply ignore the path loss effect or specifically the amount of received power so that the multipath richness property of the radio channel is highlighted. Herein the channel matrix will be normalized such that

$$H = \frac{H_{measured}}{\sqrt{\frac{1}{N_t N_r} \sum_{i=1}^{N_t} \sum_{j=1}^{N_r} |h_{ij}|^2}} \qquad (3)$$

This normalization implicitly indicates that the square of the Frobenius norm of the normalized matrix H will be equal to $N_t \times N_r$.

Having the channel coefficients it is now possible to study the marginal distribution of their phase and magnitude. From the floor plan of the measurement site (figure 1.b.), it is clear that the channel coefficients must not contain a strong line of sight (LOS) characteristics. We use the data collected from two measurement scenarios namely the indoor-indoor measurement (BS1) with the laptop as the receiver at location 8 and the outdoor-indoor measurement (BS3) with the handset as the receiver at location 1 to study their magnitude and phase distribution. The reason for selecting these two measurement scenarios is that they are, from the ray tracing point of view, most likely having a strong LOS property. The results are shown in figure 4. The distribution of the magnitude of the channel coefficients for the indoor-indoor shows a weak LOS characteristics with the best fit Ricean $\mathcal{K}$-factor of 3.5dB. As it can be seen the empirical PDF almost follows the analytical Rayleigh distribution for the outdoor-indoor scenario. The phases of the channel coefficients, although not illustrated here appear to be uniformly distributed over $[0..2\pi]$.
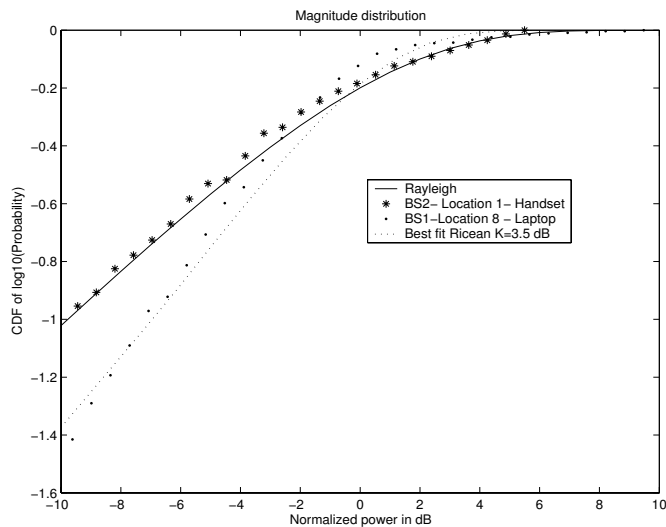


*Figure 4.* Cumulative distribution function of the magnitude of the 8x4 MIMO channel coefficients

One motivation for deploying the MIMO technique is to obtain orthogonal subchannels and therefore increasing the channel throughput at the same transmitted power and bandwidth by utilizing the radio multipath richness. Hereafter we use the eigenvalue decomposition technique as a tool to study the distribution of the subchannels' gains as well as the multipath richness property of the measured MIMO channel. In order to gather enough samples for statistical analysis, for each placement of the BS we use the data

collected from all measured locations of the receiver. The distributions of the eigenvalues or subchannels' gains are illustrated in figure 5.



a.   Handset



b.   Laptop
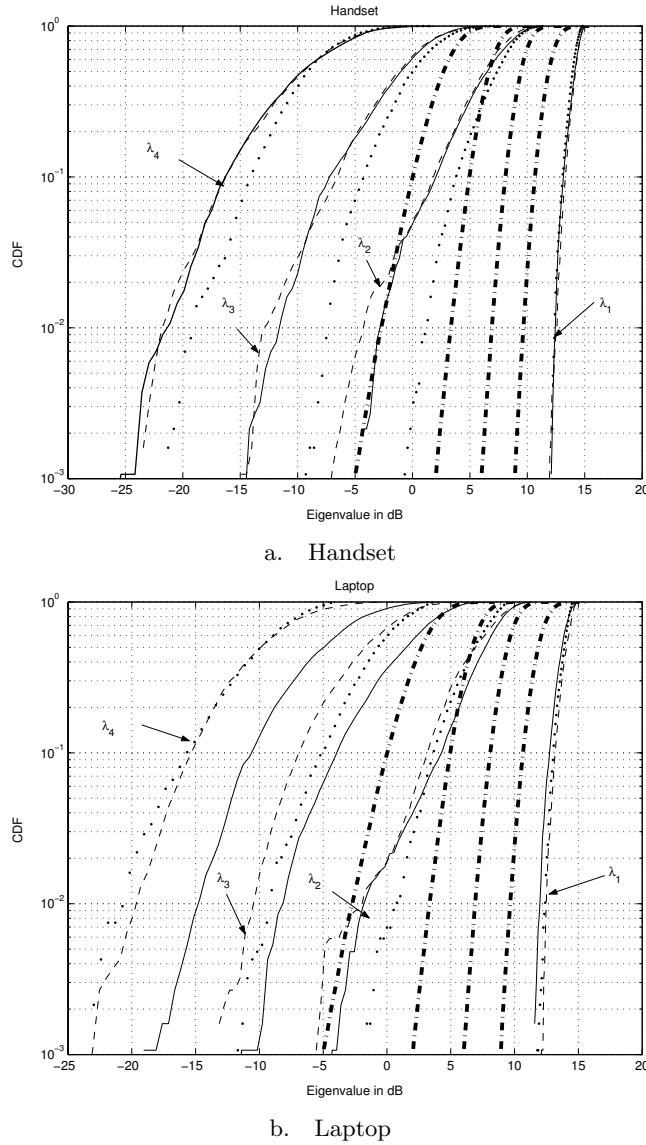
*Figure 5.* The distribution of the eigenvalues at three BS's positions, solid lines: BS1, dot lines: BS2, thin dash lines: BS3. For each BS's position the data collected at all receiver's locations are used. Thick dash lines are the distribution of eigenvalues in the IID case

In the same figure the distributions of the eigenvalues in the case where the channel coefficient is identical independently distributed (IID) with zero mean and unit variance are also plotted for reference. It is obvious from the figure that the distribution of the eigenvalues based on the measured data spread over larger range than those of the IID case. The spreads of the eigenvalues calculated as the difference in dB between the median value of the largest and smallest eigenvalues changes from 9dB to 23dB for the IID case and the measurement respectively. Interestingly the largest eigenvalue obtained from measurement has higher value than that of the IID case. This situation might be resulted from one of these main reasons:

i) A non line of sight (NLOS) environment with correlated channel that increases the largest eigenvalue.

ii) A environment that has strong LOS property (high $\mathcal{K}$-factor) that reduces the number of non zero eigenvalues.

iii) A environment with correlated channel and a slight LOS characteristics that increases the largest eigenvalue.

In our measurement, the channel coefficients are expected to be partly correlated because of the limit in the separated distance and poor cross polarization discrimination of the transmitting antennas, lack of scattering environment around the transmitter when the BS was outdoor as well as closely placed antennas at the receiver. On the other hand, as has been studied above the measured environment has more NLOS characteristics than LOS. Therefore the third reason seems to be reasonable explanation for the increase in the spread of the measured eigenvalues.

In a MIMO system we would like to have the channels to be decorrelated as much as possible so that full diversity gain can be achieved. The decorrelation degree depends on a number of factors such as the multipath environment, the configuration of the transmitting-receiving antennas, interaction of the antenna elements etc. Here we are interested in assessing the decorrealtion of the channels observed from antenna array at the receiver. From these correlation characteristics be it uncorrelated, partly correlated or correlated the benefit of using multiple antennas at a small terminal could be assessed. Based on that it is also possible to compare the correlation of the measured data with the theoretical results. For simplicity we only consider the complex correlation coefficient in the following analysis. The complex correlation coefficient between $j^{th}$ and $k^{th}$ receiving antenna is given by

$$\kappa(j,k) = \frac{1}{N_t}\sum_{i=1}^{N_t} \frac{E\left((h_{ij}-\overline{h_{ij}})(h_{ik}-\overline{h_{ik}})^*\right)}{\sqrt{E\left((h_{ij}-\overline{h_{ij}})(h_{ij}-\overline{h_{ij}})^*\right)}\sqrt{E\left((h_{ik}-\overline{h_{ik}})(h_{ik}-\overline{h_{ik}})^*\right)}} \quad (4)$$

where $E(.)$ is the expectation operator, $(.)^*$ denotes complex conjugate and $\overline{(.)}$ denotes the mean value.

In order to gather enough spatial statistic, for each measured location we used all the 32x234 IRs to calculate receiving spatial correlation coefficient. The variations of the magnitude of the complex spatial correlation coefficient at the receivers along the corridor for different placement of the BS are illustrated in figure 6. Note that the order of the receiver's location has been reversed in the third row so that the x axis reflects the relative distance from the BS to the handset or to the laptop. It is observed that the highest value of the spatial correlation coefficient is 0.85 and the lowest value is 0.05. The analytical correlation coefficient obtained from a widely used Jake model $J_o(\frac{2\pi d}{\lambda})$, are 0.47, 0.30 and 0.26 for a antennas separated distance of $0.25\lambda$, $0.5\lambda$ and $0.75\lambda$ respectively. In general, the measured spatial correlation coefficient between receiving antenna elements hardly reflects the separation between them. Mutual coupling, differences in the antenna radiation patterns which can be expected from real life scenario must be the main reason for the disagreement in the measured and theoretical results.

## 4.2. Channel capacity

As mentioned in the previous chapter it is possible to transmit up to $min(N_t, N_r)$ subchannels in a MIMO system consisting of $N_t$ transmitting antenna and $N_r$ receiving antennas. Therefore there is a significant increase in the channel spectral efficiency or the channel capacity. The theoretical amount of information or capacity the MIMO system can convey is defined as (Telatar, 1999).

$$C = log_2\left(det(I + \frac{SNR}{N_t}H*H^H)\right) = \sum_{k=1}^{K} log_2(1 + \frac{SNR}{N_t}\lambda_k) \quad (5)$$

where $()^H$ denotes the Hermitian transpose operator; $K = min(N_t, Nr)$ and $\lambda_k$ is the $k^{th}$ non zero eigenvalue derived from the eigenvalue decomposition of the normalized matrix
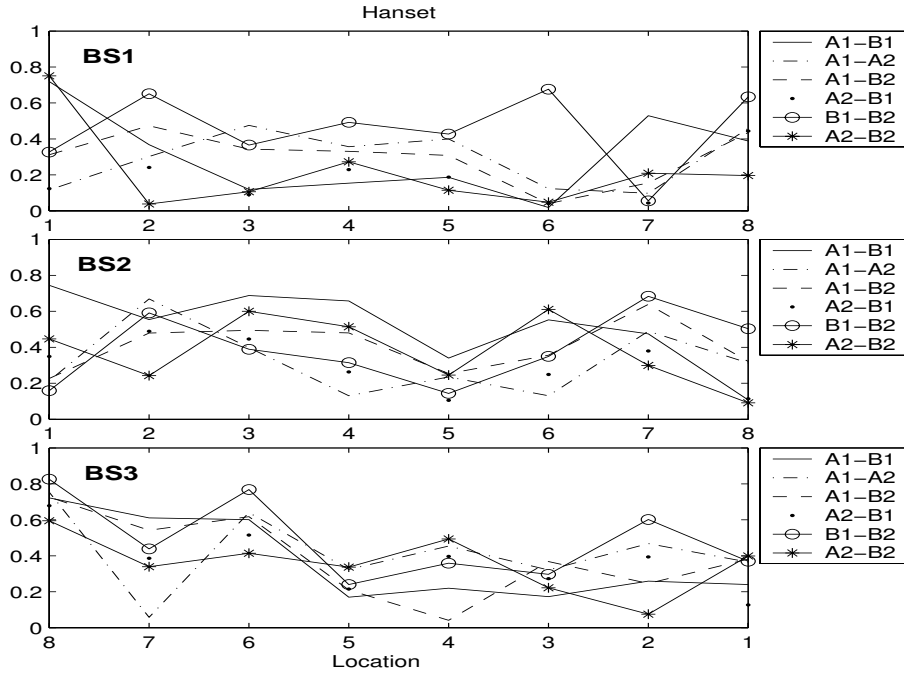
a. Handset
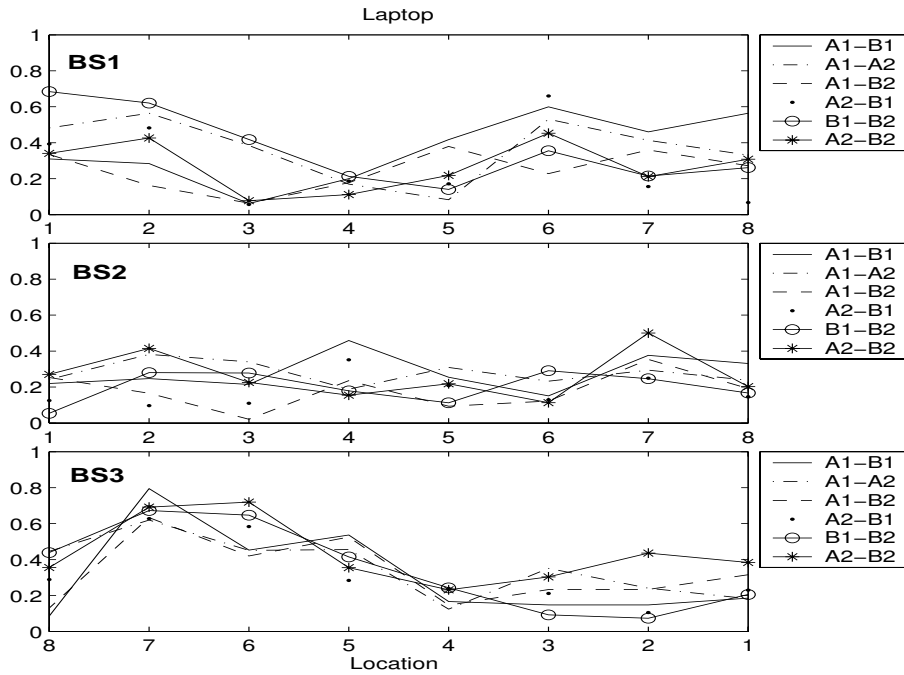


b. Laptop

*Figure 6.* Spatial correlation at the handset and the laptop along the corridor for indoor-indoor and outdoor-indoor setup

$H$. This formula is applied to the case where the channel state information (CSI) is only known at the receive side, and therefore the most reasonable way of distributing the transmitted power is to distribute it equally to each transmitting antennas.

It has been demonstrated in (Andersen1, 2000) that for a MIMO system with wide angular spread at both ends a diversity order of $N_t N_r$ can be obtained. Basically, by only knowing the CSI at the receive side it is possible to obtain the diversity gain at the receive side and full diversity order. But the mean gain is degraded because the transmitted

signal is not matched with the channel. However, in order to have full gain, knowledge of the channel must be available at both the transmitter and receiver. It has been shown that when the CSI is known at both ends of the transmission link, and with the total transmitted power constraint the maximum channel capacity can be achieved by using the waterfilling algorithm. Assuming that the noise variances are the same for all receive branches and the noise at each branches are mutually uncorrelated, the MIMO channel capacity using the waterfilling method can be described by

$$C = \sum_{k=1}^{K} log_2(1 + \lambda_k \gamma_k) \qquad (6)$$

where $\gamma_k = max(\mu - \frac{1}{\lambda_k}, 0)$ and the water level $\mu$ is chosen such that $\sum_{k=1}^{K} \gamma_k = SNR$.

When the number of the transmitting antennas is greater than the number of the receiving antennas, the advantage of having the CSI at the transmit side becomes more significant. This is because the transmitted power can be focused into the channels which have non zero eigenvalues. Meanwhile for the case where the CSI is only available at the receive side, the transmitted power is equally distributed over all channels, including the channel with zero eigenvalues. This leads to a loss in the received power and as a result reduction in the capacity.

The combination of the normalization process and the use of the fixed reference SNR imply that at the receiver we have a perfect power amplifier and attenuator so that the average SNR is always kept constant. Therefore the effect of path loss caused by the separation between the transmitter and receiver and the measured environment is always circumvented.

It should be noted that there is distinct difference in the reference SNR and the signal to noise ratio in the measurement $SNR_m$. In our measurement the system noise is mainly due to the quantization noise and the correlation noise. Even though the system noise somehow correlated with the input power, in most of the measured locations the measured $SNR_m$ is guaranteed to be well more than 40dB. Depending of its relative power as compared with the input signal power, the noise could make the channel matrix become more uncorrelated as it actually is. Therefore, we want to have a system with high $SNR_m$ so that the effect of noise is limited. Low value of the $SNR_m$ could introduce erroneous eigenvalues and therefore erroneously high value of the channel capacity especially with high reference SNR (see (Gans, 2002)). Aware of this problem we use a reference SNR value of 20dB.

In the following, we will consider both scenarios where the CSI is assumed to be known perfectly only at the receiver and at both ends on the transmission link. For each placement of the BS, the measured data collected from all measured locations of the handset and laptop were used to calculate the distribution of the channel capacity. This will give an overview picture on the effect of the measurement scenario e.g. indoor-indoor, outdoor-indoor and the laptop/handset on the theoretical capacity (figure 7).

From this figure, it is observed that the indoor-indoor scenarios with the handset as a receiver shows the largest capacity. The median capacity is accountable for at least 80% of the one obtained from the channel matrix with complex Gaussian IID entries. The availability of CSI at the transmit side leads to a significant improvement in the achievable capacity. An increase of 20% in the median capacity as compared to the case where the CSI only known at the receiver is observed. To illustrate the advantage of having the channel knowledge at the transmitter as a function of the reference SNR we calculated the improvement or gain in the channel capacity where the CSI is known at both sides as compared to the case it is only known at the receiver figure (8). At lower SNR level there is a considerable increase in the capacity of up to 240%. The advantage decreases gradually as the reference SNR value increases. It is interesting to see that the capacity gain in the IID case is always lower than the one obtained from the measured data. The reason behind it is that the waterfilling method tries to distributed more power into the
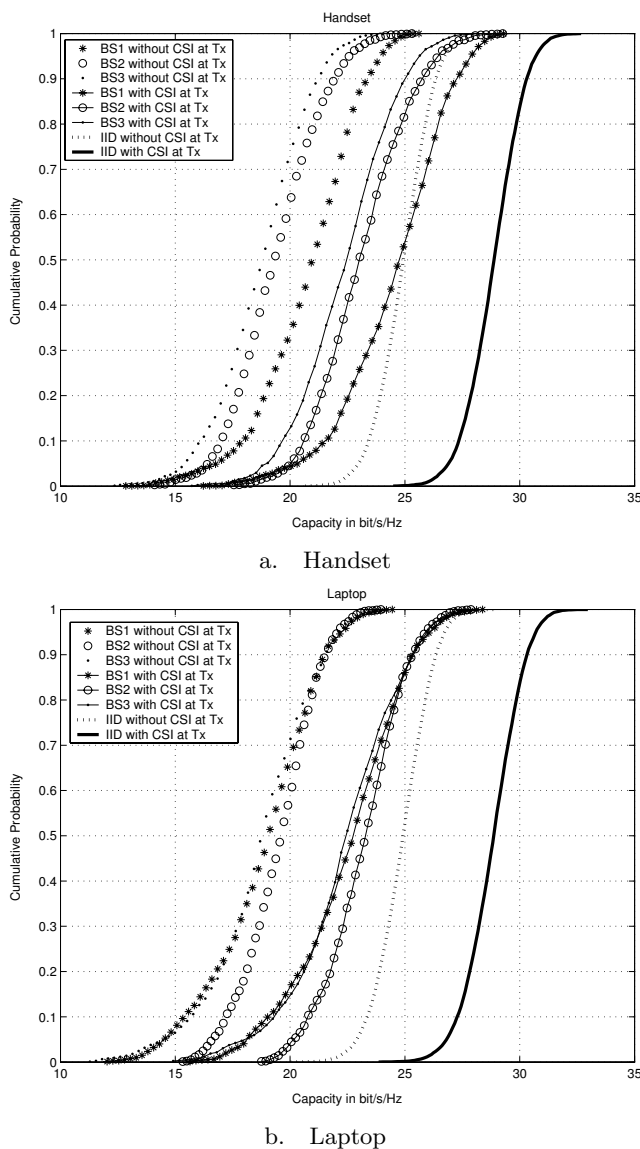
a.    Handset



b.    Laptop

*Figure 7.* Distribution of the channel capacity with the handset and laptop as receiver obtained from all measured sites at the with the system $SNR=20$dB

channels with high gains or high eigenvalues. Together with the fact that the eigenvalues achieved from the measurement distribute over a larger range than those in the IID case, the largest eigenvalue also has a higher value. Therefore the effect of using the waterfilling method becomes more prominent in the measured data than in the IID case.

Without going into the actual numerical calculations of the channel capacity the advantage of having the CSI at the transmitter can be estimated for the IID case when the number of transmitting antennas $N_t$ is much larger than the number of receiving antennas $N_r$. The approximation of the MIMO channel capacity for this case can be found in (Andersen2, 2000). When the CSI is not known at the transmit side the channel capacity can be approximated as

$$C = N_r log_2(1 + SNR) \tag{7}$$

and when the CSI is known at the transmitter

$$C = N_r log_2(1 + SNR\frac{N_t}{N_r}) \tag{8}$$
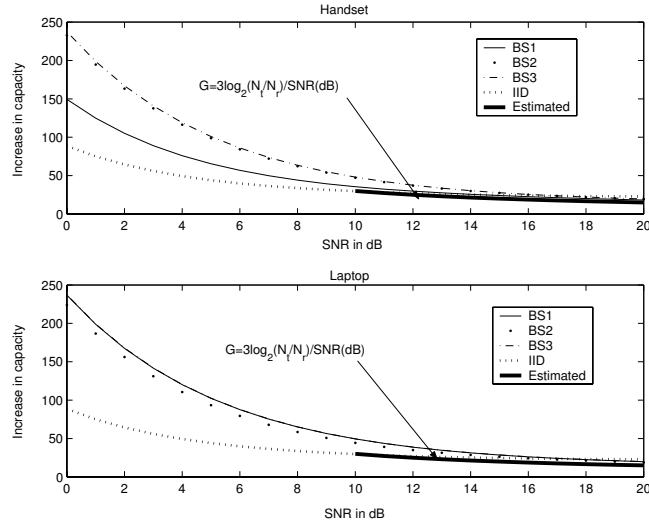
*Figure 8.* The advantage of having the knowledge of the channel at the transmitter as a function of the SNR, in percentage

It can be seen that under such circumstances the capacity of the MIMO channel increases linearly with the number of receiving antennas regardless of whether the channel is known at the transmitter or not. It follows that the advantage of knowing the CSI at the transmit side or the gain in the channel capacity for $N_t \gg N_r$ can be estimated as

$$G = \frac{N_r log_2(1 + SNR\frac{N_t}{N_r})}{N_r log_2(1 + SNR)} - 1 = \frac{log_2(1 + SNR\frac{N_t}{N_r})}{log_2(1 + SNR)} - 1 \approx \frac{3log_2\frac{N_t}{N_r}}{SNR(dB)} \qquad (9)$$

The approximation sign is for the case the value of SNR is much greater than 1. In the same figure 8 we plot the approximation of the capacity gain for the SNR values ranging from 10dB to 20dB with the 8x4 MIMO setup. The result matches with the numerical calculation for the IID data and the measured data quite well.

To highlight the site dependency of the multipath richness of the measured MIMO radio channel, we calculate the mean capacity at each measured location. The mean values of the capacity corresponding to the measured locations, the BS's placement and the receiver's types laptop/handset are plotted in figure 9.a and 9.b.

It is observed that at the same measured location the mean channel capacity does not change significantly by switching the receiver from the handset to the laptop. In some cases, having the handset as the receiver other than the laptop could lead to a higher mean channel capacity (i.e. location 5 BS1, location 6 BS2 and location 2 BS3). This can be explained by the fact that the handset and laptop's antennas are oriented on perpendicular directions. The main beams of the antenna elements at the laptop are faced toward the open door, the place where the signals with high energy are expected to arrive. Therefore the laptop has a higher chance of capturing correlated multipath components. Other thing could be contributed is that the antenna in the laptop has narrower beamwidth (more directional), which can be the result of larger ground plane, than the handset's (almost omnidirectional). Narrower radiation pattern will result in fewer multipath components being received and an increment in the correlation of the received signals at the receiving antennas. Consequently less uncorrelated multipath components impinging on the receiving antennas are captured, even though the distance between antenna elements at the laptop is slightly larger. This will give rise to the reduction of the channel capacity when the laptop is the receiver.

As also investigated in (Kyritsi1, 2002) and (Kyritsi2, 2002) for measured MIMO radio channel along the corridor, it is expected that those locations with high path loss or equivalently lower received power also have a poor multipath scattering characteristics.
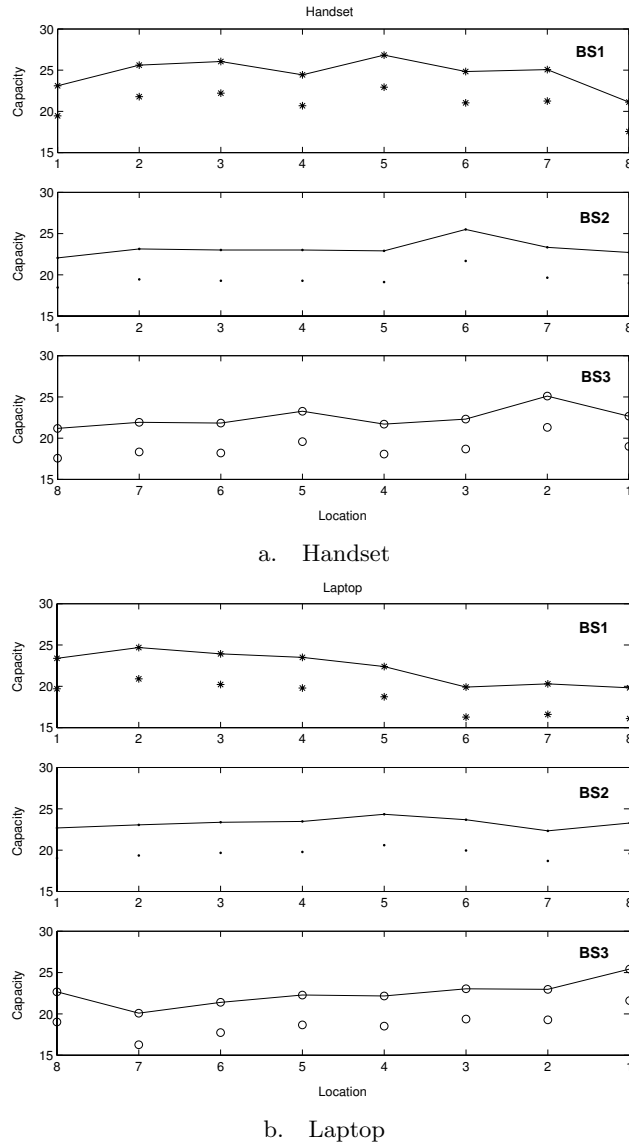
a.  Handset



b.  Laptop

*Figure 9.* The dependency of the mean channel capacity with the handset and laptop as the receiver along the corridor for indoor-indoor and outdoor-indoor setup, $SNR$=20dB, symbol with solid line: Channel is known at Tx, symbol only: Channel is unknown at Tx. Order of the receiver's location has been reversed in the third row

The corridor forming a wave guide will limit the angular spread and the propagation is dominated by a deterministic effect. As a result only components which have enough energy are able to arrive at the receiving antennas. The lack of multiple uncorrelated paths with approximately equal energy will reduce the multipath richness of the environment experienced by the receiving antennas. However, a modest decrement of the capacity along the measured location is only observed in the indoor-indoor scenario with the laptop as a receiver. Roughly speaking the channel multipath richness is independent of the measured locations as well as the type of receiver (either the handset or the laptop).

## 5.  Influence of large-scale variation to the channel capacity

The multipath richness of the radio channel or more specifically the amount of information which can be conveyed is important for any MIMO system. However, for any wireless

system to work properly the fundamental requirement on energy per bit symbol over the noise level must be fulfilled. Therefore, in a thorough assessment of the performance of any MIMO system these two fundamental characteristics: the radio channel multipath richness and the amount of received power should not be separated. It should be mentioned that having both the multipath richness and the averaged received power information is one of the advantage of measuring the MIMO radio channel.

Combining both the received power and multipath richness in the assessment of MIMO performance have been mentioned in (Wallace, 2002), (Svantesson, 2003) and (Mcnamara, 2003). In (Wallace, 2002) and (Svantesson, 2003) the measured channel matrices is normalized by a normalization factor which is the average power of the channel coefficients calculated from the entire measured data set. The channel capacity was then calculated using the normalized channel matrixes and a reference SNR. In (Mcnamara, 2003), the capacity is calculated by directly using the measured channel matrix and very high reference SNR such that after compensating for the path loss we still have positive received power in dB for all measured data set. However, the reference SNR should be chosen with care as the overall SNR (i.e. after compensating for the power loss) cannot be much larger than the actual $\mathtt{SNR}_m$ at the receiver.

Herein we use another approach where the reference SNR is not used, instead the SNR calculated as the ratio of the mean received power and a reference noise level, is used directly in the calculation of the MIMO ergodic capacity, that is

$$\overline{SNR} \approx \frac{\overline{P_{received}}}{\sigma^2_{noise}} \tag{10}$$

Note that we neglect the noise power which is inherently contained in the mean received power. This explains the $\approx$ sign in equation (10).

The capacity of the MIMO channel using this approach can be described by

$$C = \sum_{k=1}^{K} log_2(1 + \frac{\overline{SNR}}{N_t}\lambda_k) \tag{11}$$

And when the CSI in known at both link ends and the waterfilling is used

$$C = \sum_{k=1}^{K} log_2(1 + \lambda_k \gamma_k) \tag{12}$$

where $\gamma_k = max(\mu - \frac{1}{\lambda_k}, 0)$ and the water level $\mu$ is chosen such that $\sum_{k=1}^{K} \gamma_k = \overline{SNR}$.

In the equations above we use the mean received power for one SISO link as the total transmitted power for the MIMO system under consideration. Thereby the significant increase in the channel capacity of the MIMO system over the SISO system is highlighted.

As illustrated in (Amitay, 2001) the influence of the high measurement noise level or low measurement signal to noise ratio $\mathtt{SNR}_m$ to the estimated channel capacity becomes significant when:

i) The channel is correlated or in an extreme case a reflectiveness far field free space wave propagation.

ii) Using rather high reference SNR value as compared to the $\mathtt{SNR}_m$ thereby the effect of erroneous eigenvalues to the channel capacity is exaggerated.

In order to calculate the $\overline{SNR}$ stated in equation (10) care must be taken in choosing the noise level so that with this $\overline{SNR}$ the channel capacity value can be estimated with high reliability. At the same time, the variation of the mean received power is also reflected in the channel capacity. Taking these requirements into consideration and with the note that our measurement MIMO channel is partly correlated and it is measured with high $\mathtt{SNR}_m$, we decided to chose a noise level of -95dBW for all receive branches and all measured

data. As a result, the average SNR value as calculated in equation (10) ranges from -3dB to 40dB. Using this noise level, we calculate the capacity of the MIMO system for two cases where the CSI is assumed to be known at both link ends and at the receiver only. The distribution of the capacity of all measured locations for the indoor to indoor measurement and outdoor to indoor measurement are illustrated in figure 10.
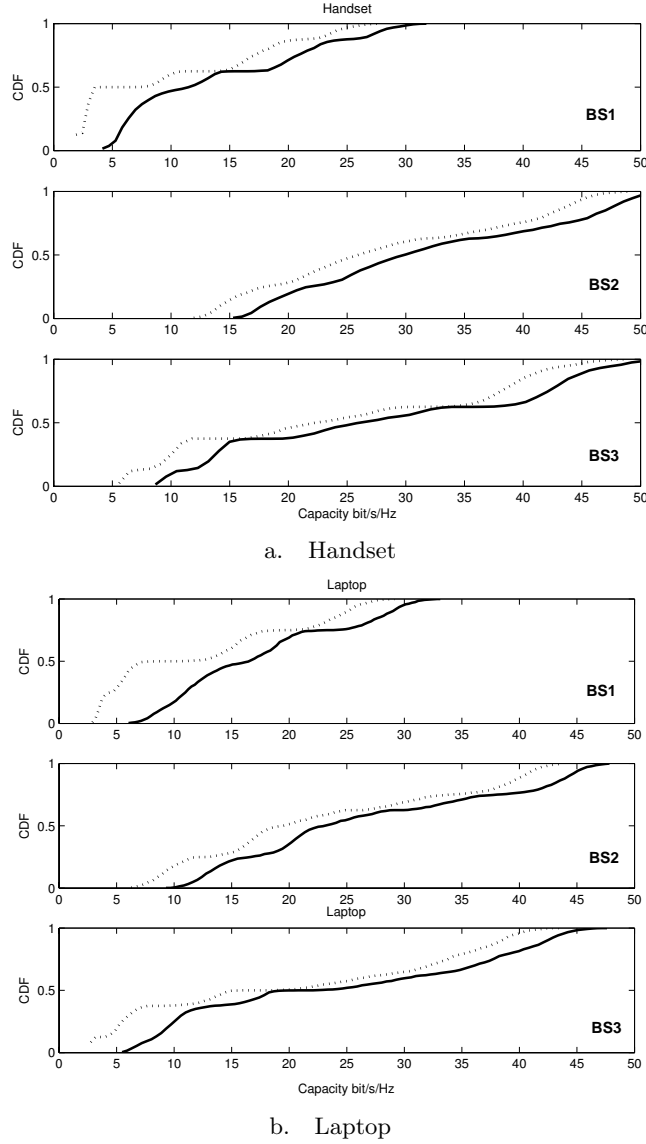


a.    Handset



b.    Laptop

*Figure 10.* Distribution of the capacity of the handset and laptop, using the average SNR for three measurement scenario, Dot lines: Channel is unknown at Tx, Solid lines: Channel is known at Tx

In general, we are interested in the relative change of the MIMO system capacity from one receiver's location to another where both the mean received power and the environmental multipath richness are included. The results of the site dependency of the MIMO capacity calculated in this way are illustrated in figure 11. Note that the mean capacity at one measured location is obtained by averaging the ergodic capacities at all measured snapshots. Because the mean received power at one measured location is retained, there is a larger spread in the MIMO capacity along the corridor.

By comparing figure 9 and figure 11 significant difference in the trend of the capacity along the measurement location can be noted. On one hand, when there are perfect amplifier and attenuator at the receiver so that the SNR for one SISO link is unchanged

regardless of the receiver's location, the capacity or the multipath richness of the measured environment along the corridor almost remains the same. On the other hand, when the capability of the amplifier and/or attenuator at the receiver is limited, which is common in practice, the variation in the mean received power has greater influence on the change of the channel capacity than variation in the multipath richness properties of the MIMO radio channel does.
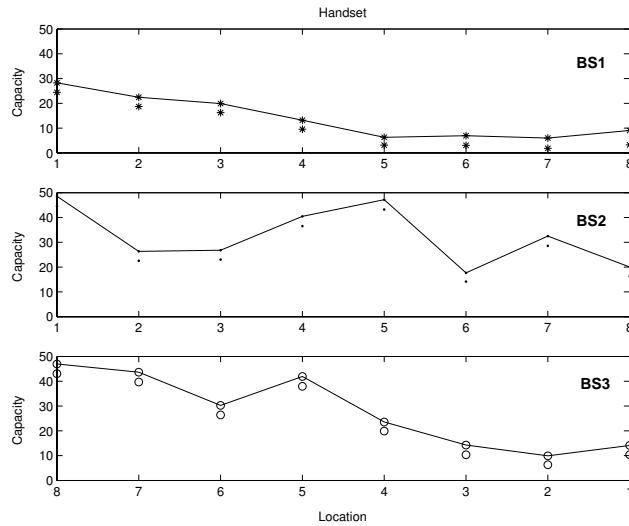


a.　Handset
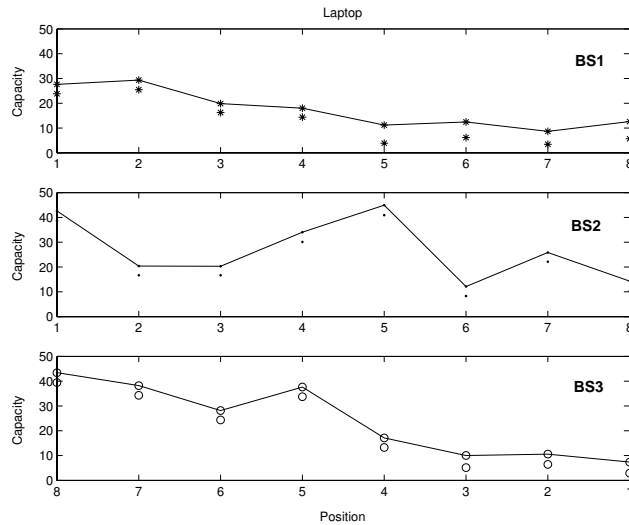


b.　Laptop

*Figure 11.* The mean channel capacity with the handset and laptop as the receiver along the corridor, using the average SNR, symbol with solid line: Channel is known at Tx, symbol only: Channel is unknown at Tx

The advantage of having the CSI at the transmitter over the case it is unknown in terms of the gain in the mean capacity is also illustrated. As expected the ergodic capacity when the channel is known to the transmitter is always higher than the ergodic capacity when the channel is unknown. However, the general trend is that the gain decreases as the received power increases. This indicates the fact that the advantage of knowing the channel at the transmitter reduces at higher SNR values.

## 6. Conclusion

In this paper, using a narrowband analysis we have evaluated the performance of the 8x4 measured MIMO system for indoor-indoor and outdoor-indoor scenarios. To mimic a real MIMO system, a prototype of a BS with eight outputs and prototypes of small terminals such as mobile handset and laptop with four patch antennas were deployed in the measurement. General properties of the measured MIMO radio channel as well as its distinct characteristics those adhere to the measurement environment and scenarios have been analyzed and discussed. The mean received power decreases steadily as the distance between the transmitting antennas and the receiving antennas increases. The multipath richness characteristics of the measured radio channel is almost independent of the measured locations as well as the type of the receiver (either handset or laptop). The distributions of the eigenvalues or the gains of the subchannels observed from the measurement data were spread over a larger range than that of the theoretical channels with identical independently distributed (IID) complex Rayleigh fading components. It is shown that when there are perfect amplifier and/or attenuator so that the mean SNR remains constant i.e. 20dB, the median capacity of the measured MIMO channel is accountable for at least 80% that of system with IID components. This indicates that in order to obtain full diversity gain and diversity order it is still make sense to deploy multiple antennas in a small terminal. The gain in channel capacity which is resulted from knowing the channel at the transmitter is significant for low SNR. At the SNR value of 20dB, using the measured data we show that by knowing the channel at both ends of the transmission link it is possible to obtain up to 20% increase in the channel capacity as compared with the case where the channel is known at the receive side only. However, the gain gradually reduces at higher received power or higher SNR value. We estimate the channel capacity where both the change in the mean received power and the change in the MIMO radio channel multipath characteristics are included. The analysis show that the variation in the mean received power can have greater influence on the overall system performance than the change in the multipath scattering property.

## Acknowledgement

## References

M.Steinbauer, A.F.Molisch, and E.Bonek  The double-directional radio channel. *IEEE Antennas and Propagation Magazine*, vol. 43, pages 51-63, August 2001.

R.Thoma, D.Hampicke, M.Landmann, G.Sommerkorn, and A.Richter  MIMO measurement for double-directional channel modelling. *IEE Seminar on MIMO: Communications Systems from Concept to Implementations*, pages 1-7, December 2001.

J.Medbo and J.E.Berg Spatio-Temporal channel characteristics at 5 GHz in a typical office environment. *IEEE Vehicular Technology Conference* vol. 3, pages 1256-1260, October 2001.

T.Fugen, G.Sommerkorn, J.Maurer, D.Hampicke, W.Wiesbeck and R.Thoma. MIMO capacities for different antenna arrangements based on double directional wide-band channel measurements. *The 13th IEEE International Symposium on Personal, Indoor and Mobile Radio Communications* vol.4, pages:1777 - 1781, September 2002

D.Chizhik, J.Ling, P.W.Wolniansky, R.A.Valenzuela, N.Costa, and K.Huber  Multiple-input-multiple-output measurements and modeling in Manhattan. *IEEE Journal on Selected Areas in Communications* vol. 21, pages 321-331, April 2003.

D.P.Mcnamara, M.A.Beach, P.Karlsson, P.N.Fletcher. Initial characterisation of multiple-input multiple-output (MIMO) channels for space-time communication. *IEEE VTS-Fall VTC 52nd*, pages 1193 -1197, Semtember 2002.

J. Kivinen, P. Suvikunnas, L. Vuokko, and P. Vainikainen Experimental investigations of MIMO propagation channels. *IEEE Antennas and Propagation Society International Symposium*, vol. 3, pages 206-209, June 2002.

J.P.Kermoal, P.E.Mogensen, S.H.Jensen, J.B.Andersen, F.Frederiksen,T.B.Sorensen, K.I.Pedersen Experimental investigation of multipath richness for multi-element transmit and receive antenna arrays. *IEEE 51st VTC 2000*, vol. 3, pages 2004-2008, 2000.

K.Yu, M.Bengtsson, B.Ottersten, P.Karlsson, D.McNamara and M.Beach Measurement Analysis of NLOS Indoor MIMO Channels. *IST Mobile Communications Summit, 2001*, pages 277 - 282.

T.Svantesson, J.Wallace On signal strength and multipath richness in multi-input multi-output systems. *IEEE International Conference on Communications*, vol.4 , pages 2683 - 2687, May 2003.

M.B.Knudsen, G.F.Pedersen Spherical outdoor to indoor power spectrum model at the mobile terminal. *IEEE JSAC Issue: 6 vol.20* pages 277 - 282, August 2002.

I.E.Telatar Capacity of Multi-antenna Gaussian Channels. *European Transactions on Telecommunications, No.6*, vol. 10, pages 585-595, 1999.

J.B.Andersen Antenna arrays in mobile communications: gain, diversity, and channel capacity. *IEEE Antennas and Propagation Magazine, Issue: 2*, vol.42, pages 12-16, 2000.

M.J.Gans, N.Amitay, Y.S.Yeh, Hao Xu, T.C.Damen, R.A.Valenzuela, T.Sizer, R.Storz, D.Taylor, W.M.MacDonald, Cuong Tran and A.Adamiecki Outdoor BLAST measurement system at 2.44 GHz: calibration and initial results. *IEEE Journal on Selected Areas in Communications, Issue: 3 , vol.20, April 2002.*

J.B.Andersen Array gain and capacity for known random channels with multiple element arrays at both ends. *IEEE Journal on Selected Areas in Communications, Issue: 11*, vol.18, pages 2172 - 2178, November 2000.

P.Kyritsi, N.Kadri, E.Thang, D.C.Cox Signal correlation in a hallway environment using waveguide mode analysis. *IEEE VTC, 2002*, vol.2, pages 787 - 791, 2002

J.W.Wallace, M.A.Jensen, A.L.Swindlehurst, B.D.Jeffs Experimental characterization of the MIMO wireless channel: data acquisition and analysis. *IEEE TWC, Issue: 2*, vol.2, pages 335 - 343, March 2003.

T.Svantesson, J.Wallace, On signal strength and multipath richness in multi-input multi-output systems IEEE International Conference on Communications vol.4, 2683 - 2687, 2003

P.Kyritsi, D.C.Cox, R.A.Valenzuela, P.W.Wolniansky Effect of antenna polarization on the capacity of a multiple element system in an indoor environment. *IEEE Journal on Selected Areas in Communications, Issue: 6*, vol.20, pages 1227 - 1239, August 2002.

D.P.Mcnamara *Characterisation and Investigation of Multiple-Input Multiple-Output Wireless Communications Channel.* PhD thesis University of Bristol Faculty of Engineering, 2003.

N.Amitay, M.J.Gans, H.Xu, R.A.Valenzuela Effects of thermal noise on accuracy of measured BLAST capacities. *IEE Electronics Letter, Issue: 9*, vol.37, pages 591 - 592, 2001

**Paper 2:**
**The influence of outdoor environment on MIMO system performance.**
H.T.Nguyen, J.B.Andersen and G.F.Pedersen.
WPMC 2005, Aalborg, Denmark.

# The influence of outdoor environment on MIMO system performance

Hung Tuan Nguyen, Jørgen Bach Andersen, Gert Frølund Pedersen
Department of Communication Technology, Niels Jernes Vej 12, DK-9220 Aalborg , Denmark
Email: {htn,jba,gpf}@kom.auc.dk

*Abstract—* In this paper, initial analyses on the performance of a MIMO system in terms of the channel capacity and the environment scattering richness are presented. The assessments are based on the wideband outdoor measurement data of an 8x4 MIMO system. Several mounted positions of a prototype mobile handset were considered in order to evaluate the influence of local scattering, shadowing and absorption on the system performance. While the multipath richness is almost the same for different local environments, the variation of the power loss is significant. We showed that it still makes sense to implement MIMO in outdoor environment and the relation between the channel multipath richness and the mean path loss could be of interest for system implementation and evaluation.

## I. INTRODUCTION

Multiple input multiple output (MIMO) systems have a potential of offering higher capacity than a traditional Single input single output (SISO) systems by utilizing space, polarization or pattern diversity [1], [2]. The gain obtained by MIMO system, however, depends on the scattering richness of the environment it is operated in. The assumption of identical independently distributed (IID) of the channel matrix's components only holds true for certain scenarios. Therefore, in order to judge the claimed potential performance, extensive measurements should be carried out.

In general, with a fixed received power level the performance of a MIMO system is heavily dependent on the decorrelation of the channels. The more uncorrelated the channels the more diversity gain can be obtained. Since the capacity of the MIMO system is a function of the eigen values of the channel matrix, channel decorrelation in return gives rise to the enhancement of the channel capacity. Hence the theoretical capacity is normally used as a metric for evaluating the performance of the MIMO system which is composed of the transmit-receive antennas and the environment under investigation. Analysis on channel capacity for outdoor environment with a fixed reference SNR can be found in [3],[4] among others.

Besides the channel decorrelation, the overall performance of a MIMO system channel, like that of any SISO system, is also determined by the received power level. While the first parameter is decided by the environmental multipath richness the second parameter depends on the radio channel characteristics such as the distance between the base station and the mobile handset, the line of sight (LOS) and non line of sight (NLOS) components, the height of transmit, receive antenna and the antenna radiation pattern. Accessing the overall performance of MIMO systems, therefore, should include both features of the propagation channels namely the multipath richness and the amount of received power into account. For indoor measurement, evaluation on the tradeoffs between multipath richness and received power levels can be found in [5], [6] and [7].

In this paper, we used both aforementioned approaches to evaluate the performance of a measured MIMO system. The analyses base on data acquired from extensive outdoor measurement campaign in downtown Aalborg. Transmitted antenna of 8 elements mounted at rooftop level and a prototype of 4 elements antenna handset on a moving car, forming a real cellular MIMO system were deployed. In order to estimate the effects of real case scenario on the channel capacity, several mounted positions of the mobile handset were deployed such as in freespace, near a phantom's head and inside a car.

The rest of this paper is organized as follows. In section II system set up and measurement environment is described. Characterizations of the measured channel are presented in section III. The capacity of the measured MIMO system with normalization of the channel transfer function and the correlation between the channel capacity and the mean received power level are investigated in section IV. Effects of the mean path loss on the channel capacity are treated in section V where influence of local absorption and shadowing caused by phantom's head and car are also investigated. The paper ends with conclusions and remarks in section VI.

## II. SYSTEM SET UP AND MEASUREMENT ENVIRONMENT

In our measurement campaign we used code phase offsetting technique to obtain the complex channel impulse response. A PN sequence of length 511 bits with the chip rate 7.665 MHz transmitted at the center frequency of 2140MHz was implemented. At the receive side, the signal was sampled at a rate of 15.36 MHz. An antenna array with 8 outputs, a BS antenna prototype made by ALLGON in Sweden was deployed at the transmit side. The total transmitted power was set to 7W or equivalently 8.45 dBW during the measurement.

A prototype of commercial mobile handset was used at the receive side. This handset was equipped with 4 patch antennas (labelled as A1,A2, B1, B2 in figure 1(a)) at the four corners and the conducting cables were replaced by optical fibres to avoid disturbance of the radiation pattern. The distance between the vertical patch antennas was 0.5 wavelength. It was 0.25 wavelength for the horizontal patch antennas. The
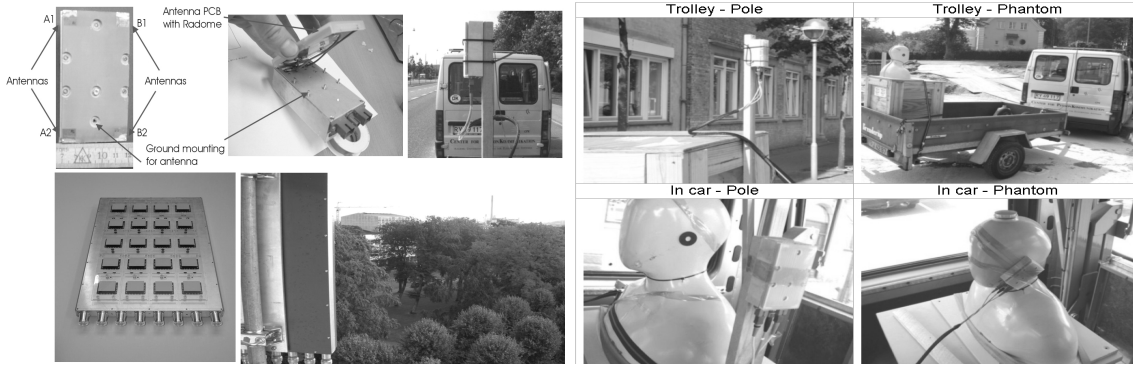
(a) Optical handset and the BS setup  (b) Setting of the handset in measurement

Fig. 1.   Measurement setup, handset and measurement scenario (top), BS and view point from the BS(bottom)

consuming power at the handset was supplied by an embedded battery.

With these setting, the measurement signal to noise ratio $SNR_m$ was well beyond 40dB from most of the measured routes. In our measurement campaign, a sampling distance of 2.04m was followed by a travelled distance of 8.07m. During the active distance of 2.04 m, 44 IR(s) of 32 channels (44 snapshots) were collected. The total number of measurement snapshots was 4400 which made up a route distance of around 1 km. The following analyses are based on the data collected from two routes with four different mounted positions of the handset. Figure 1 shows the setup of the transmitting and receiving antennas during the measurement campaign.

### III. CHANNEL PARAMETERIZATIONS FROM THE MEASUREMENT DATA

#### A. Root mean square delay spread

Root mean square (RMS) delay spread is a useful parameter to reveal the time dispersion of the channel. The RMS can be calculated from the first and second moment of the average power delay profile ($\overline{PDP}$). The $\overline{PDP}$ is calculated from the 44 IRs measured in a distance of 2 meters. To avoid quantization noise and correlation noise a threshold of 30dB was applied to the $\overline{PDP}$. Those components of the $\overline{PDP}$ which are lower than 30dB from the $\overline{PDP}$'s main peak are set to zero. In the estimation of RMS delay spread, all 32 channels and 70 out of 98 available IR's taps were used. To evaluate the frequency selective characteristics of the measured radio channel we used the data collected from the measurement where the handset was mounted on the wooden pole on a trolley. The median RMS delay spread for two routes were $0.28\mu$ and $0.6\mu$, respectively. The range of the spread is typical for outdoor, urban environment. As the chip rate of the PN sequence in our measurement was 7.665MHz, the theoretical delay resolution was $0.1305\mu$s. These median RMS delay spread values are higher than the measured delay resolution (a factor 2 for the first route and factor of 5 for the second route). Therefore in the following the analysis of the measured MIMO channel is based on its wideband information.

#### B. Average received power

The instantaneous received power at one measured snapshot is calculated as the sum of the PDP's taps. After averaging the received power over the number of SISO channels, which is 32 in our case, we have the average received power

$$\overline{P_{received}} = \left( \frac{1}{N_t N_r} \sum_{i=1}^{i=N_t} \sum_{j=1}^{j=N_r} \sum_{l=1}^{l=L} PDP_{ij}(l) \right) \quad (1)$$

where $N_t$ is the number of transmitting antennas, $N_r$ is the number of receiving antennas and $L$ is the number of used taps. In figure 3 we show the change in the average received power along the two measured routes. Notice that for particular route, the average received power decreases as in the order of "Trolley-Pole", "Trolley-Phantom", "In car-Pole" and "In car-Phantom". The decreases in the average received power are illustrated as curves with the same shape along the route but offset from each other by a certain amount depending on the mounted position of the handset. Obviously the power absorption by the phantom's head and body shadowing of the car are the main reasons for the reduction in the average received power. Table I shows the relative power loss caused by local absorption and shadowing with the free space "Trolley-Pole" scenario as a reference for the two measured routes. We note

TABLE I
MEAN RELATIVE POWER LOSS CAUSED BY LOCAL ABSORPTION AND SHADOWING

| Route | Trolley-Phantom | In car-Pole | In car-Phantom |
|-------|-----------------|-------------|----------------|
| 1 | 2.1 dB | 4.2 dB | 6.7 dB |
| 2 | 2.3 dB | 5.0 dB | 6.6 dB |

that the average absorption loss of the order of 2dB caused by the phantom's head is fairly close to the 3dB body loss measured for patch antennas reported in [8].

### IV. CAPACITY OF NORMALIZED CHANNEL MATRIX

Calculating the channel capacity from a reference SNR and normalized channel matrix is a common way of evaluating
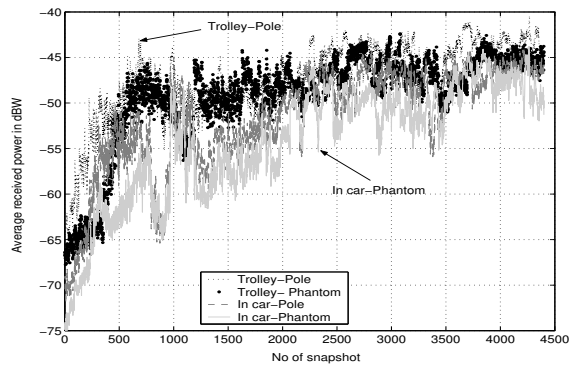
(a) The first route
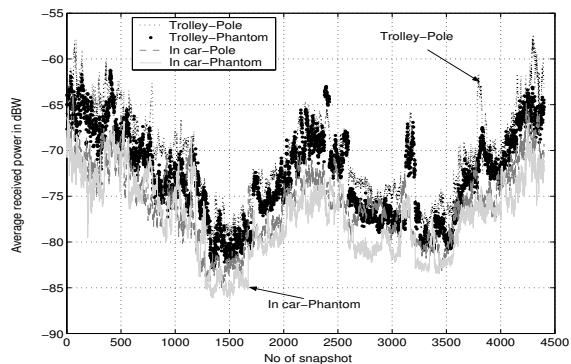


(b) The second route

Fig. 2.   Average received power along the two routes



Fig. 3.   CDF of the channel capacity with $SNR = 20dB, N_t$=8 $N_r$=4, for both measured routes

the performance of a measured MIMO channel. The capacity reveals the capability of the measured MIMO system in capturing enough multipath components and more importantly the amount of information it can theoretically convey.

Because the wideband information is used, analysis of the channel coefficients characteristics is carried out in the frequency domain. The IR(s) of 32 transmitting-receiving pairs are first converted to the frequency domain by FFT. Again, to avoid the unwanted noise we only use 70 out of 98 available taps in each measured IR. Moreover, of those 70 channel coefficients we decided to use 50 components whose corresponding frequencies are nearest to the center frequency. This corresponds to a bandwidth of 10.95 MHz. The measured channel matrix at frequency $f_l$ is normalized such that the Frobenius norm of the normalized $H_{f_l}$ is equal to $\sqrt{N_t \times N_r}$. Thereby the channel gain is ignored or removed through the normalization process.

In the calculation of the channel capacity, we assume that the channel matrix is only known at the receive side. With the knowledge of the channel only at the receiver, equally distributed power seems to be the most reasonable scheme for distributing the transmitted power. For a wideband channel, if the frequency step is small enough such that we can consider the spectrum to be flat in that step, the channel capacity can

be calculated as

$$C = \frac{1}{L} \sum_{l=1}^{L} (log_2(det(I + \frac{SNR}{N_t} H_{f_l} * H_{f_l}^H))) \qquad (2)$$

Using this way of calculation, the capacity of the measured MIMO channel is evaluated at a reference $SNR$ of 20dB. Figure 3 demonstrates the CDF of the channel capacity along both the measured routes with different mounted positions of the handset. In general, the 8x4 outdoor MIMO system has a median capacity of about 20 bit/s/Hz. This number accounts for 80% of the capacity obtained in an 8x4 MIMO system with IID components. But it is observed that as long as the reference SNR is fixed, the distributions of the channel capacity are independent from the mounted positions of the handset, whether it is in a metal cage (inside a car) or on an open platform (on a trolley). This observation may indicate that in an outdoor environment the immediate surroundings such as human, car etc. do not significantly enrich the environmental multipath richness. The environmental characteristics of the route in which numerous strong, uncorrelated multipaths were created have greater influence on the channel capacity. The median capacity of the system increases from 18 bit/s/Hz in the first route to 21 bit/s/Hz in the second route.

Because of the short range measurement distance (approximately 1 km) and dense urban environments, the contribution of the free space path loss to the variation of the overall mean path loss is negligible. The maximum variation of the free space path loss in the measured routes was found in the order of 5dB by using a well known free space path loss formula. Instead, path loss caused by the shadowing and power absorption of major obstacles such as buildings, trees as well as the surrounding objects must be the main reason. These objects in turn contribute to the scattering richness of the environment, which the channel capacity is entirely dependent of. Hence, the dependence of the channel capacity on the path loss could be explained by the relationship between the number of equivalently strong and uncorrelated components and the mean path loss. Note that the path loss has a direct influence on the amount of power that could be received. High mean path loss or equivalently low average received power could suggest that there is richer scattering environment. This

in turn, give rises to an enhancement in the diversity gain as of richer multipath environment. Of course, this argument only holds true as long as the measured $SNR_m$ is above a certain threshold so that the system noise could not significantly contribute to the randomness of each channel coefficient.

Having the average received power and the channel capacity associated with a specific position along the route it is now possible to find their dependence. The results shown in figure 4 demonstrate a strong correlation between the MIMO system capacity and the received power the same location. In order
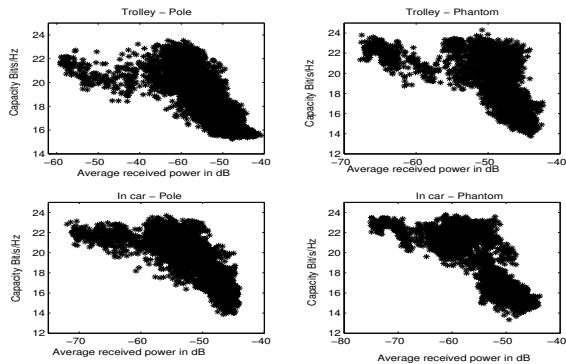


(a) Route 1
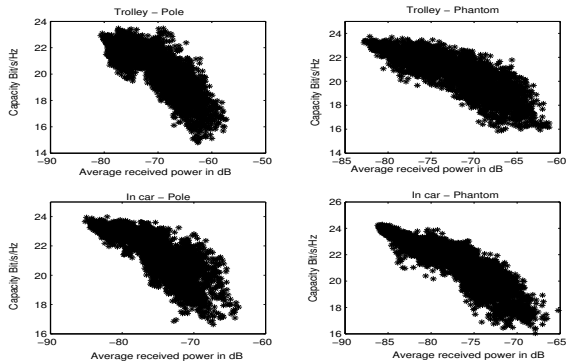


(b) Route 2

Fig. 4.   Dependence of the channel capacity and the mean received power of two measured routes

to give a sense of how correlated they are, the correlation coefficient between the channel capacity and the average received power is calculated and shown in table II. In fact, the environment in the second route which is composed of blocks of building giving denser scatterers environment than in the first route, does give lower correlation. Therefore it can be concluded that for a fixed reference SNR values the location which has higher average received power will have lower capacity and vice versa.

| Route | Trolley - Pole | Trolley - Phantom | In car - Pole | In car - Phantom |
|-------|------|---------|------|---------|
| 1 | -0.72 | -0.62 | -0.76 | -0.82 |
| 2 | -0.81 | -0.83 | -0.81 | -0.88 |

## V. DEPENDENCE OF THE CHANNEL CAPACITY ON THE POWER LOSS

In the evaluation of the MIMO system capacity presented in section IV the average received power has been deliberately ignored by means of normalization thereby the scattering characteristics of the environment is highlighted. Analysis on the channel capacity with fixed reference SNR showed that the scattering richness of the measured radio channel is independent of the mounted position of the handset. However as has been studied in section III the local absorption and shadowing caused by car and phantom's head on the other hand has certain impact on the received power levels. Thus, these changes in the received power level, which often result from real-life usage, have a greater influence on the true capacity of a MIMO system than the changes in the scattering richness do. Hence, practically, in order to compare the performance of the MIMO systems with difference settings and fixed transmitted power two important properties of the measured MIMO channel must be taken into account namely the multipath richness and the path loss.

Assuming that each receive branch has the same white noise level, one way to assess the effect of power loss on the channel capacity is to use additional received power information instead of the reference transmitted power in the formulation of the channel capacity. Thereby the average $SNR$ at one measurement snapshot is given by

$$\overline{SNR} \approx \frac{\overline{P_{received}}}{\sigma_{noise}^2} \qquad (3)$$

is directly used in the channel capacity formula. Note that the average $SNR$ is also the average $SNR$ for one SISO link. In fact the average received power contains the inherent measurement noise, this explains the approximation sign in the equation.

In our measurement campaign, the source of the noise is mainly the correlation noise and quantization noise and therefore the measured signal to noise ratio, $SNR_m$ is fairly constant. Nevertheless, the measurement noise will add more scattering richness to the measured channel matrix, causing errors in the eigenvalues (see [9]). To restrain the effect of the erroneous eigenvalues to the channel capacity the reference $\overline{SNR}$ should be smaller than the $SNR_m$ value. Herein, for each measured route we chose a noise level such that the maximum $\overline{SNR}$ as calculated in equation (3) is lower than 35dB. In doing that the effect of measurement noise causing erroneously high channel capacities is somehow limited. At the same time the effect of path loss, shadowing and absorption

loss are included in the calculation of the channel capacity. The channel capacity can be calculated as in equation 2 with the reference SNR replaced by the average $\overline{SNR}$. The variation of the channel capacity along the two measured routes is illustrated in figure 5. Capacity degradations resulting from
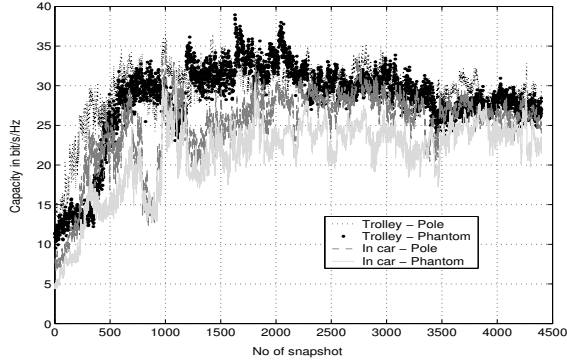


(a) Route 1
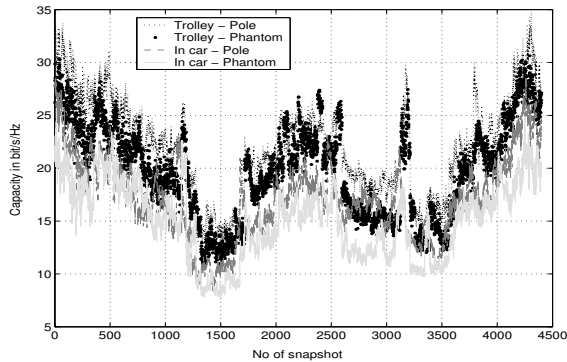


(b) Route 2

Fig. 5. Variation of the capacity along two measured route when the average received power is taken into account

the mounted positions of the handset can clearly be seen. As expected the "In car-Phantom" scenario gives the lowest capacity due to the lower $\overline{SNR}$ values associated with this setting. In general, the channel capacity spreads over a large range and closely follows the change in the average received power.

It is interesting to compare the change in system performance obtained in one mounted position of the handset relative to the other positions where both the multipath richness property and the power loss information of the measured radio channel are included. From these relative values we can estimate the penalties imposed by absorption and shadowing on the systems' performance. Using the free space scenario "Trolley-Pole" as reference, the mean capacity degradations of the "Trolley-Phantom", "In car-Pole" and "In car- Phantom", over the "Trolley - Pole" scenarios are calculated and listed in table III. By only changing the mounted position of the handset, significant degradation in the channel capacity can be

TABLE III

MEDIAN CAPACITY LOST WITH THE BEST CASE SCENARIO

"TROLLEY-POLE" AS A REFERENCE

| Route | Trolley-Phantom | In car-Pole | In car-Phantom |
|-------|-----------------|-------------|----------------|
| 1 | 10% | 26% | 45% |
| 2 | 16% | 33% | 48% |

observed. When the handset is used inside the car and close to the phantom's head the channel capacity decreases by up to 45% as compared to that in free space scenario.

## VI. CONCLUSION AND REMARKS

In this work the capacity of measured outdoor MIMO system has been evaluated. It was found that the outdoor MIMO system with 4 patch antennas handset and 8 antennas array at the BS can provide up to 80% median capacity according to that of IID case for SNR=20dB. Strong correlations between the normalized capacity and mean receiver power level have been observed. This phenomenon could be explained by the fact that the mean path loss is dependent upon the degree of multipath richness in outdoor urban environment. By including the effect of mean path loss, it is possible to compare the performance of MIMO system where local absorption and shadowing such as car, phantom are presented. The absorption and shadowing body of the phantom's head could lead to a reduction of 12% in capacity. Meanwhile, shadowing of the car alone could reduce the channel capacity by 30%.

## REFERENCES

[1] G.J.Foschini, "Layered space-time architecture for wireless communication in fading environment when using multi-element antennas" Bell Labs Tech. J., 4159, 1996.
[2] I.E.Telatar "Capacity of Multi-Antenna Gaussian Channels. AT&T Bell Labs". 522526, 1995.
[3] K.Sulonen, P.Suvikunnas, L.Vuokko, J.Kivinen, P.Vainikainen, "Comparison of MIMO antenna configurations in picocell and microcell environments" IEEE JSAC, 21(5),703-712, 2003.
[4] D.Chizhik,J.Ling, P.W.Wolniansky, R.A.Valenzuela, N.Costa, K.Huber "Multiple-input-multiple-output measurements and modeling in Manhattan" IEEE JSAC, 21(3), 321-331, 2003.
[5] D.P.Mcnamara "Characterisation and Investigation of Multiple-Input Multiple-Output Wireless Communications Channel", PhD thesis University of Bristol Faculty of Engineering, 2003.
[6] J.W.Wallace, M.A.Jensen, A.L.Swindlehurst, B.D.Jeffs "Experimental characterization of the MIMO wireless channel: data acquisition and analysis", IEEE TWC, 2(2), 335-343, 2003.
[7] T.Svantesson, J.Wallace "On signal strength and multipath richness in multi-input multi-output systems", IEEE ICC, 4, 2683-2687, 2003
[8] G.F.Pedersen, K.Olesen, S.L.Larsen, "Bodyloss for handheld phones" 49th IEEE Vehicular Technology Conference 1999, Volume: 2, Pages: 1580-1584.
[9] N.Amitay, M.J.Gans, H.Xu, R.A.Valenzuela "Effects of thermal noise on accuracy of measured BLAST capacities", Electronics Letters , 37(9), 591-592, 2001.

**Paper 3:**
**A stochastic model of spatio-temporally correlated narrowband MIMO channel based on indoor measurement.**
H.T.Nguyen, J.B.Andersen and G.F.Pedersen**.**
15th IEEE International symposium on Personal, Indoor and Mobile communications Barcelona Spain, September, 2004, Vol 3, 1827-1831.

# A STOCHASTIC MODEL OF SPATIO-TEMPORALLY CORRELATED NARROWBAND MIMO CHANNEL BASED ON INDOOR MEASUREMENT

**Hung Tuan Nguyen, Jørgen Bach Andersen, Gert Frølund Pedersen**

Department of Communication Technology, Niels Jernes Vej 12, DK-9220 Aalborg , Denmark
Email: {htn,jba,gpf}@kom.auc.dk

**Abstract -** In this work we propose a spatio-temporal model for narrowband indoor non line of sight (NLOS) MIMO channel. The model bases on the parameterization from measured 8x4 MIMO radio channel. Validation of the model performance is made by comparing the estimated capacity and the temporal characteristic with these obtained from measurement. The results show that our model is capable of capturing the essential characteristics of a temporally correlated multipath MIMO radio channel.

**Keywords -** MIMO, indoor measurement, spatial-temporal correlation, stochastic model

## I. INTRODUCTION

Multiple-input multiple-output (MIMO) systems have appeared as a new method for high capacity in wireless communication. In order to be able to evaluate the algorithm/air-interface performance at higher layer of the MIMO system, we need a model to establish the behavior of channel propagation and antennas. Although numerous channel models have been proposed for the MIMO radio channel, most of them only concentrated on the spatial domain to highlight the potential of MIMO system in providing high data rate without requiring extra bandwidth and power. The temporal variation of the channel is often ignored in these models. However, in order to make a full use of the diversity gain the channel coefficients must be appropriately known at least at the receiver. Not being able to update the channel coefficient timely could lead to system performance degradation. Because of its importance, a number of works has been devoted to the study of the temporal variation of the MIMO radio channel characteristic. Analysis on the variation in time of the measured MIMO radio channel may be found in (e.g. [1] and [2]) among others.

The main objective of this paper is to establish a stochastic model in both spatial and temporal domain based on data collected from the 8x4 MIMO system indoor measurement campaign. Here, the spatial domain refers to the small-scale spatial variation of the received signal responsible for the correlation of the closely space antennas. Meanwhile temporal domain refers to the evolution of the channel coefficients in time, which is caused by the movements of the transmitting/receiving antennas and/or movements of surrounding objects. By doing that not only the spatial characteristic but also the temporal behaviors of the measured

radio channel are retained. We show that the model is able of capturing the major MIMO channel characteristics both in time and space.

The paper is organized as follows. We first present the measurement environment and set-up. After that the proposed model is described. Next, a method for extracting the temporal and spatial parameters from the measured data is presented. Based on these measured parameterizations, the model's performance is evaluated separately in spatial and temporal domain. The paper ends with conclusion and remarks.

## II. MEASUREMENT ENVIRONMENT AND SYSTEM SET-UP

Center for Personal Kommunication's (CPK) sounder system is built on post-processing and real antenna array technology. A code phase offsetting technique with the use of pseudo noise sequence (PN) is applied. In our indoor measurement campaign a PN sequence of length 511 bits with the chip rate of 7.665MHz was transmitted at the center frequency of 2140MHz. At the transmit side we use 8 outputs antenna array, a base station (BS) antenna prototype made by ALLGON. The handset is equipped with 4 patch antennas at the four corners and conducting cable is replaced by optical fibre to avoid radiation disturbance. In the campaign the handset was mounted on a stick which is in turn carried by a sledge. The sledge was capable of moving the handset linearly over a distance of 1.638m ($11.4\lambda$) with a speed of 23.4 mm/s. The sampling distance was 7mm which made up 20 samples per wavelength. This gives a total number of 32x234 channel impulse responses (IR) at one measured location. The height of the antennas at the BS and the handset were 1.75m and 1.69m respectively. The layout of the measured site was an office building with different offices on the same floor, figure 1. The arrows in this figure illustrate the direction of displacement of the handset and the BS. The setup of the handset and BS during the measurement is illustrated in figure 2.

## III. DISCRETE TIME STOCHASTIC CHANNEL MODEL

### A. Spatially correlated model

Let us consider the narrowband MIMO system with $N_t$ transmitting antennas and $N_r$ receiving antennas. The stochastic model based on the measured data of indoor
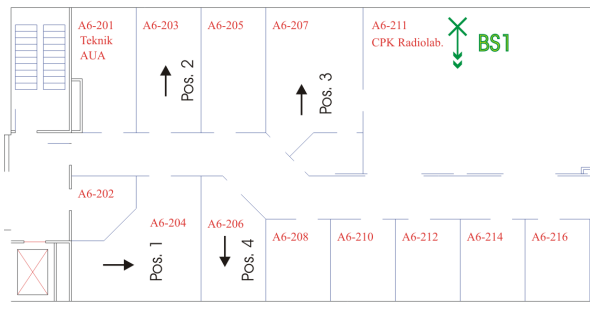
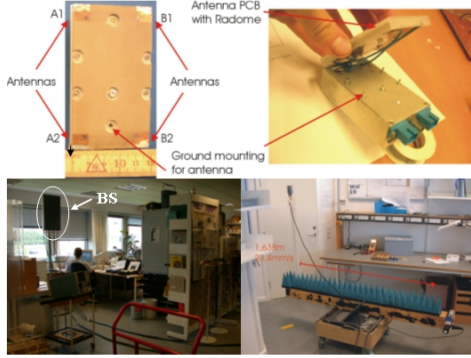Fig. 1. Top view layout of the measurement site.



Fig. 2. Measurement's setup.

narrowband MIMO system has been thoroughly study in [3], [4] and [5] among others. In the model, NLOS is assumed and more importantly the independency of the spatial correlation seen from the transmitter and the receiver must be fulfilled. With this assumption, the channel covariance matrix can be approximated as the Knonecker product of the spatial correlation matrices at the transmitter and receiver respectively, that is

$$R = E(vec(H)vec(H)^H) \approx R_{Rx} \otimes R_{Tx} \qquad (1)$$

In this equation $E(.)$ denotes the expectation operator; $(.)^H$ denotes the the complex transpose operator and $\otimes$ denotes the Knonecker product.

The correlated MIMO channel, $\widetilde{H}$ may be modelled by

$$vec(\widetilde{H}) = R^{1/2}vec(H_{iid}) \qquad (2)$$

where $R^{1/2}$ is the square root of $R$ which satisfies $R^{1/2}(R^{1/2})^H = R$. The matrix $H_{iid}$ is of size $N_t \times N_r$ and it has identical independently distributed complex entries, with zero mean and unit variance (denoted as $\mathcal{CN}(0,1)$).

Furthermore, suppose that the channel coefficients are complex Gaussian the synthetic channel matrix can be generated by filtering the complex Gaussian matrix $H_{iid}$ with the two spatial correlation matrix $R_{Rx}^{1/2}$, and $R_{Tx}^{T/2}$

$$\widetilde{H} = R_{Tx}^{1/2} H_{iid} R_{Rx}^{T/2} \qquad (3)$$

where $(.)^T$ denotes the the transpose operator.

It is noteworthy that the spatial correlation matrices $R_{Tx}$ and $R_{Rx}$ are determined by the the transmitting-receiving antennas setting and the environment the MIMO system operates in. However, when the synthetic channel matrix $\widetilde{H}$ is generated, only the spatial correlation matrices and a $H_{iid}$ matrix get involved. Hence, there is almost no temporal correlation between the generated synthetic matrices as it is expected in real-life. In other words, the well-known Kronecker model only concentrates on modelling the spatial characteristic of measured MIMO radio channel. The time variation aspect of the channel caused by the movement of the transmitting/receiving antennas themselves or the surrounding objects, which is also important, is ignored in this model.

### B. Spatio-temporally correlated model

In a temporal correlated channel, the relationship of the two channel coefficients in the past and at present is normally described by the correlation coefficient $\rho$. A widely-used model for a time-varying narrowband channel is the Jakes model with the channel correlation coefficient given by

$$\rho(t) = \frac{E\left(h_{ij}(t_o)h_{ij}^*(t_o+t)\right)}{\sqrt{E(|h_{ij}(t_o)|^2)}\sqrt{E(|h_{ij}(t_o+t)|^2)}} = J_o(2\pi f_d t) \qquad (4)$$

where $(.)^*$ denotes the complex conjugate operator. As seen from the equation the correlation coefficient is a zeroth order Bessel function of the first kind with the time delay $t$ and the maximum Doppler frequency $f_d$ as parameters. However, normally the assumption used in the model that the scatterers are horizontal isotropically distributed does not hold. Hence, in practice the correlation coefficient may not follow the Jakes model. A more precise value of the temporal correlation coefficient should be derived from the channel measurement.

The temporal correlation coefficient is a useful parameter for estimating the relation between the channel coefficients along the time axis. Based on this parameter, the decision on how frequently the channel should be probed can be made. This parameter is, however, not enough for modelling the variation of the channel with time. In [6] a simple Markov chain model of the channel state evolution is presented whereby the current channel coefficient is related to the past channel coefficient as

$$h_{ij}(t_o+t) = \rho(t)h_{ij}(t_o) + \sqrt{1-\rho(t)^2}e_{ij}, e_{ij} \sim \mathcal{CN}(0,1) \qquad (5)$$

Now, the spatio-temporally correlated narrowband model for a MIMO channel can be readily derived

$$\widetilde{H}(t_o+t) = \rho(t)\widetilde{H}(t_o) + \sqrt{1-\rho(t)^2}\widetilde{E} \qquad (6)$$

In this equation $\widetilde{H}(t_o)$ and $\widetilde{E}$ are the spatially correlated channel matrices. They are both independently generated by using the model presented in equation (3).

## IV. Parameterization from Measured Channel and Model Validation

### A. Measured parameters

Root mean square (RMS) delay spread is a useful parameter to reveal the dispersion or the multipath propagation of the channel. In order to decide whether narrowband or wideband information will be used we have assessed the RMS delay spread of the channel in all measured locations. To avoid the thermal and the correlation noise a threshold of 30 dB is used for the power delay profile (PDP). Those PDP components which are lower than 30 dB from the PDP's peak will be set to zero. We found that in all measured locations, 80% of the RMS delay is lower than $0.135\mu s$ which is an inversion of the PN chip rate. Therefore the channel under investigation could be considered as narrowband. The channel coefficient is derived by summing up all 60 bins out of 98 bins of the measured IR. The remaining bins are not used because for our indoor measurement they often contain the thermal and correlation noise rather than useful multipath information.

During the measurement, aside from the movement of the receiving antennas, the movements of other objects are limited so that the channel can be assumed to be static. Therefore, the handset's movement is the main source of the temporal variation of the channel coefficients. However the scattering richness property of the channel is expected to remain the same because in each measured location the MIMO radio channel was probed in a fairly short distance of 1.64 meters. To gather enough spatial statistic, for each measured location we use all the 32x234 IRs to calculate the transmitting and receiving spatial correlation matrices. By doing that, the correlation in time of the measured channel matrices has been somehow embedded in these two spatial correlation matrices through the calculation process. As a result, the temporal correlation of the channel coefficients is simply ignored.

An example of the magnitude of the Kronecker product of the transmitting and receiving spatial correlation matrices and the magnitude of the channel covariance matrix from one measured location are shown in figure 3. Basically, the major components (those with high values) of the channel covariance matrix and the Kronecker product matrix are almost equal. However, it is observed that at the same index the component's magnitude at the channel covariance matrix has a slightly larger value.

The time variation of the measured radio channel is assessed via the temporal correlation. Of all 234 measured IRs, 210 snapshots are used. They are divided into 14 groups with 15 IRs each. The average temporal correlation at one measured location is given as

$$\rho(t) = \frac{1}{N_t N_r} \sum_{i=1}^{N_t} \sum_{j=1}^{N_r} \frac{E\left(h_{ij}(t_o)h_{ij}^*(t_o + t)\right)}{\sqrt{E(|h_{ij}(t_o)|^2)}\sqrt{E(|h_{ij}(t_o + t)|^2)}} \tag{7}$$

where $t \in (0 \cdots 15\Delta t)$ and $\Delta t \approx 0.3s$ is the interval between two samples.

### B. Validation of the model

1) *Spatial domain:* One way to evaluate the performance of the stochastic model in spatial domain is to compare the measured capacity with the one obtained from synthetic channel matrix using equation (3) or (6). In order to calculate the measured system capacity the measured channel matrix is normalized such that

$$\| H \|_F^2 = N_t \times N_r \tag{8}$$

where $\| . \|_F$ denotes Frobenius norm. The channel theoretical capacity is calculated by well known formula

$$C = \log_2\left(det(I + \frac{SNR}{N_t}H \times H^H)\right) \tag{9}$$

where $I$ is the identity matrix. Since the spatial-temporally correlated stochastic model is built on top of the spatial correlated stochastic model, there should not be any difference in the synthetic capacity generated by the two models presented in (3) and (6). We have tried to generate the channel matrix using both models and found that statistically they give the same results in terms of the channel capacity. However, to this end we only use equation (6) so that the performance of the model in both spatial and temporal domain can be assessed. The correlation coefficients were extracted from the measured data using equation (7). In all, 1000x210 channel matrices were generated using (6). Then the synthetic channel capacity was compared with the measured capacity at 210 snapshots. The relative error between them is defined as

$$C_{error}(n, k) = \frac{|C_{estimated}(n, k) - C_{measured}(k)|}{C_{measured}(k)}$$
$$n \in [1..1000], k \in [1..210] \tag{10}$$

It can be observed in figure 4 that in general the stochastic model is able to capture the spatial characteristic of the MIMO radio channel accurately. The median relative error between capacity from synthetic channel matrices and the measured one is around 5% which is a reasonable number.

From a viewpoint of assessing the environmental multipath richness and transmitting-receiving antenna setup the measured median capacity is around 22 bit/s/Hz which is accountable for 88% of the MIMO channel with complex Gaussian independently distributed entries. This number highlights a very promising potential of the MIMO systems in indoor environment, even though the separated distances between the receiving antennas are small (0.25-0.5 wavelength).

In [7] the authors showed that the capacity of a MIMO system obtained from the Kronecker model always lower than the measured one especially at high spatial resolution. Their works base on the data collected from the NLOS

(a) Kronecker product

(b) Covariance matrix
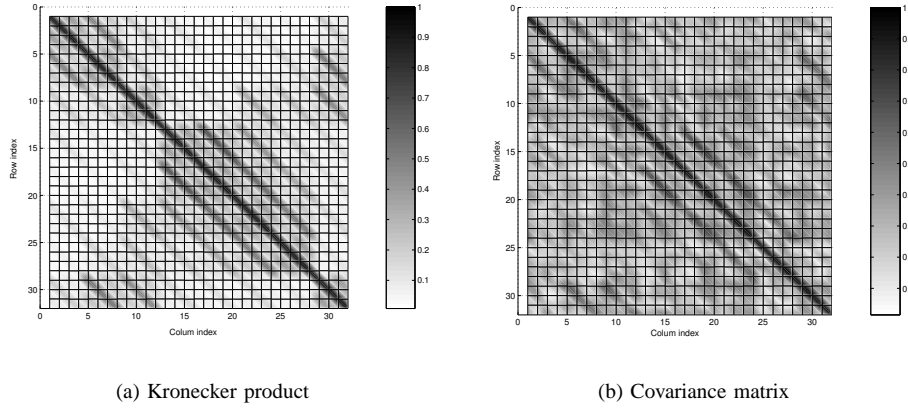
Fig. 3. Comparison of Kronecker product of the transmit-receive spatial correlation and the measured covariance matrix
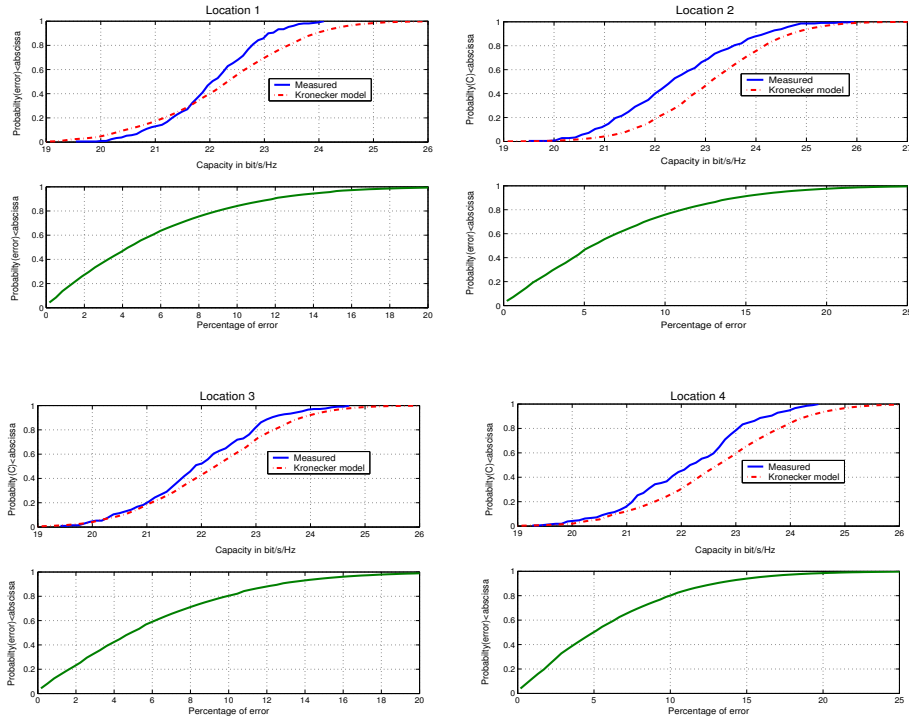


Fig. 4. Measured and estimated capacity at SNR=20dB and the average relative error at four locations

indoor measurement at 5.2 GHz. Although a good reason was given, their conclusion is not verified in our case as from our results the capacity of the synthetic channel matrix is either larger or smaller than the one calculated from measurement data with the median relative error of 5%.

*2) Temporal domain:* Because the handset was moved with constant velocity during the measurement, there is certain degree of correlation between the neighboring samples of the channel coefficient. In the evaluation of the model's performance in the temporal domain, we utilized the same

1000x210 synthetic matrices as described above. For each bunch of 210 matrix realizations, the temporal correlation is calculated as in equation (7). The averaged temporal correlations for four measured locations generated from our model together with the measured temporal correlations are plotted in figure 5. A temporal correlation generated from Jakes model is also plotted in the same figure for reference. It can be seen that the temporal correlations from the synthetic matrices are perfectly inline with those obtained from the measured data. In the first few seconds,
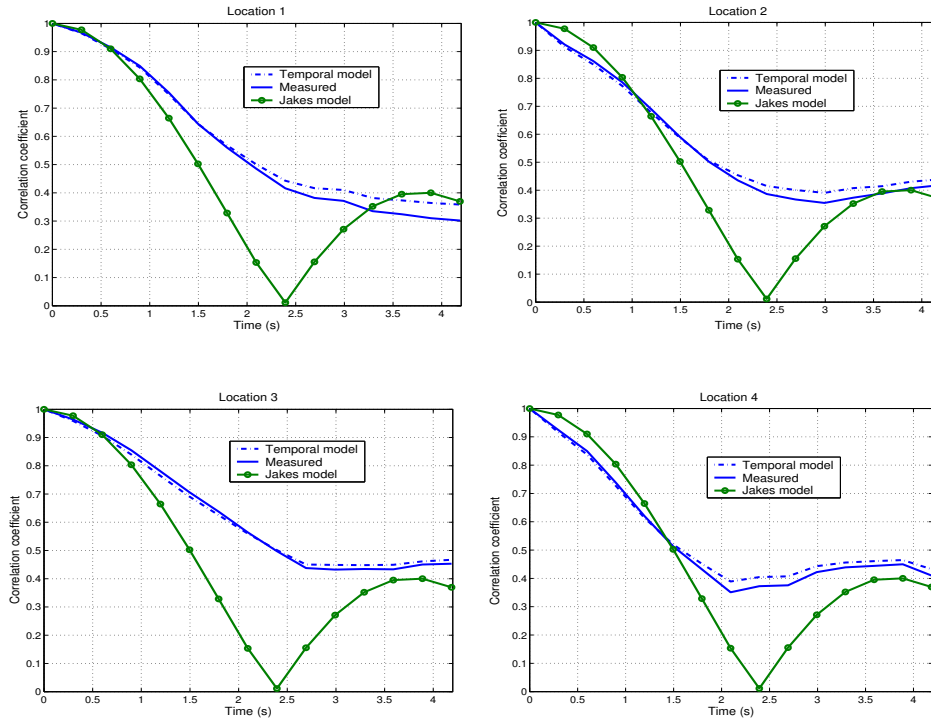
Fig. 5. Measured and estimated temporal correlation at four locations, the velocity of the handset is 23.4 mm/s

the temporal correlation changes rapidly and it follows the shape of that derived from Jakes model to a certain degree. We found that the time interval for the correlation coefficient goes below 0.9 is around 0.6s with assumably static environment. As handset's velocity is 23.4 mm/s the equivalent distance thereby the correlation coefficient goes below this level is 0.1 wavelength. This is important as it provides some insight into the required training period for MIMO adaptive modulation and coding technology which use the channel state information. However, the temporal correlation coefficient seems to flatten out along the time axis. Due to the lack of measured data, our observed window is too short for us to observe the temporal correlation coefficient gradually decreases to zero as expected.

## V. Conclusion

In this paper we have presented a stochastic model for spatio-temporraly correlated indoor MIMO channel based on measured data. We showed that the model can reproduce the essential characteristic of the MIMO radio channel both spatially and temporally. The results could be used to generate adequate channel matrices with predefined channel characteristic in time and space for evaluating the MIMO system performance at higher level.

## Acknowledgement

## References

[1] D.P.McNamara, M.A.Beach, P.N.Fletcher, P.Karlsson "Temporal variation of multiple-input multiple-output (MIMO) channels in indoor environments", 11 International Conference on A&P 2001 Page(s): 578 -582 vol.2.

[2] J.W.Wallace, M.A.Jensen, A.L.Swindlehurst, B.D.Jeffs "Experimental characterization of the MIMO wireless channel: data acquisition and analysis" IEEE Transactions on Wireless Communications, Volume: 2 Issue: 2, March 2003 Page(s): 335 -343

[3] K.I.Pedersen, J.B.Andersen, J.P.Kermoal and P.E.Mogensen, "A Stochastic Multiple-Input Multiple-Output Radio Channel Model for Evaluation of Space-Time Coding Algorithms", Proceedings of VTC Fall'00, pp. 893-897.

[4] J.P.Kermoal, L.Schumacher, K.I.Pedersen and P.E.Mogensen, "A Stochastic MIMO Radio Channel with Experimental Validation", IEEE JSAC, vol. 20, n.6, August 2002, pp. 1211-1226.

[5] K.Yu, M.Bengtsson, B.Ottersten, P.Karlsson, D.McNamara and M.Beach "Measurement Analysis of NLOS Indoor MIMO Channels" IST Communications Summit, 2001, pp. 277-282.

[6] S.Haykin "Adaptive Filter Theory", Englewood Cliffs, NJ, Prentice Hall, 1996.

[7] M.Herdin, H.Oezcelik, W.Weichselberger, E.Bonek and J.Wallace "Deficiencies of 'Kronecker' MIMO radio channel model", Electronics Letters , Volume: 39 , Issue: 16 , 7 Aug. 2003 Pages:1209 - 1210.

**Paper 4:**
**On the performance of link adaptation technique in MIMO systems.**
H.T.Nguyen, J.B.Andersen and G.F.Pedersen.
Submitted to Wireless Personal Communication, An International Journal, 2005.

# On the performance of link adaptation techniques in MIMO systems [*]

Hung Tuan Nguyen, Jørgen Bach Andersen and Gert Frølund Pedersen
*Department of Communication Technology, Niels Jernes Vej 12, DK-9220 Aalborg , Denmark*

2000/04/29

**Abstract.** Recent researches on multiple antennas system namely the multiple input multiple output (MIMO) system show that huge potential be it the spectral efficiency or the enhancement in transmission quality can be achieved. In this paper, with the assumption that the channel is narrowband and the channel coefficients are known at both link ends, we propose and evaluate several link adaptation (LA) algorithms applied to the spatial multiplexing MIMO systems. Depending on the requirements, the LA technique is designed to optimize either the system spectral efficiency or the BER. We also consider the potential use of the maximum eigen beamforming in supporting concurrent users. The results show that efficient use of the channel information could lead to a significant improvement in the system performance.

## 1. Introduction

Unlike wired communications the channel variation of wireless communications makes it a big engineering challenge. Multipath fading, path loss, time-selective fading, frequency-selective fading among others are the main obstacles in wireless communications. Recently MIMO technique (Telatar, 1999), where both the transmitter and receiver are equipped with multiple antennas has emerged as a cure for the very first phenomenal: the multipath fading. MIMO technique does not try to repair the multipath fading channel. However, it tries to utilize the multipath richness environment in a smart way such that the received signal in probability cannot be in deep fade. The reliability and spectral efficiency of the wireless communication are therefore substantially improved.

Like SISO systems, MIMO systems need a set of algorithm, coding, and transmission parameters to adapt the system to the variation of the environment. Such sets are often refereed to as Link Adaptation (LA) techniques (Catreux, 1999). The main motivation of any LA scheme is to get the best possible system performance based on some knowledge of the wireless channel. The channel knowledge could be the absolute instantaneous channel information (i.e. the channel impulse response) or in an average form (i.e. the average SNR, BER per transmitted frame, average channel covariance matrix or the statistical information of the channel coefficients). In this paper, we investigate the LA techniques for narrowband MIMO systems with the assumption that the channel state information (CSI) is instantaneously known at the both ends of the transmission link. The performance of the LA techniques adhere to different system requirements such as transmission reliability, spectral efficiency and implementation complexity is investigated.

The rest of the paper is organized in the following way. First the model for a narrowband MIMO system is described in section 2. The algorithm for optimally distributing the transmitted power to minimize the overall BER while keeping the total bit rate constant is addressed in section 3. Under a certain requirement on the transmission reliability, an algorithm which is capable of enhancing the system spectral efficiency is covered in the same section. With respect to the implementation complexity, we change the focus to the maximum eigen beamforming technique in section 4. In this section, several performance advantages of the maximum eigen beamforming technique are highlighted. Further, the potential use of this technique in a multi-user environment for the downlink is also investigated. The paper ends with conclusion and remark in section 5.

---

## 2. System model

Let us consider the scenario where there are $N_t$ transmitting antennas and $N_r$ receiving antennas. A wide angular spread at both ends of the transmission link is assumed. The channel transfer matrix $\mathbf{H}$ can be realized as a $N_t \mathrm{x} N_r$ matrix in which each element is a complex Gaussian independent identically distributed (IID) number with zero mean and unit variance. The channel transfer matrix $\mathbf{H}$ can be diagonalized using the Singular Value Decomposition (SVD) technique

$$\mathbf{H} = \mathbf{UDV}^H \tag{1}$$

In this equation $\mathbf{U}$ and $\mathbf{V}$ are unitary matrices; $\mathbf{D}$ is a $N_t \times N_r$ diagonal matrix containing the singular values which are real and non-negative; $(.)^H$ means complex conjugate transpose operator. By applying the transmitting weight matrix $\mathbf{U}^H$ at the transmit side and the $\mathbf{V}$ receiving weight matrix at the receive side the $K = min(N_t, N_r)$ orthogonal channels can be realized. Each sub-channel has a channel gain of $\lambda_i$, which is the square of the singular value. To study in more detail the realization of these, the discrete time baseband interpretation of a single transmitted symbol vector is preferred. The received symbol vector has the form

$$\mathbf{y} = \mathbf{xUDV}^H + \mathbf{n} \tag{2}$$

where $\mathbf{x}$ is the transmitted symbol vector and $\mathbf{n}$ is the additive noise. By using the weight matrix $\mathbf{U}^H$ at the transmit side and weight matrix $\mathbf{V}$ at the receive side the received symbol vector becomes

$$\widetilde{\mathbf{y}} = \mathbf{xD} + \widetilde{\mathbf{n}} \tag{3}$$

Since the $\mathbf{U}$ matrix is unitary, the variance of the noise in (2) and in (3) is the same. Equation 4 also implies that the power put into $K$ parallel channels will be amplified by the eigen values; power put into channel(s) which have index larger than $K$ will be lost.

## 3. Link adaptation in MIMO system using parallel sub-channels

As described in the previous section when the CSI is known at the both link ends it is possible to obtain up to $K = min(N_t, N_r)$ independent sub-channels. However, with the knowledge of the channel coefficient we can dynamically adapt the modulation and transmission parameters (i.e. transmitted power for each sub-channel). The results out of that would be a significant improvement in the system performance. Depending on the requirements be it maximizing the system throughput at a certain BER or minimizing the over all BER while keeping the data rate unchanged, the transmission parameters can be optimally adjusted to meet these goals. In the sequence, we will consider these two optimization problems.

### 3.1. Minimizing the overall BER with fixed spectral efficiency

We restrict ourselves to the narrowband MIMO system where the modulation is purely M-QAM or M-PSK and further assume that the phase and frequency synchronization are well established so that a coherent detection could be performed. Because of the differences in the eigenvalues, equally distributed power is not an optimum solution. Instead, the transmitted power must be distributed optimally to get an overall improvement in the average BER.

Basically, for an additive white Gaussian noise (AWGN) channel, at a certain SNR value the BER of the system using either M-QAM or M-PSK modulation is known. However, the BER expression is rather complicated and difficult to interpret. In (Chung, 2001), approximations of the BERs for both modulation types with a very simple expression are

presented. The approximations have an error of up to 1.5dB for a BER of less than $10^{-3}$. In a spatial multiplexing MIMO system, each sub-channel can be considered as an AWGN channel with a specific channel gain associated with it. Applying the BER approximations presented in (Chung, 2001), the BER of each sub-channel can be calculated as

$$M - QAM : BER_k \approx 0.2 exp\left(\frac{-1.6\lambda_k\gamma_k}{\sigma^2(2^{r_k}-1)}\right)$$

$$M - PSK : BER_k \approx 0.05 exp\left(\frac{-6\lambda_k\gamma_k}{\sigma^2(2^{1.9r_k}-1)}\right)$$

$$1 \le k \le min(N_t, N_r) = K \tag{4}$$

where $\gamma_k$ is the transmitted power allocated for the $k^{th}$ sub-channel, $\sigma^2$ is the noise variance, $r_k$ is the modulation order and $\lambda_k$ is the sub-channel gain. The easily invertible relation between the approximated BER, the transmitted power and the modulation order makes it more convenient to obtain an optimal solution for a LA scheme. Using this approximation and Gallager's multiplier procedure, it can be shown that the overall BER of a particular spatial multiplexing MIMO system using either M-QAM or M-PSK modulation will be minimized if the distributed power is satisfied

$$\gamma_k = max(\frac{1}{\beta\lambda_k}(ln(\lambda_k) - \mu), 0)$$

$$\text{where } \beta = \begin{cases} \frac{1.6}{\sigma^2(2^{r_k}-1)} & \text{for M-QAM} \\ \frac{6}{\sigma^2(2^{1.9r_k}-1)} & \text{for M-PSK} \end{cases}$$

$$\mu \text{ is chosen such that } \sum_{k=1}^{K} \gamma_k = P_t \tag{5}$$

Here we assume that all sub-channels use the same type of modulation and the same modulation order i.e. $r_k = r = const$. In case the BPSK modulation is of interest, the optimal power distribution solution for QAM or QPSK can be applied since BPSK, QAM and QPSK have the same BER expression. Note that because the power distribution algorithm presented in (5) is for any modulation type and order, it generalizes the exiting one reported in (Nguyen, 2004) and (Betu, 2004) where only BPSK modulation is considered.

The numerical BER using the optimally distributed power scheme is illustrated in Figure 1 for M-QAM and M-PSK modulation with 4x4 and 8x4 MIMO setup. The results are obtained from 10000 realizations of the channel matrix $\mathbf{H}$ with IID, zero mean and unit variance components. After having the optimally distributed power for each sub-channel $\gamma_k$, we use an exact expression of the BER to calculate the BER. The overall BER of the spatial multiplexing MIMO system can thus be expressed as

$$\overline{BER} = E(\frac{1}{T}\sum_{k=1}^{T} BER_k) \tag{6}$$

where $T$ is the number of sub-channel with the assigned transmit power greater than zero and $E(.)$ is the expectation operator.

There are two important conclusions which could be drawn from the results. Firstly, the optimum distribution of the power does indeed give a better performance as compared to the equal distribution scheme especially at high SNR values. Secondly, for low SNR values, when the eigenvalues are not large enough or not evenly distributed (i.e. in 4x4 setup), the proposed scheme does give a better BER. However, it comes the cost of lower number of activated sub-channels. In Figure 1, this fact is manifested itself as the stair case shape of the BER curves, where each step corresponds to an increase in the number of activated sub-channels. This violates the premise condition that we would like to keep

a.   M-QAM modulation



b.   M-PSK modulation
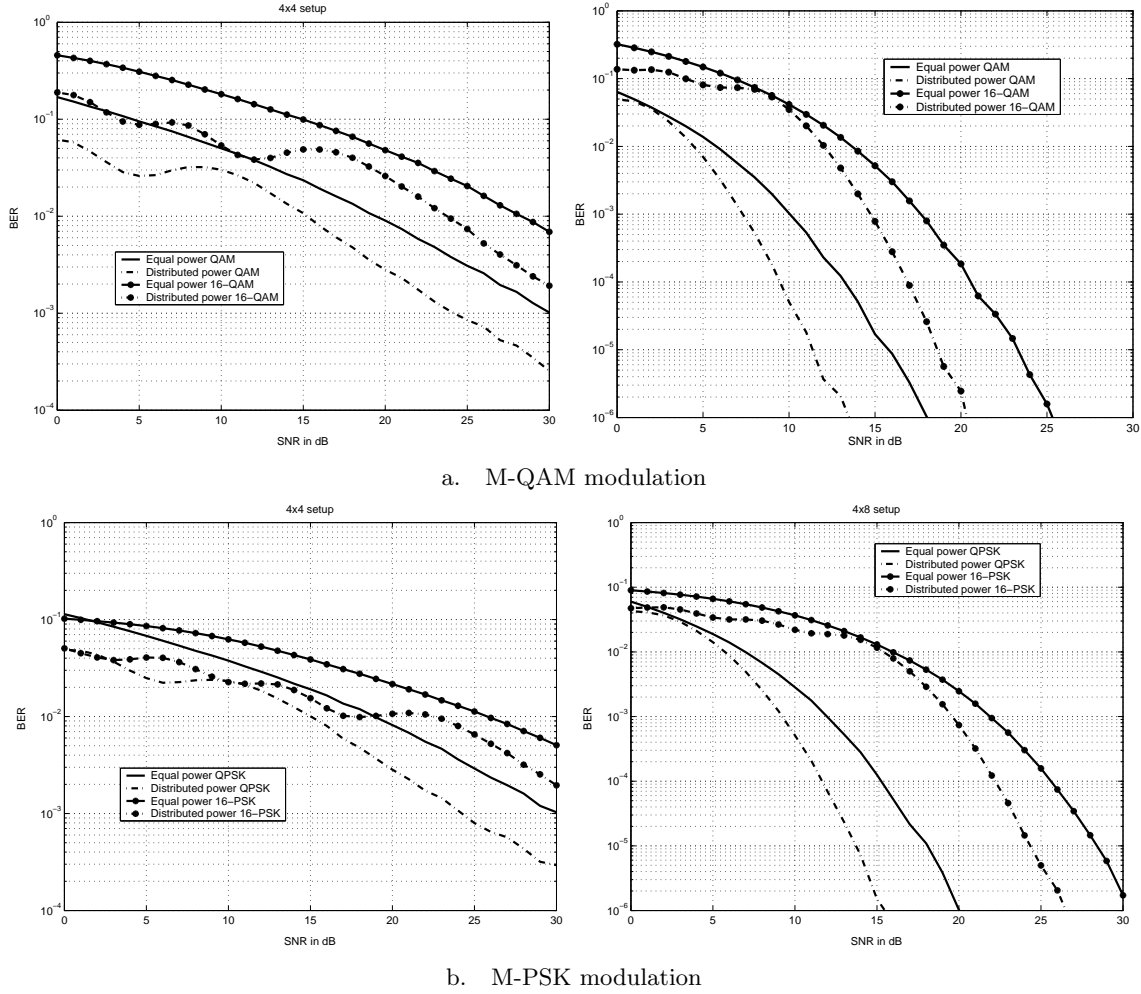
*Figure 1.* BER of MIMO system with and without optimum power distribution

the system throughput constant while minimizing the overall BER. Lower transmission rate is traded for a better system transmission quality. In other words, it is not possible to improve the overall BER in such low SNR values and/or eigenvalues without reducing the number of activated sub-channels. In such case, using equal power distribution seems to be the only solution to keep the total bit rates constant.

## 3.2.  MAXIMIZING THE SYSTEM SPECTRAL EFFICIENCY WITH FIXED BER

The above mentioned algorithm aims at minimizing the overall BER while keeping the transmission rate to be constant. The complexity of the system using this approach is reduced as only one type of modulation is used. In the contrary, there are systems which have a stringent requirement on the target BER. For such systems the available channel state information can be utilized to maximize the transmission rate. The complexity of these systems, however, will increase since a higher order modulation is required. In this section, we will investigate the feasibility and performance of the adaptive modulation scheme which focuses on maximizing the transmission rate at a target BER. For simplicity we only consider one type of modulation either M-PSK or M-QAM with different modulation orders. Without going into the detail of the algorithm one could deduce that the distribution of the transmitted power in this scheme must be similar to that of the water filling method. More power should be put into the sub-channel with higher gain. Consequently, the effective received power level of this sub-channel might be large enough

to support higher modulation order. This leads to a maximization of the overall data rate while the target BER is met.

The algorithm for optimal allocation of the modulation order and transmitted power level at each sub-channel is described in (7). Again this optimization solution stems from the useful approximation of BER in (4) and a Lagranger's multiplier procedure. Note that the same algorithm, but only for M-QAM case was also independently reported in (Wennstrom, 2003).

$$\gamma_k = max(\mu - \frac{1}{\Gamma\lambda_k}, 0)$$
$$\text{where } \Gamma = \begin{cases} \frac{-1.6}{\sigma^2 ln(5BER_{target})} \text{ for M-QAM} \\ \frac{-6}{\sigma^2 ln(20BER_{target})} \text{ for M-PSK} \end{cases}$$
$$\mu \text{ is chosen such that } \sum_{k=1}^{K} \gamma_k = P_t \tag{7}$$

The modulation order or in other words the number of bits per transmitted symbol of each sub-channel can be indirectly estimated as

$$r_k = \begin{cases} log_2(1 + \Gamma\gamma_k\lambda_k) \text{ for M-QAM} \\ \frac{1}{1.9}log_2(1 + \Gamma\gamma_k\lambda_k) \text{ for M-PSK} \end{cases} \tag{8}$$

It is interesting to see that the optimum distribution of the transmitted power for each sub-channel has the same form as that of the water filling method. The only different is a constant value $\Gamma$, which is a function of the target BER and modulation type (M-QAM or M-PSK). This constant number together with the distributed power level determine the modulation order that should be applied in each sub-channel. The essence of this algorithm can be summarized as follows. First, depending on the target BER the constant value $\Gamma$ is derived. Next, the distributed power for each sub-channel is found by iterative searching as expressed in (7). Then, depending on the modulation type, M-QAM or M-PSK the modulation order is estimated as in (8). However, it should be noted that $r_k$ in (8) is only an approximation. In practice, because of the constraint in the constellation setting, $r_k$ is calculated as the greatest even number (for M-QAM) or the greatest integer number (for M-PSK) which is less than or equal to the one estimated in (8). Figure 2 illustrates the achievable transmission rate as a function of SNR vaules for two types of modulation with the target BER of $10^{-3}$ and $10^{-5}$. The results are obtained from 100000 synthetic channel matrices with IID components for 4x4 and 8x4 MIMO settings.

The results indicate that at low SNR values, the algorithm does not work, illustrated by low spectral efficiency (e.g. 0 or 1 bit/s/Hz). It is as expected since the gain of each sub-channel is not high enough to support either types of modulation with the target BER. At high SNR region, M-QAM has better performance than than M-PSK for the same system setup and required BER. The reason could be that M-PSK modulation, by its constellation setting, has higher average BER than M-QAM modulation for the same modulation order. This forces the algorithm to select lower modulation order to fulfill the target BER. However, the M-PSK modulation does not require the gain of each sub-channel to be exactly known at the receiver as does the M-QAM modulation. Therefore M-PSK modulation has lower demodulation complexity.
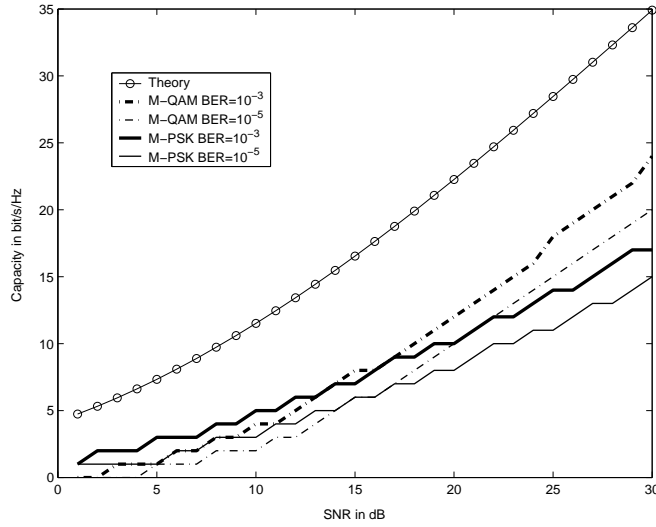
a.   4x4 setup
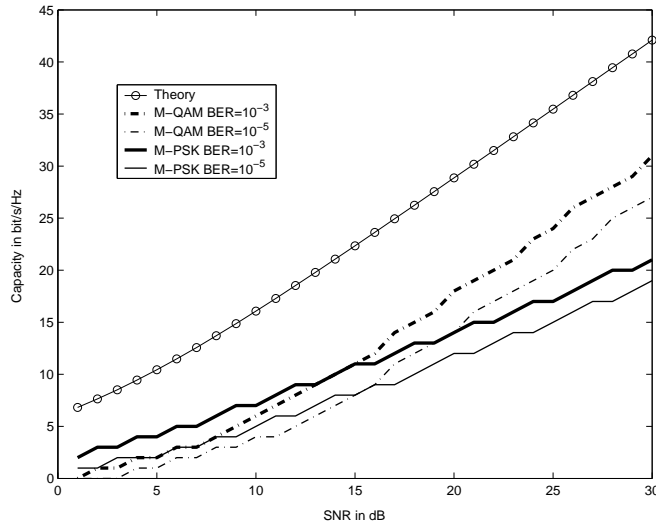


b.   8x4 setup

*Figure 2.* The obtainable throughput at different targeted BER values for M-QAM and M-PSK modulations in spatial multiplexing MIMO systems

## 4.   Maximum eigen beamforming transmission

### 4.1.   Motivation and performance comparison

In section 3 we have considered two schemes which utilize the available channel state information in an optimal way. However, the substantial performance gain can only be guaranteed if the instantaneous channel information is available at both link ends. Although the implementation complexity of the first approach could be released as only one type of modulation is considered, dense power amplification steps together with a large dynamic range could be a challenge for the design of a low noise amplifier. Signalling overhead required to inform the receiver about the modulation order and power gain of each sub-channel could also be an issue. The optimal use of the channel information turns out to be a compromise between the practical implementation issues and the achievable performance gain. In this section, we will investigate a third approach which also utilizes the instantaneous channel information, a maximum eigen beamforming scheme. Because only one sub-channel with maximum gain is used, we can get rid of several practical problems.

In this scheme, we propose that only one type of modulation with a fixed modulation order is implemented. Therefore, the complexity of the power amplifiers and signalling overhead can be significantly reduced. In a reciprocal channel, the eigen beamforming vector can be known at the transmitter by using iterative algorithm as reported in (Andersen, 2000) and (Dahl, 2002). In case the channel is not reciprocal, feedback of the eigenvector could also be possible as we only need to transmit $N_t$ complex components back to the transmitter. In the sequence, we will evaluate the advantages of the proposed transmission scheme in terms of the array gain, robust against time-varying channel and LOS condition.

### 4.1.1. Array gain advantage

When only one maximum eigenmode is activated the array gain of the channel will be the maximum eigenvalue. In case all sub-channels are combined as one channel, this gain would be the sum of all the eigenvalues. The nominal array gain of the maximum eigen beamforming method, therefore, would be at least $min(N_t, N_r)$ times larger than that of the system when all sub-channels are activated. This is because, in a spatial multiplexing MIMO system, the transmitted power must be divided among $min(N_t, N_r)$ sub-channels. On the other hand, all of the transmitted power is located for a single channel in a MIMO system deploying the maximum eigen beamforming approach.

$$P_t \lambda_{max} > \frac{P_t}{min(N_t, N_r)} \sum_{k=1}^{K} \lambda_k \tag{9}$$

The array gain advantage of maximum eigen beamforming technique could be used to support higher modulation order. In fact, we can restrict the modulation order such that the bit rates of both eigen beamforming and multiple parallel sub-channels transmission schemes are equal. In doing that, the requirement on the system spectral efficiency could be satisfied. Moreover, in some cases, the average BER of the system with one maximum eigen channel could be lower than that of the system using all sub-channels. As an example we make the BER simulations for both the spatial multiplexing and maximum eigen beamforming MIMO systems. Two MIMO system with 4x4 and 8x4 setting were considered. For the spatial multiplexing transmission BPSK modulation was used for all sub-channel and the optimum power distribution algorithm proposed in section 3 is used. To ensure that the overall throughput of the two transmission schemes is the same, in the maximum eigen transmission we used a 16-QAM modulation. The results in Figure 3 show that even with the same throughput, the maximum eigen beamforming technique does give a considerable improvement in terms of the BER. At the BER of $10^{-3}$ it gives 3dB and 17.5dB gain for the 4x4 and 8x4 setup respectively.

It should be noted here that the outcome of the example presented above is not, by any means, a general conclusion. The purpose of this example is merely to show that thorough investigation in the design of a link adaptation for MIMO system could leads to significant improvement in system performance and in reducing the system complexity.

When the average BER is required to be lower than a certain value, using the maximum eigen beamforming technique it is possible to adapt the modulation order of the transmitted symbol according to the channel gain and the SNR so that the throughput of the system is maximized. In Figure 4 the throughput of 4x4 and 8x4 MIMO setup with different required BER values. By comparing the results with those illustrated in Figure 2 we can see that the performance of the maximum eigenbeam forming method is inferior to that of the link adaptation technique applied to spatial multiplexing MIMO systems. However, the complexity of the system using the maximum eigen beamforming technique has been significantly reduced.
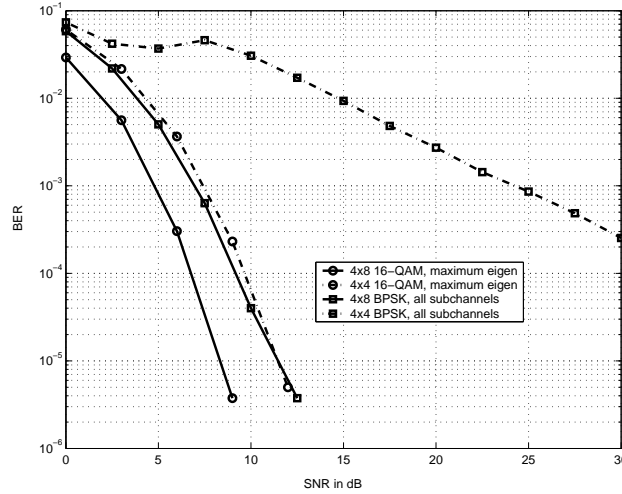
*Figure 3.* Average BER of MIMO systems using maximum eigen beamforming and spatial multiplexing approaches with the same throughput

### 4.1.2. *Robust against time-selective environment*

For mobile wireless communications, because of the time varying channel those LA techniques which are heavily dependent on the instantaneous channel information might suffer considerable performance degradation. In MIMO system, the time-varying characteristic of the channel makes the orthogonality of the weight vectors no longer holds true. This is because of the power leakage among the sub-channels generated by the out of date unitary matrices applied at both ends. The leakage would be substantially lower in case we use only one maximum eigen beamforming to communicate. As in (Nguyen, 2004) the received signal in time-varying channel is of the form

$$P_{received} \;=\; |\rho\sqrt{\lambda_{max}} + \sqrt{1-\rho^2}e|^2 P_t + \sigma^2_{noise}$$

(10)

where $e$ is a complex IID number with mean zero and unit variance; $\rho$ is the channel time-varying correlation coefficient. Since only one channel is involved in the transmission, the self interference power level caused by cross talk is lower than that of the case where all sub-channels are activated. To estimate the effect of time-varying environment, we use the same simulation setup for illustrating the gain advantage as above. The results are shown in Figure 5 with different values of $\rho$.

It is clearly seen that the effect of feedback delay on the average BER is much lower for the maximum eigen beamforming technique. It is justified by the fact that only at very high value of $\rho$ does the average BER approach the BER floor.

### 4.1.3. *Robust against LOS or correlated multipath fading*

The $K$ parallel sub-channels in MIMO system can only be realized in rich multipath environment where the received signals at each antenna element become uncorrelated. If the received signal is correlated such as in a narrow angular spread or LOS scenario the rank of the channel matrix will be reduced. In the extreme case when the received signal is totally correlated the channel matrix be come a rank one matrix and only one sub-channel can be used for data transmission. Practically, partial correlated channel matrix is a general scenario. The full $K$ sub-channels could also be obtainable in such case. However, correlated signals make the sub-channels with low gains (i.e. eigenvalues) become practically obsolete. Therefore being able to switch between multiple sub-channel mode
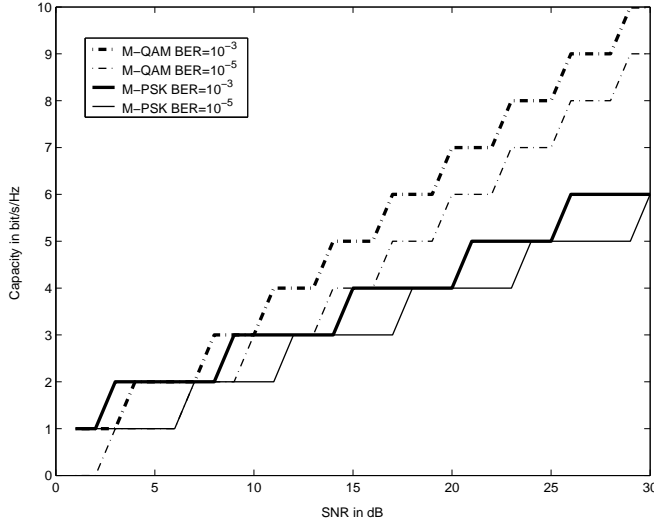
a. 4x4 setup
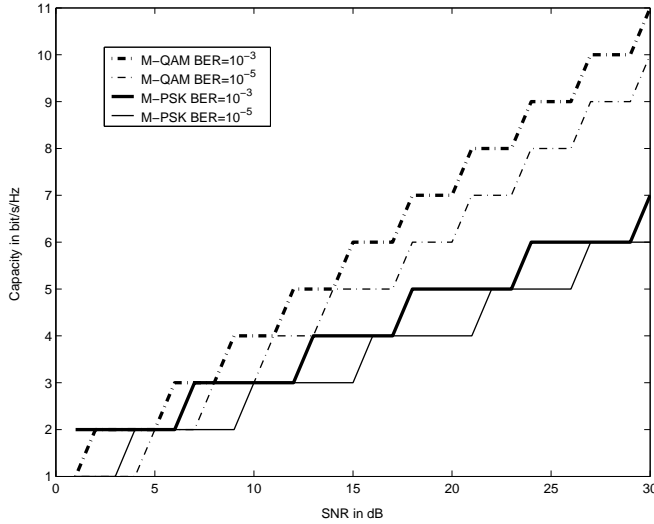


b. 8x4 setup

*Figure 4.* The obtainable throughput at different targeted BER for M-QAM and M-PSK modulations in maximum eigen beamforming MIMO systems

to maximum eigen beamforming mode according to the environment the MIMO system operated in might lead to a substantial benefit. We use the theoretical capacity as a metric to compare the performance of maximum eigen beamforming and spatial multiplexing schemes in LOS environment. Figure 6 shows the capacity of 4x4 and 8x4 MIMO systems with the Ricean factors of 10dB and 20dB.

It is observed that at a low SNR value the capacity of the maximum eigenmode is equal to that of multi sub-channels scheme using water filling method. As the Ricean factor increases, the capacities of these two transmission scheme asymptotically approaching each other. It is interesting to see that for such a high Ricean factor ($\mathbb{K} \geq 10dB$) the capacity of the maximum eigen beaforming approach does not change as $\mathbb{K}$ increases. This is illustrated in Figure 6 by the overlap of the capacity curves at the two values of the Ricean factor.
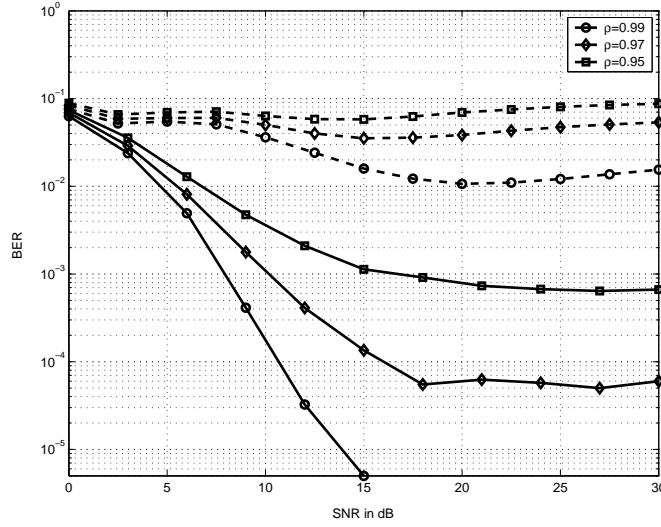
a.  4x4 setup
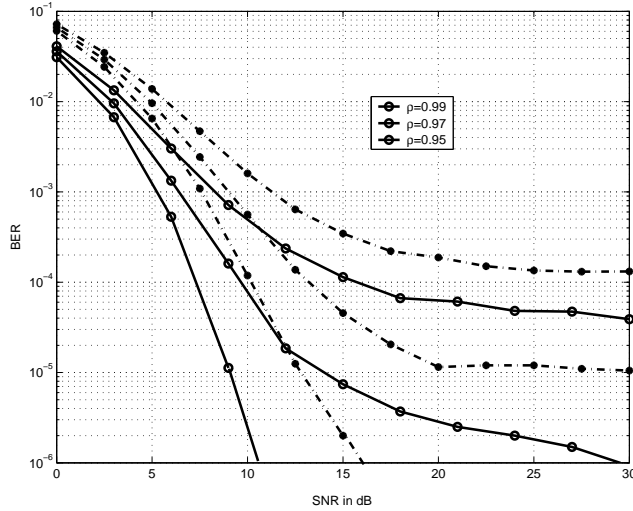


b.  8x4 setup

*Figure 5.* Effect of time-varying environment to the MIMO average BER, straight line: maximum eigenmode with 16-QAM, dot line: parallel sub-channels mode with BPSK

## 4.2. Potential of maximum eigen beamforming in multi-user environment

Obviously, by using multi-antennas at both link ends the wireless system spectral efficiency and transmission quality will be substantially improved. So far we have only investigated the adaptation link performance of a single user scenario. However it is often expected that the improvement in performance will be shared among users and single user MIMO system is hard to find for cost effective reason. Apparently, when multi-user environment is considered the result from analysis of the MIMO system implementing link adaptation above mentioned provides only an upper limit of the achievable system performance. The multi-user scenario adds complexity to the analysis of the system performance especially in MIMO system and it is out of the scope of this paper.

In this part we consider the potential of the maximum eigen beamforming technique in supporting concurrent transmissions from the transmit side to $N_u$ users with desired SIR value. The eigenvectors applied at both transmitter and receiver act as steering vectors to focus the signal to the intended users. Apparently, the focusing resolution depends on the degree of correlation among the targeted users. Here we assume that the channels
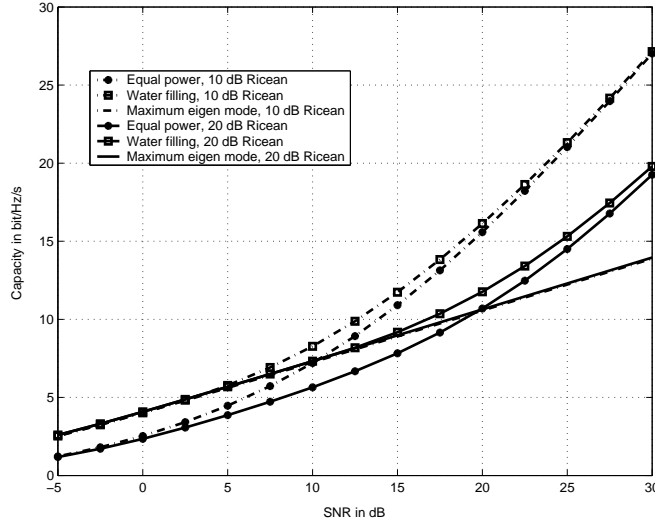
a.   4x4 MIMO setup
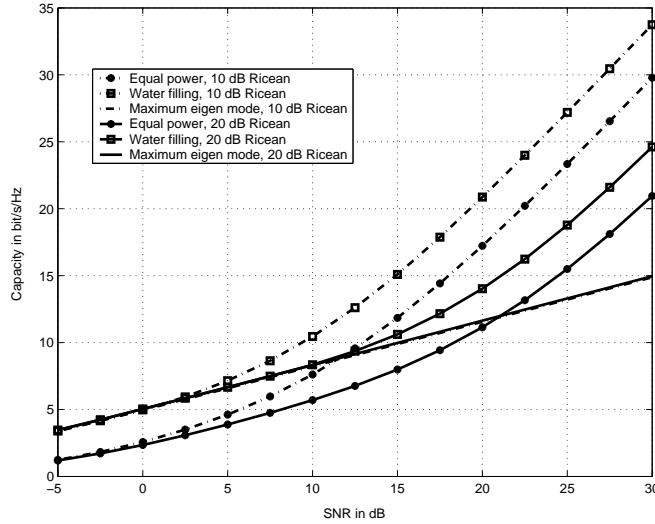


b.   8x4 MIMO setup

*Figure 6.* Capacity of MIMO system using maximum eigenmode and spatial multiplexing transmissions in LOS environment

between each user are totally uncorrelated, though this is not very lose assumption when considering the rich multipath indoor environment or the largely separated users in outdoor environment.

We denotes the channel matrix of the $p$th user is $H_p$ which is a matrix with IID mean zero and unit variance entries. Further $u_p, v_p$ are the unitary matrices derived from the SVD of $H_p$, and $s_p$ is the symbol intended for the $p$th user with constant power $P$. The received signal of a particular user becomes

$$y_{p_o} = \sum_{p=1}^{p=N_u} u_p H_{p_o} v_{p_o} s_p + n_{p_o}$$

$$= \sqrt{\lambda_{max_{p_o}}} s_{p_o} + \underbrace{\sum_{p=1, p \neq p_o}^{p=N_u} u_p H_{p_o} v_{p_o} s_p}_{Interference} + n_{p_o} \tag{11}$$

Because $u_p$ and $v_p$ are unitary vector and $H_{p_o}$ is a matrix with IID components with zero mean and unit variance, the interference term in (11) is also a random number with zero mean and the variance of $(N_u - 1)P$. Hence the average SIR of a particular user is

$$SIR = \frac{\lambda_{max}}{N_u - 1} \tag{12}$$
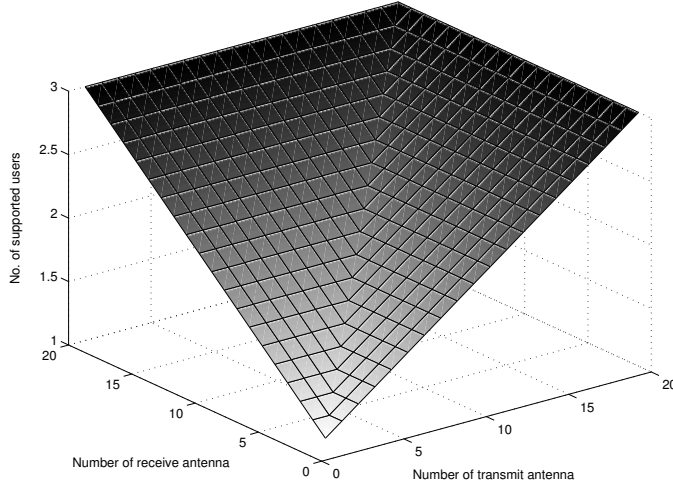


a.   Lower bound
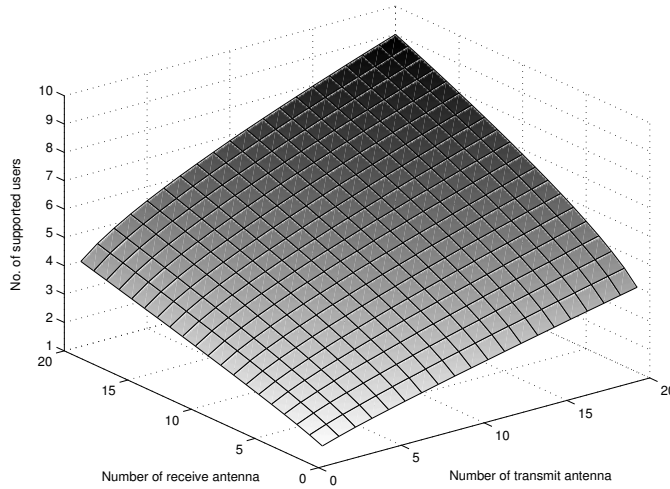


b.   Upper bound

*Figure 7.* Lower and upper bound of the number of simultaneous users with a target SIR of 10dB

It is interesting to see that the variance of the interference is a linear function of the number of supported users. Besides the number of supported users, the SIR is also determined by the maximum eigenvalue. The upper bound of the maximum eigenvalue $\lambda_{max}$ was found in (Andersen, 2000) at the limit when $N_r$ becomes infinitively large.

$$\lambda_{max} < \left( \sqrt{N_t} + \sqrt{N_r} \right)^2 \tag{13}$$

The lower bound of $\lambda_{max}$ can be derived as

$$min(N_t, N_r)\lambda_{max} > \sum_{k=1}^{min(N_t,N_r)} \lambda_k = N_t N_r$$

$$\iff \lambda_{max} > max(N_t, N_r) \tag{14}$$

Now, the upper bound and lower bound of the number of supported users with a certain SIR value can be readily found

$$1 + \frac{max(N_t, N_r)}{SIR} < N_u < 1 + \frac{(\sqrt{N_t} + \sqrt{N_r})^2}{SIR} \tag{15}$$

Figure 7 illustrates the bound of the number supported users for MIMO systems with up to 20 antennas at each ends. The target $SIR$ was 10dB as it is reasonable number for achieving $BER$ of $10^{-3}$ in Gaussian channel with BPSK modulation.

It should be mentioned that the lower bound is a lose bound as the maximum eigenvalue is often much larger than the minimum one, especially in a MIMO system equipped with large number of antennas. For the upper bound, it is not a tight bound and correct only when $N_r$ becomes infinitely large. This calls for a simulation to evaluate the actual number of supported users with this target $SIR$. We generated 10000 channel matrix realizations, calculated the mean of the maximum eigenvalue and variance of the interference caused by a single interferer. The number of supported users $N_u$ is defined as a maximum number of interferers at which the corresponding SIR value is still greater than the target SIR of 10dB. Figure 8 demonstrates the average number of supported users from this simulation.
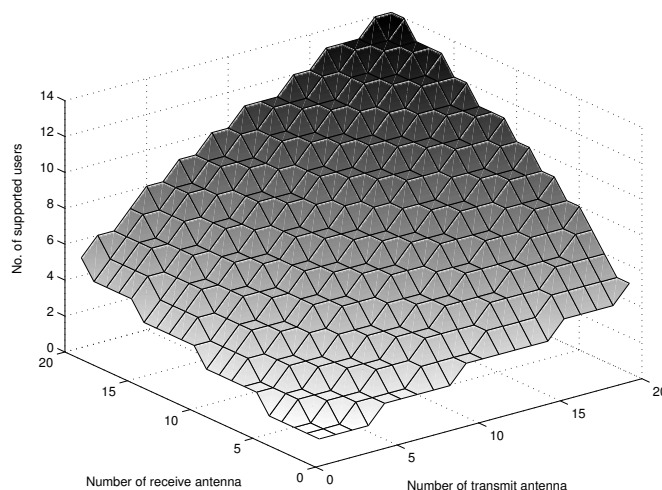


*Figure 8.* Simulation result on the average number of supported users with target SIR=10dB

It can be clearly seen that for lower number of antenna elements the result derived from simulation is even larger than the upper bound. This is expected as explained previously. The number of users $N_u$ asymptotically approaches the upper bound as the number of antenna elements at one side increases while it is fixed at the other. Nevertheless, the simulation results demonstrates the potential use of the maximum eigen beamforming technique in multi-user applications. As an example, a multi-user MIMO system with 8x4 setup can support 4 concurrent users with the target SIR of 10dB by using the maximum eigen beamforming.

Now, if we consider downlink transmission of a multi-user MIMO system consisting of $N_t$ transmitting antennas and $N_u$ users with $N_r$ receiving antennas for each user, the spectral efficiency of the MIMO cell can be estimated as

$$C_{cell} = \sum_{p=1}^{N_u} log_2(1 + \frac{\lambda_{max}P}{(N_u - 1)P + \sigma_{noise}^2}) \tag{16}$$

## 5. Conclusion

In this paper we have investigated several link adaptation algorithms for MIMO system with the assumption on the availability of the instantaneous channel coefficients at both link ends. Depending on the requirement either at target average bit rate or the BER the transmitted power is optimally distributed to each parallel sub-channel according to its associated eigenvalue. Using these algorithms, the average BER or the spectral efficiency of the spatial multiplexing MIMO system are substantially improved. To reduce the system complexity, we proposed a maximum eigen beamforming technique. We showed that this technique can provide higher array gain and not very sensitive to the time-varying environment as compared to the case where all the sub-channels are used. Moreover, the potential of this transmission technique in multi-user environment is also studied. It is interesting to see that this transmission scheme can offer a sort of spatial focusing with the resolution and the SIR depending on the number of supported users and the degree of correlation between them. The results illustrate a promising solution for reducing the co-channel interference in multi-user MIMO systems.

## Appendix

### DERIVATION OF EQUATION (5)

For M-QAM or M-PSK modulation the BER of channel $k$ can be expressed as

$$BER_k = \alpha_k exp(-\beta_k \gamma_k \lambda_k) \text{ where}$$

$$\alpha = \begin{cases} 0.2 \text{ for M-QAM} \\ 0.05 \text{ for M-PSK} \end{cases}$$

$$\beta = \begin{cases} \frac{1.6}{\sigma^2(M-1)} \text{ for M-QAM} \\ \frac{6}{\sigma^2(2^{1.9log2(M)}-1)} \text{ for M-PSK} \end{cases}$$

$$\sum_{k=1}^{K} \gamma_k = P_t \tag{17}$$

The average BER of the overall system using only one type either M-QAM or M-PSK and only one modulation order is

$$BER_{sys} = \frac{1}{K} \sum_{k=1}^{K} \alpha exp(-\beta \gamma_k \lambda_k) \tag{18}$$

Here, $\alpha$ and $\beta$ are constant for each sub-channel. Following the Gallager's multiplier procedure, the problem now is to find set of $\gamma$ so that the $BER_{sys}$ is minimized. Since $K$ and $\alpha$ are constant, it is equal to finding a set of $\gamma$ to minimize the sum

$$\Xi = \sum_{k=1}^{K} (e^{-\beta\lambda_k \gamma_k} + \varepsilon \gamma_k) \tag{19}$$

where $\varepsilon$ is a variable. The solution can be obtained if we differentiate the $\Xi$ with respect to $\gamma_k$ and set it to zero

$$-\lambda_k e^{\beta\lambda_k \gamma_k} + \varepsilon = 0 \rightarrow \lambda_k e^{-\beta\lambda_k \gamma_k} = \varepsilon$$

$$-\beta\lambda_k \gamma_k = ln(\frac{\varepsilon}{\lambda_k}) \rightarrow \gamma_k = \frac{1}{\beta\lambda_k}ln(\lambda_k) - \frac{1}{\lambda_k}ln(\varepsilon)$$

$$\gamma_k = (\frac{1}{\beta\lambda_k}(ln(\lambda_k) - \mu)), \text{ where } \mu = \beta ln(\varepsilon) \tag{20}$$

## DERIVATION OF EQUATION (7) AND (8)

From (17) we have the number of bits per symbol of the $k^{th}$ channel is

$$r_k = \begin{cases} log_2(1 + \Gamma\gamma_k\lambda_k) \text{ for M-QAM} \\ \frac{1}{1.9}log_2(1 + \Gamma\gamma_k\lambda_k) \text{ for M-PSK} \end{cases} \text{ where}$$

$$\Gamma = \begin{cases} \frac{-1.6}{\sigma^2 ln(5BER_{target})} \text{ for M-QAM} \\ \frac{-6}{\sigma^2 ln(20BER_{target})} \text{ for M-PSK} \end{cases} \tag{21}$$

The total number of bit rate of all sub-channels per unit symbol is

$$R = \sum_k^K r_k = \begin{cases} \displaystyle\sum_{k=1}^K log_2(1 + \Gamma\gamma_k\lambda_k) \text{ for M-QAM} \\ \displaystyle\frac{1}{1.9}\sum_{k=1}^K log_2(1 + \Gamma\gamma_k\lambda_k) \text{ for M-PSK} \end{cases} \tag{22}$$

Again, following the Gallager's multiplier procedure the problem of finding a optimum set of modulation order for both types of modulation now boils down to find a set of $\gamma$ to maximize the sum

$$\Xi = \sum_{k=1}^K log_2(1 + \Gamma\gamma_k\lambda_k) - \varepsilon\gamma_k \tag{23}$$

Differentiating the $\Xi$ with respect to $\gamma_k$ and set it to zero we have the results as in (8)

$$\frac{1}{ln(2)}\frac{\Gamma\gamma_k}{1 + \Gamma\gamma_k\lambda_k} = \varepsilon \tag{24}$$

$$\rightarrow \frac{1}{\frac{1}{\Gamma\lambda_k} + \gamma_k} = \frac{\varepsilon}{ln(2)} \tag{25}$$

$$\rightarrow \gamma_k = \mu - \frac{1}{\Gamma\lambda_k} \text{ where } \mu = \frac{ln(2)}{\varepsilon} \tag{26}$$

## References

I.E.Telatar. Capacity of Multi-antenna Gaussian Channels. *European Transactions on Telecommunications*, , Vol. 10, No. 6, pp. 585-595, Nov/Dec 1999.

S.Catreux,V.Erceg, D.Gesbert, R.W.Heath, Adaptive modulation and MIMO coding for broadband wireless data networks. *Communications Magazine, IEEE*,Volume: 40 Issue: 6 , June 2002 Page(s): 108 -115.

Seong Taek Chung, A.J.Goldsmith Degrees of freedom in adaptive modulation: a unified view. *Transactions on Communications, IEEE* ,Volume: 49 Issue:9 , Sept. 2001 Page(s): 1561 -1571

M.Wennstrom On MIMO systems and adaptive arrays for wireless communication.. *PhD thesis ,Signals and Systems Group, Uppsala University, Sweden*, ISBN : 91-506-1619-6.

J.B.Andersen Array gain and capacity for known random channels with multiple element arrays at both ends. *Journal on Selected Areas in Communications, IEEE*, Volume: 18 Issue: 11 , Nov. 2000 Page(s): 2172 -2178.

T.Dahl, N.Christophersen, D.Gesbert BIMA: blind iterative MIMO algorithm. *International Conference on Acoustics, Speech, and Signal Processing*, Volume: 3 , 13-17 May 2002.

H.T.Nguyen, J.B.Andersen,G.F.Pedersen MIMO system's performance and capacity under the impact of feedback delay. *15th IEEE International symposium on Personal, Indoor and Mobile Communications Barcelona Spain, September, 2004, Vol 1, 2004. s. 53- 57.*

B.N.Getu, J.B.Andersen MIMO Systems in Random Uncorrelated, Correlated and Deterministic Radio Channels.. *Wireless Personal Communications, July, 2004, vol. 30, no 1, pp 27-61, 2004*

K.Miyashita, T.Nishimura, T.Ohgane, Y.Ogawa, Y.Takatori, Cho.Keizo High data-rate transmission with eigenbeam-space division multiplexing (E-SDM) in a MIMO channel. *Vehicular Technology Conference, 2002* Page(s): 1302 -1306 vol.3

# CAPACITY AND PERFORMANCE OF MIMO SYSTEMS UNDER THE IMPACT OF FEEDBACK DELAY

**Hung Tuan Nguyen, Jørgen Bach Andersen, Gert Frølund Pedersen**

Department of Communication Technology, Niels Jernes Vej 12, DK-9220 Aalborg , Denmark
Email: {htn,jba,gpf}@kom.auc.dk

**Abstract -** Multiple input multiple output (MIMO) systems promise better performance and significant increases in the channel capacity by utilizing rich scattering environment to obtain diversity gain and spatial multiplexing. Maximum system capacity and performance can be achieved if the instantaneous channel state information (CSI) is known at both sides of the transmission link. In order to have such improvements, the CSI at both link ends must be updated timely. However, the updating process is always subject to non-ideality. In this paper we investigate the effect of delay in updating CSI on the MIMO spectral efficiency and performance with system capacity and BER as benchmarks.

**Keywords -** MIMO, feedback delay, capacity, BER

## I. INTRODUCTION

Recently MIMO technique where both the transmitter and the receiver are equipped multi antennas has emerged as a cure for the problematic short-term multipath fading. In the MIMO technique, we do not try to repair the multipath fading channel, however we try to utilize multipath richness environment in the smart way such that the received signal in probability cannot be in deep fade. The reliability and spectral efficiency of the wireless communication are therefore substantially improved. It could be fairly easy to get antenna diversity and spatial multiplexing at the receiver as the channel state can be updated using available sounding technique. However, having these at the transmit side is cumbersome in case the channel is not reciprocal i.e. in FDD scheme. In order to make full use of antenna diversity at the transmit side the channel information must be sent back from the receive side. Thereby, the updated CSI is subject to non-idealities such as channel estimation errors and feedback delay [1], [2].

In this work one dominant aspect of the non-idealities of the CSI in the feedback scheme, namely the feedback delay, will be investigated. The effect of the feedback delay to MIMO system's theoretical capacity and performance is addressed. To highlight this effect, other errors in the estimation of the CSI will be ignored. We show that when the CSI is not updated timely the orthogonality of the parallel channels no longer holds true. As a result, the signal power of one channel leaks to the others causing interference. These interferences increase linearly with the transmitted power leading to degradation of channel capacity and average BER at high SNR values.

The rest of this paper is organized as follows. Firstly the channel model is outlined in section II. Next, two models namely the Markov chain model and the scattering model for modelling the channel state evolution are presented in section III. In section IV the theoretical capacity of MIMO system at the presence of feedback delay is derived. A practical figure of merit, the average BER is used to estimate the system performance's degradation under the effect of feedback delay is investigated in section V. Monte Carlo simulation to justify the analytical results is also briefly described in this section. Finally conclusion is made in section VI.

## II. CHANNEL MODEL

Let us consider the scenario where there are $N_t$ transmitting antennas and $N_r$ receiving antennas. A wide angular spreads at both ends scenario is assumed. The channel matrix $H$ can be realized as $N_t$x$N_r$ matrix in which each element is complex Gaussian independent identically distributed (IID) with zero mean and unit variance (denoted as $\sim \mathcal{CN}(0,1)$). Each entry of $H$ i.e. $h_{n_t n_r}$ is the channel state coefficient between transmitting antenna $n_t^{th}$ and receiving antenna $n_r^{th}$. The channel transfer matrix $H$ can be diagonalized using the Singular Value Decomposition (SVD) technique

$$H = U * D * V^H \tag{1}$$

In this equation $U$ and $V$ are unitary matrices; $D$ is $N_t$x$N_r$ diagonal matrix containing the real and non-negative singular values; $(.)^H$ means complex transpose. By applying the matrix $U^H$ at the transmit side and the $V$ matrix at the receive side the $K = min(N_t, N_r)$ orthogonal channels can be realized. Each channel has a channel gain of $\lambda_k$, which is the square of the singular values in matrix $D$. The square of the singular values are the eigenvalues and could also be obtained by SVD of matrix $G$, which is

$$G = H * H^H = UDD^T U^H \tag{2}$$

where $(.)^T$ denotes transpose operator. The realization of $K$ parallel channels is achieved by processing significant uncorrelated multi-path components stemming from the environment's scattering richness. To study in more detail the realization of these parallel channels the discrete time base-band interpretation of a single transmitted vector of symbols is preferred. In the base-band, it is assumed that the frequency synchronization and sampling are perfectly achieved. The received vector of symbols will have the form

$$Y = X * U * D * V^H + N_{noise} \tag{3}$$

By using the weight vectors $U^H$ at the transmit side and weight vectors $V$ at the receive side the received vector of symbols becomes

$$\widetilde{Y} = X * D + \widetilde{N}_{noise} \tag{4}$$

The noise matrix $N_{noise}$ of size $(1,N_r)$ after being weighted has unchanged variance since the $U$ matrix is unitary. This equation implies that the power put into $K$ parallel channels will be amplified by the eigenvalues; power put into channel(s) which have index larger than $K$ will be lost.

## III. Feedback delay model

In the ideal case i.e. when we have TDD system with reciprocal and quasi-stationary channel, the CSI can be obtained timely at both ends. The channel matrix $H$ can be diagonalized and we can transmit $K$ independent channels. However, in the FDD system the transmitted and received signal will be influenced by independent fading. In order to have knowledge of the CSI at both ends the measured values must be sent back and forth (figure 1). Under the limitation of overhead, processing and updating time the CSI is subject to delay. For simplicity we assume that CSI will be updated after two consecutive frames and the delay time will be twice the time of transmitting one frame plus the processing time. It should be noted here that non-ideal updating of the CSI
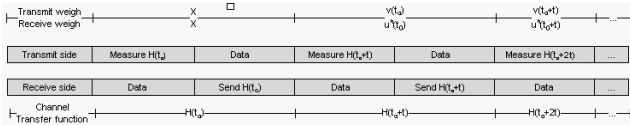


Fig. 1. Example of CSI updating scheme.

could also occur in the TDD system when the updating time is larger than the coherent time of the channel. The feedback delay model presented above can easily be extended for this case.

### A. Markov chain model

In the MIMO system, the feedback delay causes the weight vectors at both sides to be out of date. It means that the orthogonality of $K$ channels cannot be guaranteed as the channel has changed by the time the weight vectors are applied. In order to investigate the influence of feedback delay, it is necessary to build a channel state evolution model. In [3], Jakes proposed a model for a time selective narrowband channel which is interpreted by the channel state correlation coefficient $\rho$ as

$$\rho = \frac{E(h_{n_t n_r}(t_o) h^*_{n_t n_r}(t_o + t))}{\sigma^2_{n_t n_r}} = J_o(2\pi f_d t) \tag{5}$$

where $E(.)$ denotes the expectation operator, $J_o(.)$ is the zero order Bessel function of the first kind, $f_d$ is the maximum Doppler frequency, $t$ is the delay time and $\sigma^2_{n_t n_r}$ is the variance of the channel coefficient which is equal to one in our case. Although this model provides us information on

to what extent the two channel coefficients are correlated, the channel is not easy to be tracked [4]. Therefore we need a model capable of describing the evolution in time of the channel. In [6] a simple Markov chain models the channel state evolution is presented where the current channel coefficient is related to the past channel coefficient as

$$h_{n_t n_r}(t_o + t) = \rho h_{n_t n_r}(t_o) + \sqrt{1 - \rho^2} e_{n_t n_r} \sigma^2_{n_t n_r} \tag{6}$$

where $e_{n_t n_t} \sim \mathcal{CN}(0,1)$ and with $\sigma^2_{n_t n_r}=1$ the equation is reduced to

$$h_{n_t n_r}(t_o + t) = \rho h_{n_t n_r}(t_o) + \sqrt{1 - \rho^2} e_{n_t n_r} \tag{7}$$

This model allows us to track the channel state given the knowledge of the past. The channel state matrix at time $t+t_o$ can be predicted based on the channel matrix at time $t_o$ as

$$H(t_o + t) = \rho H(t_o) + \sqrt{1 - \rho^2} E \tag{8}$$

Here $E$ is the $N_t$x$N_r$ matrix with $\mathcal{CN}(0,1)$ components. In the presence of feedback delay, the channel state matrix $H(t_o)$ will be diagonalized and the $U^H$ and $V$ weights matrices are applied when the actual channel state matrix has changed to $H(t_o + t)$. The actual received signals are described by

$$\begin{aligned} \tilde{Y} &= XU^H H(t_0 + t)V + U^H N_{noise} \\ &= XU^H(\rho H(t_o) + \sqrt{1 - \rho^2} E)V + \tilde{N}_{noise} \\ &= \rho XD + \sqrt{1 - \rho^2} XU^H EV + \tilde{N}_{noise} \end{aligned} \tag{9}$$

From this equation it is clear that the orthogonality of the channels no longer holds true. The received signal of one channel is not its own amplified signal as in the ideal case but combined by the signals of other channels. In [7] Telatar showed that if $U^H$ and $V$ are two unitary matrices of size $N_t$x$N_t$ and $N_r$x$N_r$ respectively the distribution of $U^H EV$ will be the same as that of $E$. Hence the product of these three matrices is another matrix of size $N_t$x$N_r$ with $\mathcal{CN}(0,1))$ components. We denote this matrix as $Q$. Equation (9) can be rewritten as

$$\tilde{Y} = \rho XD + \sqrt{1 - \rho^2} XQ + \tilde{N}_{noise} \tag{10}$$

Expressing this equation in component-wise and considering the $k^{th}$ received signal ($1 \leq k \leq K$) we get

$$\tilde{y_k} = \rho\sqrt{\lambda_k}x_k + \sqrt{1 - \rho^2}\sum_{i=1}^{K} x_i q_{ik} + n_{noise} = \rho\sqrt{\lambda_k}x_k$$
$$+ \sqrt{1 - \rho^2}x_k q_{kk} + \sqrt{1 - \rho^2}\sum_{i\neq k,i=1}^{K} x_i q_{ik} + n_{noise} \tag{11}$$

Since $x_k$ is independent and normally has zero mean, the mean received power of channel $k^{th}$ in the presence of feedback delay can be expressed as

$$\begin{aligned} \widetilde{P_{(k)}} &= (|\rho\sqrt{\lambda_k} + \sqrt{1 - \rho^2}q_{kk}|^2)P_{(k)} \\ &+ (1 - \rho^2)\sum_{i\neq k,i=1}^{i=K} P_{(i)}|q_{ik}|^2 + \sigma^2_{noise} \end{aligned} \tag{12}$$

where $P_{(i)}$ is the transmitted power of channel $i$, $\sigma_{noise}^2$ is the variance of the noise. From the equation it can be seen that the received power is heavily dependent on the eigenvalues and the correlation coefficient factor. The interference of other channels can be assumed as Gaussian noise source having the same power. Consequently the signal to interference plus noise (SINR) of channel $k$ can be approximated as

$$
\begin{aligned}
SINR_k &= \frac{|\rho\sqrt{\lambda_k} + \sqrt{1-\rho^2}q_{kk}|^2 P_{(k)}}{(1-\rho^2)\sum_{i\neq k, i=1}^{i=K} P_{(i)}|q_{ik}|^2 + \sigma_{noise}^2} \\
&= \frac{|\rho\sqrt{\lambda_k} + \sqrt{1-\rho^2}q_{kk}|^2 SNR_{(k)}}{(1-\rho^2)\sum_{i\neq k, i=1}^{i=K} SNR_{(i)}|q_{ik}|^2 + 1}
\end{aligned} \quad (13)
$$

### B. Scattering model

Scattering model is another approach, which gives more physical insight to the evolution of channel state of moving mobile terminal. This simple model assumes that the received signal is the superposition of number of waves generated from random scattering objects. For narrowband MIMO system the discrete time CSI can be described in the base-band by

$$
h_{n_t n_r}(t_o) = \sum_{n=1}^{N} a_l e^{-j2\pi f_d t_o \cos\theta_l} \quad (14)
$$

where $\theta_l$ is uniformly distributed over $(0..2\pi)$, $a_l$ is a random complex Gaussian number with zero mean and normalised so that variance of $h_{n_t n_r}$ is 1, $f_d$ as before is the maximum Doppler frequency. $N$ is the number of scatterers and $N > 10$ is known to be large enough to approximate Rayleigh distribution [8]. If all the scatterers are assumed to be stationary, at time $t + t_o$ the channel state reads

$$
h_{n_t n_r}(t_o + t) = \sum_{l=1}^{L} a_l e^{-j2\pi f_d(t_o+t)\cos\theta_l} \quad (15)
$$

Although this model also allows us to track the channel state, based on the model it may be difficult to derive a closed form of the average SINR. Hence, the model lacks of explanation why feedback delay effect degrades the system's theoretical capacity and performance. Nevertheless, it can act as reference to verify the results obtained from the Markov chain model described in the previous section.

### IV. MIMO CAPACITY WITH FEEDBACK DELAY

It is well known that the capacity of MIMO system when the transmit side does not have knowledge of the CSI is achieved by putting equal power into the channels

$$
C = \sum_{k=1}^{K} log_2(1 + \lambda_k \frac{SNR}{N_t}) \quad (16)
$$

With the advantage of having CSI at the transmit side the eigenvalues correspond to gain of channels can be obtained by SVD technique. Under the constraint of the total transmitted power, based on the eigenvalues, water-filling method is normally used to get the maximal achievable capacity. The essence of the water-filling algorithm is that it will distribute more power to the channel with high gain (i.e. large eigenvalue) and less power, even skipping transmission on the channels with lower gain. Therefore, the MIMO channel capacity with CSI knowledge at both sides is maximized, that is

$$
C = \sum_{k=1}^{K} log_2(1 + \lambda_k \gamma_k) \quad (17)
$$

where $\gamma_k = max(\mu - \frac{1}{\lambda_k}, 0)$ and the parameter $\mu$ is chosen such that $\sum_{k=1}^{K} \gamma_k = SNR$. In the presence of feedback delay the capacity of the system is changed to

$$
C = \sum_{k=1}^{K} log_2(1 + SINR_k) \quad (18)
$$

Numerical values of channel capacity are shown in figure 2. We only consider the scenario where channel states is highly correlated in the interval $t$ (i.e. $f_d t < 0.1$). For this reason, in the simulation we chose the delay time of 1ms and three Doppler frequencies of 30, 45 and 60Hz. The influence of feedback delay is shown for three system configurations symmetric 4x4 and asymmetric 6x4, 8x4 to highlight the differences in the eigenvalue distributions. The average system capacities are plotted as a function of the SNR values. In those figures the curves with straight lines represent the capacity estimated by the Markov chain model, curves represented by symbols show the capacity estimated by the scattering model. These curves are overlapped each other indicating a good agreement in the results obtained from the two models. These figures also illustrate a reduction in system capacity at higher values of the Doppler frequency and delay time. For given $f_d t$ value, the effect of feedback delay can lead to a situation where the capacity of the MIMO system with perfect CSI at receiver only outperform that of the system with delayed CSI at both sides.

### V. MIMO'S PERFORMANCE WITH FEEDBACK DELAY

Once the performance of MIMO system is focused other than the capacity, the signal of a diversity system must be processed to have strong impact on the BER other than the spectral efficiency. It is an advantage to have the CSI at the transmit side as from that information we can improve the performance of the system optimally. However, non-ideal updating of CSI deviates the system performance from the perfect case. Therefore it is of interest to investigate the degradation of the system performance in the non-ideal situation. Here, the BER is used as a means to estimate the degradation of the MIMO system's performance under influence of feedback delay.

### A. Analytical results

We restrict ourselves to the narrowband MIMO and the performance degradation assessment will be based on BPSK

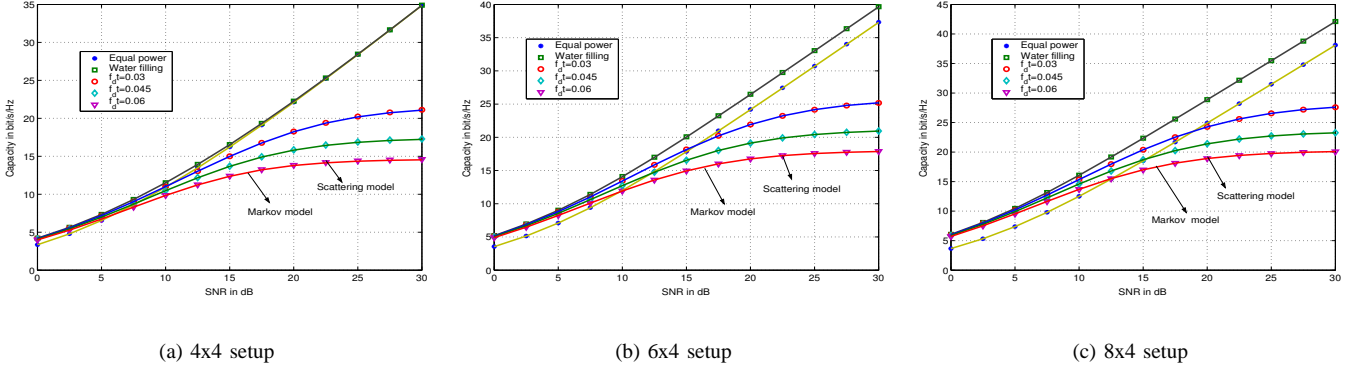| (a) 4x4 setup | (b) 6x4 setup | (c) 8x4 setup |

Fig. 2. Capacity of several MIMO system setup with and without feedback delay

modulation scheme. As mentioned in section II, having CSI at both sides it is possible to transmit up to $K$ parallel channels. However, because of the differences in the eigenvalues, equally distributed power is not an optimum solution. Instead, the total transmitted power must be distributed optimally to get overall improvement in the average BER. The essence of the algorithm can be interpreted as an inverse water filling procedure. In that more transmitted power is put into the weak channels (i.e. low eigenvalues) to reduce the average BER.

Basically for certain SNR the BER of individual M-QAM or M-PSK channel is known. By using Chernoff bound and Gallager's multiplier we can derive a solution to obtain the best performance in terms of BER. It can be shown that the overall BER of the particular system using BPSK modulation will be minimized if the distributed power is satisfied (detail derivation presented in the appendix)

$$\gamma_k = max(\frac{1}{\lambda_k}(ln(\lambda_k) - \mu), 0)$$

$$\mu \text{ is chosen such that} \sum_{k=1}^{K} \gamma_k = SNR \quad (19)$$

The average BER of the ideal system can be expressed as

$$BER_{average\_ideal} = E(\frac{1}{T}\sum_{k=1}^{T} Q(\sqrt{2\lambda_k SNR_k})) \quad (20)$$

where $SNR_k = \gamma_k$, $T$ is the number of used channel ($1 \leq T \leq K$). When there is feedback delay, the received signal will be disturbed not only by the noise but also by the signals of other channels. The average BER of such system can be approximated as

$$BER_{average} \approx E(\frac{1}{T}\sum_{k=1}^{T} Q(\sqrt{2SINR_k})) \quad (21)$$

The numerical results of average BER for 4x4 and 6x4 and 8x4 cases are presented in figure 3. As shown in this figure, with the ideal CSI at both link ends for BER of $10^{-3}$ the required SNR of the equal power scheme is up

to 5dB more than that of distributed power scheme. Besides, the average BER(s) reduces (so that the performance increases) in the order of 4x4, 6x4, 8x4 system setup. The relation between transmitting-receiving antenna setup and distribution of eigenvalues (i.e. more asymmetric meaning more even distribution of eigenvalues) is the main reason for these increments in system's performance. Like the results in the investigation of the system capacity, the performance of the MIMO system under the impact of feedback delay also degrades at high SNR values. It can be explained by the fact that when the transmitted power is increased, the power distributed into each channel is increased as well. Consequently, more interfered power will be generated. Therefore, the SINR of individual channel decreases toward a constant value and the overall BER approaches a BER floor.

*B. Monte Carlo simulation*

To justify the analytical results, Monte Carlo simulation for the three system setups 4x4, 6x4 and 8x4 are made. The results are shown in figure 4. Comparisons of the analysis and simulation results are shown in the same figure. Transmitted data used in the simulations are random. They are detected at the receive side by maximum likelihood detection method. In general, the average BER obtained from the approximation of SINR are quite in line with that from Monte Carlo simulation. The differences could be attributed to the approximation of the average SINR where the interferences from other channels are replaced by Gaussian noise source of the same power.

VI. CONCLUSION

In this work we have investigated the MIMO system performance and capacity in the presence of feedback delay. The variation in time of the channel coefficient, which causes the delay in the feedback was modelled by the Markov chain model and the scattering model. It is demonstrated that the capacity of MIMO system suffers degradation when the CSI is not sufficiently updated. Above certain SNR values, as a result of the delay the capacity of system with CSI at
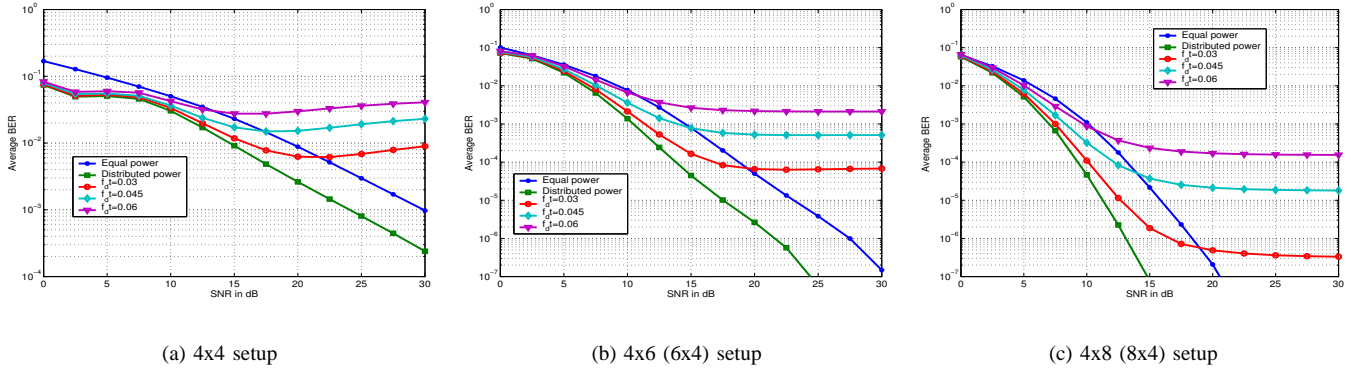
(a) 4x4 setup       (b) 4x6 (6x4) setup       (c) 4x8 (8x4) setup

Fig. 3.    BER of MIMO systems with and without feedback delay



(a) 4x4 setup       (b) 4x6 (6x4) setup       (c) 4x8 (8x4) setup
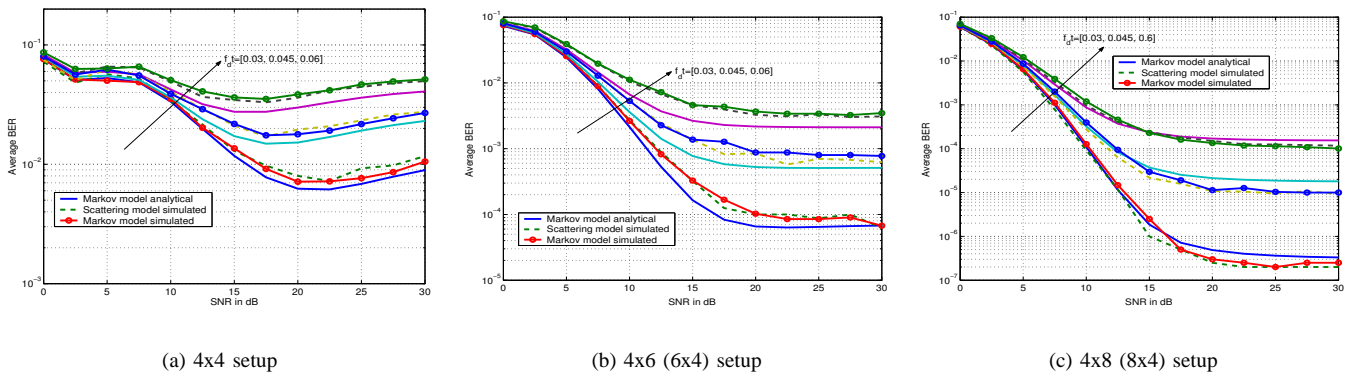
Fig. 4.    BER of MIMO systems with and without feedback delay

both sides becomes less than that of the system where CSI is perfectly known at the receive side only. The average BER with optimum power distribution considering as the performance of the MIMO system is also influenced. It approaches a BER floor when the SNR values increase.

### APPENDIX

#### *Derivation of optimal power allocation algorithm*

For BPSK modulation the BER of channel $k^{th}$ can be expressed as

$$P_{error_k} = Q(\sqrt{2\lambda_k \gamma_k}) \text{ where } \sum_{k=1}^{K} \gamma_k = SNR \qquad (22)$$

The average BER of the overall system is

$$P_{error\_average} = \frac{1}{K} \sum_{k=1}^{K} Q(\sqrt{2\lambda_k \gamma_k}) \qquad (23)$$

Using the Chernoff's bound, the BER of channel $k$ is upper bounded by

$$P_{error\_k} = Q(\sqrt{2\lambda_k \gamma_k}) \leq \frac{1}{2} e^{-\lambda_k \gamma_k} \qquad (24)$$

Following the Gallager's multiplier procedure, the problem now is to find set of $\gamma$ so that the $P_{error\_average}$ is minimized. Since $K$ is constant, it is equal to finding a set of $\gamma$ to minimize the sum

$$Sum = \sum_{k=1}^{K} (e^{-\lambda_k \gamma_k} + \varepsilon \gamma_k) \text{ where } \varepsilon \text{ is variable} \qquad (25)$$

The solution can be obtained if we differentiate the $Sum$ with respect to $\gamma_k$ and set it to zero

$$-\lambda_k e^{-\lambda_k \gamma_k} + \varepsilon = 0 \rightarrow \lambda_k e^{-\lambda_k \gamma_k} = \varepsilon$$

$$-\lambda_k \gamma_k = ln(\frac{\varepsilon}{\lambda_k}) \rightarrow \gamma_k = \frac{1}{\lambda_k} ln(\lambda_k) - \frac{1}{\lambda_k} ln(\varepsilon)$$

$$\gamma_k = (\frac{1}{\lambda_k}(ln(\lambda_k) - \mu)), \text{where } \mu = ln(\varepsilon) \qquad (26)$$

### REFERENCES

[1] P. Kyritsi, D.C. Cox, R.A. Valenzuela, "Channel and capacity estimation errors", IEEE Communications Letters, Volume: 6 Issue: 12 Dec 2002, Page(s): 517 -519

[2] G.Lebrun, T.Ying, M.Faulkner "MIMO transmission over a time-varying channel using SVD" Global Telecommunications Conference, 2002 IEEE , Volume: 1, Pages:414 - 418.

[3] W.C.Jakes"Microwave Mobile Communications", New York Wiley 1974.

[4] E.N.Onggosanusi, A.Gatherer, A.G.Dabak, S.Hosur "Performance Analysis of Closed-Loop Transmit Diversity in the presence of feedback delay", IEEE Transactions on Communications, Volume 49 Issue: 9, Sept. 2001 Pages:1618 - 1630

[6] S.Haykin "Adaptive Filter Theory", Englewood Cliffs, NJ, Prentice Hall, 1996.

[7] I.E.Telatar "Capacity of Multi-antenna Gaussian Channels", European Transactions on Telecommunications, Vol. 10, No. 6, pp. 585-595, Nov/Dec 1999

[8] R.Vaughan and J.B.Andersen Channels propagation and antennas for mobile communications, IEE Electromagnetic Waves Series 50, ISBN 085296 084 0, 2003.

# Prediction of the eigenvectors for spatial multiplexing MIMO systems in time-varying channels

Hung Tuan Nguyen
Department of Communication Technology
Aalborg University
Niels Jernes Vej 12, DK-9220 Aalborg
Email: htn@kom.auc.dk

Geert Leus
Faculty of Electrical Engineering
Delft University of Technology
Mekelweg 4 2628 CD Delft
The Netherlands
Email:leus@cas.et.tudelft.nl

Nadia Khaled
Interuniversity Micro-Electronics Center
Kapeldreef 75, B-3001 Leuven
Belgium
Email:khaledn@imec.be

*Abstract*— **In mobile communications, time varying channels make the available channel information out of date. Timely updating the channel state is an obvious solution to improve the system performance in a time varying channel. However, a better knowledge of the channel comes at the cost of a decrease in the system throughput. Thus, predicting the future channel conditions can improve not only the performance but also the throughput of many types of wireless systems. This is especially true for a wireless system where multiple antennas are applied at both link ends. In this paper we propose and evaluate the performance of a prediction scheme for multiple input multiple output (MIMO) systems that apply spatial multiplexing. We aim at predicting the future precoder/decoder directly without going through the prediction of the channel matrix. The results show that in a slowly time varying channel an increase in the system performance by a factor of two is possible.**

## I. INTRODUCTION

Multiple input multiple output (MIMO) systems have a potential of offering higher capacity than the traditional single input single output (SISO) systems by utilizing space, polarization or pattern diversity [1], [2]. In a MIMO system, it is possible to transmit a few data streams in parallel, called spatial multiplexing. Decoupling the data streams can be done by using the channel knowledge at the receiver only. One can use zero forcing (ZF), minimum mean square error (MMSE), successive interference cancellation or ordered successive interference cancellation (VBLAST) to decouple the subchannels. However, since the transmitted signals are not matched to the channel, degradation in system performance is inevitable. Once the channel information is available at both ends of the transmission link the singular value decomposition (SVD) transmission structure appears to be an elegant technique to diagonalize the channel matrices [3].

In a time-varying channel, the schemes mentioned above are subject to a performance degradation. The variation of the channel with time causes the available channel state information (CSI) at both sides to be out of date. While prediction of the future CSI for a SISO channel is possible using available methods (i.e. [4], [5], [6], [7], [9] among others) predicting

all components of the CSI matrix in a MIMO system appears to be cumbersome. Moreover the precoder/decoder obtained from the SVD of the predicted channel matrix is more prompt to estimation errors.

Having an orthonormal property and a square structure, the precoders and decoders belong to a unitary group, denoted as $\mathcal{U}(D)$ where $D$ is the dimension. This $\mathcal{U}(D)$ group is a subgroup of the Stiefel manifold which contains all rectangular matrices with orthonormal columns. On $\mathcal{U}(D)$, one can use the so-called geodesic interpolation to find the smoothest trajectory or geodesic flow between two successive points [8], [10], [11]. In this paper, by extending the geodesic interpolation idea we investigate the possibility of predicting the precoder and decoder in a time-varying frequency flat MIMO channel. The paper is organized in the following way. First, the system model is presented in section II. Section III describes the prediction algorithm. Performance evaluation of the algorithm is investigated in section IV. Finally, some conclusions and remarks wrap up the paper in section V.

## II. SYSTEM MODEL

Let us consider a spatial multiplexing narrowband MIMO system consisting of $N_t$ transmitting antennas and $N_r$ receiving antennas. Without using the precoder and decoder the received symbol vector has the form

$$\mathbf{y}_i = \mathbf{H}_i \mathbf{x}_i + \mathbf{n}_i \tag{1}$$

where $\mathbf{x}_i$ is the transmitted symbol vector and $\mathbf{n}_i$ is the additive noise, subscript $i$ is the transmitted symbol index. The precoder and decoder are obtained from the SVD of the channel matrix $\mathbf{H}_i$

$$\mathbf{H}_i = \mathbf{U}_i \mathbf{\Lambda}_i \mathbf{V}_i^H \tag{2}$$

where $\mathbf{\Lambda}_i$ is a diagonal matrix containing the singular values and $(.)^H$ denotes the complex conjugate transpose operation. The two unitary matrices $\mathbf{U}$ and $\mathbf{V}$ are in $\mathcal{U}(N_r)$ and $\mathcal{U}(N_t)$, respectively.
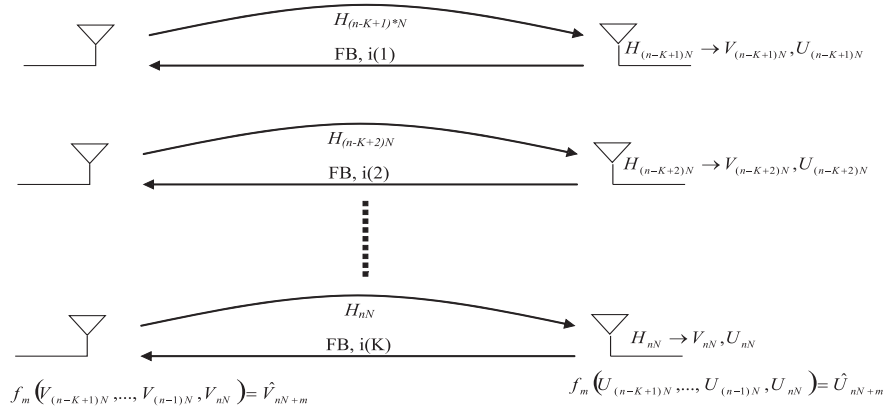
Fig. 1.   Precoder/decoder prediction in a feedback delay scheme

Applying the precoder $\mathbf{V}_i$ and the decoder $\mathbf{U}_i^H$, at the transmitter and receiver, respectively, it is possible to decouple the MIMO channel into $S = min(N_t, N_r)$ subchannels, which we can use to transmit $Q \leq S$ data streams in parallel. Applying the precoder and decoder, we obtain

$$\begin{aligned} \mathbf{y}_i &= \mathbf{U}_i^H \mathbf{U}_i \mathbf{\Lambda}_i \mathbf{V}_i^H \mathbf{V}_i \mathbf{x}_k + \mathbf{U}_i^H \mathbf{n}_i \\ &= \mathbf{\Lambda}_i \mathbf{x}_i + \widetilde{\mathbf{n}}_i \end{aligned} \qquad (3)$$

As long as the leakage among the subchannels is not severe, the individual substreams can be detected separately. Because no joint detection is required, the detection algorithm becomes rather simple.

We use the well known Jakes' model, [13] to model the time-varying channel. The maximum relative velocity is related to the maximum Doppler frequency $f_d$ by $v = c\frac{f_d}{f_c}$; where $f_c$ is the carrier frequency and $c$ is the velocity of light. Each element of the channel matrix $\mathbf{H}_i$ is simulated as a superposition of a few tens of uncorrelated plane waves. For a narrowband MIMO system the discrete time channel state information (CSI) can be described in baseband by

$$[\mathbf{H}_i]_{m,n} = \frac{1}{\sqrt{L}} \sum_{l=1}^{L} a_l e^{-j2\pi f_d T_s cos\phi_l} \qquad (4)$$

where $\phi_l$ is uniformly distributed over $(0, 2\pi]$, $a_l$ is a random complex Gaussian number with zero mean and variance 1, $f_d$ is the maximum Doppler frequency, $T_s$ is the symbol period and $L$ is the number of scatterers.

At the start of each transmitted frame, we assume the precoder and decoder are derived from the SVD of the estimated channel matrix $\mathbf{H}_i$ and the precoder is fed back to the transmitter. For simplicity we assume that the noise free precoder and decoder are instantaneously updated at the start of each frame. Because of the time-varying channel, the precoder and decoder gradually become out of date at the end of each transmitted frame. Leakage among the subchannels is more severe at the end of each frame and performance degradation is inevitable.

Figure 1 shows the proposed precoder/decoder prediction scheme in a time-varying channel. In the figure, $N$ is the number of symbols within the frame and $n$ is the frame index. The prediction scheme is based on the information that would be available for any MIMO system applying spatial multiplexing. Using the nearest $K$ past precoders/decoders, the precoders/decoders for the transmitted/received symbols within the next frame are predicted. Therefore, in a predicted precoder/decoder system the overhead required for channel probing is the same as for the unpredicted ones but the performance improves.

### III. PREDICTION OF THE PRECODER AND DECODER

Unlike other methods used to predict the future CSI, in the prediction of the precoder/decoder, the orthonormal constraint must be retained. One can use a projection based method where the precoder/decoder is first predicted in the Grassmann manifold and then projected onto the Stiefel manifold. However, for interpolation purposes, the performance of this scheme is shown to be lower than that of other methods [12].

The orthonormal property and square structure of the precoder/decoder matrix allow us to perform the exponential map, a key transformation step in geodesic interpolation. Based on the geodesic interpolation, interpolation of the precoder for spatial multiplexing MIMO-OFDM systems has been recently illustrated in [12]. Therefore, we decided to extend the geodesic interpolation method to extrapolate the precoder and decoder for a frequency flat time-varying MIMO channel.

Since the precoder/decoder as a solution of the SVD of the channel matrix $\mathbf{H}_i$ is not unique, the correlation of the consecutive precoder/decoder elements are always lower than that of the channel matrix $\mathbf{H}_i$. Therefore, to enhance the prediction performance, the precoder/decoder needs to be transformed in a way to reduce the ambiguity. For simplicity, in the following we formulate a prediction scheme for the precoder only. The future decoders are predicted in the same manner.

On the $K$ past precoder matrices denoted as $\mathbf{V}_{nN}, \mathbf{V}_{(n-1)N}, ..., \mathbf{V}_{(n-K+1)N}$ we perform the following

transformation

$$\begin{aligned}
\mathbf{V}_{nN} &\rightarrow & \mathbf{I} = \mathbf{V}_{n,o}^{Tr} = expm(\mathbf{S}_{n,0}) \\
\mathbf{V}_{(n-1)N} &\rightarrow & \mathbf{V}_{nN}^{-1}\mathbf{V}_{(n-1)N}\mathbf{\Theta}_{n,-1} = \\
& & \mathbf{V}_{n,-1}^{Tr} = expm(\mathbf{S}_{n,-1}) \\
& \vdots & \\
\mathbf{V}_{(n-K+1)N} &\rightarrow & \mathbf{V}_{nN}^{-1}\mathbf{V}_{(n-K+1)N}\mathbf{\Theta}_{n,-K+1} = \\
& & \mathbf{V}_{n,-K+1}^{Tr} = expm(\mathbf{S}_{n,-K+1}) \quad (5)
\end{aligned}$$

where $expm(.)$ is the matrix exponential operator and $(.)^{Tr}$ denotes the transformed matrix. Further information on the exponential map of matrices in $\mathcal{U}(D)$ can be found in [10] and [11].

In (5), $\mathbf{\Theta}_{n,k}$, with $k \in \{-K+1,\ldots,-1,0\}$ is the orientation matrix that makes the two matrices $\mathbf{V}_{nN}$ and $\mathbf{V}_{(n+k)N}\mathbf{\Theta}_{n,k}$ as close as possible in Euclidean distance. We use the same solution as the one proposed in [12] to find the orientation matrix $\mathbf{\Theta}_{n,k}$

$$\mathbf{\Theta}_{n,k} = diag(\mathbf{V}_{(n-k+1)N}^{-1}\mathbf{V}_{nN}) \oslash |diag(\mathbf{V}_{(n-k+1)N}^{-1}\mathbf{V}_{nN})| \quad (6)$$

where $\oslash$ represents element-wise division. The $\mathbf{S}_{n,k}$ matrix is a skew-Hermitian matrix. It can be calculated by

$$\mathbf{S}_{n,k} = \mathbf{A}_{n,k}ln(\mathbf{\Xi}_{n,k})\mathbf{A}_{n,k}^{-1} \quad (7)$$

where $\mathbf{A}_{n,k}$ and $\mathbf{\Xi}_{n,k}$ are derived from the eigenvalue decomposition of the transformed matrix $\mathbf{V}_{n,k}^{Tr}$, $\mathbf{V}_{n,k}^{Tr} = \mathbf{A}_{n,k}\mathbf{\Xi}_{n,k}\mathbf{A}_{n,k}^{-1}$. Through these $K$ skew-Hermitian matrices $(\mathbf{S}_{n,-K+1}, \mathbf{S}_{n,-K+2}, ..., \mathbf{S}_{n,0})$ we try to fit a $P^{th}$ order polynomial. When $P+1$ is equal to $K$, the $P^{th}$ order matrix polynomial goes exactly through the K skew-Hermitian matrices $\mathbf{S}_{n,k}$. The $P+1$ unknown matrix coefficients can be solved by a set of $K$ linear matrix equations:

$$\mathbf{S}_{n,k} = \sum_{p=0}^{P} \mathbf{C}_{n,p}((n+k)N)^p \quad (8)$$

where $k \in \{-K+1,\ldots,-1,0\}$.

When $P+1$ is strictly smaller than $K$, the $P+1$ unknown coefficients can be obtained by using the least squares fitting. Note that the skew-Hermitian property of the K matrices $\mathbf{S}_{n,k}$ is translated to a skew-Hermitian property for the coefficient matrices $\mathbf{C}_{n,p}$. Hence, any prediction using the obtained $P^{th}$ order matrix polynomial leads to a skew-Hermitian matrix and thus to a unitary precoder. The skew-Hermitian matrix $\hat{\mathbf{S}}_{nN+m}$ at time index $nN+m$ is estimated by

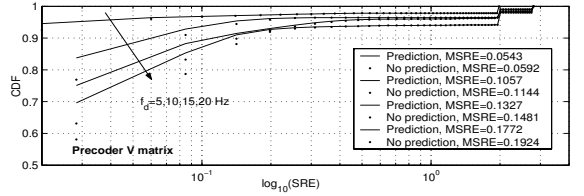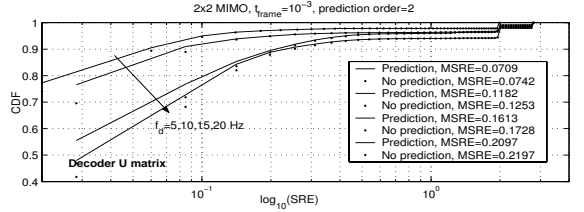$$\hat{\mathbf{S}}_{nN+m} = \sum_{p=0}^{P} \mathbf{C}_{n,p}(nN+m)^p \quad (9)$$

where $m \in \{1,2,\ldots,N-1\}$. The corresponding future precoders for the $(K+1)^{th}$ frame can thus be constructed as

$$\hat{\mathbf{V}}_{nN+m} = \mathbf{V}_{nN}expm(\hat{\mathbf{S}}_{nN+m}) \quad (10)$$

Note also that in the proposed scheme there is no restriction on the prediction resolution or the number of symbol $N$ within a frame.
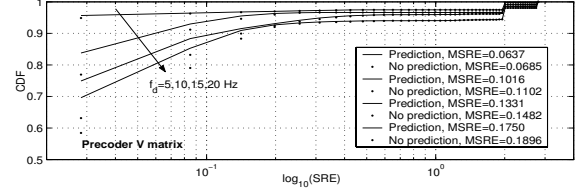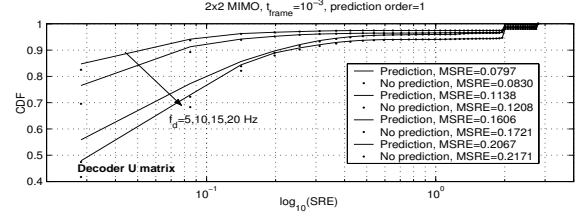


(a) 2x2 Prediction order P=1



(b) 2x2 Prediction order P=2

Fig. 2. The distribution of the precoder/decoder prediction error for various settings and maximum Doppler spread values in a 2x2 MIMO setting

## IV. PERFORMANCE EVALUATION

A natural criterion for evaluating the performance of the prediction scheme is the following square root error ($SRE$) measure

$$SRE_V = ||\hat{\mathbf{V}}_i - \mathbf{V}_i||_F \text{ or } SRE_U = ||\hat{\mathbf{U}}_i - \mathbf{U}_i||_F \quad (11)$$

where $||.||_F$ denotes the Frobenius norm. The SRE essentially is the Euclidean distance between the predicted precoder/decoder and the true ones.

Since the precoder and decoder obtained from the SVD of the channel matrix $\mathbf{H}_i$ are ambiguous up to an orientation matrix, comparing the predicted precoder/decoder with the true ones may not be a good way of evaluating the prediction performance. The predicted precoder/decoder when applied at the transmitter and receiver should create the least power leakage between the subchannels. In other words, the off-diagonal components of the matrix $\hat{\mathbf{U}}_i^H \mathbf{H}_i \hat{\mathbf{V}}_i$ should be as close

(a) 4x4 Prediction order P=1
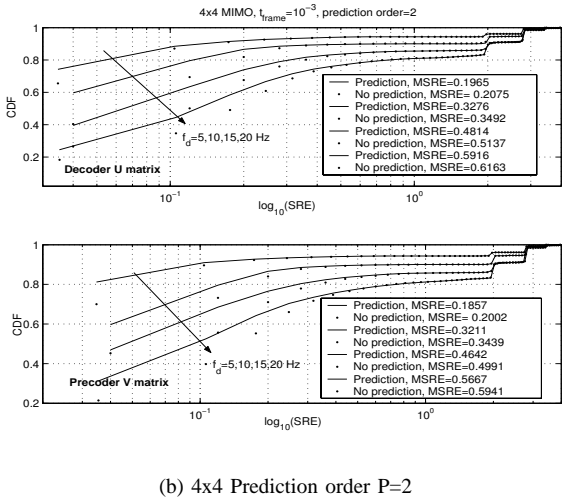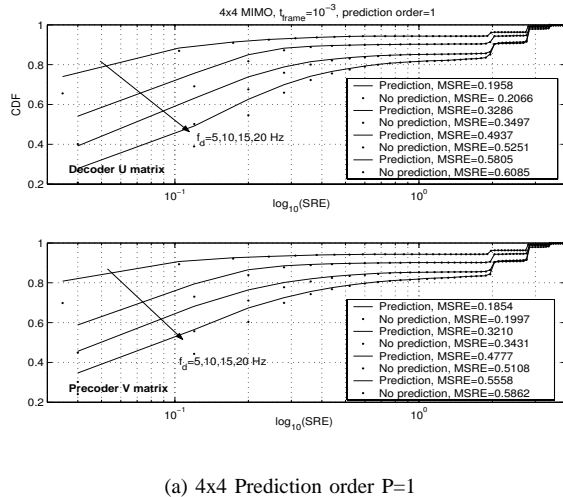


(b) 4x4 Prediction order P=2

Fig. 3. The distribution of the precoder/decoder prediction error for various settings and maximum Doppler spread values in a 4x4 MIMO setting

as possible to zero. Therefore, we chose another metric which we call the leakage level to evaluate the performance of the prediction scheme, that is

$$||\hat{\mathbf{U}}_i^H \mathbf{H}_i \hat{\mathbf{V}}_i - \mathbf{\Lambda}_i||_F \qquad (12)$$

In the prediction of the precoder/decoder we aim at a slowly time-varying channel with a maximum Doppler spread ranging from a couple of Hz to a few tens of Hz. This type of channel can occur in an indoor environment. The time required to transmit a data frame is $t_{frame} = NT_s = 10^{-3}$s. The channel matrices were generated using the model described in section II. We consider 1000 channel realizations. The total number of simulated frames was 1000.

Figures 2 and 3 show the cumulative distribution function (CDF) of the $SRE$ for different values of the maximum Doppler frequency, prediction order and MIMO settings. For comparison, we also calculate the $SRE$ for the time-varying

MIMO channel where the same precoder/decoder is used for the whole data frame (without prediction). The mean values of the $SRE$ are shown in the same figure. From the results it can be seen that when applying prediction the $SRE$ is indeed lower than for the case where no prediction is made. However, for a low Doppler spread (5Hz) and a low number of transmitting and receiving antennas (2x2) the improvement in the $SRE$ is moderate. Including more than two points ($K > 2$) in order to predict the future precoder/decoder may not enhance the prediction performance. The past frames which do not follow the variation of the newly updated frames spoil the prediction preciseness. This also reflects a general trend which can be observed in predicting the time-varying channel coefficients.



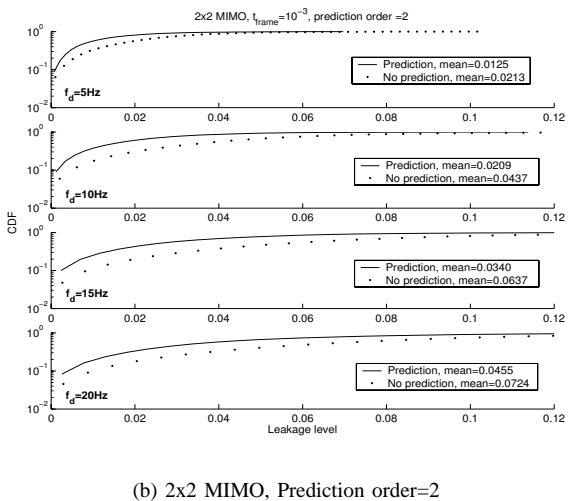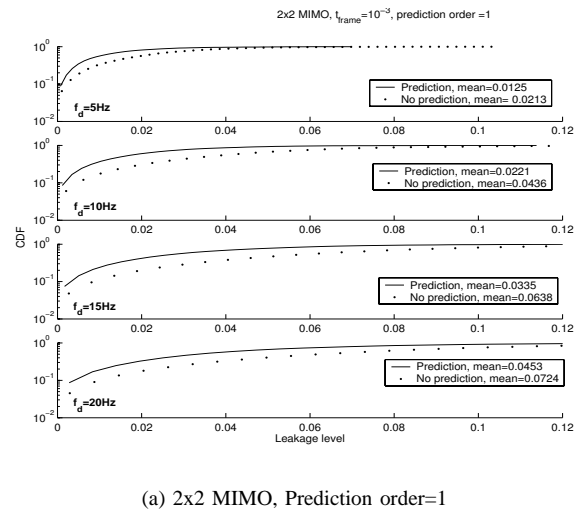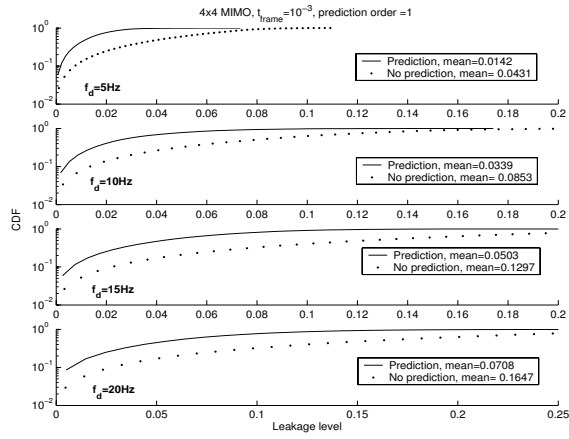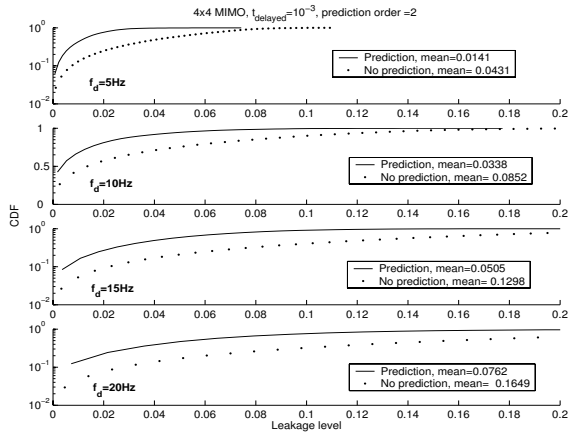(a) 2x2 MIMO, Prediction order=1



(b) 2x2 MIMO, Prediction order=2

Fig. 4. CDF of the leakage for the 2x2 setting

Figures 4 and 5 show the leakage level for a 2x2 and 4x4 MIMO system with and without precoder/decoder prediction. Using the leakage metric defined in (12) the performance improvement of the prediction scheme with the first and second
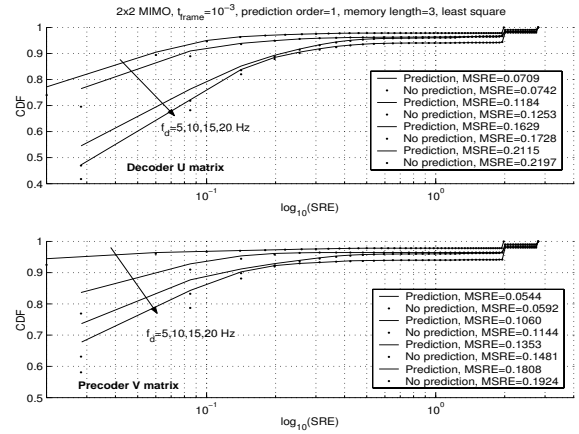
(a) 4x4 MIMO, Prediction order=1



(b) 4x4 MIMO, Prediction order=2

Fig. 5.   CDF of the leakage for the 4x4 setting



(a) 2x2 setting



(b) 4x4 Setting

Fig. 6.   The distribution of the precoder/decoder prediction error for various MIMO settings and maximum Doppler spread values

order polynomial prediction can be clearly seen. With the precoder/decoder prediction the mean leakage levels for most of the MIMO settings and time-varying channel conditions are reduced by a factor of two.

We also evaluated the performance of the prediction scheme when $P + 1$ is smaller than the number of points used for prediction $K$. In that case, the polynomial does not exactly go through the $K$ points. In the simulation, $P + 1$ and $K$ was chosen to be 2 and 3, respectively. Least squares fitting was used to find the coefficient matrices $\mathbf{C}_{n,p}$ presented in (8). The results in Figure 6 and 7 show that the prediction performance is in between linear prediction and second order prediction. Although no significant performance improvement can be obtained, it is expected that when the noise is present this scheme could lead to a smaller prediction error.

In general, based on the two metrics presented above the proposed precoder/decoder prediction scheme always outperforms the scheme with no prediction (i.e. only using a delayed

version of the precoder/decoder). A reduction in the leakage level by a factor of two is observed for most MIMO settings and time-varying channel conditions. Despite using only two past samples for the prediction, linear prediction of the precoder/decoder shows a reasonable performance improvement.

For completeness we evaluate the performance of a spatial multiplexing MIMO system using the precoder/decoder prediction scheme and compare it with the case no prediction is used. Again we consider a 2x2 and 4x4 MIMO system in a varying channel with a maximum Doppler spread $f_d$=20Hz. The precoder/decoder was predicted using a first order polynomial. For each data stream independent QPSK symbols were transmitted. At the receiver coherent detection is assumed and each data stream was detected separately. The BER of each data stream is shown in Figure 8. The results show that the performance improvement in terms of the BER is moderate for the 2x2 MIMO setting. For the 4x4 MIMO
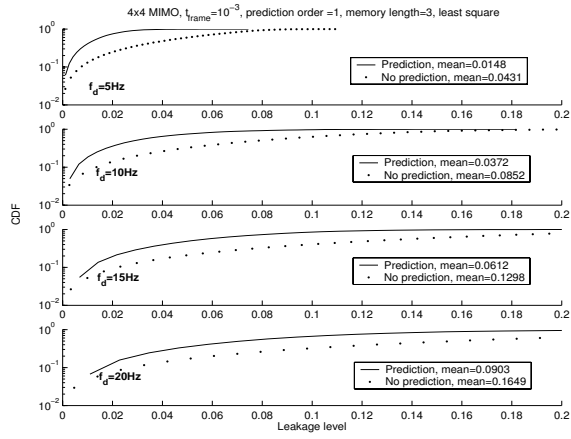
(a) 2x2 setting
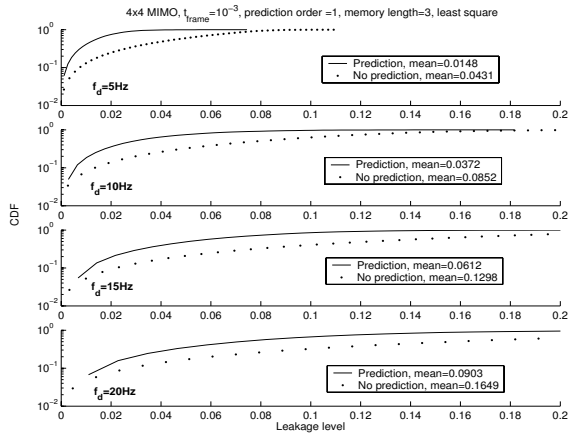


(b) 4x4 setting

Fig. 7. The distribution of the leakage for various MIMO settings and maximum Doppler spread values

setting, an improvement by a few dBs in SNR can be observed on the subchannel with low channel gain. Nevertheless, the proposed prediction scheme still remains attractive considering its simplicity.

## V. CONCLUSIONS AND REMARKS

In this paper, we have proposed and evaluated the performance of a precoder/decoder prediction scheme for a time-varying MIMO channel. The proposed prediction scheme is an expansion of the geodesic interpolation method in a unitary group where any unitary matrix can be expressed as the matrix exponential of a skew-Hermitian matrix. The prediction of the precoder/decoder is made based on the information that would be available for any MIMO system deploying spatial multiplexing. Therefore, the amount of overhead required for channel probing is the same as for the case with no percoder/decoder prediction. To evaluate the prediction performance, two metrics were defined namely the Euclidean
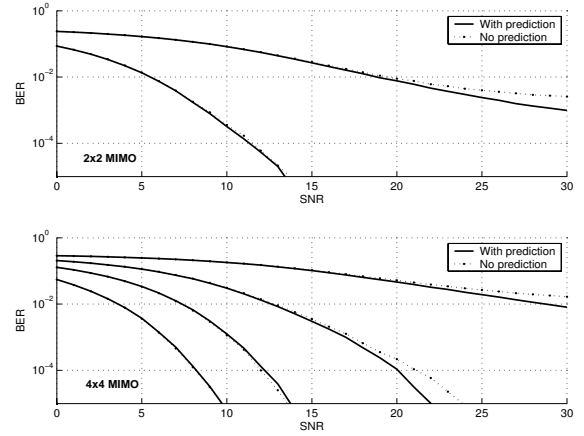


Fig. 8. BER of the time-varying MIMO channel for the 2x2 and 4x4 setting

distance between the predicted precoder/decoder and the true ones and the leakage level. Based on these two metrics, it has been shown that the proposed precoder/decoder prediction scheme can work well for a slowly time-varying MIMO channel. Evaluating the performance of the prediction scheme when the channel estimation error and quantization error are taken into account is one of the interesting problems for future work.

## REFERENCES

[1] G.J.Foschini, "Layered space-time architecture for wireless communication in fading environment when using multi-element antennas" Bell Labs Tech. J., 4159, 1996.
[2] I.E.Telatar "Capacity of Multi-Antenna Gaussian Channels. AT&T Bell Labs". 522526, 1995.
[3] J.B.Andersen "Array gain and capacity for known random channels with multiple element arrays at both ends" IEEE Journal on Selected Areas in Communications, Volume 18, Issue 11, Nov. 2000 Page(s):2172 - 2178.
[4] A.Duel-Hallen, S.Hu and H.Hallen, "Long-range Prediction of Fading Signals", IEEE Signal Processing Magazine, vol. 17, no. 3, pp. 62-75, May 2000.
[5] R.Vaughan, P.Teal and R.Raich, "Short-term Mobile Channel Prediction Using Discrete Scatterer Propagation Model and Subspace Signal Processing Algorithms", in Proc. IEEE International Vehicular Technology Conference, pp. 751-758, Sep. 2000.
[6] T.Eyceoz, A.Duel-Hallen and H. Hallen, "Deterministic Channel Modeling and Long Range Prediction of Fast Fading Mobile Radio Channels", IEEE Communications Letters, vol. 2, pp. 254-256, Sep. 1998.
[7] J.B.Andersen, J.Jensen, S.Jensen and F.Frederiksen, "Prediction of Future Fading Based on Past Measurements", in Proc. IEEE International Vehicular Technology Conference, pp. 15-155, Sep. 1999.
[8] A.Edelman, T.A.Arias adn S.T.Smith, "The geometry of algorithms with orhogonal constraints", SIAM J.MAtrix Anal. Appl. Vol. 20, No.2, pp.303-305, 1998.
[9] L.Dong, G.Xu, and H.Ling, "Prediction of Fast Fading Mobile Radio Channels in Wideband Communication Systems", in Proc. IEEE Global Communications Conference, pp. 3287-3291, Nov. 2001.
[10] D.Asimov and A.Buja" The grand tour via geodesic interpolation of 2 frames", NAS-NASA RNR technical report RNR-94-004 Feb 1994.
[11] C.Belta and V.Kumar "An SVD based projection method for interpolation on SE(3)"
[12] N.Khaled , B.Mondal, R.W.Heath J.r, G.Leus and F.Petre "Interpolation-based multi-mode precoding for MIMO-OFDM systems with limited feedback" submitted to VTC' 05.
[13] W.C.Jakes"Microwave Mobile Communications", New York Wiley 1974.

**Paper 7:**
**The potential use of time reversal technique in multiple elements antenna system**.
H.T.Nguyen, J.B.Andersen and G.F.Pedersen.

# The Potential Use of Time Reversal Techniques in Multiple Element Antenna Systems

Hung Tuan Nguyen, Jørgen Bach Andersen, *Life Fellow IEEE*, and Gert Frølund Pedersen

*Abstract*—In this paper, based on outdoor measurements we study the feasibility of applying the time reversal techniques (TR) in multiple element antenna (MEA) wireless communication systems. It is demonstrated that the use of TR in wireless communication has a promising potential in mitigating the effect of channel dispersion and especially in reducing the co-channel interference where a margin of 18dB interference reduction has been obtained.

*Index Terms*—Time reversal techniques, multiple elements antenna, MIMO system.

## I. INTRODUCTION

**T**IME reversal techniques have been studied for a long time in acoustic and medical applications (e.g. [1] among others). In most of the acoustic experiments illustrating TR's capability, the intended receiver probes the channel by transmitting a pilot sequence to the transmitters. Based on the received sequence, each transmitter estimates the channel impulse response (IR) and records it. The phase-conjugate version of the estimated IR will then be inverted in time and transmitted by each of these transmitters. If the channel does not vary with time, the transmitted waves will travel backward on the same paths they have experienced. Thereby their energies will be focused in time and space at the intended receiver. Simultaneously the actual received temporal side-slopes are reduced as later multipath components stemming from different transducers are randomly added in phase.

TR has so far only been applied to acoustics. If it can be applied in wireless communications, the advantages will be two fold: i) mitigating inter-symbol interference (ISI) without using equalizer and ii) focusing the signal to the point of interest thereby reducing the co-channel interference. In this paper the joint spatial and temporal focusing advantage of TR in MEA wireless systems is investigated. We first propose a transmission scheme and investigate the feasibility of TR in multiuser-MISO system in which the possibility of communicating with all users at one time instant is investigated. Using this scheme, the possibility of transmitting parallel channels in single user TR-MIMO system is discussed. Then based on the measurement data we evaluate the potential benefits from the use of TR. The capability to reduce the ISI effect is analyzed by means of the root mean square (RMS) delay spread.
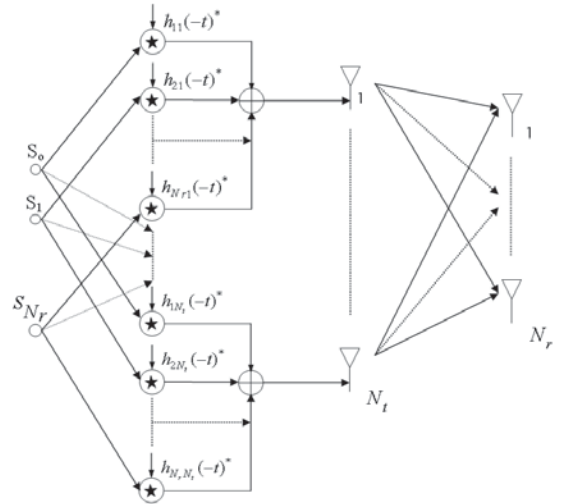
Fig. 1.   A transmission approach for MIMO system using TR.

The spatial focusing perspective of TR in MEA systems is evaluated in both single user and multiuser scenario.

## II. TIME REVERSAL TECHNIQUES AND PROPOSED TRANSMISSION SCHEME IN MEA SYSTEM

The essence of the TR is to convolve the transmitted symbol $s$ with the complex conjugate of the time reversed version of the measured IR denoted by $h$. If the channel is reciprocal and slowly varying, the received signal will be equal to a convolution of the transmitted symbol with the autocorrelation of the IR as in (1)

$$s \star h(-t)^* \star h(t) = s \star R(t) \qquad (1)$$

where $\star$ denotes convolution, $*$ indicates the complex conjugate and $R$ is the autocorrelation. Let us consider the downlink multiuser-MISO transmission using TR technique. The system consists of $N_t$ antennas at the transmitter and independent information is transmitted to $N_r$ receiving antennas (or users). Herein, we denote $i$ and $j$ as the indices of receiving antenna and transmitting antenna, respectively. A proposed transmission scheme for the multiuser-MISO system using TR is illustrated in Fig. 1. The received signal at the $i^{th}$ receiving antenna can be described as

$$y_i = \underbrace{\sum_{j=1}^{N_t} s_i \star R_{ij}}_{Signal(i)} + \underbrace{\sum_{j=1}^{N_t} \sum_{k=1; k \neq i}^{N_r} s_k \star h_{kj}(-t)^* \star h_{ij}(t)}_{Interference(i)} + \underbrace{n_i}_{Noise(i)}$$

$$(2)$$

For the multiuser scenario, the IRs are normally uncorrelated as a result of the large separation between the receiving antennas. In this case, the interference part in (2) may be suppressed. Thereby we might be able to communicate with all users in one time instant with a simple detection at the receiver. At the same time the time dispersive characteristic of the channel is mitigated.

In other aspects, where a single user MIMO system with rich multipath scattering environment is considered, it might also be possible to simultaneously transmit several independent channels. One could use the multiuser-MISO scheme mentioned above to describe the operation of a single user TR-MIMO system. Note that the number of users then becomes the number of the receiving antennas in the TR-MIMO system. The main difference between a classical MIMO system and TR-MIMO system is that in the first system the receiving antennas receive all superposed signals while in the second system each antenna receives only one dominant signal. Since the interference power increases according to the number of receiving antennas, one cannot send more information by simply adding more receiving antennas. However, with reasonably smaller number of receiving antennas than the number of transmitting antennas and a rich multipath environment the desired signal's magnitude might become larger than that of the interference. In this case, application of TR in wireless MIMO therefore could be possible.

The branch power differences at the receiving antenna elements could make the interference part in (2) become comparable with the signal of interest. One solution to limit this effect is to normalize the transmitted power or the inverse IR to the square root of its power. This scheme, which we denote a power control scheme, appears to be practical for the implementation of TR in wireless systems.

In the following, the spatial focusing potential will be characterized by the instantaneous signal to interference ratio (SIR) which is calculated as the ratio of the power of the signal of interest at the peak of their autocorrelations and the corresponding interferences power at the same time lag

$$SIR_i = \frac{|Signal(i)_{peak}|^2}{|Interference(i)_{peak}|^2} \qquad (3)$$

This SIR will be used to determine how well we can, by the TR, focus the transmitted energy into a point of interest. Here we assume that synchronization is established so that we can always sample precisely at the peak of the superimposed autocorrelations where most of the energy is contained.

## III. TR'S POTENTIAL BASED ON MEASUREMENT DATA

### A. Measurement setup and the environment

The data used for evaluation was acquired from wideband outdoor 8x4 MIMO measurements in Aalborg along two routes of length 1km each. As illustrated in Fig. 2a, the transmitter had eight antenna outputs. The receiver mimics a handset equipped with four patch antennas and was battery powered to avoid conductive cables. The transmitting antennas were mounted at a balcony on the fifth floor. The handset was placed on a car which runs with a velocity of 20km/h to 40 km/h. A pseudo noise (PN) sequence with a chip
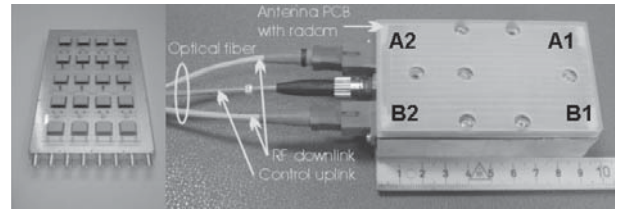


(a) BS antennas and the handset.
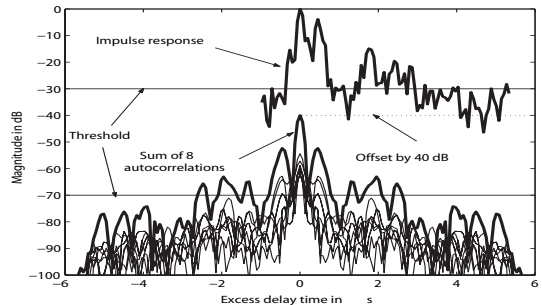


(b) Example of channel IR and autocorrelation superimposition which is offset by 40dB.

Fig. 2. Measurement setup and example of IR and autocorrelation superimposition.

rate of 7.665MHz was transmitted at 2140MHz. The center frequency and the measurement bandwidth are comparable to 3G WCDMA system. The data used to illustrate the TR potential are acquired from two measured routes with distinct multipath characteristics. In the following assessment of the TR potential, it is assumed that the measured IRs are instantaneously known at the transmitter and the channel is constant during a period in which a symbol is transmitted.

### B. Dispersion mitigation capability

To illustrate the dispersion mitigation capability of TR, we calculate the RMS delay spread of the channel IRs and the eight autocorrelations superimposed signal. Those autocorrelations are derived from the IRs between eight transmitting antennas at the transmitter and one receiving antenna at the handset. An example of the channel IR, the autocorrelations and their sum is shown in Fig. 2b. Both the IR and the sum of the autocorrelations were normalized to 0dB. For clarity the sum was offset by 40dB and the IR was shifted such that its major peak is in-line with the peak of the sum. Clearly, the autocorrelations are coherently added at their peaks as a sum of real numbers. Other complex side-lobes of the autocorrelations will add up randomly so that the actual received side-lobes are suppressed which gives rise to ISI mitigation.

The RMS delay spread is calculated from the first and second moment of the power delay profile. In both cases we use a threshold of 30dB from the peak to eliminate the noise. For the first route, the delay spread of the IRs and the superimposition of the eight autocorrelations are 0.2 $\mu s$ and 0.1 $\mu s$ respectively. These numbers are 0.6 $\mu s$ and 0.3 $\mu s$ for the second route. The RMS delay spread of the autocorrelation superimposed signal is reduced approximately a factor of 2 in comparison with that of the IRs. It is also what has been reported in [3] for 8x1 MISO system based on the acquisition

TABLE I

MEAN AND MINIMUM VALUE OF THE SIR VS DISTANCE FOR 2 ROUTES, $N_t = 8$ AND TWO USERS

| Distance (meter) | | 0.25 | 0.5 | 1 | 1.5 | 2 | 150 | 300 |
|---|---|---|---|---|---|---|---|---|
| Without power control | | | | | | | | |
| 1 | Min | -4.3 | -5.6 | -5.7 | -6.8 | -9.3 | -12.3 | -12.5 |
| | Mean | 5.7 | 6.5 | 7.1 | 7.7 | 9.4 | 11.3 | 12.1 |
| 2 | Min | -6.9 | -8.7 | -7.7 | -7.6 | -10.9 | -10.9 | -14.2 |
| | Mean | 9.5 | 11.5 | 12.7 | 14.0 | 15.5 | 17.1 | 17.8 |
| With power control | | | | | | | | |
| 1 | Min | 0.1 | 0.2 | 0.4 | 0.5 | 0.6 | 0.7 | 0.7 |
| | Mean | 6.4 | 7.3 | 8.1 | 8.7 | 10.0 | 12.0 | 13.2 |
| 2 | Min | 0.2 | 0.3 | 0.4 | 0.8 | 0.8 | 0.9 | 0.9 |
| | Mean | 8.8 | 10.8 | 12.3 | 13.5 | 15.6 | 16.9 | 17.8 |

TABLE II

SIR IN DB FOR 8X4 SETUP, WITHOUT AND WITH POWER CONTROL

| Route | Values | Antennas | | | |
|---|---|---|---|---|---|
| | | A1 | A2 | B1 | B2 |
| Without power control | | | | | |
| 1 | Mean | 2.3 | 4.8 | 7.2 | 4.0 |
| | Min | -13.4 | -16.8 | -10.0 | -17.6 |
| 2 | Mean | 1.6 | 2.5 | 6.8 | 4.2 |
| | Min | -15.3 | -22.8 | -8.3 | -16.0 |
| With power control | | | | | |
| 1 | Mean | 5.0 | 2.3 | 4.9 | 2.5 |
| | Min | -0.0 | -0.0 | 0.0 | 0.0 |
| 2 | Mean | 4.5 | 4.1 | 6.0 | 5.9 |
| | Min | -0.0 | 0.0 | -0.0 | -0.0 |

data of different measurement campaign. The reduction in the RMS delay spread values indeed illustrates the ISI mitigation capability of TR.

### C. Spatial focusing

For the multiuser scenario, the TR may possibly have a good spatial focusing resolution as antennas between users are now far apart. From the available measured data, we consider a simple scenario where there are two users separated by distance $d$ and both of them operate simultaneously. Each user is equipped with one receiving antenna and there are still eight antennas at the transmit side. We then calculate the SIRs as a function of the separation $d$ for both routes. Eight IRs measured at one location are used to calculated the power of the signal of interest as the numerator in (3). Together with these IRs, eight other IRs measured at a distance $d$ apart are used to calculate the interference power as the denominator in (3). The SIRs for the 8x1 setup with two concurrent users are evaluated independently at four receiving antennas. The averaged SIR values are presented in Table I.

With power control we get better minimum SIRs of around 0.5dB. The mean SIR tends to rise as the separation between the users increases, though it appears to approach saturation when the separated distance is above a certain value. In general the mean SIRs range from 8dB to 18dB according to the increase in the distance between the two users from 0.25 meter to 300 meters, respectively. The increment of the SIR values

may be explained by the decorrelation in the IRs' taps and the change in the relative time delay of the IRs.

For the single user MIMO system we consider the downlink transmission of the 8x4 setting and estimate the instantaneous SIR. The purpose here is to judge if it is possible, just by the TR's spatial focusing to transmit parallel channels as illustrated in the ultrasonic case [2]. The SIR is estimated from the 8x4 IRs at each measurement snapshot. The mean and minimum instantaneous SIR values for four receiving antennas with and without power control are tabulated in Table II.

From the positive mean SIR values it is concluded that the TR does give a limited spatial focusing. However, for the scheme without power control the minimum SIR value in dB is always negative. With power control better SIR are obtained with the minimum value in most case in the neighborhood of zero dB and the mean value around 4dB. Nevertheless, even with power control the marginal mean value of the SIR may not be enough for reliable detection of the desired symbol at each receiving antenna.

### IV. CONCLUSION AND REMARKS

In this paper, the potential of applying TR in wireless MEA systems is evaluated. The results show that the combination of TR and MEA techniques in multipath wireless environment is promising, especially in multiuser-MISO system. The mean RMS delay spread reduces by almost a factor of two for 8x1 setup using TR. For the single user case, the analysis of 8x4 MIMO system shows that for such closely spaced transmitting as well as receiving antennas, it may not be possible to transmit parallel channels reliably just by using TR, as the mean SIR is only around 4dB. However, for multiuser-MISO, with eight antennas at the transmit side, a mean SIR value of around 18dB was found for two concurrent users equipped with one antenna and 300m separation. Although this SIR value is significant, 9dB out of that is due to the beamforming at the transmit side and the remainder is attributed to the temporal focusing of the TR. In a coming paper, there will be further investigations on the temporal focusing characteristics of TR where the contribution of beamforming is separated as well as more detail explanations on why the SIR should increase so slowly with increasing distance.

### REFERENCES

[1] M. Fink, "Time-reversed acoustic," *Scientific American*, pp. 67-73, Nov. 1999.

[2] A. Derode *et al.*, "Taking advantage of multiple scattering to communicate with time-reversal antennas," *Phys. Rev. Lett.*, vol. 90, pp. 014301-1-014301-4, 2003.

[3] P. Kyritsi, P. Eggers, and A. Oprea, "MISO time reversal and time compression," *URSI Internatl. Symp. on Electromag. Theory*, May 2004.

**Paper 8:**
**Time Reversal in Wireless Communications: a Measurement Based Investigation.**
H.T.Nguyen, J.B.Andersen, G.F.Pedersen, P. Kyritsi and P.Eggers.

# Time Reversal in Wireless Communications: a Measurement Based Investigation

Hung Tuan Nguyen *Student Member IEEE*, Jørgen Bach Andersen *Life Fellow IEEE*, Gert Frølund
Pedersen, Persefoni Kyritsi *Member IEEE* and Patrick Eggers *Member IEEE*
Department of Communication Technology, Niels Jernes Vej 12, DK-9220 Aalborg , Denmark
Email: {htn,jba,gpf,persa,pe}@kom.auc.dk

## Abstract

Interference caused by other users in a multi-user environment degrades the system performance significantly. Conventionally, user separation in a multi-user environment is achieved by signal separation in time, frequency or code. The use of multiple elements antenna (MEA) systems can apply separation of the users in space by targeting the transmitted power to the user of interest. Inevitably in that case, the separation is not ideal and there is interference on the other users in the systems. Moreover in a wideband transmission, frequency selective fading causing inter symbol interference (ISI) is a big challenge for point to point wireless communications. In this paper, we study the feasibility of applying the time reversal technique (TR) in multiple input single output (MISO) systems to alleviate the effect of ISI. The ability of TR to focus the signal on the receiver of interest in a multi-user environment is also considered. The studies are supported by measured complex channel impulse responses with 10MHz bandwidth centered at 2.14GHz. For a 8x1 MISO system, using TR the root mean square delay spread is reduced by a factor of 2. To evaluate the capability of the TR in reducing the ISI, simulation of the Bit Error Rate (BER) was made. The irreducible BER of the TR-MISO system was shown to be lower than that of the SISO system by at least an order of magnitude. By using TR and assuming that two users are communicating simultaneously with the same BS the two signals have 17dB of isolation.

## Index Terms

Time reversal technique, multiple elements antenna, MISO system, spatial focusing, RMS delay spread, interferences reduction.

## I. INTRODUCTION

**T**IME REVERSAL (TR) has been a subject of study for some time in acoustic and medical applications (e.g. [1], [2] among others). The main purpose of TR in such applications is to focus energy in space and time on the point of interest by filtering the signal through the complex conjugate and time inverted channel impulse response. TR technique is able to offer fine focusing resolution even in high-order multiple scattering [3]. This occurs robustly despite the fading of the original channel impulse response. Simultaneously, the temporal side-lobes are reduced as the delayed multipath components are added randomly in phase. Therefore the effect of ISI can be alleviated. Nevertheless, there are two requirements for TR to work properly: the channel must be known at the transmitter and must be static during the transmission period.

The use of multiple element antenna (MEA) systems in wireless communications has recently become a well-known technique to increase the transmission reliability and channel capacity. Antenna and diversity gain can be achieved using available combining methods (selection, equal gain, maximum ratio combining). However, for wideband MEA systems where signals are mixed both in time and space a combination of advanced signal processing algorithms such as STBC-OFDM (Space Time Block Code and Orthogonal Frequency Division Multiplexing) or SVD-OFDM (Singular Value Decomposition and Orthogonal Frequency Division Multiplexing) is required to overcome the effect of multipath fading and ISI. Therefore, the receiver is expected to have a rather high complexity. Since the setup of MEA systems has some similarity to TR, it becomes an interesting question whether TR can be applied in MEA wireless systems. If this is the case the advantages will be three fold: i) reducing ISI without the use of an equalizer and ii) focusing the signal on the point of interest thereby reducing the interference iii) applying a rather simple receiver structure.

Due to its simplicity and promising performance improvement, research on the applicability of TR in wireless communication has begun to gain attention. In [4] and [5], using the data from a fixed wireless 8x1 multiple

input single output (MISO) measurement a delay compression by a factor of 3 was shown to be possible. Using the reverberant chamber in [6] the convergence of the time-reversed electromagnetic wave to the initial source was illustrated. In [7], transmission of two simultaneous channels at the same frequency in a multipath indoor environment at 2.45GHz was demonstrated. In [8], channel hardening and temporal focusing were observed for ultra wideband signals in an indoor environment.

In this paper the spatial focusing and ISI reduction advantages of TR in a wireless MISO system are investigated. A thorough investigation is presented which gives more physical insight into the working principle of TR than the initial investigation by the same authors in [9]. The studies are supported by measured complex channel impulse responses with 10MHz bandwidth centered at 2.14GHz. The paper is organized in the following way. In section II we review the transmission technique used in TR. Next, a model for the estimation of the mean signal to interference ratio (SIR) is derived in section III. Various factors which affect the SIR values are also discussed is the same section. Based on the outdoor MISO measurement data, we evaluate the potential benefits from the use of TR in section IV. The capability to reduce the ISI effect is analyzed by means of the root mean square (RMS) delay spread and the Bit Error Rate (BER). We assess the spatial focusing perspective of TR in MISO systems in terms of the SIR. In section V a comparison between the TR technique and the eigen beamforming technique with respect to the practical implementation and the spatial focusing performance is presented. The paper ends with conclusions and future work in section VI.

## II. TIME REVERSAL TECHNIQUE AND SPATIAL FOCUSING QUANTIFICATION

The TR technique requires two steps. First the channel impulse response (IR) is estimated and recorded at the transmit side. Second the desired transmitted symbol is convolved with the complex conjugate of the time reversed version of the IR(s). As long as the channel IRs are known at the transmitter and the channel is static during the transmission period, the actual transmitted signal is convolved with the same IR(s). The result is equivalent to a convolution of the transmitted symbol with the autocorrelation of the channel impulse response as in equation (1)

$$y_j(t) = x_j(t) \star h_{ij}(-t)^* \star h_{ij}(t) + n_j(t) = x_j(t) \star R_{ij}^{auto}(t) + n_j(t) \tag{1}$$

where $x(t)$ denotes the transmitted signal and $y(t)$ indicates the received signal; $\star$ denotes the convolution operator; $()^*$ is the complex conjugate operator; $i$ and $j$ are the indices of the transmitting antenna and receiving antenna respectively; $n_j(t)$ is the noise component; $R^{auto}(t)$ is the autocorrelation of the channel IR $h_{ij}(t)$. The received signal at an off-target point has the form

$$x_j(t) \star h_{ij}(-t)^* \star h_{ik}(t) + n_k = x_j(t) \star R_{ijk}^{cross}(t) + n_k(t) \tag{2}$$

where $h_{ik}(t)$ denotes the IR of the channel from the transmitting point to the off-target point and $R_{ijk}^{cross}(t)$ is the cross correlation of the channel IR $h_{ik}(t)$ to the target point and the IR $h_{ij}(t)$.

Let us consider a multi-user MISO system that applies the TR technique. The system comprises $N_u$ simultaneously operating $N_t \times 1$ MISO systems, each one targeting a different user. The signals, before being radiated by the $N_t$ transmitting antennas, are filtered by the corresponding conjugated time reversed impulse responses as described above. The proposed transmission scheme using TR in a wireless multi-user MISO system is sketched in Figure 1.

The signal received by the $j^{th}$ user can be described as

$$y_j(t) = \underbrace{x_j(t) \star \sum_{i=1}^{N_t} R_{ij}^{auto}(t)}_{S(t)} + \underbrace{\sum_{i=1}^{N_t} \sum_{k=1;k \neq j}^{N_u} x_k(t) \star R_{ikj}^{cross}(t)}_{IF(t)}$$
$$+ \underbrace{n_j(t)}_{Noise} \tag{3}$$

where $S(t)$ is the signal of interest and $IF(t)$ is the interfering signal. In the following we use the term "*equivalent channel IR, $h^{eq}$*" to denote the sum of the autocorrelation $R_{ij}$ in equation (3).

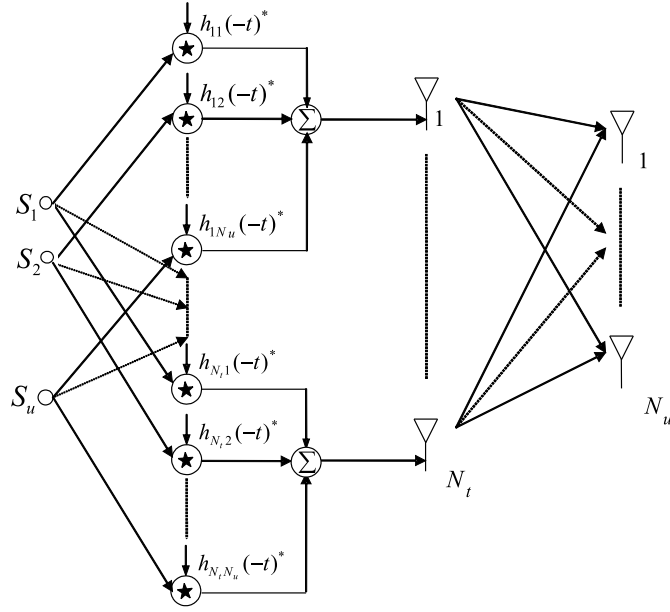$$h^{eq}(t) = \sum_{i=1}^{N_t} R_{ij}^{auto}(t) \tag{4}$$

Fig. 1.  A transmission approach for MIMO system using TR

Under certain conditions, the interference term $IF_j(t)$ in equation (3) becomes comparable to the signal of interest. Correlated IRs caused by closely placed antennas might be one of the reasons. A large number of interference paths compared to the signal of interest, or branch power differences among the receiving antennas might also contribute to this issue. One way to alleviate the influence of the branch power difference is to normalize the time-reversal filter by the square root of its power such as

$$h_{ij}^{TR}(t) = \frac{h_{ij}(-t)^*}{\sqrt{\int |h_{ij}(t)|^2}} \tag{5}$$

This scheme, which we denote as a power control scheme, appears to be practical for the implementation of TR in MEA systems.

From a wireless communication point of view, the spatial focusing capability of TR can be defined by how much the interference from other users can be mitigated. This interference comprises the signals destined for antennas other than the antenna of interest. The spatial focusing potential is characterized by the SIR. The instantaneous SIR is calculated as the ratio of the peak power of $S(t)$ and $IF(t)$.

$$SIR = \frac{|S(t)_{peak}|^2}{|IF(t)_{peak}|^2} = \frac{P_S}{P_{IF}} \tag{6}$$

This SIR is a numerical value for quantifying the capability of TR to focus the transmitted energy into a point of interest: the higher the SIR value the better the focusing resolution. Here we assume that synchronization is established so that we can always sample precisely at the peak where the received signal contains most of the energy. For simplicity in the calculation of SIR we neglect the side lobe effect caused by the tails of other received symbols at the neighbouring time slots.

## III. A SIMPLE CALCULATION OF THE MEAN SIR

In this section we derive a simple expression for the mean value of the instantaneous SIR defined in equation (6). It is approximated by the ratio of the mean signal power at the peak of the *equivalent channel IR* and the mean of the interference power at the same time lag. In order to develop an analytical expression, hereafter we only consider the discrete time signals. In the derivation process we assume i) The channel coefficient at the $l^{th}$ tap of the IR is an independent complex number with the real and imaginary parts having zero mean and variance $0.5\sigma_l^2$. Consequently, the magnitude of the tap is Rayleigh distributed, ii) Different taps of the IR are statistically

independent (uncorrelated scattering), iii) The channel coefficients between two IRs at the same tap index are mutually uncorrelated. With these assumptions the expected value of the interference power can be calculated as

$$
\begin{aligned}
\overline{P_{IF}} &= \left\langle \left| \sum_{i=1}^{N_t} \sum_{k=1,k\neq j}^{N_u} \sum_{l=1}^{L} x_k h_{ij}(l) h_{kj}(l)^* \right|^2 \right\rangle \\
&= \sum_{i=1}^{N_t} \sum_{k=1,k\neq j}^{N_u} \sum_{l=1}^{L} |x_k|^2 \sigma_l^4 \\
&= P_o N_t (N_u - 1) \sum_{l=1}^{L} \sigma_l^4 \\
&\leq P_o N_t (N_u - 1) \left( \sum_{l=1}^{L} \sigma_l^2 \right)^2
\end{aligned}
\tag{7}
$$

where $\langle\rangle$ denotes the expectation operator and $P_o = <|x_k|^2>$.

The expected value of the signal power is

$$
\begin{aligned}
\overline{P_S} &= \left\langle |x_j|^2 \left| \sum_{j=1}^{N_t} \sum_{l=1}^{L} h_{ij}(l)^* h_{ij}(l) \right|^2 \right\rangle \\
&= P_o \left\langle \left( \sum_{j=1}^{N_t} \sum_{l=1}^{L} |h_{ij}(l)|^2 \right)^2 \right\rangle \\
&= P_o \left( N_t \sum_{l=1}^{L} \sigma_l^4 + N_t^2 \left( \sum_{l=1}^{L} \sigma_l^2 \right)^2 \right)
\end{aligned}
\tag{8}
$$

In the derivation of the signal power above we used the fact that the fourth moment of a zero-mean complex Gaussian is twice the variance squared. From equations (7) and (8) the average SIR can be approximated as

$$
\begin{aligned}
\overline{SIR} &= \frac{\overline{P_S}}{\overline{P_{IF}}} \\
&= \frac{P_o(N_t \sum_{l=1}^{L} \sigma_l^4 + N_t^2 \left( \sum_{l=1}^{L} \sigma_l^2 \right)^2)}{P_o N_t (N_u - 1) \left( \sum_{l=1}^{L} \sigma_l^4 \right)} \\
&= \frac{1}{N_u - 1} + \frac{N_t \left( \sum_{l=1}^{L} \sigma_l^2 \right)^2}{(N_u - 1) \sum_{l=1}^{L} \sigma_l^4} \\
&\geq \frac{1 + N_t}{N_u - 1} = SIR_{BF}
\end{aligned}
\tag{9}
$$

In equation (9), equality occurs if the channel is narrowband and therefore the channel can be described by a single tap. This means that all the later echoes have almost zero power and, as a result, become insignificant ($\sigma_l^2 \simeq 0$ for $l > 1$). In this case the SIR is essentially a result of the beamforming at the transmit side and henceforth denoted as $SIR_{BF}$.

The derivation of equation (7) and (8) reveals two factors needed to get the best obtainable performance in spatial focusing i) the channel IRs must be uncorrelated so that the interference power is minimized ii) the IRs must have enough significant late echoes to focus the signal in time, therefore maximizing the signal power.

Equation (9) only gives us a lower bound of the mean SIR for the situation when the channel is narrowband and the IRs are uncorrelated. This lower bound is also the SIR obtained by beamforming or maximum ratio combining of the main tap of the IRs. A more exact value of the mean SIR for wideband uncorrelated IRs can be derived if

the power variance of the IR taps, $\sigma_l^2$, is known. For an urban environment, the power delay profile (PDP) can be modelled as an exponential decay [10]. The mean power at the $l^{th}$ tap of the PDP can be described by

$$\sigma_l^2 = exp\left(-\frac{(l-1)\Delta\tau}{\overline{\sigma_\tau}}\right) \tag{10}$$

where $\overline{\sigma_\tau}$ is the mean RMS delay spread measured over a particular area and $\Delta\tau$ is the tap resolution.

Applying (10) in (7), the interference power becomes

$$
\begin{aligned}
\overline{P_{IF}} &= \sum_{i=1}^{N_t}\sum_{k=1,k\neq j}^{N_u}\sum_{l=1}^{L}|x_k|^2\sigma_l^4 \\
&= P_o N_t(N_u-1)\left(\frac{1-exp\left(-\frac{2L\Delta\tau}{\overline{\sigma_\tau}}\right)}{1-exp\left(-\frac{2\Delta\tau}{\overline{\sigma_\tau}}\right)}\right)
\end{aligned} \tag{11}
$$

Using (10) in (8), the signal power can be described by

$$
\begin{aligned}
\overline{P_S} &= P_o\left(N_t\sum_{l=1}^{L}\sigma_l^4 + N_t^2\left(\sum_{l=1}^{L}\sigma_l^2\right)^2\right) \\
&= P_o\left(N_t\frac{1-exp\left(-\frac{2L\Delta\tau}{\overline{\sigma_\tau}}\right)}{1-exp\left(-\frac{2\Delta\tau}{\overline{\sigma_\tau}}\right)} + N_t^2\left(\sum_{l=1}^{L}exp\left(-\frac{(l-1)\Delta\tau}{\overline{\sigma_\tau}}\right)\right)^2\right) \\
&= P_o\left(N_t\frac{1-exp\left(-\frac{2L\Delta\tau}{\overline{\sigma_\tau}}\right)}{1-exp\left(-\frac{2\Delta\tau}{\overline{\sigma_\tau}}\right)} + N_t^2\left(\frac{1-exp\left(-\frac{L\Delta\tau}{\overline{\sigma_\tau}}\right)}{1-exp\left(-\frac{\Delta\tau}{\overline{\sigma_\tau}}\right)}\right)^2\right)
\end{aligned} \tag{12}
$$

The average SIR changes to

$$
\begin{aligned}
\overline{SIR} &= \frac{\overline{P_S}}{\overline{P_{IF}}} \\
&= \frac{1}{(N_u-1)}\left(1 + N_t\frac{\left(\frac{1-exp\left(-\frac{L\Delta\tau}{\overline{\sigma_\tau}}\right)}{1-exp\left(-\frac{\Delta\tau}{\overline{\sigma_\tau}}\right)}\right)^2}{\left(\frac{1-exp\left(-\frac{2L\Delta\tau}{\overline{\sigma_\tau}}\right)}{1-exp\left(-\frac{2\Delta\tau}{\overline{\sigma_\tau}}\right)}\right)}\right) \\
&\approx \frac{1}{(N_u-1)}\left(1 + N_t\left(1 + \frac{2exp(-\frac{\Delta\tau}{\overline{\sigma_\tau}})}{1-exp(-\frac{\Delta\tau}{\overline{\sigma_\tau}})}\right)\right) \quad \text{if } L\Delta\tau \gg \sigma_\tau
\end{aligned} \tag{13}
$$

From the average SIR expression it can be seen that for the uncorrelated IR case there are three factors which influence the spatial focusing performance of TR. i) The number of transmitting antennas $N_t$. ii) The length of the IR $L\Delta\tau$ when its value is not significantly greater than the delay spread. iii) The product of the bandwidth and the RMS delay spread (effective dispersion) $\frac{1}{\Delta\tau}\overline{\sigma_\tau}$. All these factors indirectly result from the differences in the scattering medium which the signals experience.

Equation (13) is an approximation of the SIR when applying TR for the uncorrelated IR case. However, both the beamforming and temporal focusing contribute to the spatial focusing performance of TR. From equations (9)

and (13) the contribution of the temporal focusing in TR can be easily separated as

$$
\overline{SIR}_{TF} = \frac{SIR}{SIR_{BF}} = \frac{1}{N_t+1}\left(1+N_t\frac{\left(\frac{1-exp\left(-\frac{L\Delta\tau}{\overline{\sigma}_\tau}\right)}{1-exp\left(-\frac{\Delta\tau}{\overline{\sigma}_\tau}\right)}\right)^2}{\left(\frac{1-exp\left(-\frac{2L\Delta\tau}{\overline{\sigma}_\tau}\right)}{1-exp\left(-\frac{2\Delta\tau}{\overline{\sigma}_\tau}\right)}\right)}\right)
$$

$$
\approx \frac{1+N_t\left(1+\frac{2exp(-\frac{\Delta\tau}{\sigma_\tau})}{1-exp(-\frac{\Delta\tau}{\sigma_\tau})}\right)}{N_t+1} \text{ if } L\Delta\tau \gg \sigma_\tau \tag{14}
$$

## IV. Evaluation of dispersion reduction and spatial focusing based on measurement data

### A. Measurement setup and the environment

The data used for the evaluation was acquired from wideband outdoor 8x4 MIMO measurements in Aalborg, an urban environment with hilly terrain, along three different routes of length 1 km each (4400x8x4 IR(s) per route). The transmitter was a base station (BS) antenna prototype made by ALLGON in Sweden which had 8 antenna outputs, arranged in four dual polarized columns. In the measurement campaign the transmitting antennas were mounted at the fence of a balcony on the 5th floor (rooftop level). The receiver was a prototype of a commercial mobile handset which was battery powered to avoid conductive cables. This handset was equipped with 4 patch antennas at its four corners (labelled as A1, A2, B1, B2 in Figure 2).
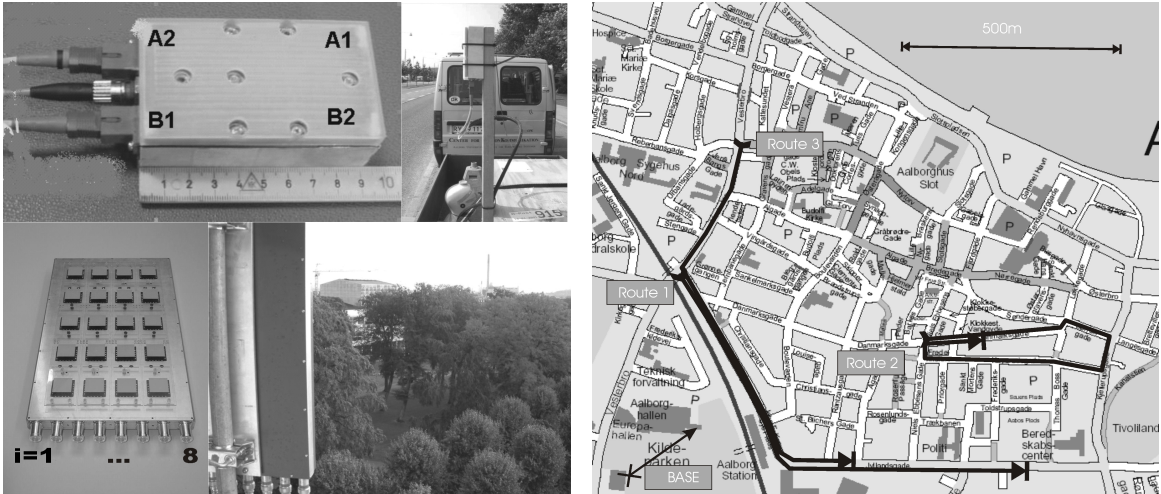


Fig. 2. Measurement setup and the map of the three measured routes, handset and measurement scenario (top left), BS and view point from the BS(bottom left), measurement route (right)

Optical cable was used to connect the handset to the measurement equipment to avoid the radiation perturbation that would have been introduced by a coaxial cable. Four antenna outputs of the handset was multiplexed into 2 parallel channels. Each channel was fitted with an antenna switch so that each vertical antenna pair was selected in turn by trigger. The switch was followed by a standard UMTS filter and a two step variable gain block. Finally it is connected to the optical transmitter, where the received signals were modulated at an optical carrier, and sent over an optical fibre to the optical receiver. The handset was placed on a trailer pulled by a car which ran at a velocity ranging between 20km/h and 40 km/h. The measurements were taken in a burst mode: the channel was measured along a distance of 2 meters during which 44 IRs were acquired, followed by 8 meters of travelled distance during which no measurements were taken.

The sounding system was based on post-processing and real antenna array gain. A code phase offsetting technique was applied, whereby each antenna element at the transmitter used the same Pseudo random Noise sequence (PN-sequence) code, but it was offset by a predefined interval. Using this technique together with the switching 8x4 channel, IRs can be almost instantaneously measured. In our measurement campaign we used a PN sequence of

511 bits length with the chip rate of 7.665MHz. The tap delay resolution of the system therefore was $0.13\mu s$. This PN sequence was transmitted at the center frequency of 2140MHz corresponding to a carrier wavelength of 14.1 cm. At the receive side, the signal was sampled at a rate of 15.36MHz so there were 1024 samples for one PN sequence length of 511 bits. The center frequency and the measurement bandwidth are comparable to the standard center frequency and bandwidth of 3G WCDMA systems. The carriers at the handset and the BS were synchronized by standard Rubidium oscillators. The instantaneous measurement signal to noise radio, $SNR_m$ for all of the measured data was well beyond 40dB. Although the length of each measured IR was 98 taps by visually inspecting the measured IRs we decided to use only 70 taps since the rest of the taps do not contain much energy and multipath information.

Figure 2 illustrates the setup of the handset, the transmitting antenna, the viewpoint from the BS as well as the measurement routes in the campaign. In the following assessment of the potential of TR it is assumed that the measured IRs are instantaneously known at the transmitter, and that the channel is static during the period in which a symbol is transmitted.

### B. Dispersion reduction capability

As mentioned in Section I, one of the most interesting properties of TR is its capability to reduce ISI. In fact, the advantage of TR in ISI reduction depends strongly on the frequency selective nature of the environment. The more wideband the channel is, the more benefit we can get out of TR in suppressing the delayed echo components. In this section, we investigate this property based on the data from the measurement campaign described in Section IV-A.

First, we consider the frequency selective fading characteristics of the measured environment. Figure 3 shows an example of the magnitude of a sample channel IR taken from the second route (normalized such that the maximum value is set to 0dB). The IR is composed of a main strong peak and several significant delayed echoes.
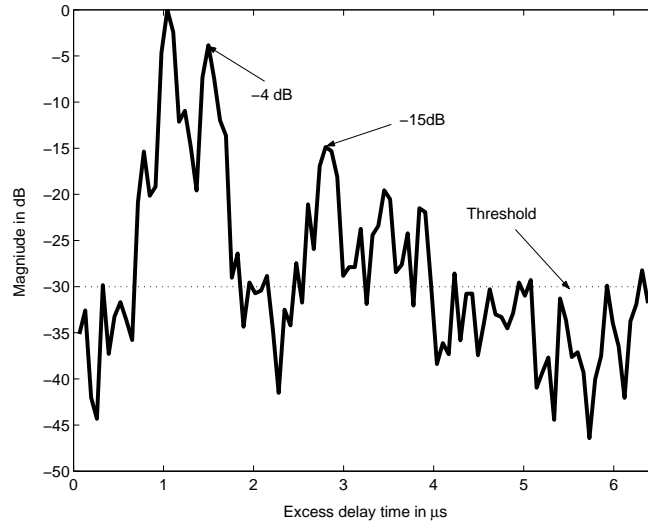


Fig. 3. An example of the channel impulse responses of route 2

Root mean square (RMS) delay spread is a useful parameter to describe the dispersion or the multipath effect of the channel. Depending on the relative magnitude of this parameter with respect to the bandwidth of transmitted signal, the channel can be described as frequency flat or frequency selective. The instantaneous RMS delay spread is calculated from the second central moment of the instantaneous PDP [11]

$$\sigma_\tau = \sqrt{\frac{\sum_{l=1}^{L} PDP(l)\tau_l^2}{\sum_{l=1}^{L} PDP(l)} - \left(\frac{\sum_{l=1}^{L} PDP(l)\tau_l}{\sum_{l=1}^{L} PDP(l)}\right)^2} \tag{15}$$

where $PDP(l) = |h_{ij}(l)|^2$ and $\tau_l$ is the excess time delay. For the calculation of the RMS delay spread, in order to reduce the thermal noise and the correlation noise, a threshold of 30dB is used for the PDP. Those components

that are lower than 30dB from the peak are set to zero. The probability distributions of the RMS delay spreads for three routes are shown in Figure 4.



Fig. 4.   Probability distribution of the instantaneous RMS delay spread based on the IRs of the three routes.

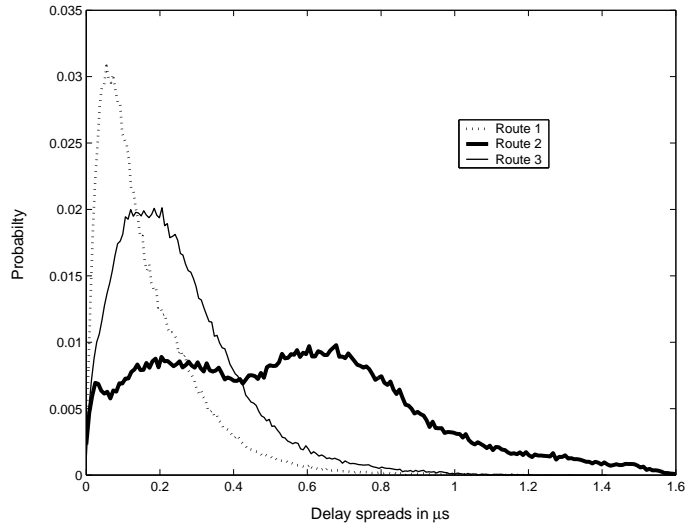The mean RMS delay spread is $0.26\mu s$, $0.62\mu s$ and $0.34\mu s$ for the first, second and third route, respectively. Obviously, $\overline{\sigma_\tau}$ is larger than the delay resolution ($0.13\mu s$) at least by a factor of 2. The delay resolution of the system is capable of resolving the multipath components in the outdoor environment for more than 50% of the measured paths.

Secondly, in order to illustrate the dispersion reduction capability of TR, we concentrate on the *equivalent channel IR*. These autocorrelations are derived from the IRs between the 8 transmitting antennas at the BS and a single receiving antenna at the handset. An example of the autocorrelations and the $h^{eq}(t)$ is shown in Figure 5.
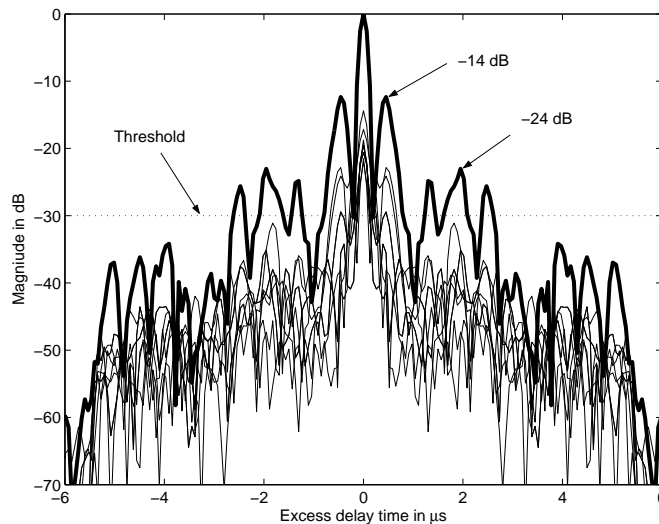


Fig. 5.   An example of the $h^{eq}$ or the sum of 8 autocorrelations, bold curve

By comparing Figure 3 and Figure 5 we can see that the later echoes have been suppressed in the *equivalent channel IR* after TR. Without TR, the second highest signal peak is 4dB lower than the peak. With TR the second highest peak is 14dB lower than the peak and therefore the sidelobes have clearly been suppressed.

The RMS delay spread of the *equivalent channel IR* is also calculated, in a manner similar to the calculation used for the measured IRs. The channel IR $h_{ij}$ in equation (15) is replaced by the *equivalent channel IR*, $h_j^{eq}$ and

TABLE I

MEAN RMS DELAY SPREAD OF THE IRs AND OF THE *equivalent channel IRs*

| Route | $\overline{\sigma_\tau}$ | |
| no | IRs, $h_{ij}$ | Equivalent channel IR, $h_j^{eq}$ |
|---|---|---|
| 1 | 0.2 $\mu$s | 0.1 $\mu$s |
| 2 | 0.6 $\mu$s | 0.3 $\mu$s |
| 3 | 0.3 $\mu$s | 0.1 $\mu$s |

the tap index $l$ ranges from 1 to $2L - 1$. A threshold of 30dB is also used. The probability density function of the RMS delay spread is illustrated in Figure 6.



Fig. 6. Probability distribution of the instantaneous RMS delay spread of the *equivalent IR*, $h^{eq}$ in the three routes.

A comparison between the delay spread of the original IRs and that of the *equivalent channel IR* is of interest in order to see how much the channel dispersion has been reduced. Table I compares these mean RMS delay spread va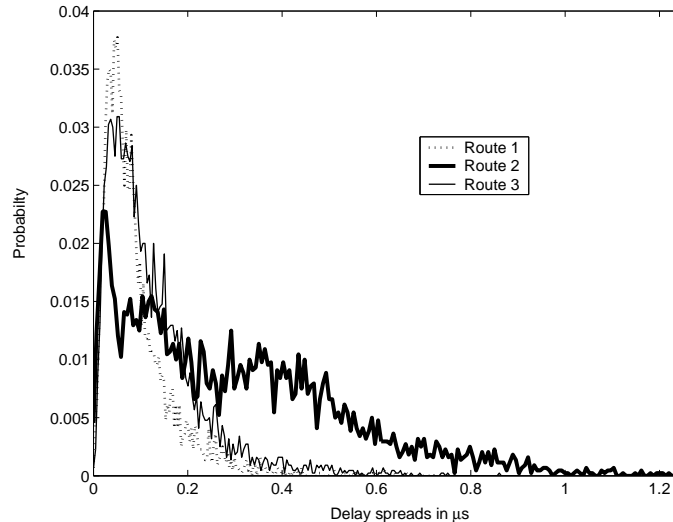lues obtained from the three measured routes. The RMS delay spread has been reduced approximately by a factor of 2. The reduction in the mean RMS delay spread values indeed reinforces the conclusion on the ISI reduction capability of TR.

Two observations can be drawn from the above results. i) if the number of transmitting antennas is increased, the ISI effect will be further reduced. This is because in the sum of the autocorrelations, the peaks add up coherently as all components have zero phase here. The side lobes add non-coherently due to independent random phase on all components, and therefore the composite sidelobes are suppressed. ii) if the environment becomes more frequency selective (more delayed echoes), the autocorrelation will be more focused in time and more energy of the signal will be concentrated at the peak of the autocorrelation. Thereby the impact of energy leakage from one symbol to its neighboring symbols will be further alleviated.

For completeness, using the measured data, we made a performance comparison in terms of the bit error rate (BER) obtained by a single user TR-MISO system and a normal single user SISO system without using TR. To highlight the influence of the ISI, no equalizer is used at the receiver. Several guard intervals of G=2, 4, 8 and 16 taps were considered. The closer the symbols are placed the higher the throughput, however it is traded for a higher ISI and a high BER as a result. For the simulation we used a simple binary phase shift keying (BPSK) modulation. The symbol width is assumed to be much smaller than the tap interval so as the convolution of the signal with the *equivalent channel IR* essentially is the multiplication of the *equivalent channel IR*'s tap with the transmitted symbol. Since the tap interval in the measurement was $T_s = 1/15.36MHz = 65.1ns$, the bit rates corresponds to the guard intervals are approximately $\frac{1}{GT_s}$ =7.68Mbps, 3.84Mbps, 1.92MBps and 0.96Mbps.

We assume that the receiver samples the received signal at the instant when the channel impulse response (or the

equivalent channel impulse response in the TR case) has the maximum energy. The power of the sampled signal $P_{max}$ is calculated as

$$P_{max} = \begin{cases} max\left(|h(l)|^2\right) P_o \text{ Original IR}, l = 1..L \\ max\left(|h^{eq}(l)|^2\right) P_o \text{ Equivalent IR }, l = 1..2L-1 \end{cases} \quad (16)$$

where $P_o$ is the transmitted signal power. The sampling instant $L_{sam}$ is defined as

$$L_{sam} = \begin{cases} \text{argmax}_l |h(l)|^2 \text{ Original IR} \\ \text{argmax}_l |h^{eq}(l)|^2 \text{ Equivalent IR} \end{cases} \quad (17)$$

Based on this observation, the receiver detects the originally transmitted symbol without performing any equalization.
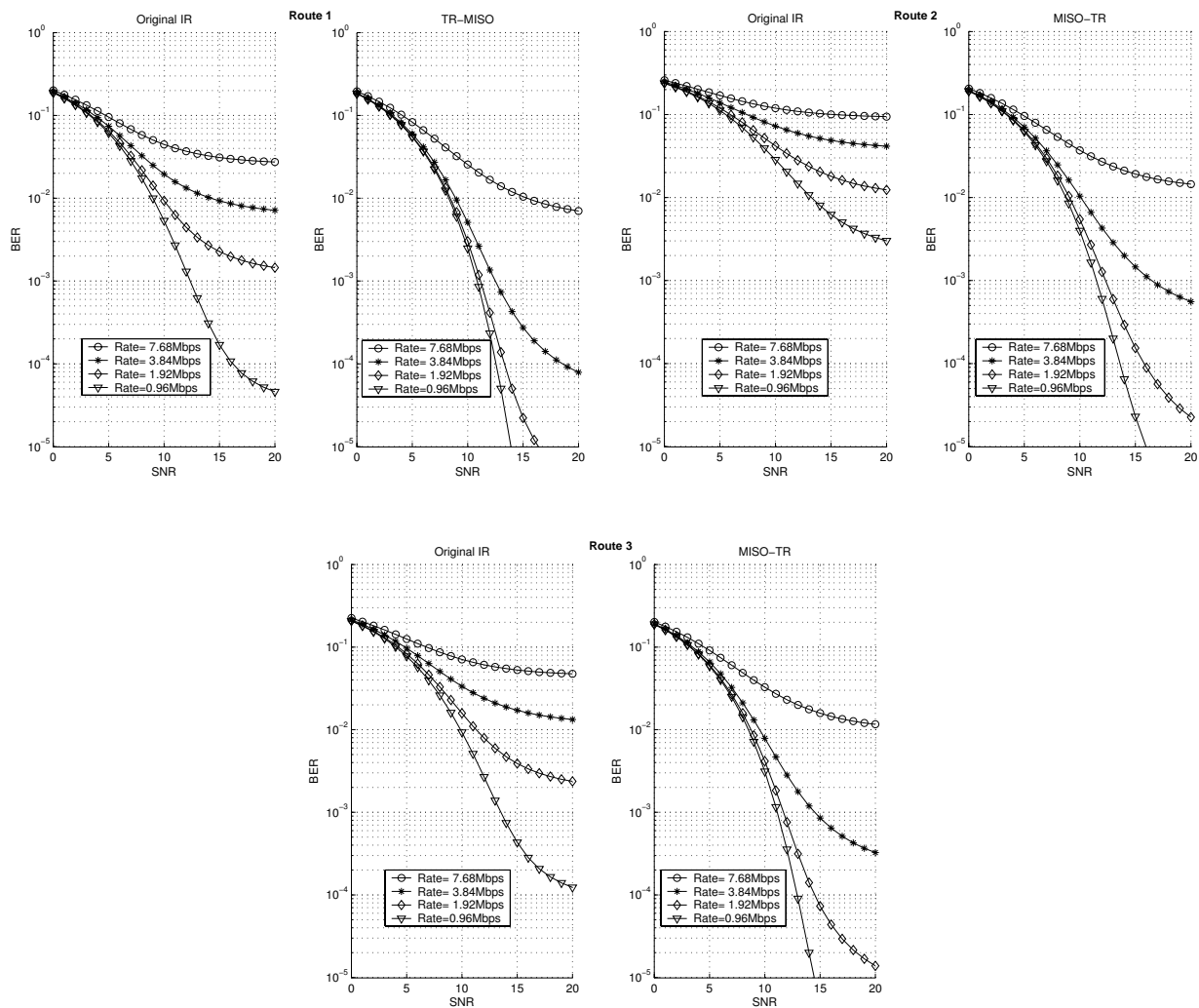


Fig. 7. BER comparision between the SISO and the TR-MISO systems at difference bit rates

In our simulations, the original channel IR for the SISO case and the *equivalent channel IR*, $h^{eq}$ for the TR-MISO case are normalized so that their signals have the same total power level $S = \sum_{l=1}^{L} |h(l)|^2 = \sum_{l=1}^{2L-1} |h^{eq}(l)|^2$. In this way the link budget is the same for both SISO and TR-MISO system. Thereby the temporal focusing characteristics of TR is highlighted. We varied the signal to noise ratio (SNR), defined as the ratio of the total received power $S$ to the variance of the additive white Gaussian noise N. We approximate the inter symbol interference as a Gaussian random variable. This simplifying assumption is within 2dB of the true performance for the range of SNRs of

interest. Therefore, if we assume BPSK modulated signals, the BER for one channel realization can be estimated as

$$BER = 0.5\text{erfc}\left(\sqrt{\frac{P_{max}}{I+N}}\right) \tag{18}$$

where erfc() is the complementary error function, $P_{max}$ is the power of the sampled signal and $N$ is the noise variance. The expected value of the inter symbol interference power $I$ is calculated as

$$I = \begin{cases} P_o\left(\displaystyle\sum_{l=L_{sam}-G}^{l=l-G,l=1} |h(l)|^2 + \sum_{l=L_{sam}+G}^{l=l+G,l=L} |h(l)|^2\right) & \text{Original IR} \\ P_o\left(\displaystyle\sum_{l=L_{sam}-G}^{l=l-G,l=1} |h^{eq}(l)|^2 + \sum_{l=L_{sam}+G,}^{l=l+G,l=2L-1} |h^{eq}(l)|^2\right) & \text{Equivalent IR} \end{cases} \tag{19}$$

where G is the guard interval. As mentioned in section IV-A the number of measured IRs per route was 8x4x4400, therefore for each SNR values there are 8x4x4400 realizations for the BER simulation of the SISO system. Similarly, there are 4x4400 realizations of the 8x1 MISO TR channel, and for each one of them the BER is calculated as in equation 18. The results are then averaged over the whole route.

The performance enhancement due to the use of TR is shown in Figure 7. At a bit rate of 7.68Mbps the BER floor of the TR-MISO system is always lower than that of the SISO system by an order of magnitude. For the bit rates less than 2Mbps, while the BER of the SISO system reaches a BER floor at some points, the SNR value where the BER floor of the TR-MISO system occurs is out of the observed SNR range. As seen from the RMS delay spread results, the highly frequency selective characteristic of the environment in the second route leads to a significant difference in the BER of these SISO and TR-MISO systems.
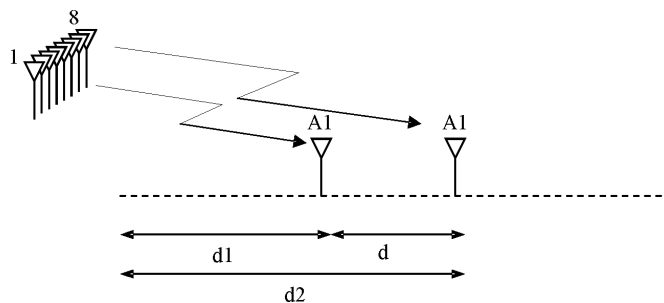


Fig. 8.   Illustration of the separation distance between users along the measurement route

### C. Spatial focusing

In this section the spatial focusing property of TR in the 8x1 down-link setup is evaluated. The available measured data can be used to mimic a multi-user environment. We consider a simple scenario where there are two users separated by distance $d$. Each user is equipped with a single receiving antenna and both users operate simultaneously. There are still 8 antennas at the transmit side. Eight IRs measured at one location are used to calculated the power of the signal of interest as the numerator in equation (6). From the measurement data, the fading correlation between transmitting antennas was estimated and it is smaller than 0.4 for most of the cases.

The eight other IRs measured at a distance $d$ far apart are used to calculate the interference power as the denominator in equation (6). Illustration of the multi-user scenario and the distance between the users is shown in Figure 8.

Figure 11 illustrates the mean of the instantaneous SIR values as a function of the distance between the two users along these three measured routes. The SIR resulting from both schemes, with and without power control, is shown. TR indeed provides a large gain in terms of the SIR in the multi-user scenario. The mean SIR value increases when the distance between the users increases. It saturates when the distance between two users is above
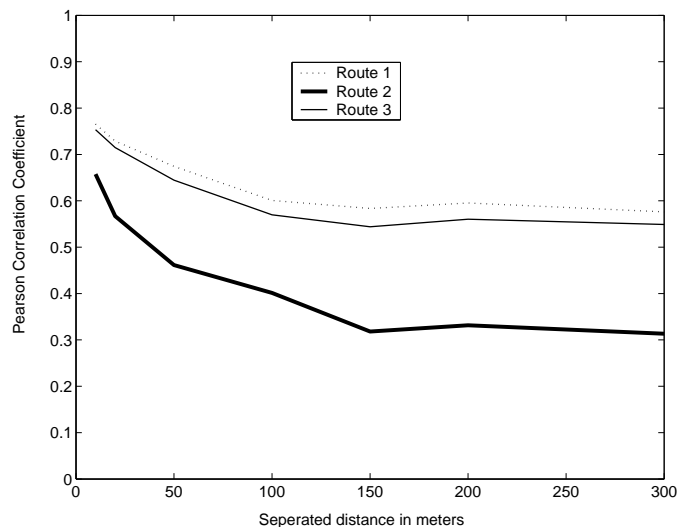
Fig. 9. Pearson's correlation coefficient of two IRs as a function of the seperation distance

a certain value (i.e. 18 dB at a distance of 300 meters). With power control we get higher SIR, its minimum value for most of the routes is around 1dB. The mean SIR ranges from 8dB to 18dB when the distance between the two users varies from 10 meters to 300 meters.

The estimation in section III gives us a lower bound of the mean SIR value of 9dB when there are 8 antennas at the transmit side and 2 antennas at the receive side. With the common measured mean RMS delay spread of $\overline{\sigma_\tau} = 0.3\mu s$ the estimated SIR is 18.7dB. The approximation of the mean SIR in section III was derived under the assumption of uncorrelated IRs. This condition is satisfied when the two receiving antennas are placed far enough apart. When the distance between the two users is around 100 to 300 meters (Figure 11) there is a good match between the mean of the instantaneous SIR value from the measurements and the approximated mean SIR from the model (17dB and 18.7dB respectively). Following up on equations (9) and (15), it is interesting to see that the beamforming ($SIR_{BF}$) and the temporal focusing of TR ($SIR_{TF}$) have almost equal contributions (i.e. each 9dB) to the overall spatial focusing performance. Therefore this simple model can be used as a guide line for estimating and understanding the potential of TR with respect to its temporal and spatial focusing characteristics.

In an urban environment, it has been confirmed by measurements that the signal arrives in clusters, and clustering of the scatterers leads to an increase in the delay dispersion (e.g. [12], [13] among others). Obviously if two receiving antennas are placed far enough apart (e.g. 200m in our measurement) the IRs to the two users are no longer described by the same Wide Sense Stationary Uncorrelated Scattering (WSSUS) model and they experience independent clusters. This leads to a difference in the shapes of the IRs observed at these two locations. In TR, the interference is calculated as the sum of the cross-correlations of two IRs as stated in equation (2). The difference in the shape of the IRs and the shift in time of their major peaks can lead to a situation where the taps of the TR filter containing significant energy are multiplied by taps of the channel with weak amplitude and vice versa. Thus, decorrelation with respect to the shapes of the IRs can also contribute to the reduction of the interference power, and consequently increase the mean SIR values. To support this conclusion, from the collected data we calculate the correlation of the magnitude of the IRs measured at two different points along the route. We use Pearson's correlation [14] as a means to estimate how similar in shape the magnitudes of the two IRs are. Pearson's correlation is defined in equation (20).

$$\rho_{Pearson} = \frac{\sum_{l=1}^{L}(|h_{d_1}(l)| - \overline{|h_{d_1}|})(|h_{d_2}(l)| - \overline{|h_{d_2}|})}{\sqrt{\sum_{l=1}^{L}(|h_{d_1}(l)| - \overline{|h_{d_1}|})^2}\sqrt{\sum_{l=2}^{L}(|h_{d_2}(l)| - \overline{|h_{d_2}|})^2}} ; \overline{|h_{d_{1,2}}|} = \frac{\sum_{l=1}^{L}|h_{d_{1,2}}(l)|}{L} \qquad (20)$$

In this equation $L$ is the number of taps, subscripts $d_1$ and $d_2$ denote the distance between the measurement location of the IR and the starting point of the measured route. The separation distance between the two points therefore becomes $d = d_2 - d_1$ as in Figure 8. The correlation $\rho_{Pearson}$ tells us both the strength and the sign of the relationship and is between $-1$ and $+1$. The closer to zero it is the more uncorrelated the two samples.

From Figure 9 it is apparent that in the first 100m the Pearson correlation of the two IRs depends strongly on the separation distance. It has a declining trend and reaches a floor as the distance between the receiving antennas increases. Interestingly, we observe that both the correlation and the SIR become saturated at the same distance (i.e. 150 meters). This observation highlights the influence of the changes in the shapes of the IRs on the spatial focusing capability of TR. The correlations are also different in the three measured routes. This can also explain the higher SIR values observed along one route relative to the others.

## V. A COMPARISON ON THE SPATIAL FOCUSING PERFORMANCE OF TR AND SVD TECHNIQUES

The success of the TR depends heavily on the availability of the IRs at the transmitter. In practice, in order to use TR at both the uplink and the downlink the channel information is needed at the receiver as well. However, from this channel information, other schemes such as Singular Value Decomposition (SVD) transmission can be applied to obtain spatial focusing. We investigate the potential of the maximum eigen beamforming in supporting concurrent independent data channels from the transmit side to $N_u$ users. The issue of frequency selective fading is assumed to be addressed by proper OFDM technique so that the SVD can be applied as if the channel were narrowband (eigen beamforming on a tone-by-tone basis) [15]. The eigenvectors applied at the transmitter and at the receiver act as steering vectors to focus the signal on the intended user. We further assume that the channels experienced by the users are totally uncorrelated, which is a reasonable assumption provided that these users are separated far enough apart. At one frequency tone, the channel matrix of the $k^{th}$ user, $k \subset (1..N_u)$, is denoted as $H_k$. Furthermore, $u_k$ and $v_k$ are the eigenvectors associated with the maximum eigenvalue of $H_k$. The symbol intended for the $k^{th}$ user is denoted as $x_k$ and its corresponding power is $P_o$. At one frequency tone, the received signal of the $j^{th}$ intended user becomes

$$
\begin{aligned}
y_j &= \underbrace{x_j u_j' H_j v_j}_{S_j} + \underbrace{\sum_{k=1,k\neq j}^{k=N_u} x_k u_k' H_j v_j}_{IF_j} + \underbrace{n_j}_{Noise_j} \\
&= x_j \sqrt{\lambda_{max_j}} + \sum_{k=1,k\neq j}^{k=N_u} x_k u_k' H_j v_j + n_j
\end{aligned}
\tag{21}
$$

where $()'$ denotes the complex transpose operator. Because $u_k$ and $v_j$ are the eigenvectors and if $H_j$ is a matrix with identical independent distributed component with zero mean and unit variance, the interference term in equation (21) is also a random complex number with zero mean and variance equal to $(N_u - 1)P_o$. Hence the average SIR obtained by the maximum eigen beamforming at one arbitrary frequency tone is

$$
SIR = \frac{\overline{\lambda_{max}}}{N_u - 1}
\tag{22}
$$

It is immediately obvious that when there are two concurrent users the SIR can be approximated by the mean of the largest eigenvalue. From the collected data, we calculated the maximum eigenvalues, or the link gain as defined in [16], for different transmitting-receiving antenna setups along each measurement route. The cumulative distribution functions of these link gains are shown in Figure 10.

The results show that the mean link gain and therefore the mean SIR values are 5.7dB, 11.5dB and 13.6dB for the 8x1, 8x2 and 8x4 setups respectively. Meanwhile, under ideal conditions i.e. assuming that two users are separated far enough apart so that their IRs are uncorrelated, the mean SIR of 8x1 setup using TR is around 17dB. The results illustrate that TR outperforms the SVD technique in the spatial focusing perspective. Concerning the complexity of the system, TR-MISO also outperforms the SVD technique as it only requires a single receiving antenna for each user. Moreover, the SVD technique requires more advanced signal processing algorithm than TR.

Since in TR the ISI can not be mitigated completely, the comparisons mentioned above are somewhat biased in favor of the TR. In addition, with the knowledge of the channel state information at both the link ends, it is possible to have better signal processing algorithms to deal with spatial focusing and ISI reduction. Nevertheless, through the comparison we have highlighted the advantage of TR concerning its simplicity in the deployment, without compromising the system performance.
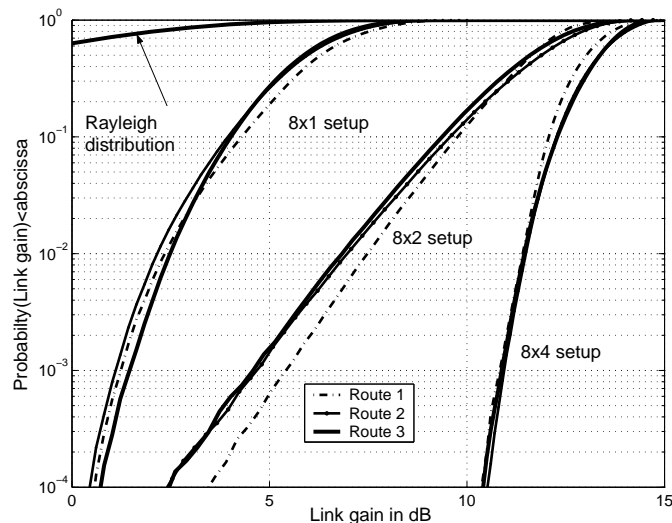
Fig. 10. Link gain obtained by the SVD for 8x1, 8x2 and 8x4 setup of the three routes.

## VI. CONCLUSION

In this paper, the potential of TR has been verified in actual MEA wireless communications. A number of investigations with the data collected from a large outdoor measurement campaign has been carried out. We showed that TR is promising with respect to ISI reduction and its spatial focusing capabilities. Using TR, for the 8x1 setup the mean RMS delay spread is reduced almost by a factor of 2 as compared to the case when no TR is used. This indicates that with the use of TR the receiver can be rather simple. Simulation based on the measured data also shown that the BER floor level due to the ISI effect is reduced significantly when applying TR. In general, the BER floor of the TR-MISO system is always lower than that of the SISO system by at least an order of magnitude. For a lower transmitted bit rate (e.g. smaller than 2Mbps), while the BER of the SISO system reach a floor at some SNR values no BER floor is observed for the MISO-TR system in the SNR range of 0dB to 20dB. For a multi-user scenario, a mean SIR value of around 17dB was found for two concurrent users equipped with single receiving antenna each and 8 transmitting antennas at the BS. This illustrates that using TR can help reduce the interference and the probability of intercept. We presented a simple model for estimating the mean SIR value which can be obtained by the use of the TR technique. The SIR value calculated from the measurements is fairly close to what has been estimated by our model. This is only an initial investigation on the potential of TR under ideal conditions such as perfect knowledge of the instantaneous IR. Nevertheless, the results from this paper can provide useful guidelines for the understanding and the potential deployment of TR in wireless MEA systems. Further investigations include the performance of TR when the transmitting antennas are distributed rather than centralized. In this case, not only are the channel IRs uncorrelated but also the scattering medium observed by transmitting antennas is different. Therefore it is expected that the spatial focusing performance of the TR in that case will improve. A model to estimate the mean SIR when both the complex and the envelope correlations of the IRs are taken into account is an interesting problem for future work. Besides, applying TR in extremely wideband signal such as UWB signals in order to improve the temporal focusing performance could also be an interesting direction [17], [18].

## REFERENCES

[1]  M. Fink "Time-reversed acoustic" Scientific American, Nov 1999, pages 67-73.
[2]  R.K.Ing, M.Fink "Ultrasonic imaging using spatio-temporal matched field (STMF) processing-applications to liquid and solid waveguides", IEEE Transactions on Ferroelectrics and Frequency Control, Vol.48, Issue 2, Mar 2001, pages 374-386

[3]   A.Derode, P.Roux, M.Fink, "Acoustic time-reversal through high-order multiple scattering" Proceedings of Ultrasonics Symposium IEEE , Vol. 2, Nov. 1995,pages 1091-1094.

[4]   P.Kyritsi, P. Eggers, A. Oprea, "MISO time reversal and time compression", URSI International Symposium on Electromagnetic Theory, May, 2004

[5]   P. Kyritsi, G. Papanicolaou, P. Eggers, A. Oprea, "MISO Time Reversal and Delay-Spread Compression for FWA Channels at 5 GHz" Antennas and Wireless Propagation Letters, Vol.3, Issue 6, 2004, pages 96 - 99.

[6]   G.Lerosey, J.de Rosny, A.Tourin, A.Derode, G.Montaldo, and M.Fink, "Time Reversal of electromagnetic waves" in Physical Review Letter, Vol.92, May 2004, pages 193904-1 193904-3.

[7]   B.E.Henty and D.D.Stancil "Multipath-Enabled Super-Resolution for rf and Microwave Communication using Phase-Conjugate Arrays" Physical Review Letters, Vol. 93, Dec 2004, pages 243904-1 243904-4.

[8]   S.M.Emami, J.Hansen, A.D.Kim, G.Papanicolaou, A.J.Paulraj, D.Cheung, and C.Prettie, "Predicted Time Reversal Performance in Wireless Communications Using Channel Measurements", Accepted for publication in IEEE Communications Letters, 2005.

[9]   H.T.Nguyen, J.B.Andersen, G.F.Pedersen, "The potential use of time reversal technique in multiple elements antenna systems", IEEE Communications Letters, Vol 9, No 1, January 2005, pages 40 - 42.

[10]   R.Vaughan and J.B.Andersen "Channels propagation and antennas for mobile communications", IEE Electromagnetic Waves Series 50, ISBN 0 85296084 0, 2003.

[11]   Theodore S.Rappaport, "Wireless Communications, Principles and practice" Prentice Hall PRT, 1996.

[12]   A.Kuchar, J.P.Rossi, E.Bonek "Directional macro-cell channel characterization from urban measurements" IEEE Transactions on Antennas and Propagation, Vol.48, Issue 2 , Feb 2000, pages 137-146.

[13]   K.I.Pedersen,P.E.Mogensen, B.H.Fleury "A stochastic model of the temporal and azimuthal dispersion seen at the base station in outdoor propagation environments", IEEE Transactions on Vehicular Technology, Vol.49, Issue 2, Mar 2000, pages 437-447.

[14]   R.Russo, "Statistics for the behavioural sciences : an introduction", Hove Psychology Press, 2003, ISBN/SKU1841693200

[15]   G.L.Stuber, J.R.Barry, S.W.McLaughlin, Y.G.Li, M.A.Ingram and T.G.Pratt, "Broadband MIMO-OFDM Wireless Communications," Invited Paper, Proceedings of the IEEE, vol. 92, no. 2, pp. 271-294, February 2004

[16]   J.B.Andersen "Array gain and capacity for known random channels with multiple element arrays at both ends ", IEEE Journal on Selected Areas in Communications, Vol.18, Issue 11, Nov 2000, pages: 2172-2178.

[17]   T.Strohmer, M.Emami, J.Hansen, G.Papanicolaou and P.J.Arogyaswami, "Application of Time-Reversal with MMSE Equalizer to UWB Communications", IEEE Global Telecommunications Conference, Vol. 5, Dec 2004, pages 3123-3127.

[18]   H.T. Nguyen, I.Z.Kovacs, P.Eggers, "A Time Reversal Transmission Approach for Multi-user UWB Communications", IEE Communications Proceeding, Jan 2005, submitted.
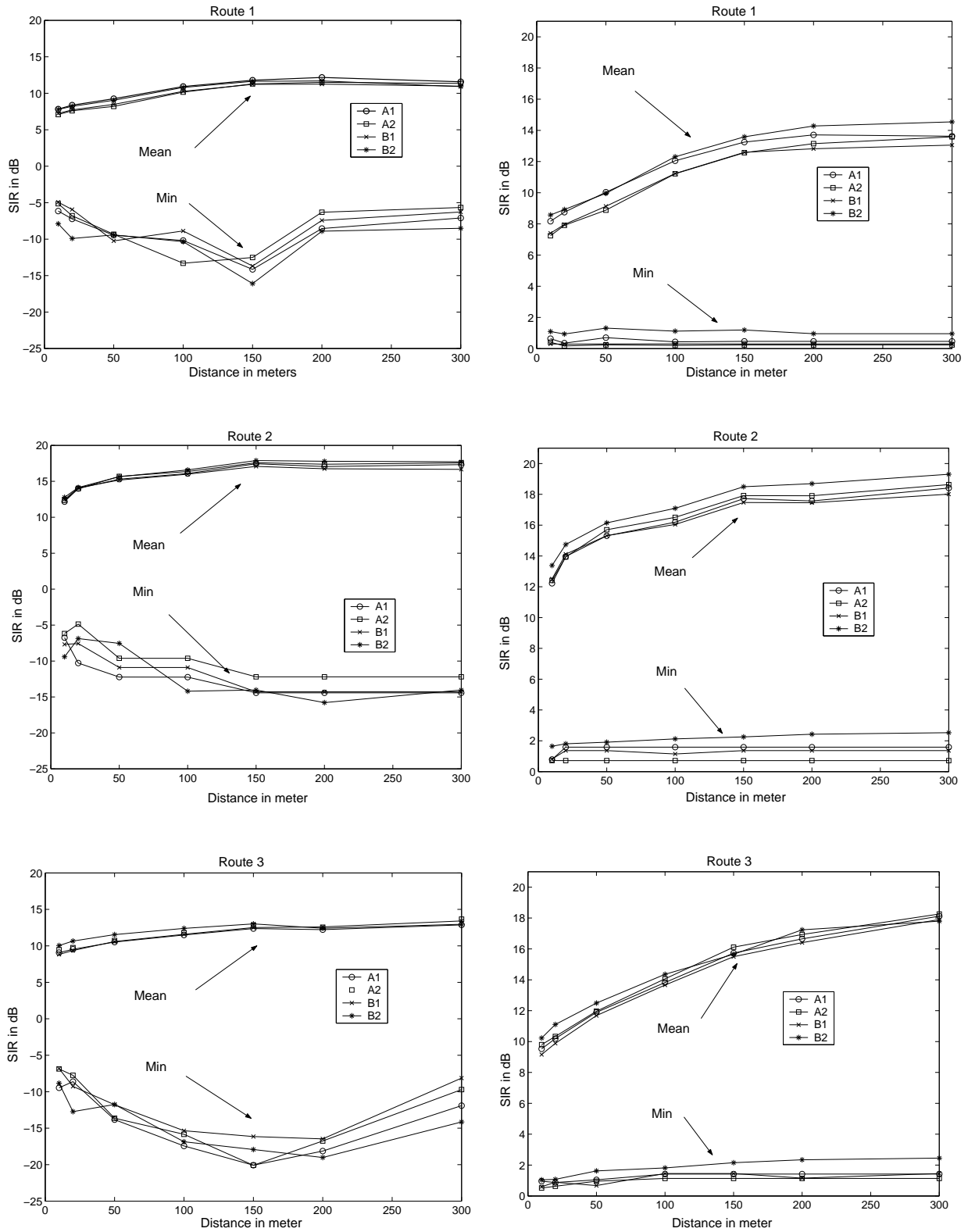
Fig. 11. Maximum, Mean and Minimum value of the SIR vs distance without power control (left column) and with power control (right column) for 3 routes

**Paper 9:**
**A Time Reversal Transmission Approach for Multi-user UWB Communications.**
H.T.Nguyen, I.Z.Kovacs and P.C.F.Eggers.

# A Time Reversal Transmission Approach for Multi-user UWB Communications

Hung Tuan Nguyen, István Zsolt Kovács and Patrick C.F. Eggers *†

## Abstract

*In this paper we propose and evaluate the performance of the time reversal technique in impulse radio UWB communications. The evaluation was based on measured channel impulse responses at the UWB frequency bandwidth of 3 to 5 GHz of a 4×1 MISO system with both vertical and horizontal polarization at the receiver. The results show that there is a great potential in combining time reversal and UWB technique with regards to both reducing the receiver complexity and improving the system performance. Simultaneous communication is illustrated with 5 users with a BER of less than $10^{-3}$ at an average SNR of 15dB.*

***Keywords:*** Time reversal techniques, UWB, multiple elements antenna, MISO system, spatial focusing.

## 1   Introduction

Ultra wide band (UWB) is among the hot topics today due to its potential in short range communications and positioning applications. With UWB, the dense multipath components can be resolved allowing the use of Rake receiver for signal demodulation [1], [2]. UWB aims at providing communications with high bit rates and low complexity devices using an extremely wide frequency range.

Time reversal (TR) techniques have been applied extensively in acoustic, medical and under water communications applications [3], [4]. In [4], it was demonstrated that in ultrasonic frequency regime just by temporal focusing it is possible to provide error free communication with 5 receivers simultaneously. Because of its simplicity and performance advantages, the idea of applying the TR in wireless communication has gained much of attention recently. It is expected that TR can reduce the effect of the inter symbol interference (ISI) significantly without the need of high complexity equalizer at the receiver. Evaluation on the performance of TR based on wireless channel measurement in [5], [6], [7] and [9] among others has shown its great potential. Recently the authors in [8] has proposed an approach using TR with MMSE equalizer to UWB communications. The use of TR has been illustrated as a promising solution in single user UWB communications.

In this work we address the applicability of TR in impulse radio UWB transmissions as one possible solution to improve the multi-user system capacity and communication range. It is expected that the extremely wide bandwidth of the UWB signal will help in increasing the temporal compression and

spatial focusing characteristics of TR. On the other hand, TR may help in reducing the complexity of the receiver devices and in lowering the required transmitting power in UWB system. In our proposed scheme, by using only a single tap which contains most of the signal energy the receiver does not need to estimate the channel. This can result in an easier synchronisation process at the receiver and, because no equalizer is used, the complexity of the receiver can be reduced significantly. These are also the major differences in our approach as compared to the approach proposed in [8]. We show that under certain assumptions, TR-UWB can fulfill the receiver's low complexity requirement as well as increase the system capacity in terms of the number of supported users. The performance of the proposed scheme was evaluated using radio channel data from recent MIMO UWB channel investigations [12].

The rest of the paper is organized in the following way. First we briefly review the TR technique and present the proposed TR-UWB transmission scheme in Section 2. The UWB measurement setup and scenarios are presented in Section 3. Based on the measured channel impulse response (IRs) the TR-UWB performance in terms of the signal to interference ratio (SIR), the number of simultaneous supported users, and the system BER are analyzed in Section 4. The conclusion wraps up the paper in Section 5.

## 2 Multi element antennas & time reversal

### 2.1 TR back ground and performance metrics

The essence of the time reversal technique is that by coherently adding the received signals in the delay domain and the spatial domain (multiple antennas) we can achieve both the spatial focusing and the time compression at the same time. Due to the spatial focusing the interference can be reduced and due to the time compression the ISI can be alleviated. The mathematical formulation of the received signal of a SISO link using TR can be described as follows

$$s(t) \star h_{ij}(-t)^* \star h_{ij}(t) = s(t) \star R_{ij}^{auto}(t) \tag{1}$$

where $\star$ denotes convolution, $(.)^*$ indicates the complex conjugate; $R_{ij}^{auto}(t)$ is the autocorrelation of the channel IR $h_{ij}$ between $i^{th}$ transmitting antenna and $j^{th}$ receiving antenna; $s$ is the transmitted symbol. The received signal at the off-target point has the form

$$s(t) \star h_{ij}(-t)^* \star h_{ik}(t) = s(t) \star R_{ikj}^{cross}(t) \tag{2}$$

where $h_{ik}(t)$ denotes the IR of the channel from the transmitting point to the off-target point and $R_{ikj}^{cross}(t)$ is the cross correlation of the channel IR $h_{ik}$ and the transmitted signal $h_{ij}$.

The three fundamental propagation mechanisms: reflection, diffraction and scattering, which in general make the propagation channel of each communication link independent and unique, contribute to the process of magnifying the intended signal and attenuating the interference at the target point. The independence of each channel forms the orthogonal property among them. It turns out that the environment can provide the artificial "orthogonal code" and that the more decorrelated the channel the better the orthogonality property of the code.

TR for SISO system works in the same manner as the traditional pre-Rake system. When there are $N_t$ transmitting antennas, under ideal conditions the received signal becomes the sum of $N_t$ IR autocorrelations.

The received signal peak is the sum of the $N_t$ real-valued correlated numbers, while the side lobe signals are the sum of $N_t$ real-valued random numbers. This gives rise to the spatial focusing in systems using TR.

Now we consider the scenario when there are $N_t$ antennas at the transmit side and $N_r$ antennas at the receive side. The received signal at the $j^{th}$ receiving antennas is

$$y_j(t) \;\; = \;\; \underbrace{s_j(t) \star \sum_{i=1}^{N_t} R_{ij}^{auto}(t)}_{Signal(j)} + \underbrace{\sum_{i=1}^{N_t} \sum_{k=1;k \neq j}^{N_r} s_k(t) \star R_{ikj}^{cross}(t)}_{Interference(j)} + \underbrace{n_j(t)}_{Noise(j)} \tag{3}$$

In the following we use the term "*equivalent IR*" or $h^{eq}$ to denote the sum of the autocorrelation $R_{ij}^{auto}(t)$ in equation (3).

$$h_j^{eq}(t) = \sum_{i=1}^{N_t} R_{ij}^{auto}(t) \tag{4}$$

As long as the channels are uncorrelated, we expect that the interference part in equation (3) can be suppressed. Thereby, it might be possible to communicate with all users simultaneously with a simple detection scheme at the receiver. Consequently, the throughput of the system can be significantly increased. It should be noted that the formulation mentioned above can be used to describe a single $N_t \times N_r$ MIMO system or $N_r$ simultaneously operating MISO ($N_t \times 1$) systems, each one targeting a different user. As in [7], we use the Signal to Interference ratio (SIR) as a metric representing the spatial focusing characteristics of the TR. The instantaneous SIR is calculated as the ratio of the peak power of the signal of interest and the corresponding interference power at the same time lag.

$$SIR_j = 10log_{10}\left( \frac{|Signal(j)_{peak}|^2}{|Interference(j)_{peak}|^2} \right) \tag{5}$$

where $||$ denotes the absolute value operation.

We note that in order to apply the TR, the channel IR must be known at the transmit side. In a reciprocal channel, the channel estimation of the backward link (from the receiver to the transmitter) can be thought of as a solution to estimate the IR of the forward link (from the transmitter to the receiver). This requirement on reciprocal channel can be approximately fulfilled in a systems employing time-division duplexing (TDD) with a quasi-stationary environment.

## 2.2    TR-UWB transmission scheme

In impulse radio UWB technique, the transmitted pulse width is much smaller than the effective length of the measured IR. Therefore the convolution of the signal with the time-reversed IR is essentially equivalent to the multiplication of time-reversed IR's tap with the transmitted UWB pulse. As long as the pulse width is smaller than the interval between two taps, the pulses between two consecutive taps are distinguishable, i.e. there is no interference between them. Therefore the spectral characteristics of the transmitted TR waveforms are essentially determined by the spectral characteristics of the transmitted pulse waveform. The receiver only needs to synchronize with the main peak of the received signal. It does not need to estimate the channel IR and can use a single tap/Rake finger tuned to the major peak. Thus the detection of the received signal can be done with a rather simple energy detection method. Because of the temporal focusing characteristics of the TR, it is expected that synchronization to the main peak of the signal at the receiver would be easy. Since no equalizer is required, the design of the receiver becomes fairly simple. Most of the complexity burden at the receiver is moved to the transmitter and thereby the cost and the size of the receiver can be reduced. Performance evaluations of the pre-RAKE scheme for SISO UWB system (TR-UWB for SISO) can be found in [10], [11] among others.

For illustration purposes, initially the interval between two transmitted symbols is assumed to be equal to the length of the measured and estimated channel IRs. The ISI effect therefore can be neglected. However, because of the TR's temporal focusing characteristics, the transmitted symbol interval can be smaller than the effective IR's length as long as the ISI effect is not severe. Figure 1 illustrates the working principle of a TR-UWB MISO system.
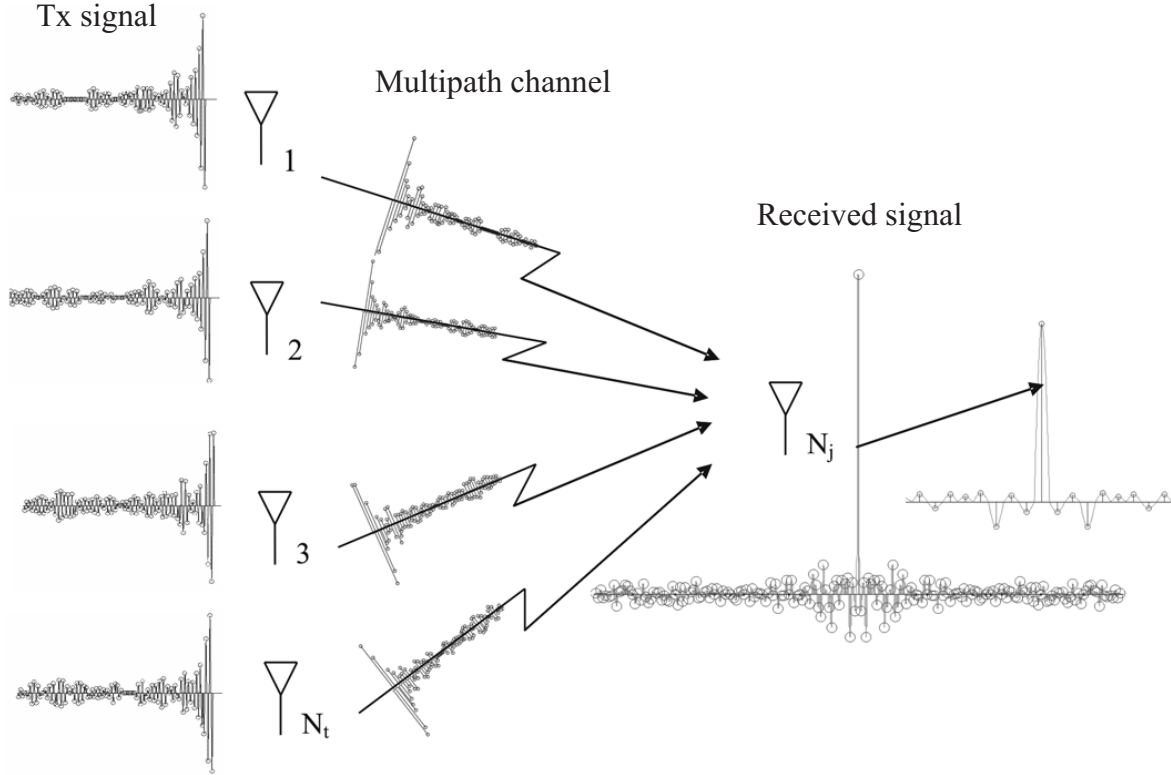


**Figure 1. Illustration of a practical MISO TR-UWB single user system of $N_t$ transmitting antennas and one receiving antenna with real IRs taken from meaurement**

Spatial focusing is the other main advantage of applying TR in UWB communications. Because the transmitted signal is focused in signal space on the target user, not only the interference to other users but also to other wireless communication system is reduced. In the context of multi-user scenario, the system capacity therefore increases (see Section 4.4 for detail).

## 2.3 Equal power control

The plain TR transmission technique described in Section 2.2 assumes that the transmitted power of each symbol for each transmission link is equal to the power of the estimated channel IR. It means that the plain TR transmission technique also introduces a sort of power control for each individual transmission link. However when there are simultaneous communication links, due to the difference in the transmitted power intended for different receiving antennas/users, the interference power as described in equation (3) can be comparable to (or a large fraction of) the intended signal. Here we use the same approach described in [7] as a solution. The time-reversed IR is normalized by the measured wideband

power so that the transmitted power intended for each receiving antenna/user will be equal

$$h_{ij}^{TR}(t) = \frac{h_{measured_{ij}}(-t)^*}{||h_{measured_{ij}}(t)||} \tag{6}$$

where $||()||$ denotes Frobenius norm operation.

### 2.4 Equal power control & Interference suppression

For a TR system with a large number of transmitting antennas as compared to the number of simultaneous receiving antennas/users and with the use of equal power control solution described in Section 2.3 to reduce the effect of branch power difference, the interference can be suppressed. However, in practice the number of transmitting antennas at a hot spot or base station cannot be infinitively large because of the constrains in the size, cost etc.

The expectation of simultaneous transmission of independent data stream requires that the time-reversed IRs should be aligned at their maximal peak/or the first arrival path, so that one can transmit $N_r$ independent symbol simultaneously (Figure 1). Because of the time alignment, even though the channel IRs are uncorrelated, the magnitude of the IRs cross-correlation $R_{ikj}^{cross}$ is still an order of magnitude smaller than that of the IR autocorrelation $R_{ij}^{auto}$. In general, the interference at the peak of the signal also increases linearly according to the number of simultaneous transmissions. Low transmission quality, i.e. low SIR is traded for more users.

Our proposal for interference suppression consists in offsetting in time the time-reversed IRs intended for each user. The transmitted signal intended for $j^{th}$ user at the $i^{th}$ transmitting antenna can be described as

$$s_j \star circshift(h_{ij}^{TR}(t), \triangle TR(j-1))$$
$$\triangle TR = \triangle l \delta_t \tag{7}$$

where $circshift()$ denotes the circular shift operation, $\triangle l$ is the shifted unit calculated as the number of taps and $\delta_t$ is the tap resolution. Figure 2 illustrates the signals transmitted at one transmitting antenna before and after shifting the time-reversed IRs' main peaks by $\triangle l = 5$ taps relative to each other.

In this way the taps in the propagation channel containing significant energy are multiplied by taps of the transmitted signal with low energy and vice versa. The peak to peak multiplication can be avoided and the interference power is significantly suppressed. Depending on the amount of the time offset $\Delta TR$, the system capacity is reduced as it requires a longer interval for all symbols to be transmitted. The communication quality is improved as the interference is decreased. The results of the SIR as a function of the time offsetting interval are shown in the Section 4. Hereafter we use the term "TR&S" to denote the shifted time reversed scheme.

## 3  Measurement and data analysis

The channel measurements were conducted with a *UWB sliding correlator* channel sounder. The measurement bandwidth was 2.5GHz centered at 4.5GHz. The effective delay resolution was $\delta_t$ =0.4ns. The antennas used were planar monopole antennas with a bandwidth of 2GHz to 15GHz. An array of four elements was used at the 'access-point' (AP) device, while a single element was used at the user terminal with vertical or horizontal polarization, (see Figure 3).

The environment was quasi-static during the measurements and only the stationary user device scenarios were used for the results presented in this paper. The environment was a large hallway (17m x
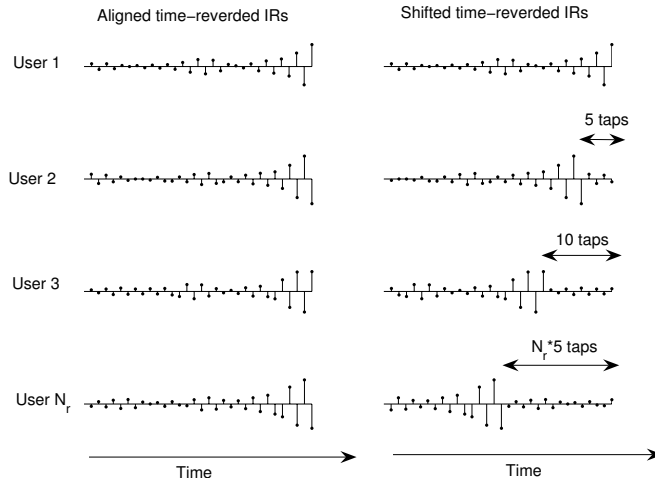
**Figure 2. Signal applied at one antenna for MISO TR-UWB multiple-user scenario: normal TR case (left), proposed shifted TR ($TR\&S$) scheme (right). The IRs were real IRs taken from measurement**

12m x 11m) with two metalised glass walls, two metallic bridges and one staircase structure. The AP antenna system was mounted at 6m height above the floor. The user terminal was moved to five different locations always at 0.8m height above the floor. The effective TX-RX distances were in the range of 6m to 17m. For one type of receiving antenna polarization, at one location 1024x4 (1024 is the number of SISO channel IRs, and $N_t = 4$ is the number of antennas at the AP) channel IRs were captured. The number of *equivalent IR*, $h^{eq}$ captured at one measured location, $N_{h^{eq}}$ therefore was 1024. The channel IRs were sampled at a rate of 40Hz. A detailed description of the equipment and investigated environment can be found in [12]. The obtained channel data was compensated for all system components.

In order to make it more natural to the concept of carrier-less UWB signal, the measured complex IRs have been converted into real-valued IRs via standard Hermitian transformation. To illustrate the working principle of the TR in UWB, in the following analysis we assumed that the measured data is noise free and the forward link can be perfectly estimated from the backward link (using the reciprocity theorem).

## 4  Results

### 4.1  Temporal focusing

From the measurement data we estimated the length of 90% energy window $W$ defined as

$$\frac{\sum_{l=1}^{W} PDP(l)}{\sum_{l=1}^{L_{meas}} PDP(l)} * 100\% = 90\% \tag{8}$$

where PDP is the power delay profile , $L_{meas}$ is the length, as a number of taps, of the measured IR. The average value of $W$ is about 100 taps or 40ns. For the purpose of illustration, we use a truncated version of the measured IR with $L = 100$ taps starting from the first arrival path, or the main peak of the IR in most case, as the effective length of the IR. To illustrate the time compression characteristics of the TR, we compare the instantaneous RMS delay spreads between the channel IRs and the *equivalent IR*, $h^{eq}$ of
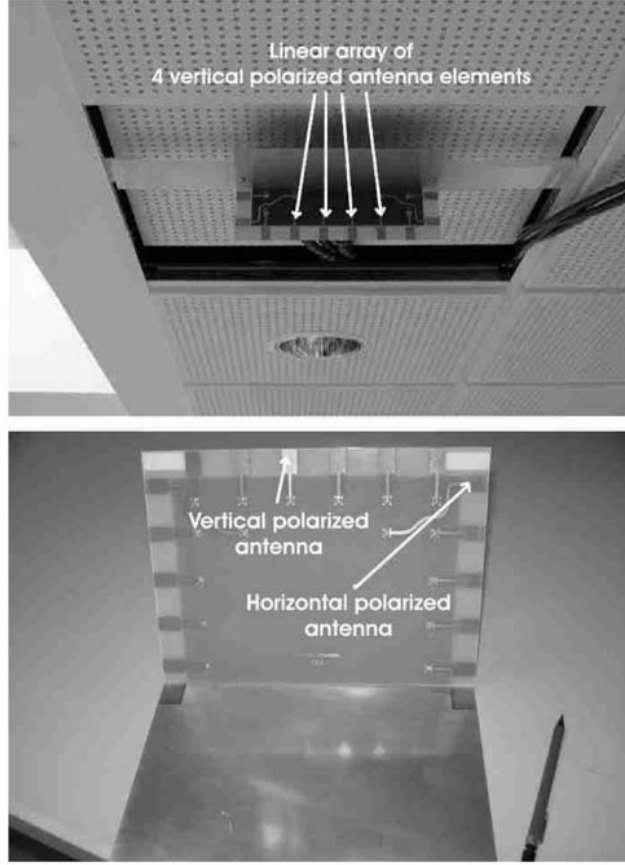
6

**Figure 3. Antenna systems used in the UWB channel investigations: AP linear antenna array with vertical polarized elements (top), User device with vertical or horizontal polarized element (bottom).**

a 4×1 MISO system. For the measured IRs, the instantaneous RMS delay spread is calculated from the first and second moment of the instantaneous IRs

$$\sigma_\tau = \sqrt{\frac{\sum_{l=1}^{L} PDP(l)\tau_l^2}{\sum_{l=1}^{L} PDP(l)} - \left(\frac{\sum_{l=1}^{L} PDP(l)\tau_l}{\sum_{l=1}^{L} PDP(l)}\right)^2}$$

$$\text{with } PDP(l) = |h_{ij}(l)|^2 \tag{9}$$

where $\tau_l$ is the excess time delay. The RMS delay spread of the *equivalent IR* $h^{eq}$ is calculated by

$$\sigma_\tau^{eq} = \sqrt{\frac{\sum_{l=1}^{2L-1} PDP(l)\tau_l^2}{\sum_{l=1}^{2L-1} PDP(l)} - \left(\frac{\sum_{l=1}^{2L-1} PDP(l)\tau_l}{\sum_{l=1}^{2L-1} PDP(l)}\right)^2}$$

$$\text{with } PDP(l) = |h_j^{eq}(l)|^2 \tag{10}$$

7

The RMS delay spread cumulative distribution function (CDF) for the measured IR and the $h^{eq}$ are shown in Figure 4. Using TR, the median RMS delay spread of the $h^{eq}$ has reduced by a factor of 1.5 as compared to that of the real channel IR. This is in agreement with the results shown in [5] and [7].
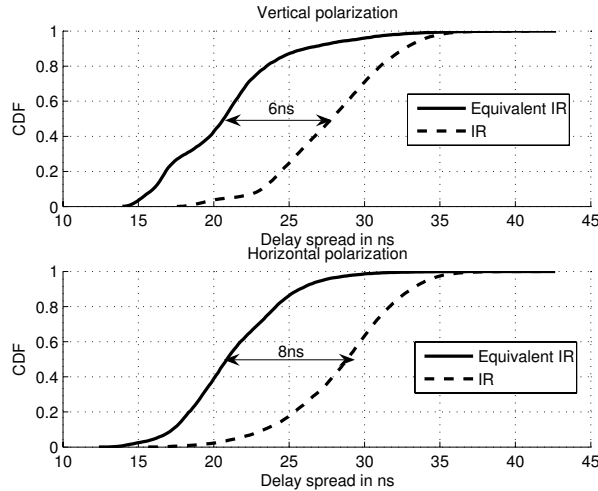


**Figure 4. Comparision of the RMS delay spread CDF, the real measured channel IR (top), the** *equivalent channel IR* **(bottom)**

## 4.2 Signal detection

As mentioned in Section 2.2, for the TR-UWB scheme to work correctly the receiver needs to be synchronized to the received signal peaks. Due to the temporal focusing effect described in Section 4.1, the fraction of the signal energy used for synchronization is higher than in the case of traditional systems without TR. Simple energy threshold detectors [13] or more complex ones, such as the chip-level post-detection integration schemes [14] can be potentially used to achieve synchronization.

We calculated the signal to side lobe ratio (SSR), defined as the power ratio of the main signal peak to the largest side lobe signal of the *equivalent IR*, $h^{eq}$ as a function of the used IR's length, $L$.

$$SSR = 20log_{10}\left(\frac{max(|h^{eq}(l)|)}{max(|h^{eq}(l)|_{l\neq L})}\right), l = 1...2L - 1 \tag{11}$$

The results are shown in Table 1. The mean SSR values do not very much depend on the used IR's length. With a mean SSR of more than 10dB, the synchronization to the main received signal peak can be fairly easily achieved.

## 4.3 Spatial selectivity and TR with time offset scheme

### 4.3.1 Results in an idealized case

As described in Section 2, by avoiding the peak to peak multiplication, the interference at the peak of the $h^{eq}$ can be further suppressed. Figure 5 shows the mean SIR values as a function of the time offset interval $\Delta TR$. It is observed that above certain offsetting value $\Delta l =5$ taps the SIR becomes saturated at the average value of 27dB.

**Table 1. Minimum, Mean and Standard deviation value of the SSR in dB vs the used IR's length for Vertical (V) and Horizontal (H) polarization**

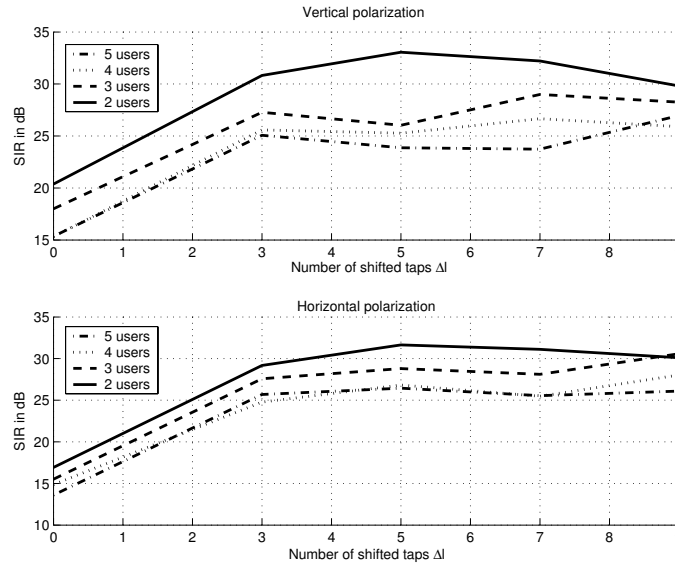| IR's length/taps | | 25 | 50 | 75 | 100 | 125 | 150 |
|---|---|---|---|---|---|---|---|
| V | Min | 3.1 | 3.2 | 3.1 | 3.2 | 3.1 | 3.1 |
| | Mean | 11.7 | 11.9 | 12.1 | 12.2 | 12.3 | 12.3 |
| | $\sigma_{SSR}$ | 4.7 | 4.8 | 4.9 | 5.0 | 5.1 | 5.0 |
| H | Min | 3.7 | 3.6 | 3.6 | 3.6 | 3.7 | 3.7 |
| | Mean | 11.1 | 11.2 | 11.4 | 11.3 | 11.4 | 11.5 |
| | $\sigma_{SSR}$ | 3.6 | 3.8 | 3.9 | 3.8 | 3.9 | 3.8 |



**Figure 5. Mean SIR as a function of the time offset and the number of users**

Figure 6 shows the CDF of the SIR calculated from the measured IRs with the effective IR's length of 100 taps (40ns). The results for both aligned time-reversed IRs and $TR\mathcal{C}S$ schemes are given. Note that the offset time described in Figure 2 can be made dynamic or static depending on the channel condition and system requirement. Henceforth, for simplicity purpose we use a static offset time of $\Delta l = 5$ taps, which is equivalent to 2ns. It is observed that by shifting the transmitted time-reversed IRs intended for each user by 2ns, significant improvement in the SIR can be obtained i.e. the median SIR increases to 23dB from 12dB for 5 simultaneous users scenario.

These results become more significant if we consider the separation distance between users/measurement locations was only 15 meters at most [12]. For a 2 users scenario, both with UWB signals the mean SIR of the aligned IRs is about 20dB. Whereas for the same value of SIR, with wideband (UMTS) signals the required separation distance is about 300m [7]. This demonstrates a much better spatial focusing performance of the TR for UWB bandwidth (GHz) than for UMTS bandwidth (MHz).

With the aligned IRs scheme, the SIR was slightly better when vertical polarized receiving antenna is used, (Figure 6(a)). However, using the $TR\mathcal{C}S$ scheme there was no significant difference in the obtained SIR between the two polarizations (Figure 6(b)).
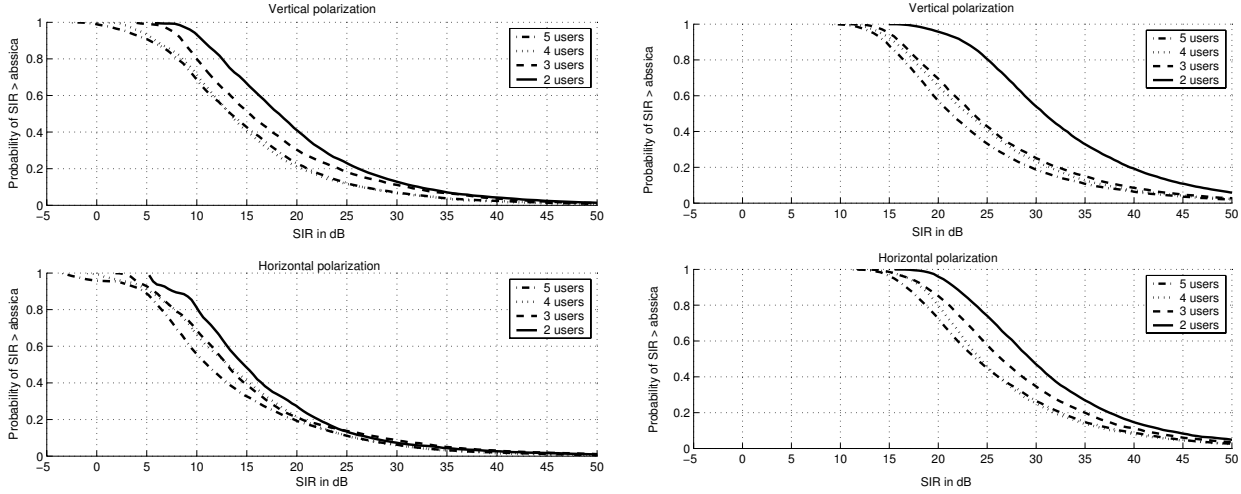
9

(a) SIR of aligned time-reversed IRs, simple TR

(b) SIR of shifted and time-reversed IRs, the peaks are shifted by 2ns relative to each other($\Delta l = 5$, $\Delta TR$ =2ns),TR&S

**Figure 6. SIR with different settings and transmission schemes**

### 4.3.2 Effect of outdated channel information

One of the most important condition for TR to work properly is that the channel IRs must be known at the transmitter. As mentioned earlier, this can be fulfilled by estimating the channel from the backward link (from the receiver to the transmitter). However, even though the measured channel is quasi-stationary there is concern about the impact of outdated channel IRs to the TR performance. For example, the channel can be varied in time due to the movement of the people or objects in the vicinity of the measurement site. To evaluate this impact, we calculated the SIR value when the time reversed version of the current channel IR is used as the TR filter for the next channel realization. Since the channel IR was sampled at the rate of 40Hz, the outdated time therefore is 2.5ms and we believe that this is a realistic interval for the loopback delay. The mean and standard deviation of the SIR values for the perfect and outdated cases are tabulated in table 2 and 3. In most cases, the loss in the mean SIR value caused by outdated TR filter is about 2dB, which is a reasonable number if we consider the outdated time of 2.5ms. Meanwhile the standard deviation value of the SIR is almost the same the for both the perfect and outdated cases. Therefore, in the following analysis we use the instantaneous TR filter in the evaluation process and the results thereof could be considered as the upper bound of the TR performance.

### 4.4 BER simulation and system throughput

Using the measured channel IRs we simulated the average BER of the multi-users TR-UWB MISO system. At one measured location, the received signal power at the receiving antenna was calculated as the average power of the signal at its peak

$$P_j = \overline{max(|h_j^{eq}(t)|)^2} \tag{12}$$

The equal power control scheme, (Section 2.3), is used in the simulations. By varying the noise variance, we can vary the synthetic Signal to Noise Ratio (SNR) at one measured location. The maximum SNR

**Table 2. Comparison of the Mean/Standard deviation values ($\mu/\sigma$) of the SIR in dB when using instantaneous and outdated TR filter, Horizontal polarization**

| No. of users | TR | | TR&S | |
|---|---|---|---|---|
| | Instantaneous | Outdated | Instantaneous | Outdated |
| 2 | 16.93/8.97 | 15.30/9.22 | 31.64/9.47 | 29.92/9.38 |
| 3 | 15.51/9.97 | 13.80/10.25 | 28.80/9.64 | 27.33/10.06 |
| 4 | 14.87/8.98 | 13.33/9.67 | 26.82/8.97 | 25.48/9.34 |
| 5 | 13.61/9.61 | 11.88/10.10 | 26.45/9.45 | 25.06/10.32 |

**Table 3. Comparison of the Mean/Standard deviation values ($\mu/\sigma$) of the SIR in dB when using instantaneous and outdated TR filter, Vertical polarization**

| No. of users | TR | | TR&S | |
|---|---|---|---|---|
| | Instantaneous | Outdated | Instantaneous | Outdated |
| 2 | 20.38/9.37 | 18.74/9.80 | 33.05/9.84 | 31.40/10.15 |
| 3 | 18.00/9.71 | 16.40/10.28 | 26.03/9.76 | 24.90/10.13 |
| 4 | 15.33/8.81 | 13.73/9.30 | 25.27/9.45 | 23.77/9.91 |
| 5 | 15.35/9.44 | 12.86/9.71 | 23.87/9.39 | 22.49/9.75 |

value is limited at 20dB to assure that it is always lower than the measured SNR [12].

For these simulations, we used the bipolar pulse amplitude modulation (BPAM) with the Gaussian pulse shape similar to the investigations in [14]. The pulse width of 0.4ns was chosen. The interval between consecutive transmitted symbols of 40ns was selected. This interval is also equal to the 90% energy window length of the IRs. Perfect synchronization is assumed in the simulation. The received signal of the $j^{th}$ user has the form described in equation (3). The received signal $y_j(t)$ is sampled at its peak. Then the sampled signal is detected based on the ideal decision threshold

$$\text{Detected bit} = \begin{cases} \text{"1" if } y_j(t = L\delta_t) \geq 0, \\ \text{"0" if } y_j(t = L\delta_t) < 0 \end{cases} \tag{13}$$

For each measured IR, some $N_{symbol} = 10000$ symbols were simulated in order to have enough data for statistical analysis. For each SNR value, the average BER for each user is calculated as

$$\overline{BER} = \frac{\sum_{n=1}^{N_{h^{eq}} * N_{symbol}} \sum_{j=1}^{N_r} err(y_j|s_j)}{N_{h^{eq}} * N_{symbol} * N_r}$$

$$\text{where } err(y_j|s_j) = \begin{cases} 1 \text{ if } y_j(t = L\delta_t) \neq s_j, \\ 0 \text{ if } y_j(t = L\delta_t) = s_j \end{cases} \tag{14}$$

where $N_r$ in this case is the number of simultaneous users. The results are shown in Figure 7. The theoretical BER of the BPAM scheme in additive white Gaussian noise (AWGN) channel is plotted in the same figure for reference. When the transmitted time-reversed IRs are aligned in time at their peaks, the performance decreases significantly for a large number of concurrent users. For more than 3 users and at a SNR value of 15dB, the BER already reaches a BER floor of $10^{-2}$, (Figure 7(a)). For the proposed *TR&S* scheme, the BER does increase with the number of users, but at a lower rate and the

detected BER floor was below $10^{-6}$. At a SNR of 15dB, a BER in the order of $10^{-3}$ can be obtained for 5 simultaneous users (Figure 7(b)).



(a) Aligned time-reversed IRs, simple TR

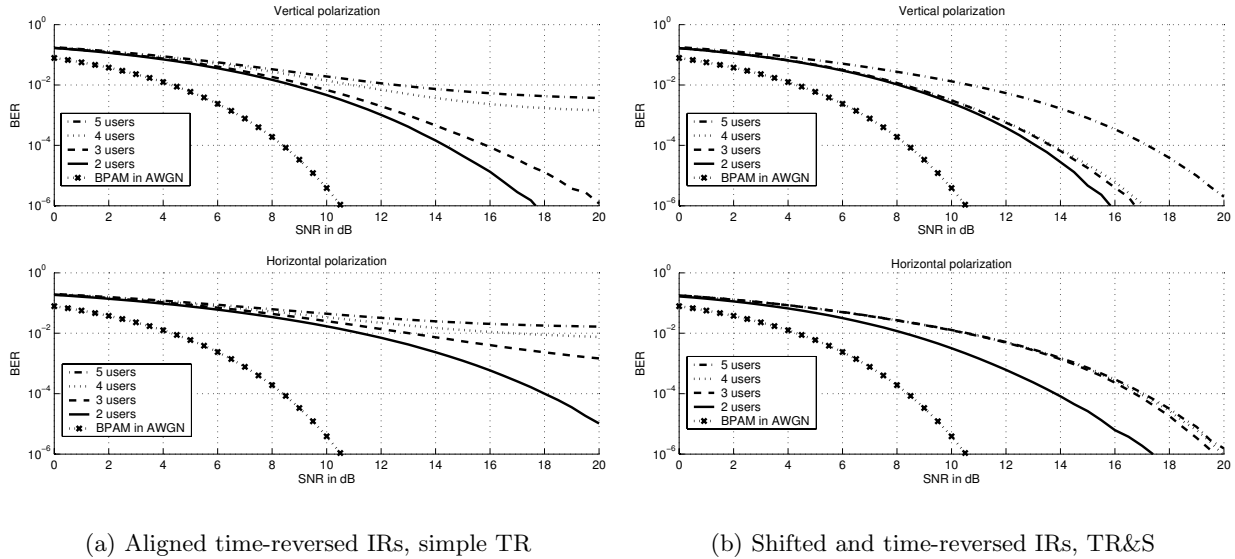(b) Shifted and time-reversed IRs, TR&S

**Figure 7. BER with different transmission scheme**

As for the system capacity, we compare the total system bit rate for a multi-user system of the classical time hopping UWB (TH-UWB) transmission scheme [1], the TR-UWB and our proposed *TR&S*-UWB schemes.

For the TH-UWB scheme, with a frame interval $T_f = 0.2\mu s$ and time slot chip duration $T_c = 40ns$, the system can serve 5 users with the total maximum bit rate of 5x5=25 Mbps (Figure 8 top). The time slot for each particular user is assigned randomly from frame to frame depending on the TH-code. The total maximum bit rate of the system (all users) in a TH-UWB scheme is

$$N_u^{TH} R_u^{TH} = \frac{1}{T_c} \tag{15}$$

where $N_u^{TH}$ is the number of served users and $R_u^{TH}$ is the bit rate of one user.

Using the simple TR-UWB scheme we can pack more users into a single time slot. The signals of 5 (or more) users can be packed into the same time slot at the same epoch and therefore overlapped in time (Figure 2 (left)). However, the performance in terms of the BER decreases fast with the number of users if the multi-user interference cannot be suppressed (Figure 7(a)). The maximum bit rate of the system (all users) in the simple TR-UWB scheme is

$$N_u^{TR} R_u^{TR} = N_u^{TR} \frac{1}{T_c} \tag{16}$$

The number of simultaneous users $N_u^{TR}$ is selected so that the requirement on the transmission quality of the system in terms of the BER is met. For example, if the target BER at 20dB SNR is $10^{-3}$ then the number of users is 4 and 3 for vertical and horizontal polarization receiving antenna respectively, Figure (7(a)).

In Figure 8 (bottom), the signal assignments of the 5 users in the *TR&S*-UWB scheme are illustrated. For clarity, only the first tap of the time-reversed IRs of the transmitted symbol is shown. With this
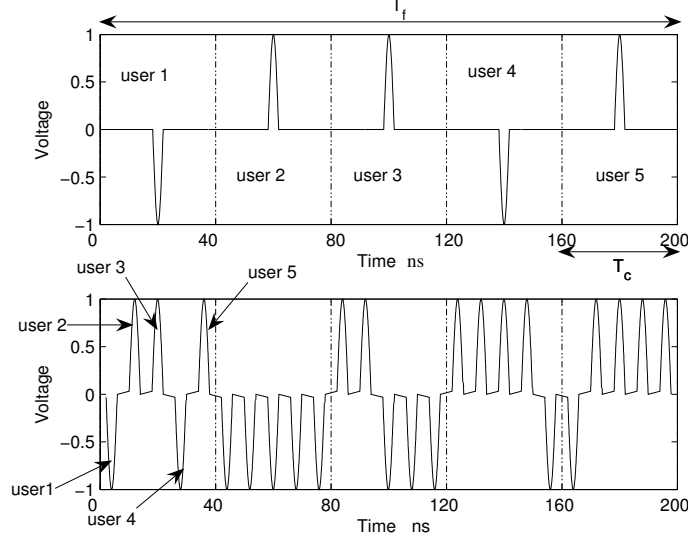
12

**Figure 8. Illustrations of the classical TH-UWB transmission scheme (top ) and the TR-UWB transmission scheme** $TR\mathscr{E}S$**-UWB (bottom)**

$TR\mathscr{E}S$-UWB scheme, it is also possible to pack 5 users in one time slot $T_c$. However, because the interference is further suppressed, better BER performance can be achieved (Figure 7(b)).

The maximum number of supported users $N_u^{TR\&S}$ in our proposed scheme (TR&S) can be roughly calculated as

$$N_u^{TR\&S} \leq \frac{T_c}{\triangle TR} \tag{17}$$

The total bit rate of all users in a $TR\mathscr{E}S$-UWB system consisting of $N_u^{TR\&S}$ therefore is

$$N_u^{TR\&S} R_u^{TR\&S} = \frac{1}{\triangle TR} \tag{18}$$

Roughly speaking, without taking the system performance in terms of the BER into account, using the proposed $TR\mathscr{E}S$-UWB scheme we can increase the total system bit rate by a factor of $N_u^{TR\&S}$ as compared with the classical TH-UWB scheme.

A combination of the $TR\mathscr{E}S$-UWB scheme and the TH-UWB scheme is also a potential option. In this $TR\mathscr{E}S$-TH-UWB scheme the time slot of each group consisting of $N_u^{TR\&S}$ users is assigned randomly depending on the TH-code. The advantage of this scheme is that the system can serve $N_u^{TH}$ times more users. However, the system maximum total bit rate is similar to that of the $TR\mathscr{E}S$-UWB scheme.

## 5   Conclusion and remarks

In this paper we have proposed and evaluated the time reversal (TR) technique in UWB communications. We considered a particular multi-user TR-UWB system consisting of 4 transmitting antennas and 5 concurrent users each of them equipped with a single antenna (with either vertical or horizontal polarization). It was illustrated that the median SIR value observed at each user/location can be as large as 18dB. Using the TR technique, spatial and temporal focusing is achieved, the receiver's architecture becomes very simple and the required maximum transmit power can be alleviated. Using the proposed shifted time-reversed transmission scheme(TR&S), the simulation results showed that under

13

certain assumptions, it is possible to communicate with 5 users simultaneously with the uncoded BER as low as $10^{-3}$ when the average SNR at the receiver is 15dB. With a typical loopback delay time of 2.5ms, the effect of outdated channel information on the TR performance was shown to be negligible i.e. 2dB reduction in the mean SIR.

For the same total throughput of 125 Mbps (5x25), the BER vs. the SNR performance of the proposed *TR&S* scheme is similar to the single user case with All-Rake receiver [14], in IEEE 802.15.3a multipath UWB channel [15]. In [8] similar performances are obtained for the TR SISO single user case in measured multipath channel. These comparisons highlight the strong potential of TR schemes in MIMO/MISO-UWB systems.

Evaluating the performance degradation of the TR in UWB system when the imperfection in channel estimation is taken into account is one of the interesting problem for future work. Besides, using a distributed instead of centralized antennas system at the AP in order to capture most of the waves emitted by the source/receiver so as to increase the spatial focusing could be an interesting investigation topic.

## Acknowledgement

## References

[1] M.Z.Win, R.A.Scholtz, "Impulse radio: how it works" IEEE Communications Letters, Vol. 2 , Issue: 2 , Feb. 1998 Page(s): 36 - 38

[2] M.Z.Win, R.A.Scholtz, "Characterization of ultra-wide bandwidth wireless indoor channels: a communication-theoretic view", IEEE Journal on Selected Areas in Communications (JSAC), Vol. 20 , Issue: 9 , Dec. 2002, Page(s): 1613 - 1627

[3] M. Fink, "Time-reversed acoustic", Scientific American, November 1999, Page(s): 67 - 73

[4] A.Derode, A.Tourin, J.D.Rosny, M.Tanter, S.Yon, M.Fink, "Taking Advantage of Multiple Scattering to Communicate with Time-Reversal Antennas", Physical Review Letters, Vol. 90, No. 1, 2003, Pages(s) 014301-1-014301-4

[5] P. Kyritsi, G. Papanicolaou, P. Eggers, A. Oprea, "MISO Time Reversal and Delay-Spread Compression for FWA Channels at 5 GHz" IEEE Antennas and Wireless Propagation Letters, Vol. 3, Issue: 6, 2004, Page(s): 96 - 99

[6] S.M.Emami, J.Hansen, A.D.Kim, G.Papanicolaou, A.J.Paulraj, D.Cheung, and C.Prettie, "Predicted Time Reversal Performance in Wireless Communications Using Channel Measurements", Accepted for publication in IEEE Communications Letters, 2005.

[7] H.T.Nguyen, J.B.Andersen, G.F.Pedersen, "The potential use of time reversal technique in multiple elements antenna systems", IEEE Communications Letters, Vol. 9, No. 1, January 2005, Page(s): 40 - 42

[8]  T.Strohmer, M.Emami, J.Hansen, G.Papanicolaou and P.J.Arogyaswami, "Application of Time-Reversal with MMSE Equalizer to UWB Communications", IEEE Global Telecommunications Conference (GlobeCom), Vol. 5, December 2004, Page(s): 3123 - 3127

[9]  B.E.Henty and D.D.Stancil "Multipath-Enabled Super-Resolution for rf and Microwave Communication using Phase-Conjugate Arrays" Physical Review Letters 10 December 2004, 243904-1 243904-4.

[10]  K.Usuda, H.Zhang, M.Nakagawa, "Pre-Rake performance for pulse based UWB system in a standardized UWB short-range channel", IEEE Wireless Communications and Networking Conference, Vol.2, March 2004, Page(s): 920 - 925

[11]  S.Imada, T.Ohtsuki, "Pre-RAKE diversity combining for UWB systems in IEEE 802.15 UWB multipath channel", IEEE Joint Conference on Ultrawideband Systems and Technologies, May 2004, Page(s): 236 - 240

[12]  IST 2004-507102 "My Personal Adaptive Global Net (MAGNET)", Deliverable D3.1.2a: "PAN Radio Channel Characterisation (Part 1)", October 2004

[13]  IST 2004-507102 "My Personal Adaptive Global Net (MAGNET)", Deliverable D3.2.2a: "Candidate Air-Interfaces and Enhancements", October 2004 (www.ist-magnet.org).

[14]  I.Oppermann, M.Hamalainen and J.Linatti "UWB theory and applications" John Wiley & Sons, Ltd ISBN 0-470-86917-8

[15]  J. Foerster, "802.15.3a Channel modelling sub-committee - Report Final", IEEE P802.15 Working Group for WPAN, November 2002.